Metabolic functions and inheritance of the microsporidian mitosome

By
Kacper M. Sendra

Thesis submitted for the degree of Doctor of Philosophy

Institute for Cell and Molecular Biosciences

October 2015

Abstract

Microsporidia are a group of obligate intracellular parasites of economic and medical importance. Many aspects of microsporidian genomes and cell biology are a result of an extensive reductive evolution during adaptation to their intracellular parasitic lifestyle. Microsporidian mitochondrial homologues called mitosomes have only a single known conserved metabolic function in biosynthesis of the essential iron-sulfur clusters. Based on genomic data an additional function of the mitosome in the alternative respiratory pathway (ARP) was proposed for some microsporidians including human pathogenic *Trachipleistophora hominis.* This thesis provides the first direct experimental evidence for a mitosomal localization of the two components of the ARP in *T. hominis.* Quantitative analyses of the immunofluorescence data together with western blotting experiments provided results consistent with the life cycle-stage specific function of the organelle. In the proliferative stages of the *T. hominis* life cycle, capable of stealing ATP from the host, mitosomes seem to function mostly in the biosynthesis of the essential iron sulfur clusters. The ARP proteins are enriched in the *T. hominis* spores, which is consistent with the hypothetical functions of the mitosome in energy metabolism of the spore that is unable to rely on its host for ATP production. This thesis also provides the first bioinformatics characterization of the molecular machineries involved in the processes required for inheritance of the microsporidian mitosomes: organelle fission and segregation during the cell division. Specific antibodies were generated and used to detect the microsporidian spindle pole body (SPB), an organelle hypothesized to play a role in inheritance of the microsporidian mitosomes. Double labelling experiments using the specific antibodies against the SPB and mitosomal markers provide evidence for a stable connection between the two organelles throughout the life cycle of the parasite.

Declaration

This thesis is submitted for the degree of Doctor of Philosophy to Newcastle University. The research was conducted in the Institute for Cell and Molecular Bioscience, Newcastle University, under the supervision of Professor Martin Embley and Professor Robert Hirt. I certify that this thesis is the result of my own investigations unless otherwise stated and that no part of it has been previously submitted by me for a degree or qualification at this or any other university.

Kacper M. Sendra

Dedication

I dedicate this thesis to my wife Ania, whose unconditional support gave me strength to pursue my dreams.

Dziękuję Kochanie.

Acknowledgements

I would like to thank my supervisors, Professor Martin Embley and Professor Robert Hirt, for their mentoring and support throughout this project.

I would also like to thank Dr Sirintra Nakjang, and Dr Alina Goldberg for providing me with initial bioinformatics and laboratory training. Dr Artur Rogowski, for his invaluable help with molecular techniques and useful discussions. Research technician, Mrs Ekaterina Kozhevnikova, whose hard work and expertise have contributed greatly to all of my projects. I am grateful to all past and present members of the Embley/Hirt lab: Dr Peter Major, Dr Shaojun Long, Dr Paul Dean, Mr Andrew Watson, Mrs Maxine Geggie, Mrs Svetlana Cherlin, Mr William Lewis, Dr Cedric Bicep, Dr Didier Ndeh, Dr Sarah Heaps for all their contributions.

I would particularly like to thank, Dr Tom Williams, who introduced me to phylogenetic analyses and set an example of an outstanding researcher and colleague.

I would like to acknowledge the members of the Institute for Cell and Molecular Biosciences, Newcastle University, for their support and technical advice. Dr Alex Laude and Dr Trevor Booth from Bio-Imaging Unit for initial microscopy and image analyses training as well helpful discussions and advice. My assessors Professor Zofia Chrzanowska-Lightowlers and Professor Jeremy Lakey for insightful discussions. The staff of ICAMB office for their kindness and practical support throughout my PhD.

This PhD project was generously funded by the European Union as a part of a Marie Curie Initial Training Network Symbiomics.

Table of contents

List of Figures

List of Tables

List of Abbreviations

AAC	ADP/ATP carrier
ADP	Adenosine diphosphate
AIDS	Acquired immune deficiency syndrome
AOX	Alternative oxidase
ARP	Alternative respiratory pathway
ATM1	Mitochondrial type ABC transporter
ATP	Adenosine triphosphate
BCA	Bicinchoninic acid
BSA	Bovine serum albumin
cdETC	Cytochrome-dependent electron transport chain
cytG3PDH	Cytoplasmic glycerol-3-phosphate dehydrogenase
DAPI	6-Diamidino-2-phenylindole dihydrochloride
ddH_2O	double destilled water
DHAP	Dihydroxyacetone-3-phosphate
DIC	Differential interference contrast
DMEM	Dulbecco's minimal essential medium
DNA	Deoxyribonucleic acid
Drp1, Dnm1p	Dynamin related proteins
DTT	Dithiothreitol
EDTA	Ethylenediaminetetraacetic acid
ER	Endoplasmic reticulum
ETC	Electron-transport chain
FAD	Flavin adenine dinucleotide
FBS	Fetal bovine serum
G3P	Glycerol-3-phosphate
GapDH	Glyceraldehyde-3-phosphate dehydrogenase
GED	GTPase effector domain
GFP	Green fluorescent protein
GTP	Guanosine-5'-triphosphate
HIV	Human immunodeficiency virus
HMM	Hidden Markov models
HRP	Horseradish peroxidase
HSP	Heat shock protein
Ig	Immunoglobulin
IPTG	Isopropyl β-D-1-thiogalactopyranoside

ISC	Iron-sulfur clusters
LB	Luria-Bertani
LCMA	Last common microsporidian ancestor
LCSM	Laser scanning confocal microscopy
LECA	Last eukaryotic common ancestor
LGT	Lateral gene transfer
LRR	Leucine rich repeat
MCF	Mitochondrial carrier family
MCL	Markov clustering
MD	Middle domain
MPP	Mitochondrial processing peptidase
MSA	Multiple sequence alignment
mtG3PDH	Mitochondrial glycerol-3-phosphate dehydrogenase
mtHsp70	Mitochondrial heat shock protein 70
MTOC	Microtubule organizing center
MTS	Mitochondrial Targeting Signal
NADP	Nicotinamide adenine dinucleotide phosphate
NCBI	National Centre for Biotechnology Information
NSP	N-terminal signal peptide
NTT	Nuleotide transporter
OCT	Optimal cutting temperature compuond
ORF	Open reading frame
PAGE	Polyacrylamide gel electrophoresis
PAM	Presequence translocase-associated motor
PBS	Phosphate Buffered Saline
PC	Phase contrast
PCR	Polymerase chain reaction
PDB	Protein Data Bank
PDH	Pyruvate dehydrogenase
PFA	Polyformaldehyde
PFO	Pyruvate:ferredoxin oxidoreductase
PGK1	Phosphoglycerate kinase
PH	Plecktrin homology
PMSF	Phenylmethylsulfonyl fluoride
PRD	Proline rich domain
Q	Ubiquinone
QH_2	Ubiquinol
RK13	Rabbit kidney cells

rMW	Relative molecular weight
RNA	Ribonucleic acid
RNAi	RNA interference
rRNA	Ribosomal RNA
RT	Room temperature
SAM	Sorting and assembly machinery
SDS	Sodium dodecyl sulfate
SPB	Spindle pole body
SHAM	Salicylohydroxamic acid
TAE	Tris- Acetate-EDTA buffer
TBS	Tris-Buffered Saline
TBST	Tris-Buffered Saline and Tween 20
TCA	Trichloroacetic acid
TIM	Translocase of the inner membrane
TMHMM	Transmembrane hidden Markov models
TOM	Translocase of the outer membrane
TPR	Tetratricopeptide repeat
WGS	Whole-genome shotgun
ZWF1	Glucose-6-phosphate dehydrogenase
v/v	Volume per volume

Chapter 1. General introduction

1.1 Microsporidia

1.1.1 Host range and relevance

Microsporidia are a group of highly successful eukaryotic intracellular parasites of economic and medical importance. There are over 1000 described species of microsporidia (Vavra & Lukeš, 2013) that can infect a broad range of eukaryotic hosts including humans (Franzen & Müller, 2001; Didier & Weiss, 2011), other mammals (Didier et al., 2000; Wasson & Peper, 2000), fish (Jiří Lom & Nilsen, 2003; Kent et al., 2014), insects (Becnel & Andreadis, 2014), crustaceans (Stentiford & Dunn, 2014), nematodes (Bakowski, Luallen, et al., 2014) and potentially apicomplexans (Sokolova et al., 2014; 2013). Microsporidian dispersive spores seem to be widely distributed in the environment (Fayer & Santin Duran, 2014; Favet et al., 2013) and microsporidian infections were identified in hosts living in a variety of terrestrial, fresh water and marine habitats (Vossbrinck & Debrunner-Vossbrinck, 2005) possibly including deep-sea methane seeps (Sapir et al., 2014). Spores of microsporidian species known to infect humans can be found in treated waste waters, recreational bathing waters, drinking water sources (Izquierdo et al., 2011) as well as fresh food produce including strawberries, raspberries and lettuce (Jedrzejewski et al., 2007; Galván et al., 2013). Microsporidia pathogenic to humans are classified as a Category B Food- and waterborne pathogens on the National Institute of Allergy and Infectious Diseases (NIAID) list of Emerging Infectious Diseases/Pathogens (US Department of Health and Human Services. National Institute of Allergy and Infectious Disease, 2015.).

The first descriptions of microsporidia date back to the mid 19th century when microsporidian infection of silkworms caused a significant damage to the European silk industry (Franzen, 2008). More recently bee infection by microsporidian species *Nosema apis* and *Nosema ceranae* have been suggested as a source of significant losses to the beekeeping industry (Fries, 2014). Microsporidian infections of economically important fish species were also associated with considerable losses to the fishing industry (Kent et al., 2014). On the other hand, infective spores of microsporidian species *Antonospora locustae* are used as a specific biological

insecticide in control of the grasshopper population (e.g. NOLO BAIT^{TM}, M&R Durango Inc.), (Bjørnson & Oi, 2014) and a similar strategy has been suggested to fight mosquitos transmitting malaria (Chapman, 1974; Bjørnson & Oi, 2014).

In the 1980s after the outbreak of the HIV pandemic, microsporidia emerged as a causative agent of opportunistic infections in patients with AIDS (Franzen &. Müller, 2001). Recently, more cases of infection in organ transplant recipients, children, the elderly, diabetics, cancer patients and immunocompetent humans have been described (Didier & Weiss, 2011). Cases of foodborne (Decraene et al., 2012) and possible waterborne (Hunter, 2000; Cotte et al., 1999) microsporidian infection outbreaks were described in Sweden (Decraene et al., 2012) and in France (Hunter, 2000; Cotte et al., 1999) respectively.

Microsporidian infections of immunocompetent and immunocompromised humans usually seem to be limited to the gastrointestinal tract and manifest as a self-limiting diarrhoea or are asymptomatic (Franzen & Müller, 2001; Didier & Weiss, 2011). In immunocompetent patients microsporidia were also found to be a cause of ocular infections that in some cases were initially misdiagnosed as a viral infection (Sharma et al., 2011). More severe forms of microsporidiosis diagnosed in immunocompromised patients include chronic diarrhoea, wasting, myositis, hepatitis and systemic infections (Franzen & Müller, 2001; Didier & Weiss, 2011). Choice of effective anti-microsporidian drugs is limited and although in most of the described cases treatment with either albendazole or fumagillin was successful the first drug is not effective against all microsporidia and the second drug has toxic side-effects (Weiss, 2014).

Microsporidia are also common pathogens of model laboratory animals such as rabbits (*Oryctolagus cuniculus*), (Gannon, 1980; Künzel & Joachim, 2009) and fish (*Danio rerio*), (Kent et al., 2012; Ramsay et al., 2009). Subclinical infections can be prevalent in laboratory conditions and regular screening is required in order to avoid using infected animals in experimental work (Künzel & Joachim, 2009; Ramsay et al., 2009).

1.1.2 Life cycle and transmission

The only stage in the microsporidian life cycle (Figure 1.1) that can survive outside the host cell is an infective, nonmotile spore (Vavra & Larsson, 2014). The microsporidian spores range in size from 1 μm to 40 μm, are mostly of ovoid shape and are surrounded by a thick two-layer wall composed of a proteinaceous exospore and chitin-containing endospore that provide the spore with a high degree of resistance against environmental insults (Vavra & Larsson, 2014; Keeling & Fast, 2002). The most distinctive morphological feature of the spore is its unique infection apparatus, the polar tube (Xu & Weiss, 2005). When faced with particular, but still poorly understood, environmental conditions the spore discharges its polar tube possibly after the sudden increase of osmotic pressure followed by influx of water and swelling (Vavra & Larsson, 2014). The extended polar tube ranges in length from 50 μm to 100 μm (potentially up to 100 times longer than the spore), and serves as a conduit to inject the spore contents (sporoplasm) into the host cell (Franzen, 2004). It was hypothesized that the polar tube can pierce through the host cell membrane in order to deliver the sporoplasm directly into the host cytosol, however it is also possible that the tip of the polar tube interacts with the host cell membrane and facilitates delivery of the sporoplasm to the host cell surface where it can enter the host cell by yet unspecified mechanism (Weiss et al., 2014). Alternatively, the polar tube can also be used by microsporidian spores that were taken up by the host via phagocytosis in order to escape from the phagosome (Franzen, 2004).

After the infection process the parasite goes through two consecutive obligate intracellular life cycle stages: proliferative merogony and spore forming sporogony. The intracellular proliferative forms may develop in direct contact with the host cytoplasm or nucleoplasm, or inside parasite or host-derived vesicles (parasitophorous vesicle), (Cali & Takvorian, 1999).

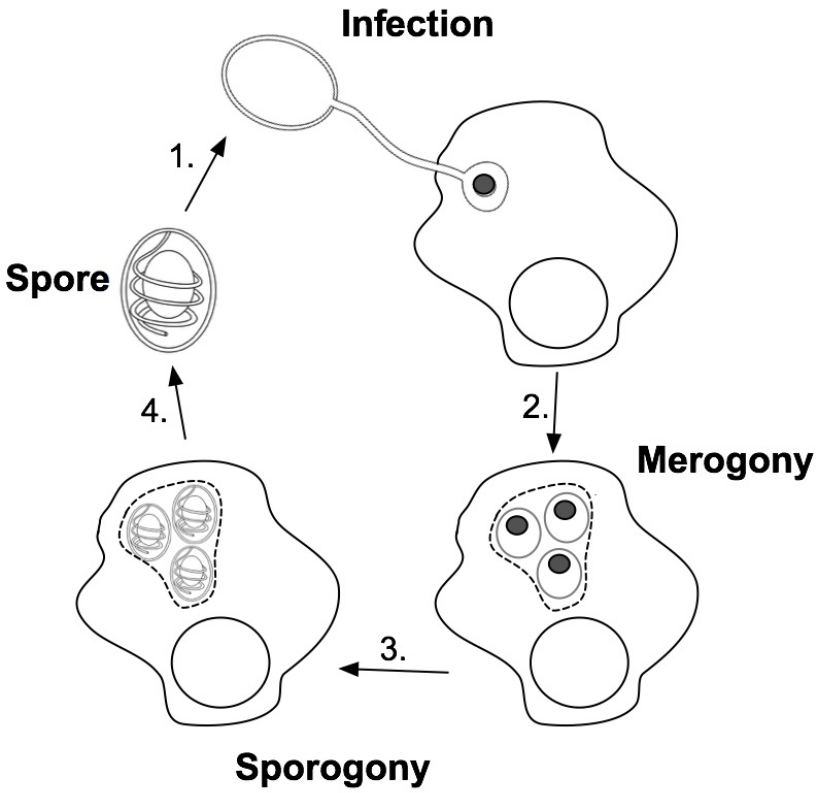

Figure 1.1 Diagram of a microsporidian life cycle
During the infection process (1.) the extracellular spore discharges its polar tube and uses it as a conduit for the delivery of the spore contents (sporoplasm) into the host cell. While inside the host cell the intracellular forms of the parasite divide (2.) and finally differentiate into spores (3.) that can be released into the environment (4.). Many of the microsporidian species develop inside parasite or host-derived vesicle called a parasitophorous vesicle (dashed line). The details of proliferative stage (merogony) and spore differentiation stage (sporogony) as well as the definition of transition between the two stages can vary greatly between different microsporidians (see section 1.1.6).

While inside the host microsporidia seem to be able to acquire metabolites required for proliferation and spore formation from their hosts using a range of membrane transport proteins (see *section 1.1.4 Metabolism of microsporidia*). Microsporidia also seem to be able to manipulate the host cells causing such various effects as formation of xenomas (Lom & Dyková, 2005), (hypertrophic cells filled with the microsporidian spores), rearrangement of the host actin cytoskeleton (Estes et al., 2011), and accumulation of the host mitochondria around the parasitophorous vesicle (Scanlon et al., 2004; Hacker et al., 2013). The intracellular stage of microsporidian development ends with formation of new spores that can be released into the environment and infect the other cells of the same host (autoinfective spores) or other hosts (environmental spores). Release of the microsporidian spores into the environment can follow a lysis of the host cell, although spore of microsporidian *Nematocida parisii* exit the infected intestinal epithelium cells of a nematode

Caenorhabditis elegans without causing cell lysis (Estes et al., 2011). This non-lytic exit mechanism seems to be facilitated by the rearrangement of the host actin cytoskeleton caused by the parasite (Estes et al., 2011).

Uptake of the environmental spores by the host (horizontal transmission) seems to be the only mode of transmission for some microsporidian species including a parasite of honey bees *Nosema apis* (Dunn & Smith, 2001). Other microsporidians such as *Nosema granulosis* seem to be transmitted only vertically, from the female host to its progeny (Dunn & Smith, 2001). Both modes of transmission have been observed in a complex life cycle of microsporidia from genus *Amblyospora* that include at least two different hosts (mosquitos and an intermediate crustacean host), three different developmental cycles and three distinct spore morphotypes (Andreadis, 1985; Lucarotti & Andreadis, 1995; Becnel & Andreadis, 2014).

1.1.3 Phylogeny of microsporidia

All characterized microsporidia share a set of common features that altogether make them a distinct group of eukaryotes including, an intracellular parasitic lifestyle with seemingly unique adaptations such as a polar tube (infection apparatus) (Franzen, 2004; Xu & Weiss, 2005) and a proteinaceous external layer of a spore wall (exospore), (Vavra & Larsson, 2014), overall reduction of genomes with an extreme reduction of their metabolic capacity (Bakowski, et al., 2014; Katinka et al., 2001; Williams, Lee, et al., 2008; Chen et al., 2013; Heinz et al., 2012; Campbell et al., 2013; Corradi et al., 2010; 2009; Pombert et al., 2012; Pan et al., 2013; Keeling et al., 2010; Akiyoshi et al., 2009), presence of remnant mitochondria that do not seem to have genomes (Williams et al., 2002) and apparently are unable to generate ATP via oxidative phosphorylation (Katinka et al., 2001), presence of a bacteria-like plasma membrane-located nucleotide transport proteins (NTTs), (Heinz et al., 2014; Tsaousis et al., 2008) and fusion of 5.8 S and 23 S ribosomal subunits (Vossbrinck et al., 1987; Franzen, 2008; Vavra & Lukeš, 2013). Some of these features were initially used to classify microsporidia into Archezoa, a phylum then believed to comprise descendants of the primitive Eukaryotes that have diverged before acquisition of mitochondria (Cavalier-Smith, 1989; Corradi & Keeling, 2009). Discovery of apparent reduced forms of mitochondria in all members of Archezoa together with increasing number of available genome sequencing data have prompted a reclassification of

former ‘Archezoans’ including microsporidia into other eukaryotic taxa (Embley & Martin, 2006). The available evidence from molecular phylogenetic analyses supports a placement of microsporidia either as a highly derived Fungi or a sister group of Fungi (Williams & Keeling, 2011; Adl et al., 2012; Capella-Gutiérrez et al., 2012; Heinz et al., 2012). The relationship with Fungi seems to be further supported by a set of unique characteristics shared between Fungi and microsporidia including, detection of chitin and trehalose in the spore stages, apparent nuclear division via a closed mitosis and presence of an organelle resembling fungal spindle pole body in diverse microsporidian lineages (Vavra & Lukeš, 2013).

Additional evidence for the close relationship between fungi and microsporidia has been provided by genome sequencing projects of two endoparasites closely related to microsporidia, namely *Rozella allomycis* (James et al., 2013) and *Mitosporidium daphnia* (Haag et al., 2014). In the published phylogenies *R. allomycis* and *M. daphniae* together with microsporidia form a sister group of Fungi (Figure 1.2) while *M. daphniae* forms a monophyletic group with microsporidia *sensu stricto* and based on this grouping was classified as a basal microsporidian (Haag et al., 2014), (However, in this thesis the term microsporidia refers to microsporidia *sensu stricto,* and does not include *Mitosporidium daphniae*). Both *R. allomycis* and *M. daphniae* are obligate intracellular parasites of respectively water moulds (*Allomyces*) and crustaceans (*Daphnia*) and have seemingly less reduced protein coding - and metabolic - capacities than that of microsporidia (James et al., 2013; Haag et al., 2014).

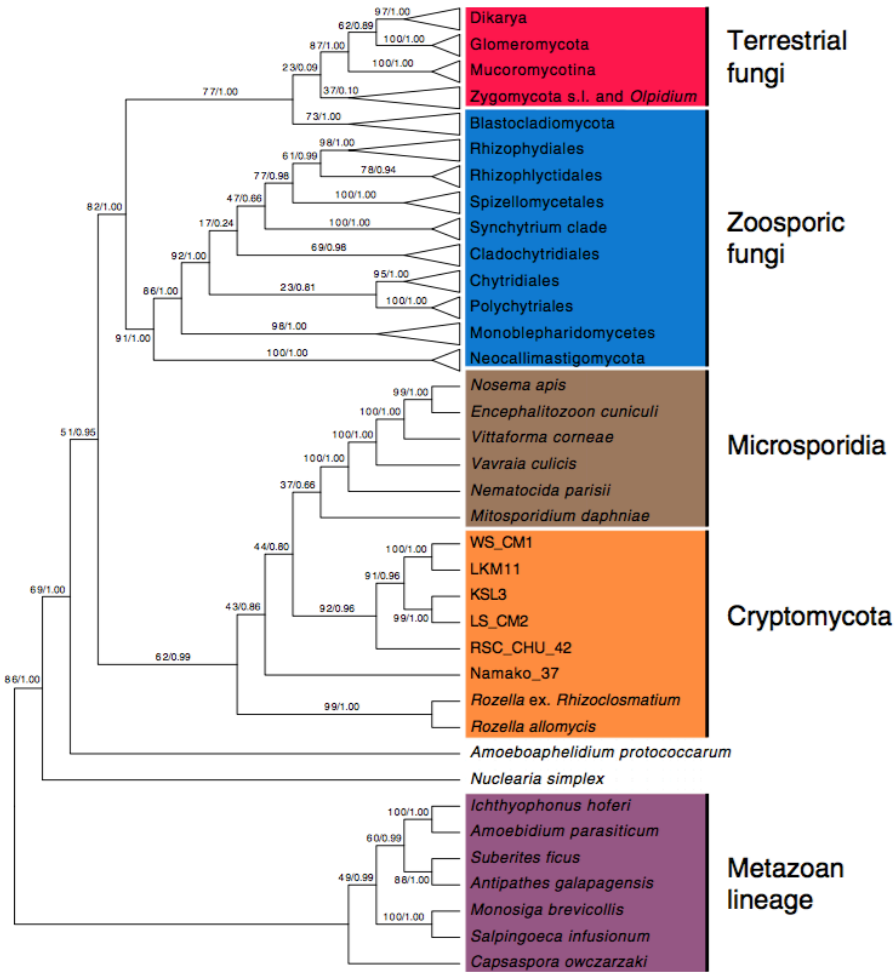

Figure 1.2 Microsporidia together with *M. daphniae* and Cryptomycota form a sister group of Fungi

Figure reproduced from Haag *et al.*, 2014. The tree was generated using RAxML and MrBayes under GTR+I+G model based on concatenated alignment of 18 S, 28 S, and 5.8 S rRNA genes. Bootstrap percentage/Bayesian posterior probabilities values are indicated.

R. allomycis seems to form two distinct types of spores, a flagellated motile zoospores and a non-motile 'resting' spores without any evidence for a polar tube-like infectious apparatus (James et al., 2013). *M. daphniae* appears to have only one form of a non-motile spores with a microsporidian-like double-layered spore wall and what seems to be an infection apparatus resembling microsporidian polar tube (Haag et al., 2014). Both *R. allomycis* and *M. daphniae* seem to have mitochondria with an organelle genome, and genes coding for enzymes of the Krebs cycle and some components of the electron transport chain (James et al., 2013; Haag et al., 2014). *R. allomycis* has bacteria-like NTT nucleotide transporters that seem to be related to the microsporidian NTTs and has lost the metabolic pathways for *de novo* biosynthesis of nucleotides indicating that these traits were already present in the last

common ancestor of the microsporidia and *R. allomycis* (James et al., 2013; Heinz et al., 2014). *M. daphniae* seemingly also does not have any pathways for *de novo* biosynthesis of nucleotides, however, it does not seem to have NTT transporters potentially due to a lineage specific gene loss and likely has an alternative membrane transports for importing nucleotides from the host (Haag et al., 2014). Thus it seems that *R. allomycis* and *M. daphniae* are nucleotide auxotrophs like the microsporidia however they appear to have a capacity to generate ATP via oxidative phosphorylation in their mitochondria. Neither *R. allomycis* nor *M. daphniae* seem to have the microsporidian-specific fusion of the 5.8 S and 23 S ribosomal subunits (Haag et al., 2014; Vossbrinck et al., 1987; Vavra & Lukeš, 2013).

Studies of the apparently less reduced relatives of microsporidia provide evidence that the lack of capacity for *de novo* biosynthesis of nucleotides and presence of bacteria-like nucleotide transporters apparently required to steal nucleotides from the host (NTTs) are likely to have been present in the last common ancestor of *R. allomycis*, *M. daphniae* and microsporidia indicating these feature as possibly important adaptations to their intracellular parasitic lifestyle (James et al., 2013; Haag et al., 2014; Heinz et al., 2014) however the loss of the mitochondrial genome and capacity to generate ATP via oxidative phosphorylation in mitochondria seem to be specific to the microsporidia (Haag et al., 2014).

1.1.4 Metabolism of microsporidia

Metabolism of microsporidia seems to have been extremely reduced during adaptation to their intracellular parasitic lifestyle (Nakjang et al., 2013; Katinka et al., 2001). Complete metabolic pathways for *de novo* biosynthesis of nucleotides and amino acids as well as pathways involved in energy metabolism including the tricarboxylic acid cycle, beta-oxidation of fatty acids and the electron transport chain are apparently absent from all of the studied microsporidians (Bakowski, et al., 2014; Katinka et al., 2001; Williams, Lee, et al., 2008; Chen et al., 2013; Heinz et al., 2012; Campbell et al., 2013; Corradi et al., 2010; 2009; Pombert et al., 2012; Pan et al., 2013; Keeling et al., 2010; Akiyoshi et al., 2009).

The lack of the *de novo* biosynthetic pathways of amino acids and nucleotides implies that microsporidia cannot rely on their own metabolism to provide building blocks for synthesis of proteins and nucleic acids (DNA and RNA), (Nakjang et al., 2013; Katinka et al., 2001). In order to fill in the gaps in their reduced metabolism

microsporidia seem to be able to import the required metabolites from their hosts using a repertoire of membrane transport protein families (Katinka et al., 2001; Heinz et al., 2012; Nakjang et al., 2013), (Figure 1.3). Most notably, NTTs from two distantly related microsporidians infecting humans namely *Trachipleistophora hominis* and *Encephalitozoon cuniculi* were shown to localize to the cell membrane of the intracellular stages of these parasites and to transport radio labeled purine nucleotides across the *E. coli* cell membrane in heterologous expression experiments (Tsaousis et al., 2008; Heinz et al., 2014). Therefore, it seems that intracellular stages of *T. hominis* and *E. cuniculi* are able to use NTTs to steal purine nucleotides from their hosts in order to compensate for the apparent loss of nucleotide biosynthesis pathways in these microsporidia (Tsaousis et al., 2008; Heinz et al., 2014).

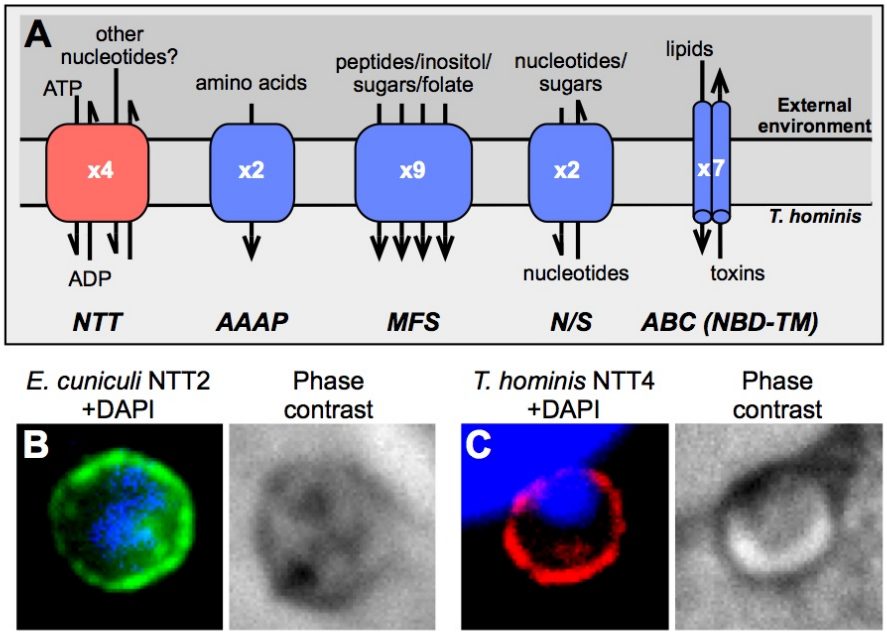

Figure 1.3 Microsporidian cell membrane transporters
A. A schematic representation of a selection of characterized (red) or predicted (blue) cell membrane transporters of *T. hominis* (based on the analyses by Heinz *et al.*, 2012). The name of the protein family to which the transporters were classified; the number of the family members identified in the *T. hominis* genome; as well as predicted substrates are indicated. **B.** and **C.** Immunofluorescence localization of the purine nucleotide transporters (NTT) to the cell membrane of the intracellular stages of *E. cuniculi* (A) and *T. hominis* (B) using previously characterized (Tsaousis et al., 2008; Heinz et al., 2014) specific antibodies.

NTT-type transport proteins are also used by bacterial obligate intracellular parasites including a pathogen of humans *Chlamydia trachomatis* in order to provide nucleotides for their own reduced metabolism (Tjaden et al., 1999; Haferkamp et al., 2006; Trentmann et al., 2007; Audia & Winkler, 2006). Different NTT homologues

from *C. trachomatis* seem to use different transport mechanisms including import of ATP in counter exchange with ADP (Class I) providing the bacteria with energy, and unidirectional proton-driven nucleotide import (Class II) providing a net gain of different nucleotides required for DNA and RNA biosynthesis (Tjaden et al., 1999; Haferkamp et al., 2006). Similar to *C. trachomatis* microsporidian genomes encode multiple NTT homologues that could potentially include transporters using Class I or Class II import mechanism providing microsporidia with not only essential building blocks for biosynthesis of their DNA and RNA but also energy required for the parasite metabolism and protein synthesis (Heinz et al., 2014). In addition to the relatively well characterized microsporidian NTTs a range of transport protein candidate families including predicted amino acid transporters have been identified in bioinformatic analyses of microsporidian genomes (Katinka et al., 2001; Heinz et al., 2012; Nakjang et al., 2013). Many of these uncharacterized transport protein-candidates have a predicted cell membrane localization and some of them have undergone microsporidia-specific protein family expansion as it is in the case of microsporidian NTT family (Nakjang et al., 2013; Heinz et al., 2014). It was hypothesized that some of these predicted transport proteins could also play a role in acquiring essential metabolites such as amino acids from the host in order to compensate for the extreme reduction of microsporidian metabolism (Nakjang et al., 2013; Heinz et al., 2012). Dependence on the host for production of essential nutrients seems to be most evident in *Enterocytozoon bieneusi* that can infect humans and has probably almost completely lost its core carbon metabolism (Keeling & Corradi, 2011). While most of the functional gene categories that are present in other microspordia seem to be well represented, genes encoding only one glycolytic enzyme (glyceraldehyde-3-phosphate dehydrogenase), one enzyme of pentose phosphate pathway (glucose-6-phosphate dehydrogenase) and no enzymes involved in trehalose metabolism have been identified in two genome surveys of *E. bieneusi* (Akiyoshi et al., 2009; Keeling et al., 2010). The possible loss of all known pathways capable of generating ATP in *E. bieneusi* would suggest not only a complete reliance of its proliferative intracellular stages on the ATP stolen from the host (Akiyoshi et al., 2009; Keeling et al., 2010) but also inability of its spores to generate energy (Williams et al., 2014). It was suggested that the loss of the core carbon metabolism in *E. bieneusi* could be due to a loss of specific physiological functions that require these pathways such as an ability to infect using microsporidian specific infection apparatus (polar tube), (Williams et al., 2014). This extreme

dependence on its host may partially explain difficulty in establishing a continuous *in vitro* culture of *E. bieneusi* in mammalian host cell lines as opposed to other human pathogenic microsporidia; such as *E. cuniculi* and *T. hominis* (Keeling et al., 2010; Visvesvara, 2002).

Apart from *E. bieneusi* all of the studied microsporidian species seem to have retained a set of conserved metabolic pathways including a biosynthesis of chitin, and a core carbon metabolism consisting of: glycolysis, trehalose metabolism, and pentose phosphate pathway (Nakjang et al., 2013; Keeling et al., 2010), (Figure 1.4). With an exception of pentose phosphate pathway, hypothesized to play a role in generating reduced potential in form of NADPH for biosynthesis (Heinz et al., 2012), these conserved metabolic pathways have been mostly linked to a formation, survival and/or germination of the microsporidian resistant spores (Heinz et al., 2012), (Figure 1.4).

Chitin is a major component of the inner layer (endospore) of microsporidian spore wall, while trehalose seems to be the only reserve carbohydrate found in spores of different microsporidian species and may potentially serve as an osmoregulator, energy source and/or anti-desiccation agent (Vavra & Lukeš, 2013). Glycolysis seems to be the only pathway capable of generating ATP retained by most microsporidia as genes encoding enzymes from all other pathways known to be involved in generation of this essential cellular energy currency are missing from available microsporidian genome assemblies (Bakowski, et al., 2014; Katinka et al., 2001; Williams, Lee, et al., 2008; Chen et al., 2013; Heinz et al., 2012; Campbell et al., 2013; Corradi et al., 2010; 2009; Pombert et al., 2012; Pan et al., 2013; Keeling et al., 2010; Akiyoshi et al., 2009).

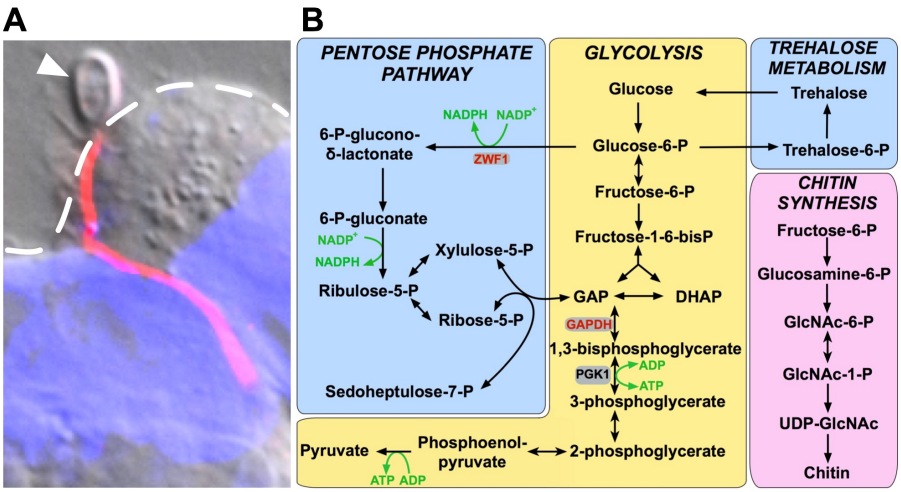

Figure 1.4 Microsporidian spore and a model of metabolic pathways conserved in microsporidia

A. A microscopy image of a *T. hominis* spore (arrowhead) with an extended polar tube labeled with a non-specific rabbit polyclonal serum (red) possibly during the process of infecting the rabbit kidney (RK13) host cell (dashed line). Nuclei of the host were stained with DAPI (blue).

B. A simplified model of conserved microsporidian pathways including a biosynthesis of chitin, and a core carbon metabolism consisting of: glycolysis, trehalose metabolism, and pentose phosphate pathway. The model was based on the published data (Keeling et al., 2010; Nakjang et al., 2013). Names of three enzymes were indicated: phosphoglycerate kinase (PGK1), glyceraldehyde-3-phosphate dehydrogenase (GAPDH), and glucose-6-phosphate dehydrogenase (ZWF1). PGK1 (indicated in black) seems to be enriched in spores rather than intracellular stages of *T. hominis* (Heinz et al., 2012). GAPDH and ZWF1 (indicated in red) are the only of the core carbon metabolism enzymes that were identified in the genome surveys of *E. bieneusi* (Akiyoshi et al., 2009; Keeling et al., 2010). Some of the major products of the metabolic pathways (ATP and NADPH) are indicated in green.

Quantitative immunoelectron microscopy and proteomics investigations indicated enrichment of glycolytic enzymes in spores rather than in proliferative intracellular stages of human-pathogenic *T. hominis* (Heinz et al., 2012), and seem to be consistent with the results of western blotting experiments that detect enzymes involved in energy metabolism (alternative oxidase, glycerol-3-phosphate dehydrogenase, and pyruvate dehydrogenase E1α and E1β) in protein extracts from spores but not in purified intracellular stages of a microsporidian infecting insects *Antonospora locustae* (Dolgikh et al., 2009; 2011; Williams et al., 2014). Microsporidian dispersive spore as opposed to the intracellular stages of these parasites cannot rely on its host for generation of ATP and may use glycolysis in order to generate energy that is possibly required for its survival and/or germination process (Heinz et al., 2012; Williams et al., 2014).

The enzyme catalyzing the first committed step of the glycolysis (phosphorylation of glucose to glucose-6-phosphate), namely the hexokinase from various microsporidian species (*Nematocida parisii, Nosema ceranae, Encephalitozoon cuniculi* and *Antonospora locustae*) was shown to posses a predicted secretion signal that can be recognised by *S. cerevisiae* secretion machinery and lead to secretion of an invertase fusion protein outside of the yeast cells in yeast secretion trap experiments (Cuomo et al., 2012). Based on that it was hypothesized that microsporidian hexokinases can be secreted into the host cell where they could upregulate the host metabolism (Cuomo et al., 2012). Bioinformatics analyses of microsporidian protein families (see *section 1.1.5 Microspordian genomes*) identified hexokinases as one of the protein families that have undergone a lineage-specific protein family expansion that may represent an adaptation to the intracellular parasitic lifestyle (Nakjang et al., 2013).

1.1.5 Microspordian genomes

Microsporidia are not only emerging pathogens of humans (Franzen & Müller, 2001; Didier & Weiss, 2011) and parasites of economically important insects (Becnel & Andreadis, 2014) and fish (Lom & Nilsen, 2003; Kent et al., 2014) but also an important model for studying a reductive evolution of eukaryotic genomes (Katinka et al., 2001; Heinz et al., 2012) and adaptations to the intracellular parasitic lifestyle (Tsaousis et al., 2008; Heinz et al., 2014; Szumowski & Troemel, 2015; Vavra & Lukeš, 2013). Comparative studies of relatively large number of available microsporidian genome sequences reveal conserved patterns of genome reduction as well as an apparent diversity across these genomes with a lineage specific protein family gain and expansion (Heinz et al., 2012; Nakjang et al., 2013; Desjardins et al., 2015).

Currently the smallest characterized microsporidian genome from the mammalian parasite *Encephalitozoon intestinalis* is estimated to have a size of approximately 2.3 Mbp (11 chromosomes) and is one of the smallest known eukaryotic nuclear genomes (Corradi et al., 2010). The small size of the *E. intestinalis* genome has been attributed to a small number of often truncated genes (predicted 1944 open reading frames of a mean length of 999 bp), (Pombert et al., 2015), short intragenic spaces (on average 100 bp), (Pombert et al., 2015), a small number of introns and repetitive elements, and an absence of any known mobile

genetic element (Corradi et al., 2010). Available sequences of other *Encephalitozoon* genomes: *E. cuniculi* (Katinka et al., 2001), *E. romaleae* (Pombert et al., 2012) and *E. hellem* (Pombert et al., 2012) are similar to that of *E. intestinalis* both in composition and in size but these seem to be the most reduced outliers rather than a representative example of the microsporidian genome architecture (Heinz et al., 2012; Nakjang et al., 2013; Desjardins et al., 2015). Available genome assemblies from a range of microsporidian lineages include, intermediate-sized genomes of a fish parasite *Spraguea lophii* (estimated genome size of 6.2-7.3 Mbp), (Campbell et al., 2013) and *Trachipleistophora hominis* isolated from an HIV/AIDS patient (estimated at 8.5-11.6 Mbp), (Heinz et al., 2012) as well as relatively large genomes of *Daphnia magna* parasite *Hamiltosporidium tvaerminnensis* (estimated at 24 Mbp), (Corradi et al., 2009) and mosquito parasite *Anncaliia algerae* also known to be able to infect immunocompromised humans (estimated at 23 Mbp), (Peyretaillade et al., 2012).

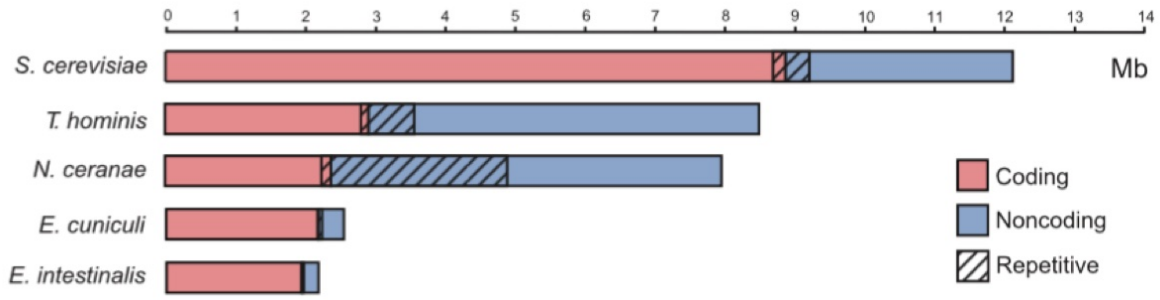

Figure 1.5 Size of microsporidian genomes and proportion of coding and noncoding genomic DNA sequences

Figure reproduced from Heinz et al., 2012. Length of a bar corresponds to a size of the genomes of four microsporidians (*Encephalitozoon intestinalis, E. cuniculi, Trachipleistophora hominis* and *Nosema ceranae*) and *Saccharomyces cerevisiae* in mega bases (Mb). Proportion of coding sequences (red) and noncoding sequences (blue) was overlaid on the bars.

Despite the differences in size all available microsporidian genomes share a set of conserved features including an apparent absence of entire metabolic pathways such as the tricarboxylic acid cycle, beta-oxidation of fatty acids, the electron transport chain, and *de novo* biosynthesis of purine and pyrimidine nucleotides (Bakowski, et al., 2014; Katinka et al., 2001; Williams, et al., 2008; Chen et al., 2013; Heinz et al., 2012; Campbell et al., 2013; Corradi et al., 2010; 2009;

Pombert et al., 2012; Pan et al., 2013; Keeling et al., 2010; Akiyoshi et al., 2009). The protein coding capacity of the sequenced microsporidian genomes seems to vary approximately twofold within a range of estimated 1,801 – 4,474 protein coding sequences (Pombert et al., 2015). Based on the comparative genome analysis representatives of diverse microsporidian lineages seem to share a conserved core of protein families (predicted 802 protein families in analysis by Nakjang et al. (2013), that was likely present in the last common microsporidian ancestor (LCMA), (Peyretaillade et al., 2012; Nakjang et al., 2013; Desjardins et al., 2015; Campbell et al., 2013; Cuomo et al., 2012). Protein families that have homologues in other Opisthokonta (group of Eukaryotes containing animals and Fungi), include housekeeping genes and seem to account for majority of the conserved microsporidian core protein families (767/802), (Nakjang et al., 2013). Microsporidian-specific protein families, that do not have any detectable homologues outside of microsporidia, including structural proteins of microsporidian dispersive spore and infection apparatus (polar tube), seem to make up a smaller part of the conserved core (32/802), (Nakjang et al., 2013). Three microsporidian core protein families, namely small conductance mechanosensitive ion channels (MscS), (Nakjang et al., 2013), cysteine-rich secretory protein (CAP) domain-containing proteins (Nakjang et al., 2013) and bacteria-like membrane transporters from the ATP/ADP translocases family (NTTs), (Tsaousis et al., 2008), appear to have been acquired via lateral gene transfer (LGT). Microsporidia seemingly use NTTs to import host generated purine nucleotides, as they do not appear to have any known complete pathways for *de novo* biosynthesis of these nucleotides (Tsaousis et al., 2008; Heinz et al., 2014). Although functions of the remaining conserved microsporidian LGT candidates and a majority of the microsporidian specific core protein families are unknown their retention in all of the analyzed microsporidian genomes suggests potentially important functions of these proteins in microsporidian parasitic lifestyle as it seems to be in the case of NTTs (Nakjang et al., 2013).

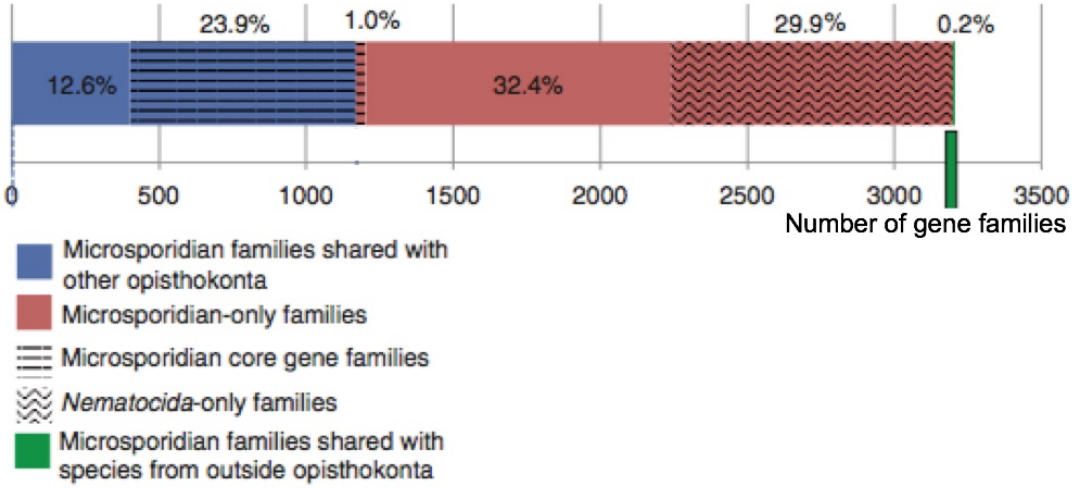

Figure 1.6 The proportion of microsporidian protein families that are microsporidian-specific or have homologs in taxa outside the microsporidia

Figure adapted from Nakjang et al., 2013. Microsporidian protein families that are shared with other opisthokonta (blue), are microsporidia specific (red), or have homologues in taxa outside opisthokonta (green) were indicated on the bar that represents 3,204 protein families each containing at least one sequence from the microsporidian genomes sampled in the analyses by Nakjang et al., 2013. Protein families were constructed using Markov Clustering (MCL) with sequences from 11 microsporidian, 7 fungal, and 3 animal genomes (Nakjang et al., 2013). Microsporidian core gene families (identified in at least 9 out of 11 analyzed genomes), and protein families identified only in *Nematocida spp.* were also indicated. Large number of the *Nematocida spp.*-specific protein families seems to reflect *Nematocida ssp.* being a phylogenetic outgroup to the rest of the analyzed microsporidia (Nakjang et al., 2013).

While microsporidian-specific protein families account for only a small fraction of the conserved microsporidian core a high number of these protein families (approximately 2000 in analysis by Nakjang *et al.*), seems to be present only in specific microsporidian lineages (Nakjang et al., 2013; Desjardins et al., 2015). These apparent lineage-specific microsporidian protein families are likely to be not only protein families that were present in the LCMA and later lost in some lineages, but also possible protein family acquisitions within the specific lineages (Nakjang et al., 2013; Heinz et al., 2012). The microsporidian-specific protein families seem to be significantly enriched for proteins predicted to be targeted to a secretory pathway, thus likely to be secreted into the host cytosol or to localize on the parasite's surface (Nakjang et al., 2013). Secreted proteins and proteins exposed on the surface of the microsporidian cell could potentially serve as effectors in the interactions of the parasite with its hosts (Nakjang et al., 2013; Cuomo et al., 2012). The apparent acquisition of the new protein families seems to be complemented by a lineage-specific protein family expansion (Nakjang et al., 2013; Heinz et al., 2012). The

expanded protein families include NTTs and many predicted membrane transport proteins that are likely to localize on the parasite's cell membrane where they could function to steal metabolites from the host in order to fill in the gaps in reduced microsporidian metabolism (Nakjang et al., 2013; Heinz et al., 2012).

The twofold variation in the protein coding capacity of the available microsporidian genomes does not seem to fully explain the tenfold variation in estimated sizes of these genomes indicating a possibly significant differences in a length of the intragenic regions (Heinz et al., 2012; Peyretaillade et al., 2012). Consistent with that gene densities of the available microsporidian genome assemblies range from estimated 0.09 Gene/kbp in *A. algerae* (Peyretaillade et al., 2012) and estimated 0.21 Gene/kbp in *H. tvaerminnensis* (Corradi et al., 2009) up to approximately 0.85 Gene/kbp in *Encephalitozoon* species (Pombert et al., 2015). Potential partial genome duplications (Pan et al., 2013) and presence of mobile genetic elements (Parisot et al., 2014) were also identified as mechanisms playing a possibly significant role in evolution of microsporidian genomes.

Recently published direct comparison between genomes and transcriptomes of two distantly related microsporidia infecting mosquitoes, namely *Edhazardia aedis* (51.3Mbp genome assembly) and *Vavraia culicis* (6.1Mbp genome assembly) seems to be consistent with the trends observed across other microsporidian genomes including an estimated 8-fold variation in genomes size, an approximately 1.5-fold variation in gene coding capacity and a significant differences in gene density (9% and 47% coding regions in *E. aedis* and *V. culicis* respectively), (Desjardins et al., 2015). Both genomes encode genes from the conserved microsporidian core and major differences between their coding capacities appear to be in the numbers of seemingly species-specific genes (Desjardins et al., 2015). *E. aedis* with an expanded repertoire of species-specific genes encoded in its relatively large genome apparently infects only one species of mosquitos (*Aedes aegypti*), has a relatively complex life cycle with both lateral and horizontal transmission modes as well as possible sexual cycle whereas *V. culicis* with the smaller genome and a smaller number of the species-specific genes can be found infecting different species of mosquitoes and seems to have less complex life cycle without any evidence for vertical transmission or sexual cycle (Desjardins et al., 2015).

Overall, an extremely reduced set of encoded metabolic pathways and in some cases a highly reduced general architecture of diverse microsporidian genomes are contrasted by a protein family expansion and a lineage-specific protein

family gain (Nakjang et al., 2013). The protein family gains and expansions may represent important adaptations to the intracellular parasitic lifestyle (Nakjang et al., 2013) and in case of *E. aedis* and *V. culicis* seem to correlate with different adaptations to the same group of hosts (Desjardins et al., 2015).

1.1.6. Encephalitozoon cuniculi and Trachipleistophora hominis - model microsporidian species infecting humans used in this study

Two microsporidians used in this study, namely *Trachipleistophora hominis* and *Encephalitozoon cuniculi* are distantly related pathogens of humans (Hollister et al., 1996; Curry et al., 2005; Deplazes et al., 1996), that have a well-established protocols for cultivation in mammalian cell lines (Visvesvara, 2002).

Possibly the first description of *Encephalitozoon cuniculi* comes from the studies of infected rabbits where acute inflammation of the rabbits brains (Encephalitis) was associated with presence of the parasite in brain tissue samples, hence the name of the genus, *Encephalitozoon* (Künzel & Joachim, 2009). In later studies *E. cuniculi* infections where described in various mammals including dogs, pigs and cows (Didier et al., 2000). In immunocompromised humans such us AIDS patients and organ transplant recipients both localized and systemic *E. cuniculi* infections were diagnosed (Weiss, 2014).

Trachipleistophora hominis was initially isolated from the skeletal muscle biopsy of an infected AIDS patient (Hollister et al., 1996). Isolated spores (Figure 1.7 A) were later used for establishment of infection in mammalian cell lines (COS-1 and RK13) and experimental infection of athymic mice (Hollister et al., 1996). *T. hominis* infections were only diagnosed in a few AIDS patients although spores of *T. hominis* isolated from infected patients were capable of infecting mosquito larvae and the spores that were subsequently isolated from adult mosquitoes and injected into mice caused a muscle infection at the side of inoculation (Weidner et al., 1999). *T. hominis* is closely related to the mosquito parasite *Vavraia culicis* and piggyBac elements possible acquired via lateral gene transfer from an insect were found in its genome indicating the possibility that the infections in humans are of zoonotic origin (Heinz et al., 2012; Weidner et al., 1999).

Inside the mammalian host cells the multinucleate *T. hominis* meronts seem to develop in a direct contact with the host cytoplasm and the parasitophorous vesicle surrounding the parasite cells becomes apparent only at the onset of sporogony (Figure 1.7 B), (Hollister et al., 1996). As opposed to *T. hominis* all intracellular stages of *E. cuniculi* seem to be single nucleate and appear to develop within a parasitophorous vesicle of a possible host origin (Figure 1.7 C), (Cali & Takvorian, 1999). Mitochondria of the mammalian host infected with *E. cuniculi* accumulate around a parasitophorous vesicle membrane and are observed in close proximity of the vesicle's membrane in electron micrographs (Scanlon et al., 2004; Hacker et al., 2013).

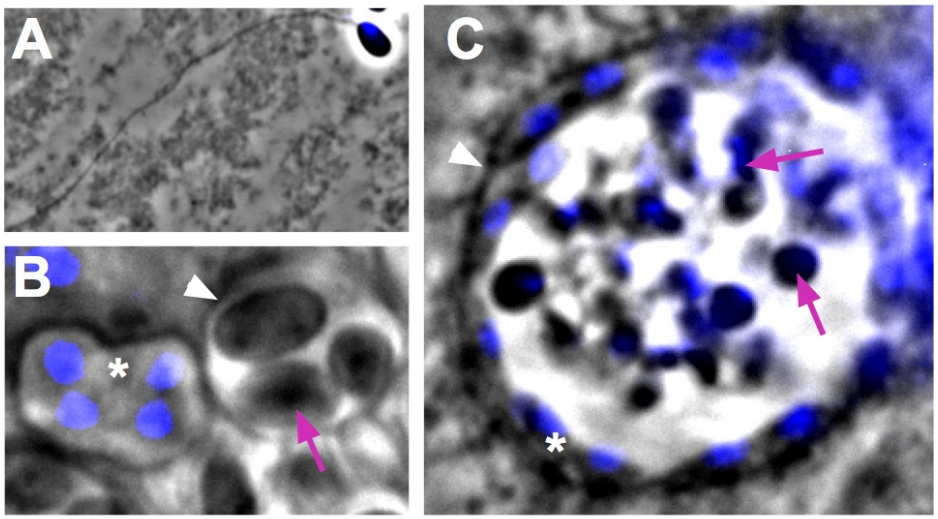

Figure 1.7 *T. hominis* and *E. cuniculi* cells inside infected rabbit kidney cells (RK13 cell line)

A. Single extracellular *T. hominis* spore with an extended polar tube. The spore seems to have been fixed at the moment of the polar tube discharge, as the DAPI stained nucleus appears to be inside the spore. B. A multinucleate (4 nuclei) *T. hominis* meront (star) seems to be in a direct contact with surrounding host cytosol. The spore-forming stages (arrow) are enclosed within a parasitophorous vesicle (arrowhead). C. Both meronts (star) and spore-forming stages (arrows) of *E. cuniculi* can be observed inside the parasitophorous vesicle (arrowhead). Meronts appear to localize to the periphery of the vesicle while spore-forming stages seem to localize mainly to the center of the vesicle.
All images where acquired with 100x phase contrast lens; (A) was fixed in 4% paraformaldehyde in PBS; (B) and (C) were fixed in ice cold methanol : acetone (1:1).

T. hominis and *E. cuniculi* are not only emerging pathogens of humans but also models for studying reductive evolution on both a genomic and cellular level. The genome of *E. cuniculi* has an extremely reduced coding capacity and is one of the smallest known eukaryotic genomes (Katinka et al., 2001) while genome of *T.*

hominis is less reduced and forms a phylogenetic outgroup to the *Encephalitozoons* making comparative studies of both species particularly relevant for studying general features of microsporidian genome evolution (Heinz et al., 2012). In contrast to *E. cuniculi,* homologues of components of RNA interference (RNAi) machinery were identified in the genome of *T. hominis* and could potentially be used to develop the first genetic manipulation methods in microsporidia (Heinz et al., 2012). Williams *et al.* (Williams et al., 2002), Tsaousis *et al.* (Tsaousis et al., 2008) and Goldberg *et al.* (Goldberg et al., 2008) have developed protocols for protein immunolocalization on fluorescence- and electron-microscopy levels using specific antibodies in *T. hominis* and *E. cuniculi*. These techniques have been used to identify extremely reduced microsporidian mitochondria (mitosomes) and characterize their only known function in biosynthesis of essential iron-sulfur clusters in both species (Williams et al., 2002; Goldberg et al., 2008). The genome of *T. hominis* also encodes a homologue of a respiratory enzyme (alternative oxidase) that was shown to localize to the mitochondria of other Eukaryotes indicating the possibility that mitosomes of this microsporidian have additional functions in the parasite's metabolism.

1.2 Mitochondria

1.2.1. The origin and functions of classical mitochondria

Mitochondria are double membrane-bound organelles of eukaryotes known to play a role in numerous key cellular processes such as energy generation (Scheffler, 2002b) and biosynthesis of essential iron sulfur clusters (Lill & Mühlenhoff, 2005). According to the endosymbiotic theory mitochondria are derived from an endosymbiotic α-proteobacterial ancestor (Embley & Martin, 2006). Evidence supporting this theory include a presence of mitochondrial genome encoding proteins essential for some of the organelle functions (Chen & Butow, 2005) some of which group with the homologues from bacteria in phylogenetic analyses (Esser et al., 2004; Gray et al., 2004; Rodríguez-Ezpeleta & Embley, 2012).

Although mitochondria have retained their genomes most of the mitochondrial proteins are encoded in the nucleus, translated in the cytosol and have to be imported into the organelle using specialized protein import system that translocates these proteins through mitochondrial membranes (Dolezal et al., 2006), (for more

details see *section 3.1.2 The mitochondrial protein translocation machinery*). This could be readily explained by a transfer of some mitochondrial genes to the nuclear genome, and subsequent loss of the transferred genes from the organelle genome (endosymbiotic gene transfer theory), however this theory does not explain why some genes remained in the organelle (Timmis et al., 2004). One of the possible explanations for retention of mitochondrial genome is that it is required for a tight control of expression of genes encoding the electron-transport chain (ETC) components in response to changes in redox environment inside the organelle ('redox control' theory), (Allen, 2015). The ETC components localize to the inner mitochondrial membrane where they are involved in the formation of the proton gradient across the membrane that can drive production of ATP via ATP synthase (Hatefi, 1985). Mitochondrial capacity to generate ATP is increased by formation of characteristic infolds in inner mitochondrial membrane called cristae that expand its surface area (Scheffler, 2002b). The role of mitochondria in production of ATP may have contributed to evolution of increased complexity of eukaryotic cell in comparison to that of prokaryotes, which is a likely prerequisite to evolution of multicellular life (Lane & Martin, 2010). As the inner mitochondrial membrane is not freely permeable to solutes a range of nuclear-encoded transporter proteins is required in order to mediate the exchange of metabolites between the organelle and the host cytosol including an ADP/ATP carrier (AAC) that plays role in ADP/ATP exchange (Klingenberg, 2008). Insertion of the host encoded nucleotide transporter into the inner membrane of mitochondrial ancestor seems to have been an important step in the transition from the endosymbiont into the organelle that allowed the host to tap into the symbionts derived ATP (John & Whatley, 1975).

In modern eukaryotes mitochondrial functions are not limited to energy conversion and can include involvement in such important cellular processes as heme biosynthesis, amino acid metabolism (Scheffler, 2002a; Scheffler 2002b), and programmed cell death (Estaquier et al., 2012). Mitochondria also have a function in biosynthesis of small inorganic protein cofactors that are vital in all living cells, namely iron-sulfur clusters (ISC), (Lill et al., 2012). ISC containing proteins are involved in central metabolic processes such as electron transport, various biosynthetic reactions, protein translation, and the synthesis and maintenance of DNA (Lill & Mühlenhoff, 2005; Netz et al., 2012). Based on phylogenetic analyses (Tovar et al., 2003; Emelyanov, 2003) the mitochondrial iron sulfur clusters biosynthesis machinery was hypothesized to be derived from the endosymbiotic

bacterial ancestor of mitochondria and retained as an essential function of the organelle in virtually all of the studied eukaryotes (Lill & Mühlenhoff, 2006; Lill, 2009).

1.2.2. Mechanisms of mitochondrial division and segregation

Size, numbers, shape and distribution of mitochondria can vary between organisms, different cells of the same organism or different stages of the cell's life cycle and in most of the studied eukaryotes it is dependent on a balance between the organelle division and fusion events (Yaffe, 1999; Mishra & Chan, 2014). Mitochondrial fusion can be responsible for the formation of interconnected network of organelles (Bach et al., 2003) while mitochondrial fission produces many smaller mitochondria that may be easily transported along the cytoskeleton (Westermann, 2011). One of the key components of the characterized mitochondrial division machineries is the force generating dynamin related protein (Drp1 in human; Dnm1p in yeast) that works with various interaction partners in constriction of the organelle membrane that can lead to the membrane scission (Kageyama et al., 2011), (more details in section 5.1).

Division of the mitochondria plays a key role in their faithful inheritance during cell division (Yaffe, 1999). Besides the organelle division, diverse mechanisms of organelle segregation during cytokinesis exist in order to provide daughter cells with the organelles (Mishra & Chan, 2014). Many of these mechanisms seem to require transport of the mitochondria along the cytoskeleton. In fission yeast *Schizosaccharomyces pombe,* mitochondria are tethered to microtubules and two different models of interaction with the filaments have been proposed (Yaffe et al., 2003). In the first model, mitochondria are tethered to microtubules by the Mmb1p protein and transported by the polymerization of filaments (Fu et al., 2011). In the second model, Peg1p is proposed to attach mitochondria to microtubules and stabilize filaments maintaining mitochondrial position inside the cell instead of moving them (Chiron et al., 2008). In the most recent studies expression of chimeric protein containing a microtubule binding domain and the mitochondria outer membrane protein (tom22p) rescued the mitochondria aggregation defects in mmb1-deletion strain, which is consistent with the Mmb1p-dependant model of mitochondrial distribution in *S. pombe* (Li et al., 2015).

Actin microfilaments rather then microtubules are used by *Saccharomyces cerevisiae*, *Aspergillus* and plants (Boldogh & Pon, 2007) whereas in animal cells,

mitochondria can be transported along both microtubules and actin microfilaments (Saxton & Hollenbeck, 2012). The actin-dependent transport can be driven by movement of motor proteins along the actin filaments or by microfilament polymerization. Tethering of mitochondria in *S. cerevisiae* is dependent on a protein complex called a mitochore, that comprises three proteins: Mdm10p, Mdm12p and Mmm1p (Peraza Reyes et al., 2010). Mitochondrial transport was proposed to be driven by polymerization of actin which in case of anterograde (towards the bud) movement is caused by the mitochondria associated protein complex Arp2/3 (Boldogh et al., 2001). In addition, Myo2p a member of myosin V family was shown to bind to mitochondria and is needed for a correct distribution of mitochondria inside the cell (Altmann et al., 2008). The active transport of mitochondria to the daughter cell is balanced by retention of mitochondria in the mother cell by anchoring of a subpopulation of the organelle to the cell cortex via a cell cortex-associated protein Num1p (Mishra & Chan, 2014).

1.2.3. Mitochondrial homologues

Some eukaryotes were once thought to primitively lack mitochondria due to divergence of their ancestor from the main branch of the eukaryotic tree before the mitochondrial endosymbiotic event (Archezoa hypothesis), (Embley, 2006). Genomes of these eukaryotes were later shown to encode homologues of mitochondrial proteins that were subsequently localized to double membrane-bound mitochondria-derived organelles (Embley & Martin, 2006). All studied eukaryotes are now considered to contain mitochondria in one form or another (Figure 1.8) that most likely originate from a single endosymbiotic event (Zimorski et al., 2014). Only two traits seem to be shared by all of these organelles namely the double membrane and a conserved protein import mechanism (Embley & Martin, 2006). Traits usually associated with canonical mitochondria of model plants, mammals, and fungi; such as organelle genome, presence of cristae, synthesis of ATP via ATP synthase, or use of oxygen as the final electron acceptor in their electron transport chain are not shared across all mitochondrial homologues (Müller et al., 2012; Hjort et al., 2010).

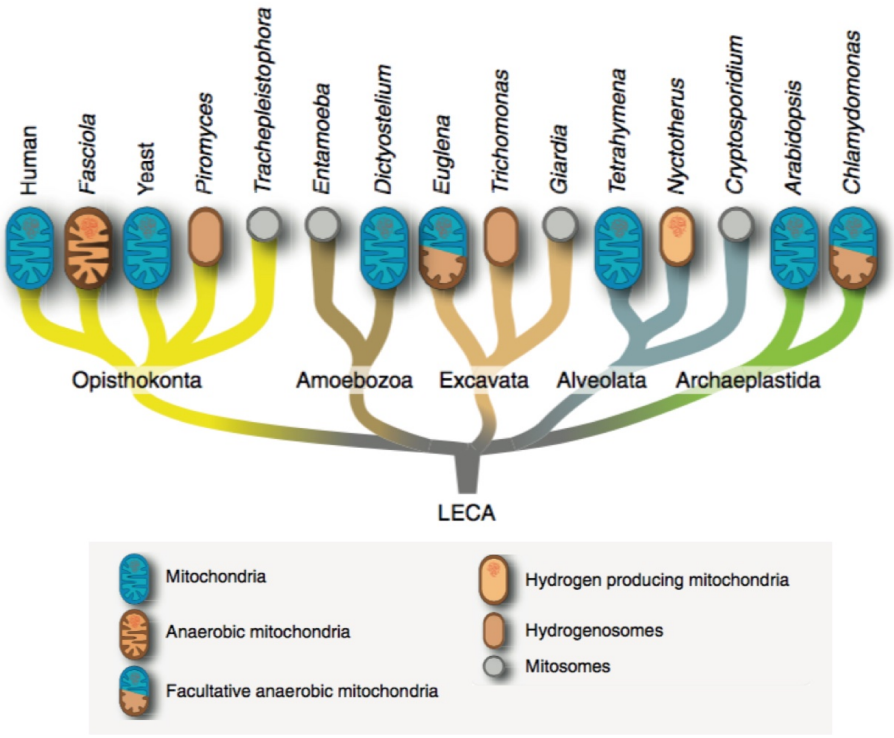

Figure 1.8 Mitochondria and mitochondrial homologues

Figure adapted from (Zimorski et al., 2014). Studied representatives of all major eukaryotic lineages contain mitochondria or mitochondrial homologues that most likely have evolved from a mitochondrion of the last eukaryotic common ancestor (LECA). Different types of mitochondrial homologues can be found in representatives of distantly related taxa indicating multiple independent origins of these organelles.

Hydrogenosomes are double membrane-bound organelles that produce molecular hydrogen, are oxygen-sensitive and produce ATP exclusively via substrate level phosphorylation (Müller et al., 2012; Embley et al., 2003). In hydrogenosomes, an oxidative decarboxylation of pyruvate by a pyruvate:ferredoxin oxidoreductase (PFO) is coupled to reduction of protons to molecular hydrogen catalyzed by an iron only [FeFe]-hydrogenase (with possible exception of some chytrid fungi where PFO activity might have been replaced by the activity of pyruvate:formate lyase), (Müller et al., 2012). The hydrogenomes have been identified in many distantly related eukaryotes adapted to anaerobic environments including some ciliates (e.g. *Nyctotherus ovalis*), (Hackstein et al., 2008), trichomonads (e.g. *Trichomonas vaginalis*), (Hrdý et al., 2008) and chytrid fungi (e.g. *Piromyces* sp E2), (Hackstein et al., 2008; Müller et al., 2012; Hjort et al., 2010). No evidence for a hydrogenosomal genome has been found in *Piromyces* and *Trichomonas* however it has been identified in *Nyctotherus* hence the mitochondrial homologue from *N. ovalis* is now classified by some authors (Müller et al., 2012) as a hydrogen producing

mitochondrion, and is considered to be an intermediate between the hydrogenosome and classical mitochondrion (Hackstein et al., 2008; Müller et al., 2012). Mitochondrial homologues with an organelle genome and [FeFe]-hydrogenase are also present in an anaerobic stramenopile (a group that also includes brown algae and diatoms) *Blastocystis sp.* (Stechmann et al., 2008), and potentially in the breviate (Brown et al., 2013), *Pygsuia biforma* (Stairs et al., 2014) as well as the free-living amoeba *Mastigamoeba balamuthi* (Gill et al., 2007).

Between hydrogenosomes and aerobic mitochondria, there is a diversity of anaerobic mitochondria that can use electron acceptors other than protons (Müller et al., 2012). The anaerobic mitochondria can be classified based on the electron acceptor into two categories: those that use an environmental electron acceptor (e.g. nitrate), and those that use an endogenously generated electron acceptor (e.g. organic acids), (Tielens et al., 2002). The endogenous terminal electron acceptors can be used in the organelles of animals such as *Ascaris* (giant roundworm) and *Fasciola* (liver fluke), as well as single-celled euglenid *Euglena gracilis.* Nitrate is used as the terminal electron acceptor in anaerobic mitochondria of denitrifying foraminiferans, some fungi and diatoms (Müller et al., 2012).

Mitosomes are the most reduced form of known mitochondrial homologues that seemingly have lost both the organelle genome and capacity to produce ATP. They are bound by two lipid bilayers without a clearly defined intermembrane space or any apparent inner compartmentalization (cristae), (Tachezy & Šmíd, 2008a). They have been identified in microsporidia, *Giardia lamblia* (Excavata), (Tovar et al., 2003), *Entamoeba histolytica* (Amoebozoa), (Tovar et al., 1999) and *Cryptosporidium parvum* (Alveolata), (Keithly et al., 2005) all of which have adopted a parasitic lifestyle (Hjort et al., 2010). An electrochemical potential across the mitosomal membranes has not been detected in the mitosomes of *G. lamblia* (Tachezy & Dolezal, 2011), *E. histolytica* (Mai et al., 1999) or microsporidia (Williams et al., 2002) but there is some evidence for a membrane potential in the mitosomes of *C. parvum* (Roberts et al., 2004; Henriquez et al., 2005). With an exception of possible function in reoxidation of cytosolic NADH in *Cryptosporidium* (Abrahamsen et al., 2004; Xu et al., 2004; Mogi & Kita, 2010) and some microsporidia (Williams et al., 2010), mitosomes from *G. lamblia, C. parvum* and microsporidia seem to function mostly in biosynthesis of essential iron-sulfur clusters (ISC), (Hjort et al., 2010). This function of the mitosomes requires a presence of protein import system for import of nuclear encoded ISC machinery components (Hjort et al., 2010; Heinz & Lithgow, 2012).

The presence of the ISC biosynthesis- and protein import-machinery components in the most reduced forms of the organelle reflects a retention of these two key mitochondrial functions across virtually all studied mitochondria and mitochondrial homologues (Lill & Mühlenhoff, 2006; Embley & Martin, 2006). The only exceptions seem to be the mitochondrial homologues where the ISC machinery may have been replaced by similar bacterial- or archaeal-derived systems that have most likely been acquired *via* lineage specific horizontal gene transfer (Stairs et al., 2014; Mi-ichi et al., 2009). Sulfur-mobilisation system (SUFCB) components of possible archaeal origin were identified and localized to the mitochondrial homologue in *P. biforma* (Stairs et al., 2014). Bacterial-derived NifU/NifS (ε-proteobacterial nitrogen fixation system) was identified in closely related *M. balamuthi* and *E. histolytica* and shown to localize to mitochondrial homologue of *M. balamuthi* (Nývltová et al., 2013). Localization of NifU/NifS to the *E. histolytica* mitosomes is unclear (Ali et al., 2004; Mi-ichi et al., 2009; Dolezal et al., 2010; Maralikova et al., 2010) and the only confirmed function of this organelle is its seemingly unique role in a sulfate-activation pathway required for synthesis of various sulfated metabolites (Mi-ichi et al., 2009; 2015).

1.2.4. Microsporidian mitosomes

Microsporidian mitosomes were initially identified in *Trachipleistophora hominis* using immunoelectron and immunofluorescence microscopy techniques with specific antibodies against a *T. hominis* homologue of mitochondrial heat shock protein 70 (*Th*Hsp70) (Williams et al., 2002). Immunofluorescence and electron microscopy were subsequently used to identify the mitosomes in *Encephalitozoon cuniculi* (Tsaousis et al., 2008). In transmission electron micrographs mitosomes appear as tiny (around 50 nm by 90 nm in *T. hominis* and 66 nm by 110 nm in *E. cuniculi*) elongated double membrane-bound organelles (Figure 1.9 A and B) (Williams et al., 2002; Tsaousis et al., 2008). Similar structures were also observed in other microsporidian species but their identity as the mitosomes still needs to be confirmed using molecular techniques (Vavra, 2005; Heinz et al., 2012). As in the case of the mitosomes of *Entamoeba* (Leon-Avila, 2004), no evidence for the presence of the organellar genome has been found in microsporidia (Burri et al., 2006; Heinz et al., 2012). The apparent lack of the organellar genome indicates that all of the mitosomal protein are encoded in the microsporidian nuclear genomes

(genes encoding for 22 mitochondrial homologues were found in *E. cuniculi* genome (Katinka et al., 2001) and have to be imported into the organelle using a specialized protein import system (Burri et al., 2006). Consistent with that, homologues of mitochondrial protein import machinery components were identified in microsporidian genomes (Katinka et al., 2001; Burri et al., 2006).

Genes encoding homologues of proteins involved in only one mitochondrial metabolic pathway, namely biosynthesis of essential iron-sulfur clusters (ISC) were found in all available microsporidian genomes (Katinka et al., 2001; Heinz et al., 2012; Nakjang et al., 2013). Some of the ISC machinery components from *E. cuniculi* (*Ec*Isu1, *Ec*Yhf1 and *Ec*Nfs1) and *T. hominis* (*Th*Nfs1) were shown to co-localize with mtHsp70 to the mitosomes in immunofluorescence experiments with specific antibodies (Figure 1.9 C and D) (Goldberg et al., 2008). Several of the ISC biosynthesis proteins from *E. cuniculi* (*Ec*Yfh1 and EcGrx5) and *T. hominis* (*Th*Isu1) were also able to functionally replace their homologues in *Saccharomyces cerevisiae* mitochondria (Goldberg et al., 2008).

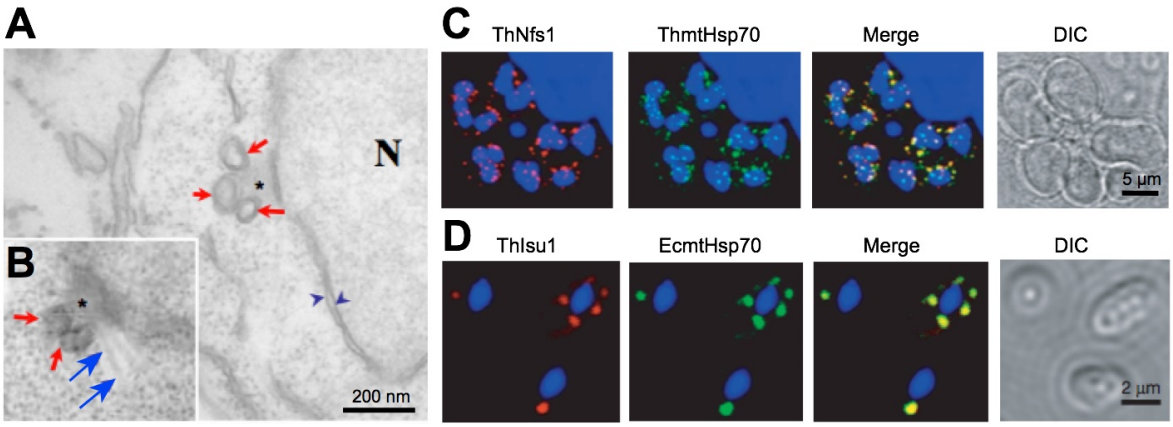

Figure 1.9 Intracellular localization and functions of the microsporidian mitosomes

(A) and (B) were adapted from Tsaousis et al., (2008). (C) and (D) were adapted from Goldberg et al., (2008)

(A) and **(B)** Microsporidian mitosomes are tiny (around 50 nm by 100 nm) double membrane bound organelles (red arrows) often observed in a proximity of an electron dense structure (star) embedded within nuclear envelope (blue arrowheads). The localization of the structure and observation of what seem to be microtubules (blue arrows) projecting out of it indicate that it may be an organelle homologous to fungal spindle pole body. **(C)** and **(D)** Microsporidian components of iron-sulfur clusters biosynthesis machinery localize to the mitosomes of *T. hominis* and *E. cuniculi.* (C) Rabbit antisera raised against *T. hominis* Nfs1 (red) co-localize with biotinylated rabbit antisera against mitosomal marker *T. hominis* mtHsp70 (green) to the mitosomes of *T. hominis. E. cuniculi* (D). Rabbit antisera raised against *T. hominis* Isu1 (red) co-localize with biotinylated rabbit antisera against mitosomal marker *E. cuniculi* mtHsp70 (green) to the mitosomes of *E. cuniculi.* Numbers of the punctate fluorescent signals labeled with antibodies per single DAPI stained nucleus (blue) of the parasite seem to be higher in *T. hominis* than in *E. cuniculi.* Large DAPI stained structure in (C) is a nucleus of the infected rabbit kidney (RK13) host cell.

In addition to the apparent loss of their genomes, mitosomes seem to have completely lost the ability to produce ATP (Tsaousis et al., 2008). As some of the mitosomal proteins including chaperonin mtHSP70 (involved in protein import and iron sulfur clusters biosynthesis in mitochondria of model organisms (Kampinga & Craig, 2010)) require ATP for their activity a mechanism for ATP import into the organelle has to exist (Tsaousis et al., 2008; Goldberg et al., 2008; Williams, Haferkamp, et al., 2008). The *E. cuniculi* genome encodes four characterized membrane transport proteins that are capable of transporting purine nucleotides including ATP when expressed in bacterial cells (Tsaousis et al., 2008). Three of these transporters (NTT1, NTT2, NTT4) were localized using specific antibodies to the cell membrane of the intracellular stages of *E. cuniculi* and seem to enable the parasite to steal ATP from its host (Tsaousis et al., 2008). However specific antisera against *E. cuniculi* NTT3 detect punctate fluorescence signals that co-localize with signals detected with antibodies against mitosomal marker mtHSP70 in immunofluorescence experiments (Tsaousis et al., 2008). Four NTT homologues that can also import ATP when expressed in bacteria are present in *T. hominis* however all of them localize to the parasite cell membrane and no evidence for the mitosomal localization has been found using immunofluorescence and quantitative immunoelectron microscopy techniques (Heinz et al., 2014). As the mitosomes of *T. hominis* seem to have similar requirements for ATP as these of *E. cuniculi* a mechanism of ATP import into the organelle has to exist indicating a possible presence of an uncharacterized mitosomal ATP transporter in *T. hominis* (Dean et al., 2014). Localization of NTT homologues has not been investigated in *Antonospora locustae,* however a different ATP transporter belonging to the mitochondrial carrier family (MCF) was detected in an expressed sequence tag (EST) library for this species (Williams & Keeling, 2005). It was subsequently shown to transport ATP in a bacterial system and to localize (when fused with GFP) to *S. cerevisiae* mitochondria in heterologous expression experiments but the mitosomal localization of this transporter has not been experimentally verified (Williams, Haferkamp, et al., 2008). No MCF transporters were found in genomes of other microsporidians (Katinka et al., 2001; Heinz et al., 2012; Cuomo et al., 2012) indicating a possible presence of lineage-specific mitosomal ATP import systems at least in some microsporidia (Williams, Haferkamp, et al., 2008; Dean et al., 2014; Heinz et al., 2014).

Although the mitosome is not capable of generating its own ATP, in some microsporidian species it could potentially be involved in ATP production *via*

glycolysis (Williams et al., 2010; Heinz et al., 2012). Genomes of *T. hominis* and some other microsporidians encode homologues of two mitochondrial homologues, namely the alternative oxidase (AOX) and mitochondrial glycerol-3-phosphate dehydrogenase (mtG3PDH) that together could function in reoxidation of NADH, a process required for continuous production of ATP in glycolysis (Williams et al., 2010). Glycolytic markers including a *T. hominis* phosphoglycerate kinase detected with specific antibodies seem to be enriched in microsporidian spores rather than in the intracellular stages indicating that glycolysis could potentially function with the mitosomal AOX and the mtG3PDH to generate ATP in microsporidian spore as opposed to the intracellular stages that can steal ATP from their hosts (Heinz et al., 2012).

The estimated number of the punctate fluorescent signals detected with antibodies against mitosomal proteins ranges from only a few in *Encephalitozoon cuniculi* (Tsaousis et al., 2008) cells to between 7 and 47 in *Trachipleistophora hominis* meronts (Williams et al., 2002). Given the apparently small number of the mitosomes in microsporidian cells, microsporidia cannot rely on a stochastic inheritance of the organelle indicating an existence of a specific organelle segregation mechanism. Mitosomes are often observed close to the electron dense structure inside the nuclear envelope that resembles fungal spindle pole body (Vavra, 2005; Tsaousis et al., 2008). It was hypothesized that anchoring of the mitosomes to this organelle is a mechanism responsible for the mitosomal inheritance (Vavra, 2005; Tsaousis et al., 2008). In addition to organelle segregation mechanism an organelle division mechanism is required for its inheritance during the cell division but the microsporidian mitosomal division machinery has not been characterized yet.

Mechanisms responsible for the mitosomal inheritance as well as the potential involvement of the mitosome in the energy metabolism of *T. hominis* spores require further investigation and constitute the aims of this thesis.

1.3. Aims and hypotheses of the thesis

The extremely reduced microsporidian mitochondrion called the mitosome has lost all known pathways for the ATP generation and its only identified metabolic function seems to be that in the biosynthesis of essential iron sulfur clusters (Goldberg et al., 2008). Intracellular stages of the microsporidian parasites are able to steal ATP from their hosts (Tsaousis et al., 2008; Heinz et al., 2014). However, extracellular spores cannot rely on the host for energy generation. The only known pathway capable of ATP production identified in microsporidian genomes is glycolysis but NADH generated in this pathway needs to be oxidized to NAD in order to sustain continuous generation of ATP (Heinz et al., 2012). In some microsporidians including *Trachipleistophora hominis* homologues of two mitochondrial proteins namely, alternative oxidase (AOX) and mitochondrial glycerol-3-phosphate dehydrogenase (mtG3PDH) could be involved in NADH oxidation (Williams et al., 2010).

Aim 1

The first aim of this PhD project is to investigate the intracellular localization of the AOX and mtG3PDH in different stages of *T. hominis* life cycle by testing the following hypotheses:

1. **Homologues of alternative oxidase and mitochondrial glycerol-3-phosphate dehydrogenase localize to the mitosomes of *T. hominis.***
2. **Alternative oxidase and mitochondrial glycerol-3-phosphate dehydrogenase are enriched in spores rather than the intracellular stages of *T. hominis.***

Due to the presence of only a small number of mitosomes in each microsporidian cell a specialized segregation mechanism is to be required in order to ensure inheritance of the organelle by all daughter cells during the cell division. In electron micrographs the mitosomes are often observed close to the electron dense structure close to the nuclear membrane that resembles the fungal spindle pole body (Vavra, 2005; Tsaousis et al., 2008). In addition to the segregation during cell fission organelles need to divide in order to be inherited but the mitosomal division machinery has not been characterized.

Aim 2

The second aim of this project is to investigate the mechanisms required for the inheritance of the microsporidian mitosomes by testing the following hypotheses:

3. The microsporidian electron-dense spindle plaque is a homologue of the yeast spindle pole body.

4. Mitosomes of *T. hominis* are associated with the spindle pole body in all stages of the microsporidian life cycle.

5. Microsporidian genomes encode homologues of the mitochondrial division machinery components.

Chapter 2. Materials and methods

2.1 Bioinformatic analyses tools

Table 2.1 Bioinformatic tools used in this thesis

Program or program package name	Function	Citation	Website
BLAST	Protein and nucleotide homologue searches. Generation of custom databases.	(Altschul et al., 1990)	http://blast.ncbi.nlm.nih.gov/Blast.cgi
HAMMER 3.1	Protein homologue searches using hidden Markov model (HMM) profiles. Generation of custom HMM profiles.	(Eddy, 2001)	http://hmmer.janelia.org
ExPASy tools (Compute pI/Mw tool)	Protein sequence analyses including computation of theoretical molecular weight.	(Gasteiger et al., 2003)	http://www.expasy.org
Sequencher 4.2.2	Analysis of the results from Sanger DNA sequencing.	(Codes, 2000)	https://www.genecodes.com
MUSCLE	Multiple sequence alignment generation	(Edgar, 2004)	http://drive5.com/muscle/
T-Coffee	Multiple sequence alignment generation and analyses	(Notredame et al., 2000)	http://tcoffee.crg.cat/
trimAL	Automated alignment trimming	(Capella-Gutiérrez et al., 2009)	http://trimal.cgenomics.org
Seaview	Multiple sequence alignment viewing and editing	(Gouy et al., 2010)	http://doua.prabi.fr/software/seaview
Jalview	Multiple sequence alignment viewing and editing	(Waterhouse et al., 2009)	http://www.jalview.org
ALINE	Multiple sequence alignment viewing and editing	(Bond & Schüttelkopf, 2009)	http://bondxray.org/software/aline.html
DSSP 2.0	Calculation of DSSP entry from PDB entry	(Touw et al., 2015)	http://swift.cmbi.ru.nl/gv/dssp/
RAxML (PThreads)	Maximum likelihood based inference of phylogenies	(Stamatakis et al.,2014)	http://sco.h-its.org/exelixis/web/software/raxml/index.html
PhyloBayes 3 PhyloBayes-MPI 1.5	Bayesian based inference of phylogenies and evaluation of model fit	(Lartillot et al., 2009)	http://www.atgc-montpellier.fr/phylobayes/
ProtTest 3.1	Selection of the best fitting amino acid replacement models for phylogenetic inference	(Darriba et al., 2011)	https://github.com/ddarriba/prottest3
Dendroscope 3	Phylogenetic trees viewing and editing	(Huson & Scornavacca, 2012)	http://dendroscope.org
FigTree v1.3.1	Phylogenetic trees viewing and editing	(Rambaut, 2007)	http://tree.bio.ed.ac.uk/software/figtree/

Table 2.1 continued

Program or program package name	Function	Citation	Website
Phyre2	Protein structure prediction, modelling and analyses	(Kelleyet al., 2015)	http://www.sbg.bio.ic.ac.uk/phyre2/html/page.cgi?id=index
PyMOL v1.7.4	Generation and viewing of 3D protein structure models.	(DeLano, 2002)	http://pymol.org
TargetP 1.1	Prediction of the presence of N-terminal targeting sequences in proteins	(Emanuelsson et al., 2000)	http://www.cbs.dtu.dk/services/TargetP/
Predotar	Prediction of the presence of N-terminal targeting sequences in proteins	(Small et al., 2004)	https://urgi.versailles.inra.fr/predotar/predotar.html
Mitoprot II	Prediction of the presence of N-terminal mitochondrial targeting sequences in proteins.	(Claros & Vincens, 1996)	https://ihg.gsf.de/ihg/mitoprot.html
PONDR-FIT	The prediction of intrinsic disorder from amino acid sequence.	(Xue et al., 2010)	http://www.disprot.org/pondr-fit.php
TMHMM2.0	Transmembrane helices prediction.	(Krogh et al., 2001)	http://www.cbs.dtu.dk/services/TMHMM/

2.2 Image processing and analyses software

Table 2.2 Image processing and analyses software used in this thesis

Program or program package name	Function	Citation	Website
FIJI	Image processing, relative band intensity measurements.	(Schindelin et al., 2012)	http://fiji.sc/
Volocity	Image deconvolution, detection and quantification of fluorescent signals.	PerkinElmer	http://www.perkinelmer.co.uk/
Image Lab™ Software	Acquisition and processing of images of western blots and stained polyacrylamide gels. Molecular weight analyses. Relative band intensity measurements	Bio-Rad	http://www.bio-rad.com/

2.3 Statistical analyses

All statistical tests with an exception of those performed in phylogenetic analyses were performed using the SigmaPlot package (version 12.5, Systat Software, www.sigmaplot.com).

2.4 Identification of microsporidian protein homologues

Microsporidian homologues of proteins of interest were identified using Blast (Altschul et al., 1990) and HMM profile searches (Eddy, 2001). Amino acid sequences of proteins of interest were downloaded from online databases (NCBI, GenBank; JGI, Genome Portal MycoCosm; Broad Institute, Microsporidia Comperative Database) and used as queries in BlastP and tBlastN searches performed using a local version of the Blast package 2.2.29+ or online NCBI Blast server (Altschul et al., 1990). HMM profiles were, downloaded from Pfam-A database, generated with hmmbuild (HMMER3) using alignments downloaded from Pfam-B, or generated using custom alignments. All profiles were used in HMM profile searches with hmmsearch (HMMER3), (Eddy, 2001). BlastP and HMM searches were performed against local protein sequence databases containing microsporidian sequences including: *Nosema ceranae* BRL01, *Nosema bombycis* CQ1, *Nosema apis* BRL 01, *Encephalitozoon cuniculi GB-M1*, *Encephalitozoon intestinalis* ATCC 50506, *Encephalitozoon hellem* ATCC 50504, *Encephalitozoon romaleae SJ-2008*, *Vittaforma corneae* ATCC 50505 (http://www.broadinstitute.org/), *Enterocytozoon bieneusi* H348, *Edhazardia aedis* USNM 41457, *Vavraia culicis floridensis*, *Trachipleistophora hominis*, *Spraguea lophii* 42_110, *Nematocida parisii* ERTm1, *Nematocida parisii* ERTm3, *Nematocida sp1* ERTm2 downloaded from GenBank (http://www.ncbi.nlm.nih.gov/) or Broad Institute, Microsporidia Comperative Database (http://www.broadinstitute.org/). tBlastN searches were performed against microsporidian NCBI WGS (Whole Genome Shotgun) sequences.

2.5 Multiple sequence alignments and phylogenetic analyses

Multiple sequence alignments (MSA) were generated using MUSCLE (Edgar, 2004) or T-Coffee with M-Coffee, Expresso, or PSI coffee mode T-Coffee. For phylogenetic analyses MSAs were trimmed using trimAL with the automated1 or gappyout method (Capella-Gutiérrez et al., 2009). Maximum likelihood trees were generated with RAxML (Stamatakis, 2014) under models determined with ProtTest3 (Darriba et al., 2011) and with 100 rapid bootstrap replicates. Bayesian analyses

were performed using PhyloBayes in four chains that were run in parallel until convergence as determined using the bpcomp and tracecomp programs of the PhyloBayes package (Lartillot et al., 2009). The fit of models used to construct Bayesian phylogenies was evaluated using posterior predictive analysis implemented in the ppred program of the PhyloBayes package (Lartillot et al., 2009).

Formatting and analysis of multiple sequence alignments was performed in Jalview (Waterhouse et al., 2009), Seaview (Gouy et al., 2010) and ALINE (Bond & Schüttelkopf, 2009). The pairwise percentage of sequence identity were calculated using the -output=sim function implemented in T-coffee (Notredame et al., 2000).

2.6 Design of PCR primers

Oligonucleotide primers were designed in order to amplify genes of interest from the genomic DNA and clone them into the expression vectors. All primers were designed so that the genes could be fused in frame with epitope tags and start codons of the expression vectors. For TOPO cloning protocol (Invitrogen) 4 base pair sequence (CACC) was added to the 5' terminus of the forward primer. For the standard cloning by restriction enzyme digestion and ligation the 5' termini of forward and reverse primers incorporated a restriction site, and a 6-nucleotide long extension to the restriction site added in order to increase the efficiency of the restriction digest. In cases where a 3' terminus of a gene was not amplified (i.e. amplified sequence did not contain an endogenous stop codon) a stop codon (TAA) was added at the 3' terminus of the amplified sequence (before a restriction site in a reverse primer).

Table 2.3 Sequences of primers used in PCR amplification

Primer name	Restriction enzyme	Sequence (5' – 3')
ThMps3pQE40F	KpnI	GGGCCC**GGTACC**GACCGAAGAAAAATGTTAAAACTT
ThMps3pQE40R	PstI	GCGCGC**CTGCAG**TTAGTGATCCTTAGCACCGTGGTTGGAC
ThMps3pQE40intF	EcoRI	GGCCGG**GAATTC**AGAACACATGGTACGACCGAGGAGG
ThMps3pQE40intR	EcoRI	CGGCGC**GAATTC**CTTTAGGAAATACGTTAGTTTGTTC
ThSpc98pET16F	NdeI	GGGCCC**CATATG**GATGTGTTAAGCATCACAAAGAAATACA
ThSpc98pET16R	BamHI	GCGCGC**GGATCC**TTAGAGACACTCCTGTTCCAGAACATTGAGA
EcHex_NSP_F	SalI	CGACAT**GTCGAC**TGGCCTGCGCTAGCTGTAAGTACG
EcHex_NSP_R	NotI	GTACCT**GCGGCCGC**CTAAGGAGTCTGATCGGCAAATG
ThHex443F	SalI	CGACAT**GTCGAC**ATGTACATTAGCTTGTGGTTG
ThHex443R	NotI	GTACCT**GCGGCCGC**TTAATGGTTATCCCTAGCTATTG
ThHex_NSP_443F	SalI	CGACAT**GTCGAC**GAGTATTCCCAACGAGATTTGG
ThHex897F	SalI	CGACAT**GTCGAC**ATGAAATTTTTGTCTTCTATAAC
ThHex897R	NotI	GTACCT**GCGGCCGC**TTATGAGAATAAATCAATTATATTACC
ThHex_NSP_897F	SalI	CGACAT**GTCGAC**ACTGATAATTTGTTGTACACAG
ThHex937F	SalI	CGACAT**GTCGAC**ATGCGTCTATTCGCCATTC
ThHex937R	NotI	GTACCT**GCGGCCGC**TTAATTATGACTAACGAGACGAG
ThHex_NSP_937F	SalI	CGACAT**GTCGAC**AGCGAGTTTCTTCACAGCGATG
ThHex1847F	SalI	CGACAT**GTCGAC**ATGGAAGAGAACTCAAACAACTC
ThHex1847R	NotI	GTACCT**GCGGCCGC**TTAATCAACCTGGAGAAGAATTC
ThmtG3PDHpET100F	- (TOPO)	**CACC**TTGAGAGAAAGAAAATACGTGATT
ThmtG3PDHpET100R	- (TOPO)	TTACAAGCTCTCTAGCATCTGCAAGCAT
ThGammaTubpET16F	NdeI	GGGCCC**CATATG**AGAGAAATCATAACATTACAAATA
ThGammaTubpET16R	BamHI	GCGCGC**GGATCC**CTATCTCTCACAGAAGGACGTTAA
ThHsp70pET100F	- (TOPO)	**CACC**AGCAAACCAGCAATCGTAGGCATT
ThHsp70pET100R	- (TOPO)	CTATAGAATTTCTTCGTTTTTGTCACCA
EcGammaTubpET16F	NdeI	GGGCCC**CATATG**CGCGAGGTGGTCACACTGCAGGTT
EcGammaTubpET16R	XhoI	GCGCGC**CTCGAG**TCAATGGTTTGGATATGCTGCCAT
ThActin_pQE40F	KpnI	GGGCCC**GGTACC**AGCTCAGAGAATGCGCCAGCAATA
ThActin_pQE40R	PstI	GCGCGC**CTGCAG**TTAACTGAGCACGATGTTGCTGTA
ThActin_pQE40intF	EcoRI	GGCCGG**GAATTC**TTCATCAAGCTGCTCAAGGAGAGC
ThActin_pQE40intR	EcoRI	CGGCGC**GAATTC**CTGGTGCCTGGGCGTGCCCACGAT

Names of the primers include: name of the microsporidian species (Ec, *E. cuniculi;* Th, *T. hominis*), name of the encoded protein (Hex, hexokinase), and target plasmid for cloning (if only one was used). Bold in the primer sequences indicate a restriction site or CACC sequence required in TOPO (Invitrogen) cloning protocol. Primers used to amplify the hexokinase genes without the predicted N-terminal secretion signals were indicated (NSP).

2.7 Polymerase Chain Reaction (PCR)

All PCRs were performed using KOD hotstart polymerase (Merck Millipore) or Phusion® High-Fidelity DNA Polymerase (NEB) in 25 to 50 µl volumes according to the manufacturers' protocols. Cycling conditions are listed in (Table 2.4). In cases when initial annealing temperature (55°C) was not optimal a gradient of the annealing temperatures (usually ranging from 50°C to 65°C) was tested in order to identify the optimal temperature.

Table 2.4 PCR conditions

	Number of cycles	KOD hotstart polymerase	Phusion® High-Fidelity DNA Polymerase
Initial denaturation	-	5 min, 95°C	30 sec, 98°C
Denaturation	35	1 min, 95°C	10 sec, 98°C
Annealing		30 sec, usually 55°C	30 sec, usually 55°C
Extension		1 min / 1 kbp, 70°C	30 sec-1 min / 1 kbp, 72°C
Final extension	-	10min, 70°C	10min, 72°C
Storage	-	4°C until stopped	4°C until stopped

2.8 Molecular cloning

PCR products were purified using either QIAquick PCR Purification Kit (QIAGEN) or QIAquick Gel Extraction Kit (QIAGEN). Plasmids were isolated and purified from bacterial cells using QIAGEN Plasmid Mini kit (QIAGEN). Purified PCR products and plasmids (usually 1 µg) were digested using appropriate restriction enzymes (Table. 2.3). All double digestions were performed sequentially using conventional restriction enzymes (Thermo Scientific) in recommended buffers and recommended conditions (usually 1h incubation at 37°C with 5-10U of restriction enzyme). QIAquick PCR Purification Kit (QIAGEN) was used to purify digested DNA fragments after the first and the second digest. Purified digested PCR products were ligated into the digested plasmids using Rapid DNA Ligation Kit (Thermo Scientific). Ligation products were used to transform chemically competent *E. coli* cells. Transformed *E. coli* cell were plated out onto LB (Luria Bertani) agar plates with the appropriate antibiotics and incubated overnight at 37°C. Colonies from the plates were used to start an overnight liquid (LB) culture with appropriate antibiotics at 37°C. Plasmids were isolated and purified from bacterial cells using QIAGEN Plasmid Mini kit (QIAGEN) and digested using the same restriction enzymes that were used in cloning in order to verify the presence of an insert. The sequence of the

insert and its integration into the vector was verified by Sanger sequencing (GATC Biotech) of the positive clones with primers specific to regions of the plasmid upstream and downstream from the cloning site.

All commercial kits were used according to the manufacturer's protocol.

2.9 Preparation of chemically competent *Escherichia coli* cells

One ml of an overnight culture of *E. coli* (strains used in this study were listed in sections *2.11 Transformation of chemically competent E. coli cells* and *2.12 Protein expression in E. coli cells*) was used to inoculate 100 ml of LB medium (with 34 µg/ml of chloramphenicol for pLysS strains or 15 µg/ml kanamycin for M15). The culture was incubated with shaking at 220 rpm at 37^{o}C and stopped by placing on ice when an optical density (OD_{600}) of 0.4 - 0.5 was reached. The culture was centrifuged at 4000 x g at 4^{o}C for 5 minutes and the supernatant was discarded. The cell pellet was resuspended in 6 ml of ice cold filter sterile 0.1 M $MgCl_2$, incubated on ice for 10 minutes and then centrifuged at 4.000 x g at 4 ^{o}C for 5 minutes. The supernatant was discarded and the pellet resuspended in 4 ml of ice-cold 0.1 M $CaCl_2$ was incubated for 2 h on ice. 2 ml of sterile 50% glycerol was added to the 4 ml of bacterial suspension, aliquoted (100 µl aliquots) and stored at -80^{o}C.

2.10 Agarose gel electrophoresis of DNA samples

PCR products, genomic DNA preparations, and plasmids were resolved and visualised by standard agarose gel electrophoresis. Agarose gels (0.6 – 2.0 % depending on the expected DNA molecule size) were prepared in 1X TAE buffer (40mM Tris acetate, 1 mM EDTA pH 8.0). Ethidium bromide (final concentration 0.5 µg/ml) was added to a cooled gel solution. Samples were mixed with 4X gel loading buffer in a 1:3 ratio (buffer : sample) prior to loading. MassRuler DNA ladder (Fermentas) was loaded onto each gel (5 µl per well) alongside the samples. Electrophoresis was performed in 1X TAE, at 10 V/cm until the marker dye left the gel. The DNA was visualised under UV light and photographed using Bio-Rad ChemiDoc XRS+ system.

2.11 Transformation of chemically competent *E. coli* cells

General cloning strains of *Escherichia coli* used in this study: DH5α, TOP10 (Invitrogen), JM109.

Aliquots of chemically competent *E. coli* cells were thawed on ice. 1-5 µl of the ligation mix or plasmid was added to the thawed cells and incubated on ice for 20

minutes. After incubation the cells were promptly transferred to a 42°C water bath for 45 seconds followed by an additional incubation on ice for 10 minutes. Thereafter, 300 µl of a room temperature LB medium was added to 100 µl of transformed bacterial cells and incubated for 1 hour at 37°C with shaking at 220 rpm. Cells were finally plated out onto the LB agar plates (50 µl on one plate and the rest on a second plate) containing the appropriate antibiotics and incubated overnight at 37°C.

2.12 Protein expression in *E. coli* cells

E. coli expression strains used in this study: BL21 (DE3), BL21 (DE3) pLysS, BL21 Star (DE3) pLysS, Tuner, Tuner pLysS, Rosetta, Rosetta pLysS, C41 (DE3), Origami B pLysS, M15.

Expression plasmids used in this study: pET16b, pET30b, pET32b, pET100 TOPO, pQE40, pGEX6-1.

Suitable *E. coli* expression strain transformed with the recombinant expression vector was grown in LB medium containing the appropriate antibiotic overnight at 37°C with shaking at 220 rpm. The overnight culture was used to inoculate a 500 ml of LB medium containing the appropriate antibiotic followed by an incubation at 37°C with shaking at 220 rpm until an OD_{600} of 0.4 - 0.6 was reached. The culture was placed on ice and 1 ml aliquot (0 h) was collected as a non-IPTG induced control. The protein expression was induced using 1 mM (final concentration) of IPTG (isopropyl β-D-1-thiogalactopyranoside). After the induction the culture was incubated for a 4 hours at 37°C with shaking at 220 rpm. The culture was placed on ice, OD_{600} was measured, and 1 ml aliquot (4 h) was taken to test the expression of the recombinant protein. Both 0 h and 4 h aliquots were centrifuged at 16,000 x g, resuspended in 100 µl of a 1x Laemmli sample buffer, syringed through a 19 G needle (in order to reduce a viscosity of the solution caused by release of the bacterial DNA), boiled at 95°C for 10 minutes, and finally centrifuged at 16,000 x g. The rest of the culture was centrifuged at 6,000 x g for 20 min, the supernatant was discarded, and the pellet was either used immediately for protein extraction or stored at -20 °C.

In order to test the expression of the recombinant protein 1 - 10 µl (based on the OD_{600} values) of the 0 h and 4 h protein extracts were separated on polyacrylamide gels that were later stained with InstantBlue (Expedeon) following the manufacturers protocol or used in western blotting experiments (usually with anti-His tag antibodies). Expression of the recombinant protein was verified by the detection

of the signals corresponding to the expected molecular weight of the protein in the 4h protein extracts and not in the 0 h control.

If no expression was detected in Coomassie blue and western blotting analysis the following alternative conditions were tested: incubation temperature after the IPTG induction (16°C, 22°C, 30°C), time of the incubation (1 h – 16 h), IPTG concentrations (0.04 mM; 0.1 mM; 0.4 mM). If different expression conditions had no effect different expression strain and/or expression plasmid were tested.

2.13 Protein extraction and purification from *Escherichia coli* cells

Bacterial cells were lysed either using a BugBuster™ protein extraction reagent (Novagen) or with a sonication (for 2 minutes using B. Braun Labsonic U sonicator set at low intensity ~42 watts and 0.5 second cycling on ice). The BugBuster™ reagent utilizes a mixture of non-ionic detergents that are capable of cell wall perforation without denaturing soluble proteins (Novagen). Pellets of bacteria expressing the recombinant proteins were lysed by incubating in the BugBuster™ reagent following the manufacturer's protocol with the addition of optional Benzonase (nuclease specific towards both DNA and RNA, Novagen) and lysozyme. Bacterial lysate was centrifuged at 16,000 x g for 20 min at 4°C and the supernatant (usually around 5 ml) was collected (soluble protein fraction). The pellet was further incubated in the BugBuster™ reagent with the addition of lysozyme followed by three washes in the BugBuster™ reagent following the manufacturer's protocol for the 'inclusion body purification'. The final pellet (insoluble protein fraction) was resuspended in the 1 x Laemmli sample buffer, boiled at 95°C for 10 minutes, and finally centrifuged at 16,000 x g. A 300 µl aliquot of the supernatant was mixed with 100 µl of the 4 x Laemmli sample buffer, boiled at 95°C for 10 minutes, and centrifuged at 16,000 x g. Usually 8 - 10 µl of both soluble and insoluble fractions were loaded onto polyacrylamide gels.

2.14 SDS-polyacrylamide gel electrophoresis (PAGE) and staining of polyacrylamide gels

All Tris-glycine SDS polyacrylamide gels were prepared using Mini-PROTEAN Handcast system (Bio-Rad) with 1 mm spacers and 10 or 15 well combs. Protein extracts were prepared by addition of Laemmli sample buffer (1x final concentration: 63 mM Tris-HCl pH 6.8, 2 % SDS, 10 % Glycerol, 0.01 % Bromophenol Blue and 50 mM DTT) incubation at 95°C for 10 min and centrifugation at 16,000 x g. Samples

were loaded onto a 10 % or 12 % polyacrylamide gels, alongside PageRuler protein ladder (Thermo Scientific) or Precision Plus Protein™ WesternC™ standard (Bio-Rad). Gels were separated at a constant voltage (usually 180 V) in a Tris-Glycine running buffer (25 mM Tris, 0.192 mM glycine, 0.1% SDS, pH 8.3) using Mini-PROTEAN Tetra cell system and PowerPac Basic power supply (Bio-Rad) until the marker dye left the gel.

Proteins in gels were stained with Coomassie blue-based gel stain, Instant blue (Expedeon). Gels after electrophoresis were incubated in the Instant blue for 1h and than left in ddH_2O overnight to destain. Images of the gels were acquired using Bio-Rad ChemiDoc XRS+ system.

2.15 Western blotting

After SDS-PAGE proteins from the gel were transferred to a nitrocellulose membrane in a wet transfer (Bio-Rad Mini Trans-Blot® Cell, 100 V, 60 min; or Bio-Rad Criterion™ Blotter, 100 V, 30-60 min or 10 V overnight in a cold-room) or semi-dry transfer (Bio-Rad Trans-Blot® Turbo™ 25 V, 30 min) system according to the manufacturer's protocol. Wet transfers were carried out in Towbin buffer (25 mM Tris, 192 mM glycine, pH 8.3, 20% (v/v) methanol) whereas semi-dry transfers were carried out in the Bjerrum Schafer-Nielsen buffer (48 mM Tris, 39 mM glycine, pH 9.2, 20 % methanol). Efficiency of transfer was assessed by Instant blue (Expedeon) staining of the gel and reversible Ponceau S (Sigma) staining of the membrane after transfer. After transfer the membrane was blocked by 1h incubation in filtered TBST buffer (50 mM Tris-HCl, pH 7.6; 150 mM NaCl; 0.1 % Tween-20) with 5 % milk at room temperature followed by incubation with primary antibodies in TBST buffer with 1 % milk (1 h at room temp. or overnight at 4°C). Incubations with primary antibodies were followed by three 10-minute washes with TBST buffer and incubation with secondary antibodies conjugated to HRP (horseradish peroxidase) for 1 hour at room temperature. The blots were finally washed three times (10 minutes) in TBST buffer and once in TBS buffer (10 minutes). Antibodies conjugated to HRP were detected using Clarity™ Western ECL Blotting Substrate (Bio-Rad) according to the manufacturer's protocol and visualized using Bio-Rad ChemiDoc XRS+ system.

2.16 Immunization of animals

Instant blue stained bands (1 mg of protein based on comparison with an albumin standard) corresponding to the proteins of interest were cut out of the

polyacrylamide gel and sent to a company for immunization (Agrisera or Eurogentec). All recombinant proteins sent to Agrisera were used to immunize rabbits (*Th*AOX, *Th*mtG3PDH) or rats (*Th*MPS3, *Th*Actin, *Th*mtHSP70, *Th*SPC98). Each of the recombinant proteins was used to immunize two animals. Each of the animals was immunized three times (week 1, week 5 and week 9) followed by the ELISA test and test bleeding (20 ml rabbit; 0.1 ml rat; week 11). The final immunization (week 13) was followed by the final bleed (50-70 ml rabbit; 3-4 ml rat; week 15).

Only animals that did not show any significant cross-reactivity with the recombinant proteins and protein extracts from the host (RK13 cell line) or the microsporidian parasite (*T. hominis* or *E. cuniculi*) based on western-blotting and immunofluorescence microscopy screening of pre-immune sera were selected for production of antibodies.

2.17 Affinity purification of antibodies

Approximately 500 µg of protein used as an immunogen for immunisation of animals was separated on SDS polyacrylamide gels (100 µg/gel) and transferred onto a nitrocellulose membrane (*section 2.15 Western blotting*). After the transfer membranes were stained with Ponceau S (Sigma) and bands corresponding to the full-length recombinant protein were cut out. Slices of the membrane (containing the recombinant protein) were blocked in TBST buffer with 5 % milk (*section 2.15 Western blotting*). Blocking buffer was discarded and the slices were incubated in polyclonal sera (final bleeds) + TBST with 1 % milk (final concentration) in 12 ml or 50 ml falcon tubes on a tube rotator overnight in a cold room. Dilution of the serum differed depending on the titre of the antibodies and total volume of the available serum (usually 5 ml – 20 ml of rabbit polyclonal sera was diluted to final volume of 50 ml and 1 ml - 2 ml of rat polyclonal sera was diluted to final volume of 12 ml). After the overnight incubation blots were washed four times 10 minutes in TBST with 1 % milk, one times 10 min in TBST buffer, and one times 10 min in TBS buffer. Following the washes, the membrane strips were transferred into the elution buffer (2 – 5 ml of 0.2 M glycine-HCl, pH 2.5) for 10 min at RT. After the incubation the membrane stripes were removed from the elution buffer and the buffer was neutralized with 1M non-titrated Tris (final concentration 60 mM) and 2.5 M NaCl (final concentration 50 mM). The neutralized buffer was split in half and one aliquot was stored at -20°C.

Buffer in the second was exchanged for PBS using Amicon® Ultra-15 Centrifugal Filter Concentrator (Millipore®, 100kDa NMWL) and concentrated to final volume 100 µl - 500 µl. The final concentrations of the antibodies in PBS were usually between 0.1 mg/ml and 1 mg/ml. Antibodies were aliquoted and stored at -20°C. Concentration of the purified antibodies was measured with absorbance spectroscopy (A280, IgG mass extinction coefficient of 13.7), in NanoDrop (Thermo Scientific).

2.18 Extraction of proteins from microsporidian spores and RK13 cells

Approximately 1 x 10^8 - 1 x 10^9 of Percoll purified microsporidian (*E. cuniculi* or *T. hominis*) spores were suspended in 300 µl of a lysis buffer: an ice cold PBS with Protease Inhibitor Cocktail (Sigma P8340), PMSF (Sigma) and $MgCl_2$ (0.6 mM final concentration). The spore solution was subjected to a three cycles of bead beating for 30 seconds at 6.5 m/sec (Bio101 FastPrep120) with 400 mg of 0.1 - 0.11 mm ∅ glass beads and 1 of minute incubation on ice. The bead beating was followed by incubation of the lysate in the lysis buffer with 2 % SDS and Benzonase (25 U, Novagen) on ice for 10 minutes.

Confluent monolayers of rabbit kidney RK13 cell line infected with *T. hominis* or *E. cuniculi*, and uninfected rabbit kidney cells grown in 175 cm^2 tissue culture flask were washed three times with PBS and lysed in a lysis buffer consisting of PBS with 2 % SDS, Protease Inhibitor Cocktail (Sigma P8340), PMSF (Sigma), $MgCl_2$ (0.6 mM final concentration), and Benzonase (25 U, Novagen). The lysate was incubated on ice on a rocker shaker for about 10 minutes in order to reduce its viscosity caused mainly by the release of genomic DNA.

Protein concentration in the lysates was measured using BCA Protein Assay Kit (Pierce) followed by the addition of Laemmli sample buffer (1X final concentration). The total protein extracts were aliquoted and stored at -20°C. Prior to polyacrylamide electrophoresis extracts were incubated at 95°C for 10 min and centrifuged at 16,000 x g for 1 minute.

2.19 Collection of microsporidian spores

Culture medium containing microsporidian spores was collected from cultures of rabbit kidney RK13 cell line infected with *T. hominis* or *E. cuniculi*, grown in 175 cm^2 tissue culture flasks. The spore suspension was centrifuged at 2,500 x g for 5 minutes, the supernatant was discarded and the pellet was washed three times by

resuspending in PBS and repeating the centrifugation step. The final pellet was resuspended in 5 ml of PBS and used immediately for the purification in density gradient centrifugation in Percoll or stored at -20°C.

In order to collect a high number of highly infective microsporidian spores (required to initiate infection in time course of infection experiments), cultures of rabbit kidney RK13 cell line infected with *T. hominis* or *E. cuniculi* were grown in 175 cm^2 tissue culture flasks until most of the host cells were filled with a large number of bags of spores. Monolayers were washed three times in PBS and scraped off the surface of the flasks with a cell scraper. The cells were resuspended in 10 ml of PBS and subjected to three cycles off sonication (spores are not lysed by sonication and it does not seem to affect their infectivity, sonication conditions as described in section 2.13 Protein extraction and purification from *Escherichia coli* cells), resuspended in the tissue culture medium, and used to infect the uninfected host cell monolayers.

The spores were counted using a haemocytometer (usually ~10^5 per sonicated flask).

2.20 Purification of microsporidian spores by density gradient centrifugation in Percoll

5 ml of microsporidian spores in PBS was placed on top of a Percoll (Sigma-Aldrich) : PBS (10 ml : 30 ml) solution in a 50ml tube and centrifuged for 30 minutes at 900 x g at 4°C. All but 5 ml of the supernatant at the bottom of the tube was slowly removed, 45 ml of PBS was added and centrifuged 2,500 x g for 5 minutes at 4°C. This washing step was repeated once, followed by removal of as much of the final supernatant as possible without disrupting the pellet. The pellet was resuspended in 9 ml of PBS containing 0.05 % saponin and 0.05 % Triton X-100 and passed through a syringe with a 25 G needle. 1.5 ml of the spore solution was placed on top of a Percoll gradient and centrifuged at 45.000 x g for 15 minutes. The Percoll density gradient was formed by centrifuging thinwall tubes (Beckman Coulter, 14 mL, 14 x 95 mm, cat. number: 344060) containing two separate layers of two Percoll solutions: 2.25 ml of 88% Percoll (bottom) and 8.25 ml Percoll 26% (top) at 45.000 x g for 15 minutes in an ultracentrifuge (Beckman SW 40 Ti rotor). Spores were detected (light microscopy) in two thick bands close to the bottom of the tube. Both bands were carefully collected, washed twice in PBS (2,500 x g for 5 minutes at 4°C) and used immediately for the protein extraction or stored at -20°C.

The spores were counted using a haemocytometer.

2.21 Tissue culture of rabbit kidney cells

The tissue culture of non-infected rabbit kidney cells (RK-13) or the host cells infected with ~1 x 10^8 of either *Trachipleistophora hominis* or *Encephalitozoon cuniculi* Strain II spores were grown Dulbecco's Minimal Essential Medium (DMEM, Invitrogen 41090028) with 10% heat-inactivated fetal bovine serum (FBS, Sigma F9665) and antibiotics (100 µg/ml, Kanamycin; 100 µg/ml, Penicillin-Streptomycin; 1 µg/ml, Fungizone) in incubator at 33°C, with 5% of CO_2. The cultures were routinely examined using light microscopy and the media were changed every four days.

Cells that reached 100 % confluence were washed three times with PBS, dissociated from the flask's surface by incubating for 2-10 minutes at 33°C with 5 ml of 0.25 % trypsin-EDTA (Invitrogen), neutralized by addition of fresh DMEM medium with 10 % FBS and antibiotics, and passaged to new flasks. During the passage RK-13 cells infected with microsporidia were usually split into 2 or 3 new flasks whereas non-infected RK-13 cells split into 4 flasks. If the infection reached high-level, non-infected RK cells were added to the culture of the microsporidian infected cells during the passage. After 10 passages RK-13 cells were usually discarded and new culture was started from a liquid nitrogen stock.

2.22 Extraction of DNA from microsporidian spores

The purified microsporidian spores were washed with ddH_20, pelleted at 500 x g for 5 minutes, and re-suspended in cell lysis solution (Puregene Tissue Core A kit, Gentra, QIAGEN). The spore solution was subjected to a three cycles of bead beating for 30 seconds at 6.5 m/sec (Bio101 FastPrep120) with 0.1 - 0.11 mm ∅ glass beads and 1 of minute incubation on ice. The bead beating was followed by quick centrifugation in order to remove the beads and incubation with RNase A solution (1 mg/ml, Qiagen). Tubes were inverted several times and placed on ice for 1 minunte. Protein precipitation solution was added (Puregene Tissue Core A kit, Gentra, QIAGEN), samples were mixed vigorously and incubated on ice for 5 minutes. The samples were then centrifuged at 13,000 x g for 3 min, and the supernatant was transferred to a new tube. Isopropanol was carefully added to the supernatant, the tubes were inverted gently 50 times to mix the solution, and centrifuged at 13,000 x g for 5 min at 4°C. This final pellet was washed with 70% ethanol once, and most of the ethanol was removed gently with a pipette. The DNA pellet was dried at room temperature and rehydrated with DNA hydration solution

(Puregene Tissue Core A, Gentra, Qiagen).

2.23 Measuring band intensity in western blots

The amount of the protein loaded onto the gels, antibodies concentration and exposure times were normalized and set so that neither of the detected bands was over-saturated (based on the blot's histogram examination) or had signal below the detection limit, and that the overall background was low and evenly distributed on the blot surface (based on the intensity line profiles across the blot). Intensities were only compared between bands of the same apparent molecular weight detected with a single antibody on a single western blot.

In Image Lab (Bio-Rad) lanes and bands were selected manually using Lanes and Bands tool. Profiles of the detected bands were adjusted using Lane Profile tool (only volume under the pick corresponding to the band was measured) with Background subtraction values used so that measured values did not include volume below the threshold level. Volumes of the bands defined as 'the sum of all the intensities within the band boundaries' were recorded. As a control bands intensities were also measured as a volume (int) of a rectangle enclosing the band of interest subtracted by a volume (int) of a rectangle of the same size that did not enclose any bands (background, usually measured in non-infected RK-13 control).

In FIJI (Schindelin et al., 2012) lanes were selected using Rectangular selection tool and Select lanes function and lane profile plots were generated using Plot lanes function. The line tool was used to close off the peaks so that only values above the background were measured.

2.24 Cell fractionation by means of differential centrifugation

Rabbit kidney RK13 cells infected with *T. hominis* were grown in 175 cm^2 tissue culture flasks until bags of spores could be seen in at least 10% of the host cells and high numbers of proliferative intracellular stages (meronts) could be observed in methanol : acetone (1:1) fixed samples grown in parallel on cover slips. Monolayers were dissociated from the flask's surface by trypsinization (see section 2.21 Tissue culture of rabbit kidney cells), washed in PBS and resuspended in a lysis buffer (10 mM HEPES-KOH pH 7.2 with 0.25 M sucrose), and stored at -20°C. Cell suspensions from 20 - 30 flasks were thawed on ice and Protease Inhibitor Cocktail

(Sigma P8340), PMSF (1 mM), and DTT (5 mM) were added to the solution. Cells were lysed with a glass tissue homogenizer on ice. The lysate was subjected to four subsequent centrifugation steps (1,000 x g for 10 minutes, 12,000 x g for 20 minutes, 25,000 x g for 1 h and 100,000 x g for 2 h) at 4°C. After each centrifugation step the supernatant was transferred to a new tube and the pellet was stored on ice. The pellet centrifuged at 1.000 x g (1 kg) was resuspended in 3000 µl of the lysis buffer with proteinase inhibitors whereas the remaining pellets were resuspended in 300 µl of the same buffer. Sonication was used to lyse the nuclear membranes and reduce viscosity (by fragmenting the DNA) of the 1 kg solution followed by the addition of Benzonase (25 U, Novagen) and incubation on ice on a rocker shaker for 10 minutes. Aliquots (20 µl) of all resuspended pellets and the final supernatant were collected in order to measure protein concentration with the BCA Protein Assay Kit (Pierce) following the addition of SDS (1%). All of the resuspended pellets and the final supernatant were mixed with Laemmli sample buffer (1X final concentration), boiled at 95°C for 10 minutes and stored at -20°C.

2.25 Proteinase K protection assay

25,000 x g pellet from the cell fractionation experiment (see *section 2.24 Cell fractionation by means of differential centrifugation*) experiment was washed twice with ice-cold HSDP buffer (0.25 M sucrose, 10 mM HEPES-KOH 7.2) without protein inhibitors and DTT. The pellet was resuspended in 300 µl of HSDP buffer and divided into three 100 µl aliquots. The first aliquot was left untreated on ice, the second aliquot was treated with 1 mg/ml (final concentration) of proteinase K, the third aliquot was treated with 1 mg/ml proteinase K and 0.25 % (final concentration) Triton X-100. All aliquots were incubated on ice for 1 hour followed by a TCA precipitation by an addition of 20 µl of 100% ice cold Trichloroacetic acid (TCA) to the sample and incubtion on ice for 30 minutes. The precipitates were spun down at 25,000 x g for 20 minutes at 4°C (Eppendorf 5417R benchtop centrifuge), the supernatant was discarded and the pellet was washed twice with an ice-cold acetone (100 %) each followed by a centrifugation at 25,000 x g for 20 minutes at 4°C. The final supernatant was discarded and the final pellet was left at room temperature for 30 minutes to 1 hour in order to evaporate the residual acetone, resuspended in the 1X Laemmli sample buffer, boiled at 95°C for 10 minutes, and finally centrifuged at 16,000 x g.

2.26 Time course of infection experiment

Infection in the time course experiment was initiated by addition of *T. hominis* spores purified using Percoll gradient to a growth medium over a confluent monolayer of rabbit kidney cells (RK13) grown on round cover slips in 24-well plates (0 h). After 30 min of incubation, spores were removed by three thorough washes with PBS. Washes were followed by addition of fresh medium. Samples (cover slips) were collected at the following time points after addition of spores (post infection): 30 min, 1 h, 2 h and later every 2 h for the period of 42 h. Every sample was washed three times with PBS and immediately fixed in methanol:acetone (1:1) at -20°C for 10 min. Fixed cells were labelled with affinity purified rabbit anti-AOX polyclonal antibodies, rat anti-mtHSP70 polyclonal serum, goat anti-rabbit Alexa 594 antibodies and goat anti-rat Alexa 488 antibodies**.**

2.27 Immunofluorescence detection

Rabbit kidney cells (RK13) infected with *T. hominis* or *E. cuniculi* were grown on round cover slips (VWR, 13 mm diameter, thickness No. 1, Borosilicate Glass) in 24-well plates until around 70 % confluent, washed three times with PBS. Fixation was usually performed in methanol : acetone (1 : 1) at -20°C for 10 minutes as this fixation method seems to be the most optimal for all antibodies and samples tested in this study. Alternative fixatives tested for all antibodies included: methanol (100 %) at -20°C for 10 minutes; acetone (100 %) at -20°C for 10 minutes; methanol (100 %) at -20°C for 10 minutes, followed by acetone (100 %) at -20°C for 10 minutes; 4 % paraformaldehyde (in PBS, pH 6.9) for 10 minutes at room temperature followed by 0.2% Triton X-100 in PBS for 10 minutes at room temperature; 4 % paraformaldehyde followed by methanol (100 %) or acetone (100 %). Fixed samples were washed four times with PBS and incubated with 1 % milk (skimmed milk powder, Merck) in PBS (filtered using Whatman grade 3 filter paper), for 30 minutes at room temperature on rocker shaker. 1 % bovine serum albumin (BSA) in PBS instead of 1 % milk was also tested however the signal to noise ratio observed in fluorescence microscopy seemed to be higher in the samples prepared with milk. Cover slips were transferred onto 20 µl drops of primary antibody solution (diluted in 1 % milk/PBS) on a parafilm and incubated in a humid chamber at 4°C overnight (fluorescent signals of the samples incubated for 1 hour at room temperature usually

had lower signal to noise ratio). The tested dilutions of the primary polyclonal antisera or affinity-purified antibodies (1 mg / ml): 1 : 20, 1 : 100, 1 : 250, 1 : 1000. The cover slips were then transferred into 24 well plates, washed three times with PBS for 5 minutes at room temperature, and incubated with the solution of the Alexa Fluor (usually 488 or 594) conjugated secondary goat antibody (against the species in which the primary antibody was raised) in 1 % milk/PBS for 1 hour at room temperature on a tilt-shaker. After addition of the fluorophores all subsequent steps were performed in the dark. Incubation with the secondary antibodies was followed by three 5-minute washes in PBS. In double labelling experiments the second round of incubation with different primary and secondary antibodies, and PBS washes was performed. After the final PBS wash cover slips were incubated for 10 minutes in DAPI solution in PBS (1 µg / ml), washed once with PBS, rinsed in sterile ddH_2O and mounted onto the glass slides. Different mountants were tested including: VECTASHIELD (Vector), VECTASHIELD HardSet (Vector), Mowiol with PDD, and ProLong Gold (Life technologies). In experimental system used in this study the ProLong Gold was the most effective and convenient mountant. Samples were stored at 4°C in the dark.

Chapter 3. Characterization and immunolocalization of homologues of mitochondrial glycerol-3-phosphate dehydrogenase and the alternative oxidase homologues in *Trachipleistophora hominis*

3.1 Introduction

Microsporidian remnant mitochondria are tiny double membrane bound organelles that seem to have lost almost all of the canonical functions of mitochondria with the exception of their role in biosynthesis of essential iron sulfur clusters (ISC), (Goldberg et al., 2008). However, in addition to components of ISC biosynthesis machinery two proteins known to be involved in metabolic activities of mitochondria from other eukaryotes, namely alternative oxidase (AOX) and mitochondrial glycerol-3-phosphate dehydrogenase (mtG3PDH) have been detected in some microsporidian genomes including that of human pathogenic *Trachipleistophora hominis* (Williams et al., 2010; Heinz et al., 2012).

3.1.1 Alternative oxidase

The AOX is a non-proton motive cyanide-resistant terminal quinol oxidase (EC 1.10.3.11) in eukaryotes typically localized to the inner surface of the inner mitochondrial membrane (Siedow & Umbach, 2000; McDonald, 2008). It has a non-heme diiron carboxylate active site and catalyzes the four-electron reduction of oxygen to water by transferring electrons from reduced ubiquinone (ubiquinol) to molecular oxygen (Shiba et al., 2013; Moore & Albury, 2008). A nuclear encoded AOX gene has been found in a variety of eukaryotes including representatives of: plants (*Arabidopsis thaliana*), red (*Cyanidioschozn merolae*) and green (*Chlamydomonas reinhardtii*) algae, Amoebozoa (*Dictyostelium discoideum*), Alveolates (*Tetrahymena thermophila*), Stramenopiles (*Thalassiosira pseudonana*), Excavates (*Trypanosoma brucei*), Fungi (*Candida albicans*) and animals (*Ciona intestinalis*), yet it has been apparently lost in numerous lineages including vertebrates and some Fungi (e.g. *Saccharomyces cerevisiae and Schizosaccharomyces pombe*), (McDonald et al., 2009; McDonald & Vanlerberghe, 2006). This wide but discontinuous distribution of the AOX across eukaryotes together with detection of the AOX encoding gene in some proteobacteria led to the

formulation of the hypothesis that AOX was acquired from the primary endosymbiotic bacterium that gave rise to mitochondria and was subsequently independently lost in multiple eukaryotic lineages (Figure 3.1), (McDonald et al., 2003; McDonald & Vanlerberghe, 2006).

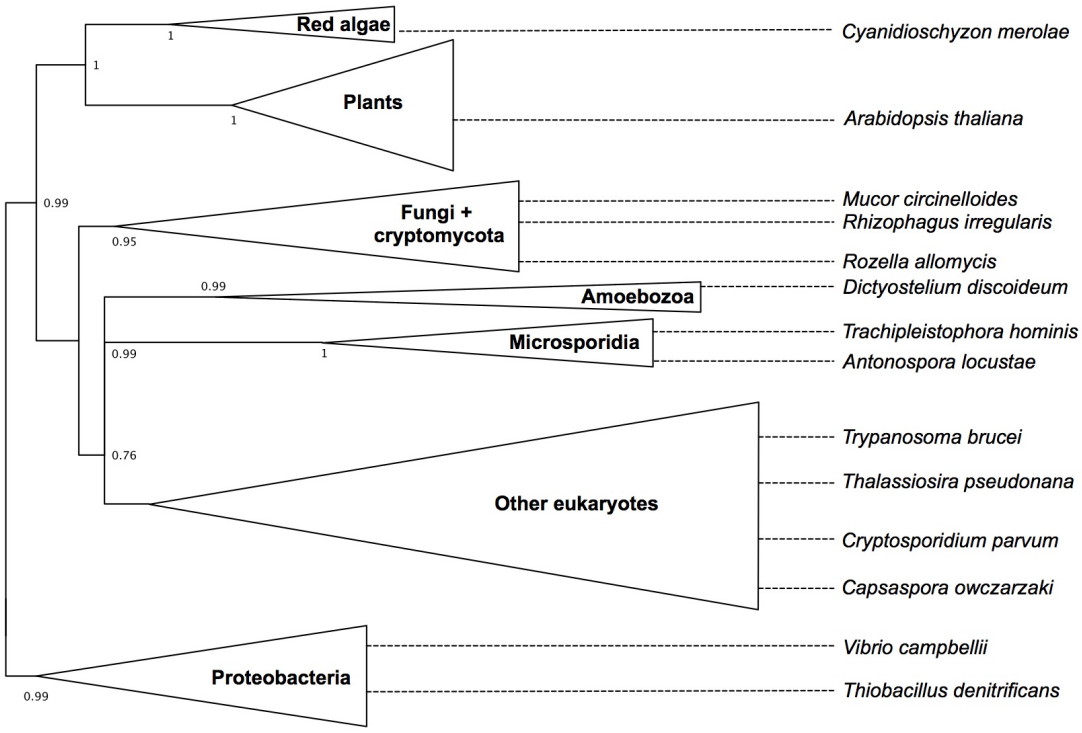

Figure 3.1 Phylogenetic tree of the alternative oxidase homologues including sequences from all major eukaryotic lineages (according to Adl et al., 2012) and representatives of Proteobacteria

AOX is widely distributed across eukaryotes and is also present in some representatives of proteobacteria. Topology of AOX phylogenietic trees is discussed in detail in section 3.4.5. Proteobacteria were used as an outgroup to eukaryotes based on published phylogenies (Williams et al., 2010). Only representative species of the groups present in the collapsed branches are indicated.
The tree was generated using PhyloBayes under the CAT60 model based on trimmed (trimAL, gappyout method) alignment of 121 sequences of 197 amino acid positions. Posterior probability support values were displayed only for the key branches.

Unlike cytochrome C oxidase, the activity of the AOX is not coupled with a proton-pumping process but instead dissipates the change in free energy as heat (McDonald, 2008; Moore et al., 2013). In mitochondria the activity of the AOX bypasses complexes III and IV of the cytochrome-dependent electron transport chain (cdETC) resulting in a reduced formation of the proton gradient across the inner mitochondrial membrane that can cause a decreased net ATP production by the mitochondrial ATP-synthase (Figure 3.2), (McDonald, 2008; Moore et al., 2013).

However, in the conditions that inhibit the cdETC such as limited phosphate and ADP supply, or presence of inhibitors (e.g. cyanide or nitric oxide) AOX can facilitate a continuous oxidation of mitochondrial ubiquinone pool (McDonald, 2008). This mechanism can allow for a continued activity of the upstream pathways (such as glycolysis or citric acid cycle) that generate a reducing potential in form of NADH that needs to be reoxidized via the cdETC (Millenaar & Lambers, 2003; El-Khoury et al., 2013). It can also alleviate an oxidative stress due to the production of excess reactive oxygen species by the over-reduced respiratory chain (Millenaar & Lambers, 2003; El-Khoury et al., 2013).

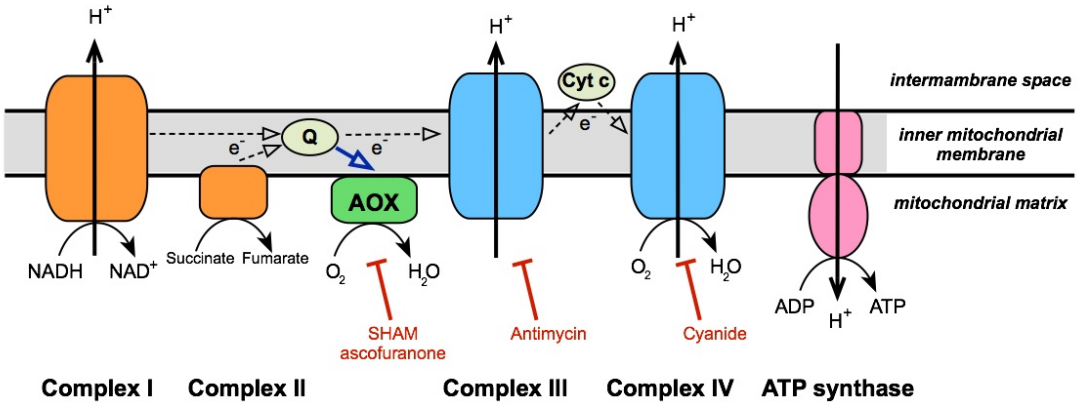

Figure 3.2 A model of electron transport chain and ATP synthase in the inner membrane of plant mitochondria

Dashed arrow lines represent a transfer of electrons (e^-) via the electron transport chain that is coupled with translocation of protons (H^+) out of the mitochondrial matrix across the inner mitochondrial membrane into the intermembrane space. This process generates an electrochemical gradient across the inner mitochondrial membrane (proton-motive force) that can be dissipated by the flow of protons back to the mitochondrial matrix through ATP synthase driving phosphorylation of ADP to ATP. The blue arrow line indicates oxidation of the reduced ubiquinone pool (Q) by the alternative oxidase (AOX), an alternative pathway for the electrons that bypasses complex III (cytochrome BC_1) and complex IV (cytochrome C oxidase). Activity of the AOX does not contribute to the formation of the proton gradient across the inner mitochondrial membrane but can contribute to reduction of ubiquinol pool in the presence of inhibitors (red) of the complex III (e.g. antimycin) or the complex IV (e.g. cyanide). Activity of the AOX can be inhibited by salicylhydroxamic acid (SHAM) or ascofuranone. Complex I, NADH dehydrogenase; Complex II, succinate dehydrogenase; Cyt C, cytochrome C.

In plants the AOX seems to function in variety of physiological processes including, a defence against environmental stresses and a heat generation in thermogenic organs of some plants (McDonald, 2008; Millenaar & Lambers, 2003). In pathogenic fungi the AOX seems to function in a defense against oxidative stress and in the conditions that limit the activity of the cdETC (Joseph-Horne et al., 2001; Juárez et al., 2004; Thomazella et al., 2012). An AOX knockout strain of human-

pathogenic yeast *Cryptoccocus neoformans* has significantly reduced virulence in mice (murine inhalation model) and a significantly impaired intracellular growth inside a macrophage-like cell line in comparison to wild type- and reconstituted- strains (Akhter et al., 2003). Strains of pathogenic fungi *Aspergillus fumigatus* and *Paracoccidioides brasiliensis* with a reduced expression of the AOX (using RNAi silencing techniques) were more susceptible to an oxidative stress and had a significantly decreased viability in macrophages in comparison to wild type strains and in case of *P. brasiliensis* decreased virulence in the murine model of infection (Ruiz et al., 2011; Magnani et al., 2009). In *P. brasiliensis* inhibition of both AOX and cdETC resulted in complete and irreversible inhibition of the transition between mycelium and pathogenic yeast forms (Martins et al., 2011). Inhibition of AOX is also an effective treatment against the causative agent of African sleeping sickness *Trypanosoma brucei brucei* in the mice model (Clarkson & Brohn, 1976; Yabu et al., 2003). Bloodstream stages of the *T. brucei* rely exclusively on glycolysis for ATP production and use the AOX as a sole final electron acceptor (Figure 3.3), (Chaudhuri et al., 2006). Energy metabolism based on the substrate level phosphorylation as the only source of ATP and the AOX as the final electron acceptor has been also proposed for apicomplexan intracellular parasites infecting humans *Cryptosporidium parvum* and *Cryptosporidium hominis* (Abrahamsen et al., 2004; P. Xu et al., 2004; Mogi & Kita, 2010).

In studied eukaryotes, the AOX is localized to the inner surface of the-NAD^+/ NADH-impermeable inner mitochondrial membrane where it has an access to the electron donor, ubiquinol (Jagow & Klingenberg, 1970; McDonald, 2008). Transfer of electrons from cytosolic NADH to the mitochondrial pool of ubiquinone is facilitated by different mitochondrial NADH oxidases and electron shuttles (Bakker et al., 2001). Components of only one such transfer system, namely glycerol-3-P shuttle are encoded in available assemblies of microsporidian genomes (Williams et al., 2010; Heinz et al., 2012). In this shuttle, cytoplasmic glycerol-3-phosphate dehydrogenase (cytG3PDH) oxidizes NADH and reduces dihydroxyacetone-3-phosphate (DHAP) to glycerol-3-phosphate (G3P), (Figure 3.3), (Bakker et al., 2001). In mitochondria protein bound to the outer surface of the inner mitochondrial membrane (via hydrophobic interactions) mitochondrial glycerol-3-phosphate dehydrogenase (mtG3PDH) oxidizes G3P back to DHAP and transfers electrons via a FAD cofactor to ubiquinone (Janssen et al., 2002; Larsson et al., 1998; Shen et al., 2006). In bloodstream stage of *T. brucei* G3P shuttle is the only active mitochondrial electron

transfer system and functions together with AOX in order to sustain continuous production of ATP via glycolysis (Figure 3.3), (Opperdoes, 1987; Chaudhuri et al., 2006).

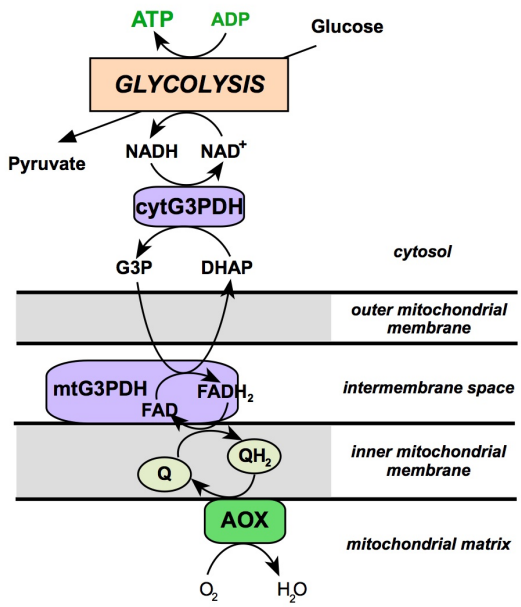

Figure 3.3 A model of an energy metabolism in bloodstream stage of *T. brucei*
Components of the glycerol-3-phosphate shuttle: NAD-dependent cytoplasmic glycerol-3-phosphate dehydrogenase (cytG3PDH) and FAD-dependent mitochondrial glycerol-3-phosphate dehydrogenase (mtG3PDH) are indicated in violet.
Abbreviations: G3P, glycerol-3-phosphate; DHAP, dihydroxyacetone-3-phosphate; Q, ubiquinone; QH_2, ubiquinol

In microsporidia the AOX gene has been found in *T. hominis* (Williams et al., 2010; Heinz et al., 2012), *A. locustae* (Williams et al., 2010), and *Octosporea bayeri* (Corradi et al., 2009) but not in the extremely reduced genomes of *Encephalitozoon* species (Williams et al., 2010) or the genome assemblies of *Entreocytozoon bieneusi* that also seems to have lost glycolysis (Keeling et al., 2010). Nuclear genomes of two intracellular parasites closely related to microsporidia, namely *Rozella allomycis* and *Mitosporidium daphniae* encode the AOX gene alongside an almost complete ETC with a terminal cytochrome C oxidase (James et al., 2013; Haag et al., 2014). Both genes encoding the components of glycerol-3-phosphate shuttle are present in all studied microsporidian genomes with an exception of *E. bieneusi* that seems to have retained only a homologue of cytG3PDH (Keeling et al., 2010). Homologues of cytG3PDH and mtG3PDH were also detected in *R. allomyces* and *M. daphniae* although, genome of *R. allomyces* also encodes a gene for a homologue of external mitochondrial NADH dehydrogenase (in model organisms localized to the inner mitochondrial membrane facing intermembrane space) that has not been detected in *M. daphnia* (James et al., 2013; Haag et al., 2014).

The microsporidian AOX from *T. hominis and A. locustae* seem to have a well conserved primary structure when aligned to the AOX from trypanosome and plants with a conserved iron and a substrate binding motifs (Williams et al., 2010). When expressed in *Escherichia coli* the AOX from both *A. locustae* and *T. hominis* catalyze a cyanide- and antimycin-resistant reduction of an ubiquinol-1 and the measured activity is inhibited by an ascofuranone, a potent inhibitor of the trypanosome AOX (Williams et al., 2010).

In immunoelectron microscopy experiments specific antibodies to *A. locustae* AOX and mtG3PDH co-localize with antibodies against mitosomal marker *A. locustae* mtHSP70 to small (50-200nm) double membrane-bound round structures - on ultrathin cryo-sections of the spore stages of the parasite (Dolgikh et al., 2011). Observed structures resemble mitosomes characterized in *T. hominis* (Williams et al., 2002) and *E. cuniculi* (Tsaousis et al., 2008), and the labeling pattern is consistent with a mitosomal localization of *A. locustae* AOX and mtG3PDH (Dolgikh et al., 2011). In western blotting experiments the same antibodies detect AOX and mtG3PDH in protein extracts from spores but not in protein extracts from purified intracellular stages of *A. locustae* as opposed to antibodies against mtHSP70 that detect specific signals in both extracts from intracellular stages and spores (Dolgikh et al., 2011). The AOX and mtG3PD together with glycolytic enzymes and neutral trehalase were also detected in spore proteomics of the human opportunistic pathogen, *T. hominis* (Heinz et al., 2012). Quantitative immunoelectron microscopy with antibodies to *T. hominis* PGK-3, the enzyme catalyzing the first ATP-generating reaction of glycolysis, indicated an enrichment of immunogold particles in the cytosol of spores compared to the cytosol of the intracellular stages of *T. hominis*. These results are consistent with enrichment of glycolytic enzymes in spores rather than the intracellular stages of *T. hominis* and are further supported by a detection of the subunit α of pyruvate dehydrogenase in *A. locustae* spores (Heinz et al., 2012; Dolgikh et al., 2011).

Some microsporidian including *Encephalitozoon cuniculi* seem to have lost the AOX but have retained both of the G3P shuttle components (Keeling et al., 2010). Results of heterologous expression and immunofluorescence experiments do not seem to be consistent with the mitosomal localization of the mtG3PDH homologue from *E. cuniculi* (Williams et al., 2010; Burri et al., 2006). The full-length protein fused with GFP is not imported to the *S. cerevisiae* mitochondria but instead seems to localize to the yeast cytosol (Burri et al., 2006). In immunofluorescence experiments

specific antibodies raised against *E. cuniculi* mtG3PDH label a large number of the parasite-specific punctate structures that seem to be distributed evenly in *E. cuniculi* cells unlike the antibodies against the mitosomal marker mtHSP70 that on average detect 3 punctate structures usually associated with DAPI stained nuclei (Tsaousis et al., 2008*;* Williams, et al., 2008; Williams et al., 2002).

3.1.2 The mitochondrial protein translocation machinery

All mitosomal proteins as well as the great majority of mitochondrial proteins including mtG3PDH and AOX are nuclear encoded, translated on the cytosolic ribosomes and have to be imported into the organelle (Chacinska et al., 2009). Targeting of the precursor proteins to the mitochondrion and later to the distinct subcomparment of the organelle is facilitated by the presence of specific targeting signals in the imported polypeptides (Neupert & Herrmann, 2007). Most often mitochondrial targeting signals have a form of a cleavable N-terminal α-helical presequence or less well-defined internal signals (Neupert & Herrmann, 2007). In the mitochondria of animals and Fungi these signals are initially recognised be receptor proteins (e.g. Tom20 and Tom70) of a translocase of the outer membrane (TOM) complex exposed on the outer surface of the outer mitochondrial membrane (Dudek et al., 2013; Opalińska & Meisinger, 2015; Hewitt, Lithgow, & Waller, 2014). The recognized polypeptides are translocated across the outer membrane of these mitochondria through a hydrophilic channel formed by the central component of the TOM complex, namely Tom40. After the passage through the outer membrane the polypeptides are selectively distributed to their target subcompartments *via* specialized sorting pathways (Dudek et al., 2013; Opalińska & Meisinger, 2015), (Figure 3.4).

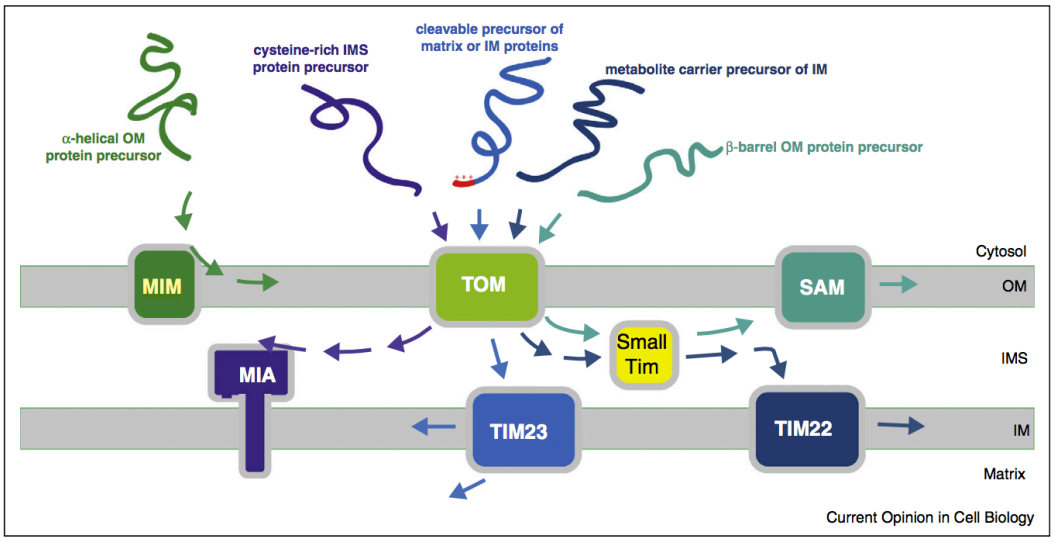

Figure 3.4 Overview of yeast mitochondrial protein import and sorting pathways

Figure reproduced from (Opalińska & Meisinger, 2015). Usually nuclear encoded mitochondrial proteins enter the mitochondrion *via* the translocase of the outer membrane (TOM) complex. Proteins targeted to the inner mitochondrial membrane (IM) or the mitochondrial matrix including those with N-terminal cleavable presequence (indicated in red) are sorted by the translocase of the inner membrane 23 complexes (TIM23). Precursors of the inner membrane metabolite carriers are transported in the mitochondrial membrane space (IMS) with the help of the small Tim chaperones and are inserted into the inner membrane through the translocase of the inner membrane 22 complex (TIM22). Small Tim chaperones are also involved in the transport of outer membrane β-barrel proteins that are later sorted into the outer membrane (OM) by the sorting and assembly machinery (SAM). Precursors of the IMS proteins that contain cysteine-rich signals are sorted *via* the mitochondrial intermembrane space import and assembly machinery (MIA). The MIM (mitochondrial import) machinery appears to be involved in import of a few outer membrane proteins including some of the components of the TOM complex.

The general protein import mechanisms seem to be conserved in mitochondria and mitochondrial homologues from distantly related eukaryotes (Hewitt, Lithgow, & Waller, 2014; Heinz & Lithgow, 2012). Microsporidian homologues of the core components of the major protein import complexes (TOM, TIM, SAM, PAM) were identified in genomes of *T. hominis* and *E. cuniculi* (Figure 3.5), (Katinka et al., 2001; Heinz et al., 2012). Receptor protein *E. cuniculi* Tom70 localized with the correct topology into the outer membrane of *Saccharomyces cerevisiae* mitochondria but was unable to functionally replace yeast Tom70 (Waller et al., 2009). Microsporidian homologue of mtHsp70, which in addition to its functions in iron-sulfur cluster biosynthesis is also involved in translocation of precursor proteins across the mitochondrial membranes (Schilke et al., 2006), is the only component of the mitochondrial protein import machinery with an experimentally demonstrated localization to the mitosomes of *T. hominis* and *E. cuniculi* (Williams et al., 2002; Tsaousis et al., 2008).

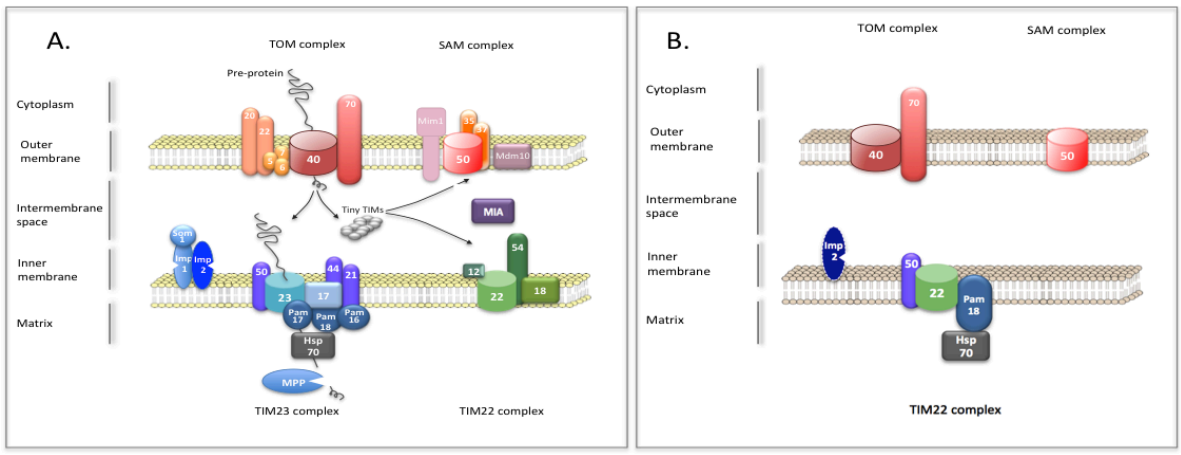

Figure 3.5 Comparison of *S. cerevisiae* (A.) and microsporidian (B.) mitochondrial protein translocation machineries

(A.) Subunits of the mitochondrial protein import complexes described in (Figure 3.4) are indicated with the corresponding numbers (e.g. 40 corresponds to Tom40). The import motor PAM (presequence translocase-associated motor complex) facilitates translocation across the inner membrane. Proteins targeted to the mitochondrion can be processed by one of two processing peptidase complexes IMP (inner membrane peptidase) or MPP (mitochondrial processing peptidase).

(B.) Microsporidian mitosomes seem to have retained only a backbone of the mitochondrial protein translocation machinery. Coding sequences for only two TOM proteins have been identified in microsporidian genomes: the receptor Tom70 and the beta-barrel channel Tom40 (Heinz & Lithgow, 2012; Waller et al., 2009). A single member of a Tim17/22/23 family annotated as Tim22 is most likely responsible for both insertion into, and translocation across, the mitosomal inner membrane. Only two components of the PAM motor were identified in microsporidian genomes: the chaperone mtHsp70 and its co-chaperone Pam18 (Heinz & Lithgow, 2012). Sam50 is the last of the main protein translocation components found in microsporidia and most probably is responsible for insertion of outer membrane proteins including Tom40 (Chacinska et al., 2009).

The broken line around the Imp2 homologue indicates that it was detected in EST library from *A. locustae* but not in the genome sequences of *E. cuniculi* and *T. hominis* (Heinz & Lithgow, 2012).

After import of the protein precursors into the mitochondria N-terminal targeting presequences are usually removed by different processing peptidases (Mossmann et al., 2012). AOX in plant mitochondria (Szigyarto et al., 1998) and possibly in mitochondria of *T. brucei* (Williams et al., 2008; Hamilton et al., 2014) as well as some fungi (Nargang et al., 2012) is processed by the activity of the mitochondrial processing peptidase (MPP). The MPP is also involved in processing of many of the protein precursors that are imported into the yeast mitochondrial matrix including Frataxin (Branda et al., 1999). N-terminal targeting signals that could be removed by the activity of the MPP were not detected in any of the microsporidian proteins that localise to the mitosomes of *E. cuniculi* (NFS1, mtHSP70, ISU1 and Frataxin) or *T. hominis* (NFS1, mtHSP70), (Williams et al., 2002; Tsaousis et al., 2008; Goldberg et al., 2008), and it seems likely that these mitosomal proteins rely on the non-cleavable internal targeting signals (Burri et al., 2006). MPP homologues have not been found

in available genome sequences of *E. cuniculi* and *T. hominis* (Katinka et al., 2001; Heinz et al., 2012) although MPP homologues can be highly divergent and difficult to identify using standard bioinformatics tools as was demonstrated in another mitosome-containing organism, *Giardia intestinalis* (Šmíd et al., 2008).

In *Saccharomyces cerevisiae*, another peptidase complex, the inner membrane peptidase (IMP), is responsible for the processing of proteins targeted to inner membrane and intermembrane space such as the cytochrome B2 and mtG3PDH precursors (Teixeira & Glaser, 2013). Imp2 gene was detected in an expressed sequence tag (EST) library from *A. locustae* (Williams & Keeling, 2005) and when expressed in *S. cerevisiae* (fused with GFP) it localized to the mitochondria of yeast (Burri et al., 2006). *A. locustae* mtG3PDH is so far the only microsporidian protein with a detectable targeting signal that seems to be cleaved off (Burri & Keeling, 2007; Burri et al., 2006). Two bands that migrate on polyacrylamide gels with the apparent relative molecular weights corresponding to a mature and a processed forms of mtG3PDH were detected in western blotting analysis of protein extracts from purified mitochondria from yeast expressing *A. locustae* mtG3PDH as well as from the purified *A. locustae* spores using specific antibodies (Burri et al., 2006). Relative intensity of the band corresponding to the mature mtG3PDH was seemingly lower when expressed in yeast lacking one of the IMP complex components (Imp1), which is consistent with processing of the *A. locustae* mtG3PDH by the IMP in yeast mitochondria (Burri et al., 2006). The IMP homologue has not been identified in the available genome sequences of *E. cuniculi* and *T. hominis* (Katinka et al., 2001; Heinz et al., 2012). *E. cuniculi* mtG3PDH does not localize to mitochondria when expressed in yeast and only one band that corresponds to the size of the full-length protein was detected in purified spores of *E. cuniculi* (Burri et al., 2006).

3.2 Aims

The presence of the genes encoding the AOX and glycerol-3-phosphate shunt components in *T. hominis* genome suggests that in addition to their role in iron sulfur cluster biosynthesis, the mitosomes of *T. hominis* might have retained their function in reoxidising NADH (Figure 3.6), a process required for continuous generation of ATP in glycolysis (Williams et al., 2010; Heinz et al., 2012). Intracellular stages of microsporidia are capable of stealing ATP from their hosts indicating that the alternative respiratory pathway may function in the environmental spores that cannot rely on the host rather than in the intracellular stages of the parasite (Heinz et al., 2012), (Figure 3.6).

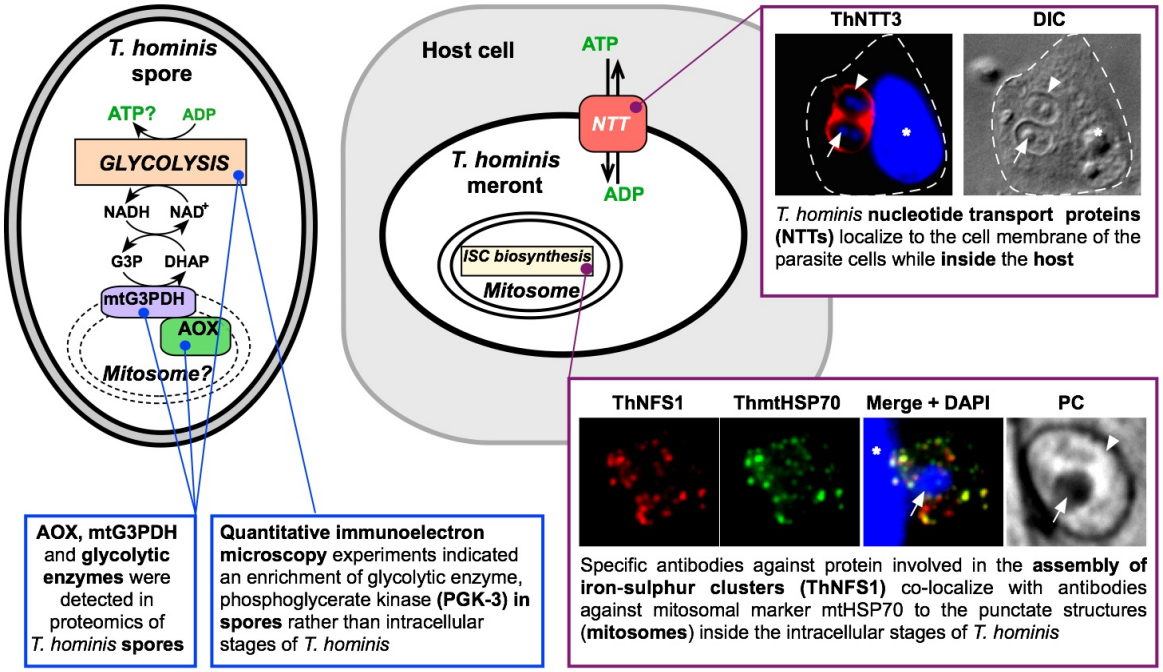

Figure 3.6 Summary of the available experimental data on functions of the mitosomes and the energy metabolism in the intracellular (meront) and the extracellular (spore) stages of *T. hominis*

Question marks indicate hypothetical role of glycolysis in ATP generation in spores and hypothetical localization of the AOX and mtG3PDH to *T. hominis* mitosomes.
Annotation of images: asterisk, host nucleus; dashed line, host cell; arrowhead, parasite cell; arrow, parasite nucleus.
Abbreviations: ISC, iron-sulfur cluster; mtG3PDH, glycerol-3-phosphate dehydrogenase; AOX, alternative oxidase; PC, phase contrast; DIC, Differential interference contrast

The main aim of this project was to generate specific polyclonal antibodies against the *T. hominis* alternative oxidase and mitochondrial glycerol-3-phospate dehydrogenase and use them in experiments designed to test the hypotheses that:

1. Homologues of alternative oxidase and mitochondrial glycerol-3-phosphate dehydrogenase localize to the mitosomes of *T. hominis.*

2. Alternative oxidase and mitochondrial glycerol-3-phosphate dehydrogenase are enriched in spores rather than the intracellular stages of *T. hominis.*

3.3 Results

3.3.1 Identification and bioinformatic analyses of microsporidian alternative oxidase and glycerol-3-P dehydrogenase homologues

Alternative oxidase

In published studies, a gene encoding microsporidian alternative oxidase (AOX) was identified in the partial genome sequence of *Antonospora locustae* as well as in DNA isolated from *Glugea plecoglossi*, *Spraguea lophii*, and *Trahipleistophora hominis* using PCR with degenerate primers (Williams et al., 2010). BlastP and tBlastN searches (Altschul et al., 1990) were performed using protein sequences of *Arabidopsis thaliana* AOX 2 (gi|9759397) and published *A. locustae* AOX (Williams et al., 2010) as queries in order to confirm a presence of the AOX gene in the available genome assemblies of microsporidia. In addition to *T. hominis* and *S. lophii* BlastP searches identified the AOX among annotated protein sequences of *Edhazardia aedis, Nematocida parisii* (isolates ERTm3, ERTm2, ERTm6) and *Vavraia culicis subsp*. *floridiensis.* tBlastN searches have identified additional sequences in the NCBI whole-genome shotgun contigs (WGS) databases of *Hamiltosporidium tvaerminnensis* and *Nematocida parisii* isolate ERTm1. Identified microsporidian protein sequences together with AOX sequences from diverse eukaryotes including *Trypanosoma brucei,* Fungi, and plants were used to generate a multiple sequence alignment (Figure 3.8). With the exception of a weakly conserved N-terminus microsporidian AOXs share a high level of identity with their homologues from other eukaryotes. Highly conserved residues involved in substrate and iron cofactor binding as well as proposed membrane interaction regions (Shiba et al., 2013) are

present in all microsporidian AOXs. One noticeable feature of microsporidian AOXs is the lack of an otherwise highly conserved tryptophan residue (W151 in *T. brucei*) that was suggested to play a role as an electron donor during catalysis (Moore & Albury, 2008).

In order to investigate a presence of the N-terminal mitochondrial targeting sequence, microsporidian AOXs were analysed using three different prediction programs (Table 3.1). Mitochondrial targeting signal was detected with high scores in *T. hominis* AOX by all three programs whereas in *V. culicis, S. lophii, and A. locustae* by at least one of the programs used. Neither of the programs detected the targeting signals with score above 50 % in *E. aedis* and *N. parisii.*

Table 3.1 Output of the analyses of the AOX homologues using different N-terminal targeting presequences prediction software

Species	Software used for prediction of mitochondrial localization		
	TargetP 1.1 (Emanuelsson et al., 2000)	Predotar (Small et al., 2004)	MitoProt II (Claros & Vincens, 1996)
T. hominis	**86.7%**	**81%**	**90%**
V. culicis	**50.5%**	**61%**	41%
S. lophii	44.6%	**70%**	46%
A. locustae	26.4%	0%	**73%**
E. aedis	11.2%	0%	44%
N. parisii	16.5%	1%	6%
T. brucei	**77.2%**	**61%**	**94%**
A. thaliana AOX2	**51.20%**	**56%**	**93%**

Scores over 50% are indicated in bold.

Length of the N-terminal region of microsporidian AOXs is variable and is the shortest in *N. parisii* AOX (Figure 3.7). Manual examination of the region upstream from the nucleotide sequence of the *N. parisii* AOX genes (in genome assemblies of all four *N. parisii* isolates available in NCBI: ERTm1, ERTm2, ERTm3, ERTm6) did not reveal any alternative start codons or any apparent insertions and/or deletions that could introduce a frameshift masking the alternative start codon (not shown). Cleavage site prediction in MitoProt II (Claros & Vincens, 1996) predicted a presence of a processing site in *A. locustae*, *T. hominis,* and *V. culicis.* TargetP 1.1 (Emanuelsson et al., 2000) analyses predicted presence of the cleavage site only in *T. hominis,* and *V. culicis* (Figure 3.7).

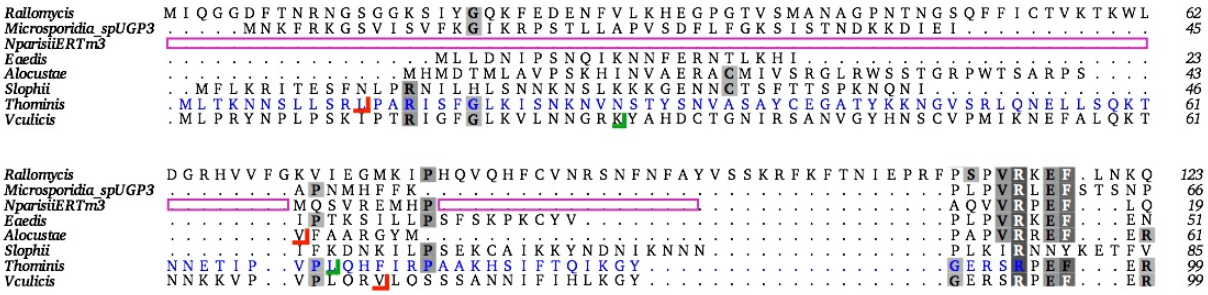

Figure 3.7 Alignment of N-terminal region of AOX homologues from microsporidia and Cryptomycota

N-terminus of *N. parisii* AOX is considerably shorter than the corresponding regions in other microsporidia as indicated with magenta box. TargetP 1.1 (green) and MitoProt II (red) cleavage site predictions were indicated. Blue text indicates a disordered region of *T. hominis* AOX predicted with high confidence in a Phyre2 analysis.

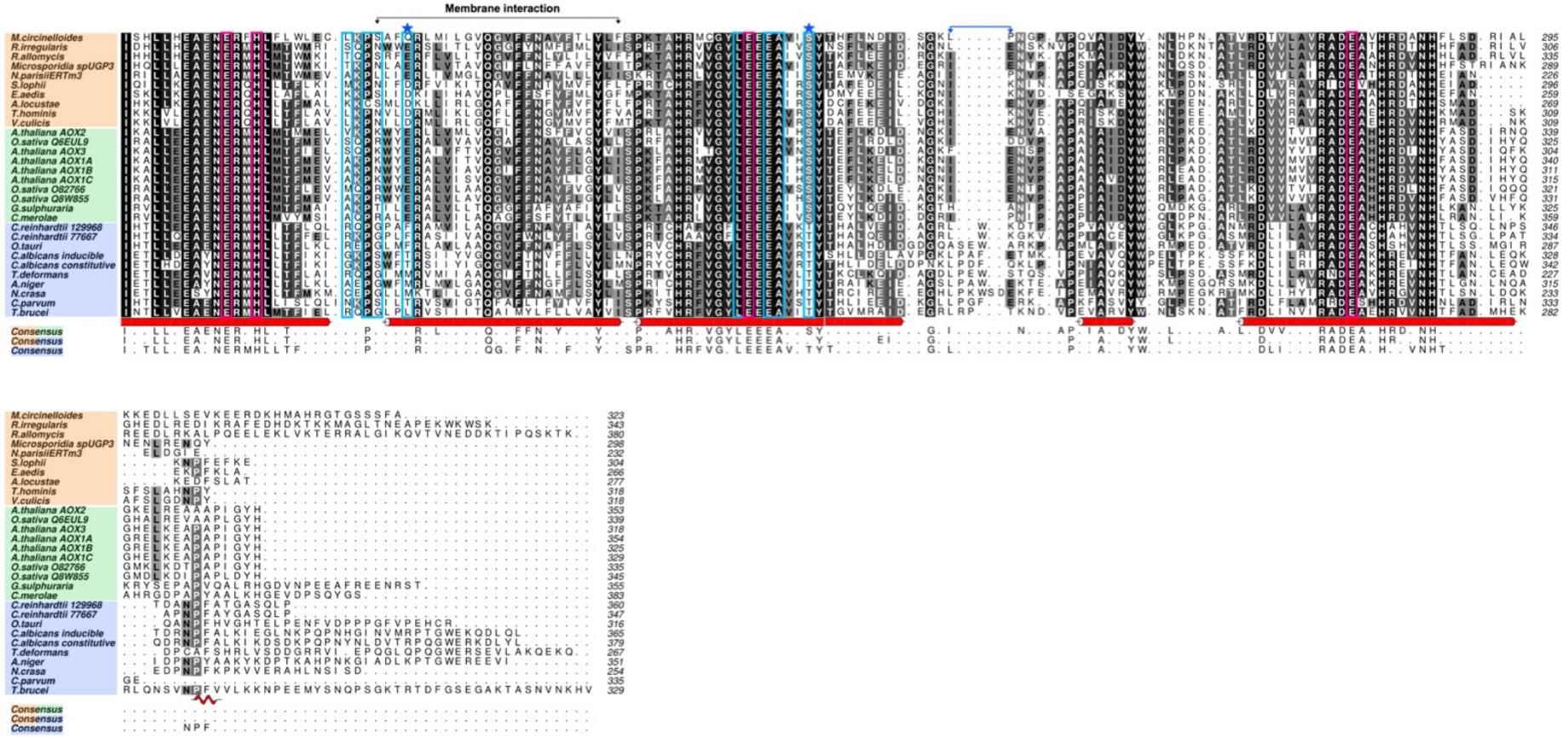

Figure 3.8 continued

Black arrow lines above the alignment indicate hydrophobic regions of AOX that were proposed to interact with the inner surface of the inner mitochondrial membrane. Some of the regions (blue arrow line) and sites (blue stars) that share high identity between microsporidia, Cryptomycota, basal fungi, plants and Red algae (Group 1) but not with Ascomycetes, Basidiomycetes, Green algae, *T. brucei* and *C. parvum* (Group 2) were indicated over the alignment. Three consensus sequences below the alignment correspond to the 80% consensus between the groups indicated by the colour coding. Alignment was generated using MUSCLE and formatted in ALINE, conserved residues were coloured using 'colouring by similarity' function implemented in ALINE with 0.5 low similarity cut-off.

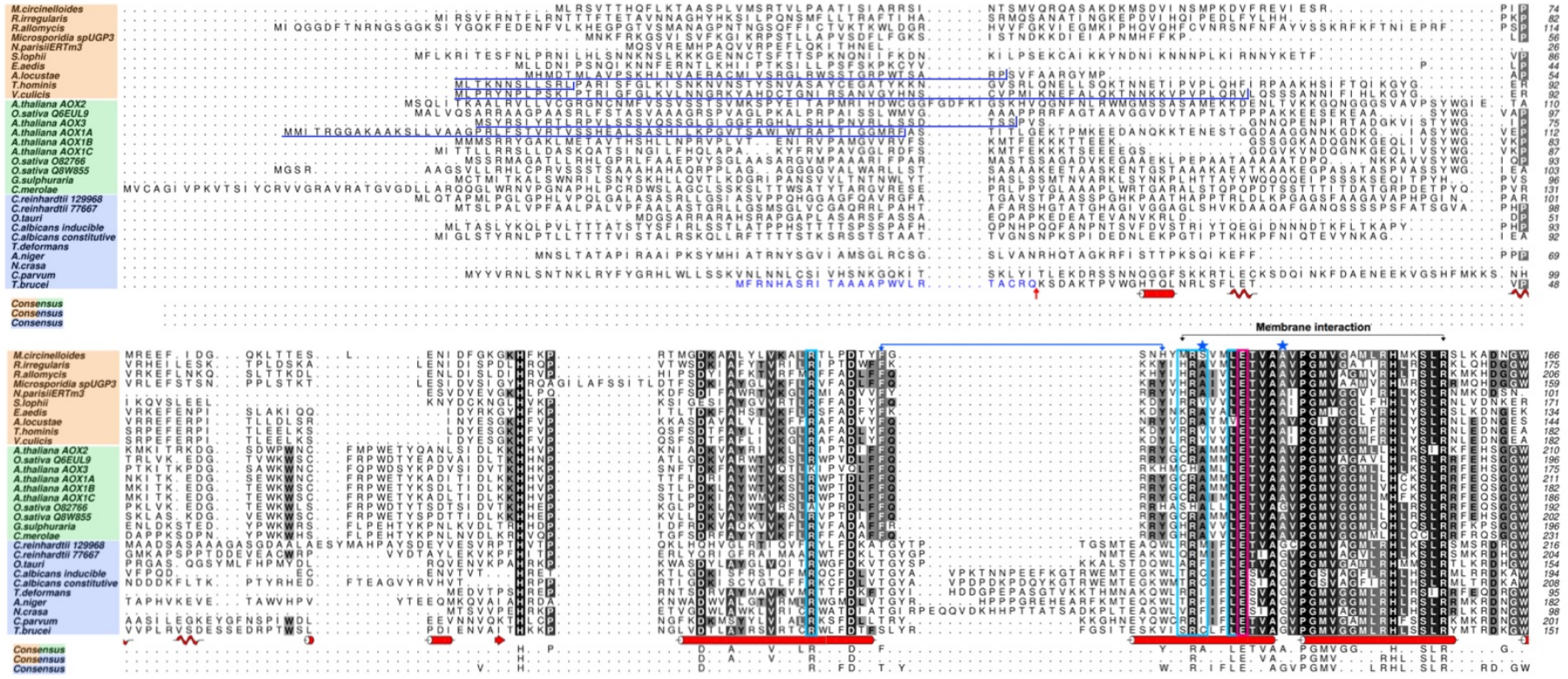

Figure 3.8 Multiple sequence alignment of AOX from different eukaryotes including Fungi, microsporidia and plants

Based on the results of phylogenetic analyses (**Figure 3.9)** AOX sequences were colour coded as follows: microsporidia, Cryptomycota and basal fungi (orange); plants and red algae (green); green algae, Fungi (Ascomycetes and Basidiomycetes), *Trypanosoma brucei* and *Cryptosporidium parvum* (blue). Secondary structure below the alignment corresponds to the structure of *Trypanosoma brucei* AOX (PDB id: 3W54), with α-helices presented as cylinders. The sites involved in binding of the iron cofactor (magenta box) and ubiquinol analogue Colletochlorin B (turquoise) in *T. brucei* AOX were mapped on the alignment. N-terminal sequences predicted to be cleaved off in MitoProt II analyses were indicated by a blue underline (all microsporidian sequences and two from *A. thaliana*: AOX3 and AOX1A were used in this analyses). The cleavage site predicted for A. thaliana AOX1A corresponds to that of *Glycine max* AOX (Tanudji, Sjöling, Glaser, & Whelan, 1999a). Blue text indicates a proposed processed N-terminus of *T. brucei* and red arrow indicates the cleavage site based on results from (Hamilton et al., 2014). (Figure legend continued below).

The secondary and tertiary structure of the *T. hominis* AOX was investigated using tools for protein structure prediction, modelling and analysis implemented in Phyre2 (Kelley et al., 2015). Both normal and intensive modes of Phyre2 identified structure of *T. brucei* AOX (PDB id, 3VVA; Chain, D) as the highest scoring homologue and used it as a template for modelling of *T. hominis* AOX (Figure 3.9). Models were generated with 100% confidence for 74% of the sequence (235 residues) excluding the N-terminus (75 residues). 3D model generated with the normal mode has a shape of a compact cylinder consisting of six α-helices and an extended N-terminal arm, similar to the *T. brucei* AOX (Shiba et al., 2013), (Figure 3.9 B and D). As sequences with significant similarity to N-terminus of *T. hominis* AOX were not identified in the intensive mode of Phyre2 the first 75 amino acids were modelled *ab initio* with the lowest confidence scores (Figure 3.9 F)**.** The N-terminal region modelled in the intensive mode seems to be poorly defined with a high proportion of loops to α-helices (turquoise) and has an additional α-helix at the N-terminus (blue), (Figure 3.9 C). The disordered region prediction implemented in the Phyre2 indicated the first 90 amino acids of *T. hominis* AOX as disordered with high confidence (Figure 3.9 G and Figure 3.7). Comparison of disordered region predictions for *T. hominis* AOX and *T. brucei* AOX using PONDR-FIT (Xue et al., 2010) showed similar pattern with the highest scores in the N-terminal and C-terminal regions of both sequences (not shown). In TMHMM (Krogh et al., 2001) analyses two hydrophobic helices were predicted (with probabilities of being a transmembrane helix ranging between 0.1 and 1) in all analysed AOX homologues in the regions that are predicted to be involved in interaction with a single leaflet of inner mitochondrial lipid bilayer (Figure 3.8), (Shiba et al., 2013).

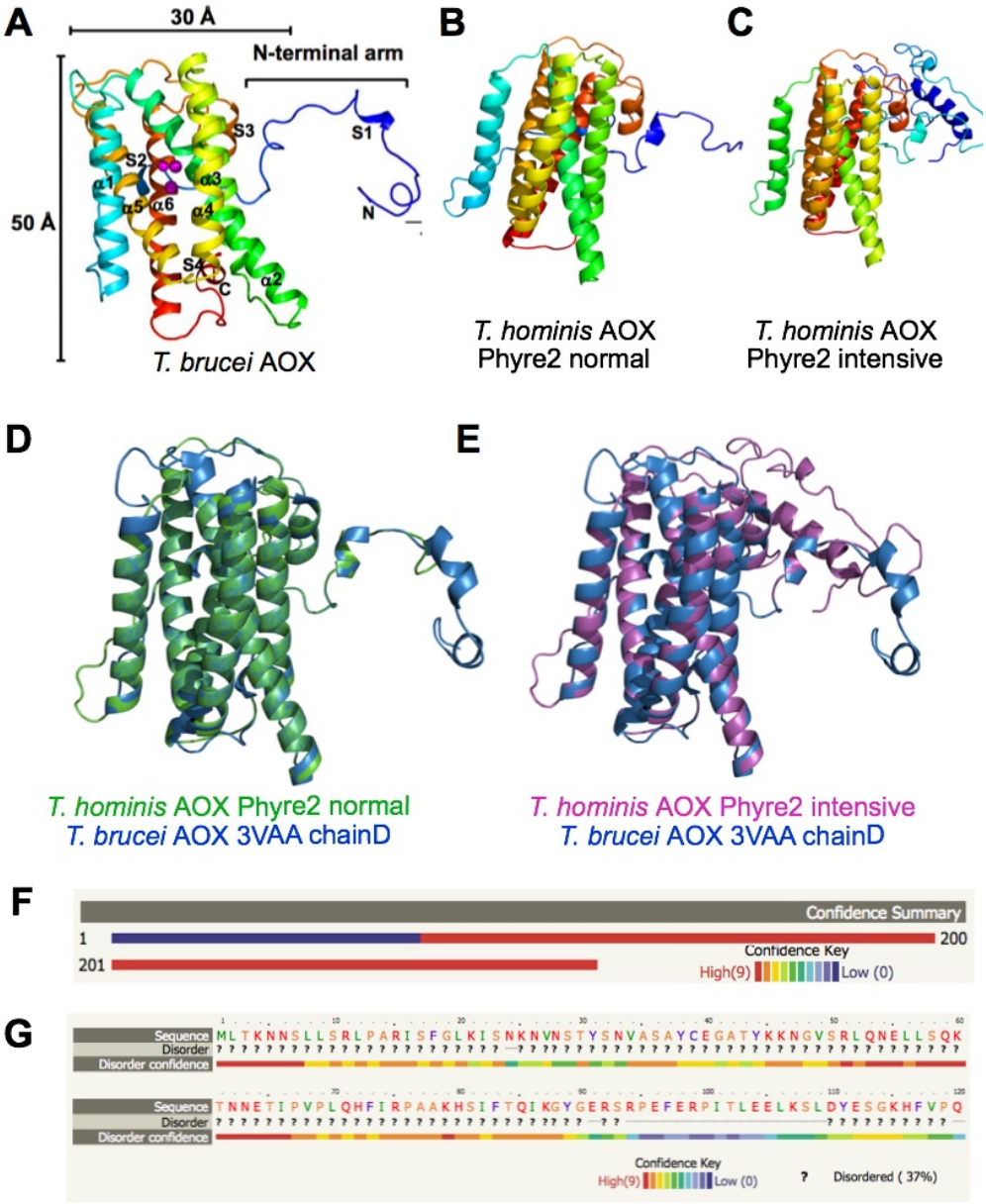

Figure 3.9 Models of *T. hominis* AOX structure generated using Phyre2
(A) was adapted from (Shiba et al., 2013).

The solved structure of *T. brucei* AOX (A) was used as a template to build 3D models of *T. hominis* AOX using normal (B) and intensive (C) modes in Phyre2. The solved structure of *T. brucei* AOX (A) lacks around 30 residues in both N- and C-terminal regions due to a low electron density (Shiba et al., 2013). Structures with significant similarities to the N-terminus of the *T. hominis* AOX were not identified and the first 75 amino acids are missing from the normal model (B). In the intensive mode of Phyre2 (C) the first 75 amino acids were modelled *ab initio* with the lowest confidence scores (F). Structure of *T. brucei* AOX was superimposed with the normal (D) and intensive (E) models of *T. hominis* AOX using PyMOL (Schrödinger, LLC, 2010). Models (A, B and C) were coloured with rainbow spectrum from N-terminus (blue) to C-terminus (red). (G) In Phyre2 analyses 37% of the *T. hominis* AOX structure (117 amino acids) was predicted to be disordered including the first 90 amino acids in the N-terminus of the protein. (F and G) were adapted from the output of Phyre2.

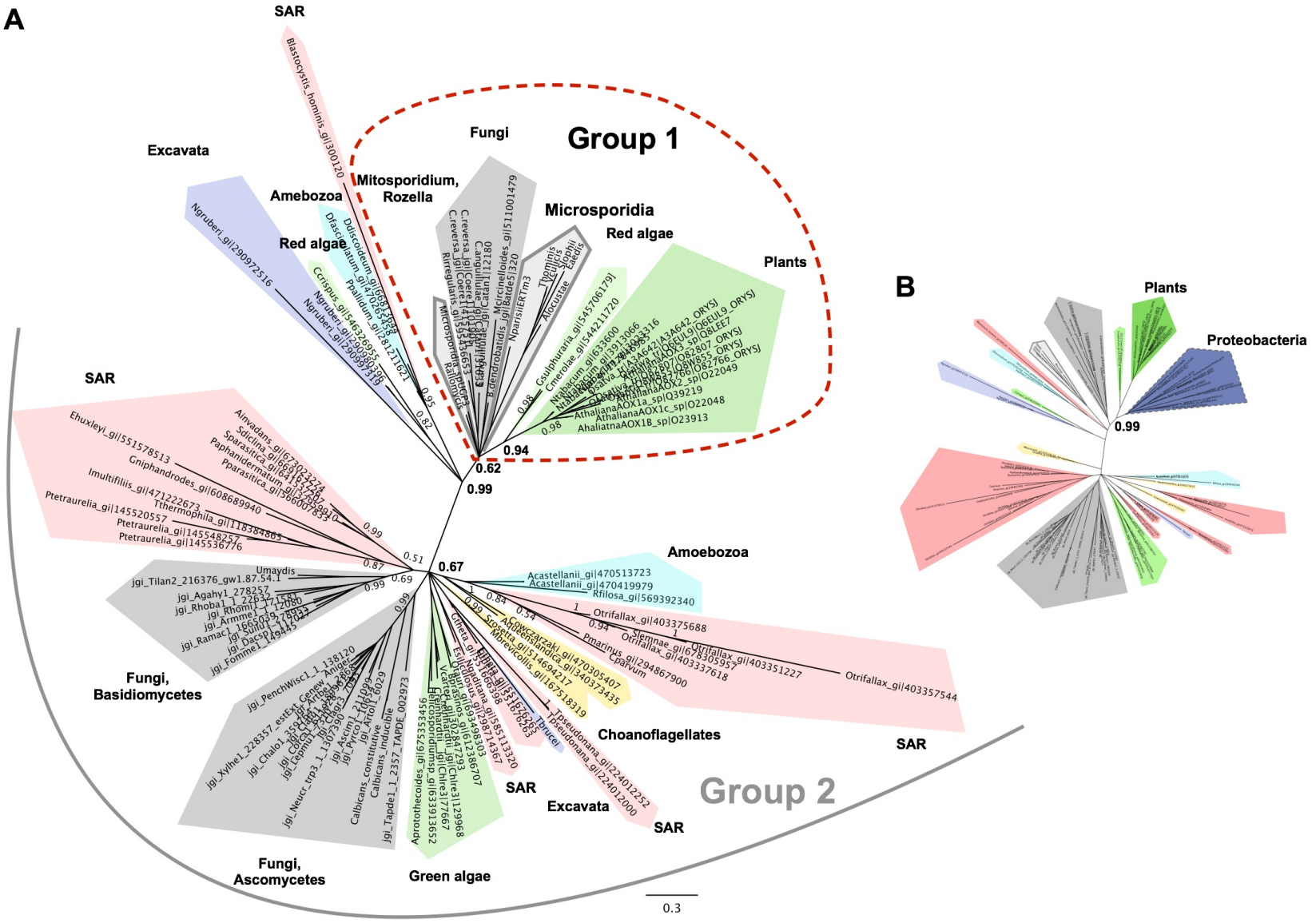

Figure 3.10 Bayesian phylogenetic trees of alternative oxidase homologues (figure legend on the next page)

Figure 3.10 Bayesian phylogenetic trees of alternative oxidase homologues

(A) Microsporidian alternative oxidases group together with the AOX homologues from basal fungal lineages, *Rozella allomycis*, *Mitosporidium sp*., plants and two species of red algae (Group 1, indicated with red dashed line). Ascomycetes, Basidiomycetes and green algae together with a majority of the eukaryotic lineages used in the analysis form a weakly resolved clade (Group 2) separated from microsporidia-plants clade by a relatively long branch with a high support (posterior probability of 0.99). A few distantly related eukaryotes including red alga (*Chondrus crispus*)*,* stramenopile (*Blastocystis hominis),* amoebozoan (*Dictyostelium discoideum*) and excavate (*Naegleria gruberi*) form long branches that originate at the polytomous node between Group 1 and Group 2. Observed tree topology is robustly supported in trees generated with different phylogenetic models (not shown) both in Bayesian (CAT20, CAT60, CAT60+LG, CAT+GTR, JTT+WLSR5) and Maximum likelihood framework (LG+I+G) and is consistent with previously published phylogenies of the AOX (Williams et al., 2010). The tree (A) was generated using PhyloBayes under the CAT model based on trimmed alignment of 106 sequences of 199 amino acid positions. Posterior probability support values were displayed only for the key branches. Scale bar represents estimated number of substitutions per site. SAR is a clade that includes stramenopiles, alveolates, and Rhizaria. AOX sequences were downloaded from NCBI and JGI Fungi Portal (ncbi, 'gi number'; jgi, 'protein id').

(B) After addition of AOX homologues from bacteria overall topology of the phylogenetic trees with a highly supported (posterior probability of 1) polytomous node between the Group 1 and the Group 2 remains unchanged. The bacterial homologues group together with plants and red algae with high support (posterior probability of 0.99). The tree (B) was generated using PhyloBayes under the JTT+WLSR5 model based on trimmed alignment of 120 sequences of 197 amino acid positions. Trees with similar topologies and support values were generated using CAT60 model in PhyloBayes and LG+I+G model (selected based on ProtTest analyses) in RAxML (not shown). Posterior probability support values were displayed only for the bacteria/plants/red algae branch. Same colours as in (A) were used to indicate different eukaryotic lineages. Bacterial AOX sequences downloaded from NCBI ('gi number' sequence identifiers): *Roseovarius sp* (gi495554606), *Erythrobacter sp* (gi494287767), *Caulobacter sp* (gi659861944), *Sphingomonas sp* (gi657924111), *Methylotenera versatilis* (gi502914340), *Acidovorax sp* (gi495130245), *Thiobacillus denitrificans* (gi|499631708), *Marinobacter sp* (gi504684205), *Fangia hongkongensis* (gi517109453), *Rheinheimera perlucida* (gi648657488), *Methylophaga thiooxydans* (gi697966896), *Methylophaga thiooxydans* (gi495565675), *Psychromonas sp* (gi646619169), *Vibrio campbellii* (gi498332416).

Phylogenetic analyses of the eukaryotic alternative oxidases generate the trees with large number of unresolved relationships (polytomies) and with two relatively well-defined polyphyletic groups (Figure 3.10). The first group includes alternative oxidases from plants, Red algae, microsporidia and closest relatives of microsporidia: Cryptomycota (*Rozella allomycis), Mitosporidium daphniae,* and basal fungi including representatives of Glomeromycota (*Rhizophagus irregularis*), Mucoromycotina (*Mucor circinelloides*), and Chydridomycota (*Batrachochytrium dendrobatidis*). The grouping of microsporidian AOX with the homologues from their closest relatives is consistent with a vertical inheritance from the last common ancestor of these organisms. The second group includes the AOX homologues from the majority of the diverse eukaryotic taxa used in the analyses. Both groups are poorly resolved (polytomies) and are weakly supported (posterior probabilities of: Group 1, 0.62; Group 2, 0.67) but they are separated by a relatively long branch at the base of the Group 2 and the polytomous node between them is highly supported (posterior probability of 0.99). Similar trees were generated in phylogenetic analysis using different evolutionary models both in Bayesian (CAT20, CAT60, CAT60+LG, CAT+GTR, JTT+WLSR5) and Maximum likelihood framework (LG+I+G).

It is noteworthy that the AOX from Dikarya (Ascomycota and Basidiomycota) do not group with homologues from their closest relatives (i.e. basal fungi), and AOX from Green algae do not group with the homologues from Red algae and plants. The AOX from both Dikarya and green algae group together with AOX from unrelated taxa within the group 2. In order to investigate the possible presence of conserved structural features that can be used to discriminate between the Group 1 and the Group 2, the multiple sequence alignment of the AOX homologues was re-examined. Manual analyses of the alignment together with the analyses of consensus of the sequences from either the Group 1 or the Group 2 has revealed a presence of some conserved features that seem to be present in sequences from one of the groups but not the other (Figure 3.8). These group-specific features include a presence of an insertion in N-terminal region of the AOX homologues from the Group 2.

Bacterial homologues of the AOX were identified only in Proteobacteria using BlastP and tBlastN searches. In phylogenetic analyses the bacterial homologues group strongly (posterior probabilities of 1) with the AOX from plants and Green algae (Figure 3.9 B).

Cytoplasmic glycerol-3-phosphate dehydrogenase

BlastP searches identified homologues of cytoplasmic NAD-dependent glycerol-3-phosphate dehydrogenase (cytG3PDH) in all microsporidian genomes available in the NCBI database. Multiple sequence alignment (Figure 3.11) indicates that primary structure of the microsporidian cytG3PDH seems to be well conserved in comparison to the homologues from other eukaryotes. Residues involved in substrate (1,3-dihydroxyacetone phosphate) binding are conserved in all microsporidian sequences with the exception of that from *S. lophii.* Sites involved in binding of nicotinamide adenine dinucleotide (NAD) cofactor in the *Homo sapiens* GPD1 are more variable in microsporidian homologues as they are also less conserved in a number of other eukaryotes including glycosomal GAPDH from *T. brucei*.

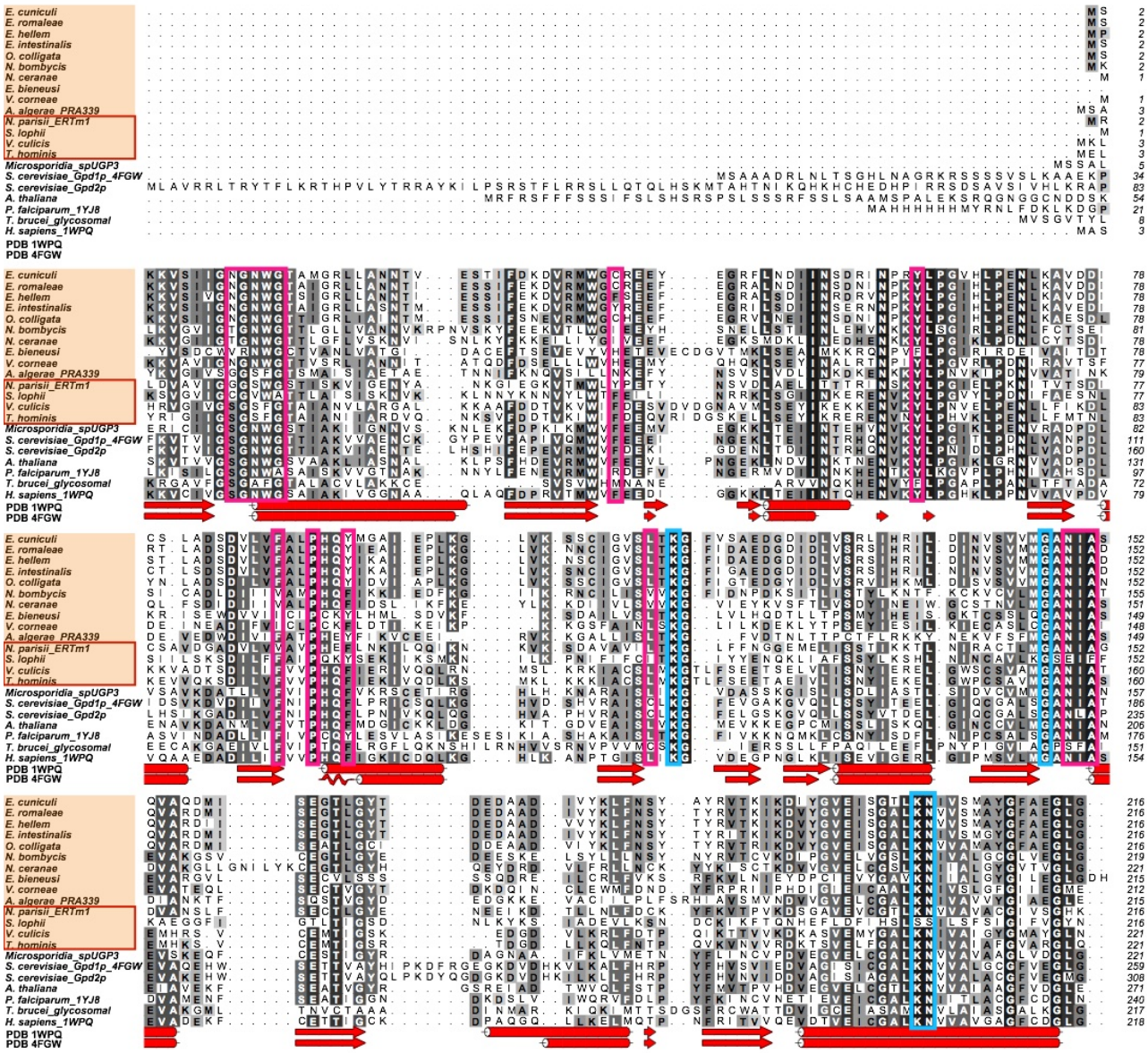

Figure 3.11 Multiple sequence alignment of cytoplasmic G3PDH homologues from microsporidia and other eukaryotes, and glycosomal homologue from *T. brucei*

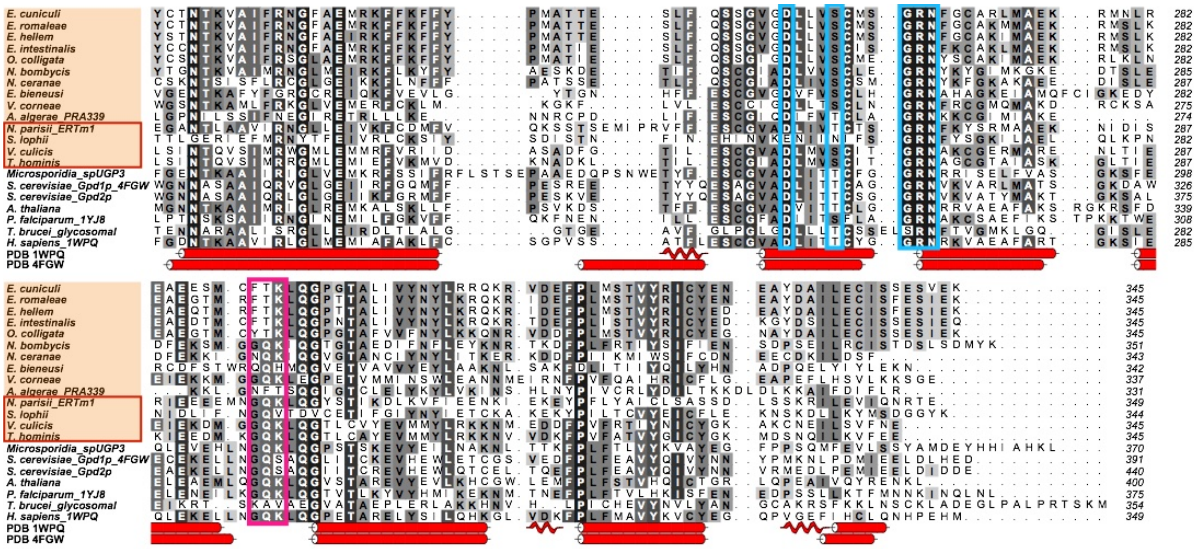

Figure 3.11 continued

Sequences of microsporidian cytG3PDH are indicated in orange. The AOX coding gene was found in genomes of species indicated with the red boxes. Secondary structures below the alignment correspond to the structure of *Homo sapiens* GPD1 (PDB id: 1WPQ) and *Saccharomyces cerevisiae* Gpd1p (PDB id: 4FGW). α-helices are presented as cylinders and β-strands are presented as arrows. The sites involved in binding of the nicotinamide adenine dinucleotide (NAD) cofactor (magenta) and 1,3-dihydroxyacetone phosphate (turquoise) in *Homo sapiens* GPD1 were mapped on the alignment. Alignment was generated using MUSCLE and formatted in ALINE, conserved residues were coloured using 'colouring by similarity' function implemented in ALINE with 0.15 low similarity cut-off.

Mitochondrial glycerol-3-phosphate dehydrogenase

Microsporidian homologues of a mitochondrial FAD dependent glycerol-3-phosphate dehydrogenase (mtG3PDH) were identified in all analysed microsporidian genomes with the exception of *E. bieneusi* and *A. algerae.* The sequences of microsporidian mtG3PDH share a high level of identity with the homologues from other eukaryotes and bacteria including the residues involved in binding of a substrate (1,3-dihydroxyacetone phosphate) and a cofactor (NAD), (Figure 3.12). The N-terminus of the protein is the least similar region of the eukaryotic homologues and is missing from the bacterial homologues. TargetP 1.1 (Emanuelsson et al., 2000) and Predotar (Small et al., 2004) analyses predicted the presence of N-terminal mitochondrial targeting signals (scores above 50 %) only in homologues from *E. romaleae* and *V. corneae* (Table 3.2). The same analyses also failed to detect the targeting signal in the characterized mitochondrial mtG3PDH from *T. brucei*. Targeting signals were detected in mtG3PDH from model organisms (*S. cerevisiae* and *A. thaliana*) as well as a putative mtG3PDH from *T. brucei* that as opposed to the other mtG3PDH homologue was suggested to localize to the outer

mitochondrial membrane (Škodová et al., 2013). MitoProt II (Claros & Vincens, 1996) analyses have detected the presence of mitochondrial targeting signals with score above 50 % in all sequences analysed except homologues from *T. hominis, V. culicis, N. parisii, O. colligata* and *N. bombycis.* In TMHMM analyses (Krogh et al., 2001) all microsporidian sequences with the exception of *E. hellem*, *E. romaleae* and *N. parisii* had a predicted (with probabilities ranging between 0.8 and 1) N-terminal transmembrane (TM) helix of around 20 amino acids in length. In the output of the analysis this TM helix was indicated as a possible N-terminal targeting signal. Outside of microsporidia the TM helix was only predicted in *T. brucei* (putative) mtG3PDH. Additional TM helix was predicted with high probability (probability score: 0.9) in the *A. locustae* mtG3PDH (residues 160 – 182) while the same region was indicated with low probabilities in *T. hominis* (0.3) and *V. culicis* (0.7). In *S. cerevisiae* regions corresponding to the predicted *A. locustae* TM helices were also predicted in TMHMM analysis with low probability scores (N- terminal helix, 0.2; the internal helix 0.4).

Table 3.2 Output of the analyses of the mtG3PDH homologues using different N-terminal targeting presequences prediction software

Species	Software used for prediction of mitochondrial localization		
	TargetP 1.1 (Emanuelsson et al., 2000)	Predotar (Small et al., 2004)	MitoProt II (Claros & Vincens, 1996)
T. hominis	13.9% (ER 57.5%)	2% (ER 89%)	45.3%
V. culicis	7.3% (ER 81.2%)	1% (ER 85%)	18.2%
S. lophii	4.7% (ER 84.9%)	3% (ER 99%)	96.9%
A. locustae	32.2% (Other 44.3%)	25% (Other 74%)	65.6%
E. cuniculi	19% (ER 92.1%)	2% (ER 99%)	61.4%
N. parisii	4% (ER 78%)	1% (Other 97%)	14.3%
E. hellem	22.5% (ER 82.2%)	3% (ER 99%)	84%
E. romaleae	31% (Other 66.6%)	92%	72.4%
E. intestinalis	18.6% (ER 82%)	3% (ER 99%)	64.7%
O. colligate	26.4% (ER 79.2%)	2% (ER 99%)	42.7%
N. ceranae	11.1% (ER 78.4%)	4% (ER 99%)	60.7%
E. aedis	10.3% (Other 73%)	10% (Other 89%)	56.6%
N. bombycis	8.5% (ER 92.3%)	2% (ER 99%)	11.2%
V. corneae	50.1%	6% (Other 94%)	58.5%
N. apis	4.2% (ER 93.2%)	3% (ER 99%)	69.9%
S. cerevisiae	80.2%	80%	62%
T. brucei	12.5% (Other 60.9%)	5% (Other 94%)	79%
T. brucei (putative)	88.4%	61%	90%
R. allomycis	56.2%	25% (Other 44%)	83%
A. thaliana	50.4%	49% (Other 42%)	68%

Scores over 50% were indicated in bold. In case of the scores below 50% the score for predicted presence of a signal peptide targeting to the endoplasmic reticulum (ER) or an unspecified (Other) was indicated.

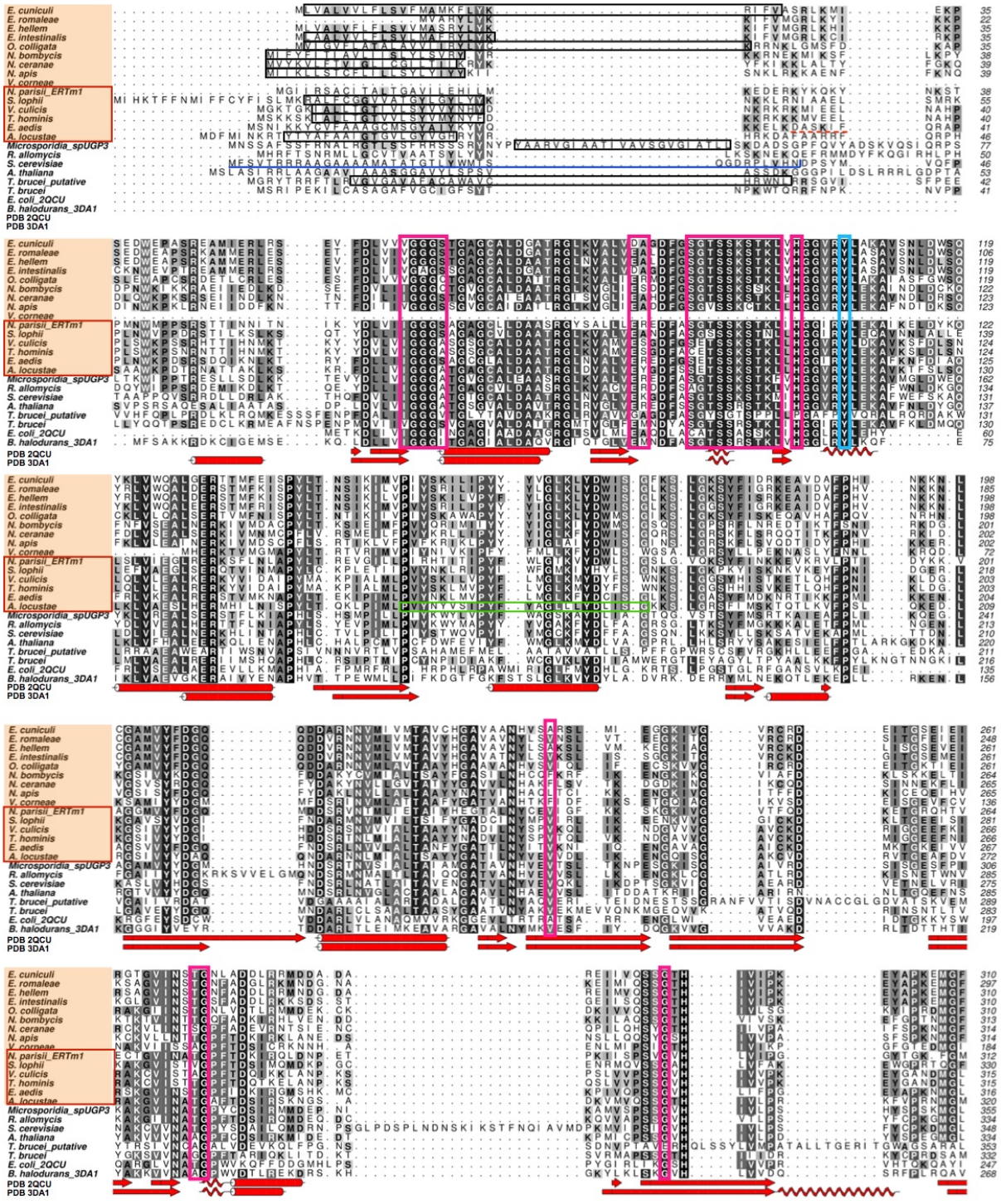

Figure 3.12 Multiple sequence alignment of mitochondrial G3PDH homologues from microsporidia, other eukaryotes and bacteria

Sequences of microsporidian cytG3PDH were indicated in orange. The AOX coding gene was found in genomes of species indicated with the red boxes. Secondary structures below the alignment correspond to the structure of sn-glycerol-3-phosphate dehydrogenase (GlpD) from *Escherichia coli* (PDB id: 2QCU) and *Bacillus halodurans* (PDB id: 3DA1). Black and green boxes indicate transmembrane helices predicted in TMHMM analysis. Red dashed underline indicates a region where a potential processing site in *A. locustae* sequences was indicated in analysis by (Burri et al., 2006), (figure legend continued on next page)

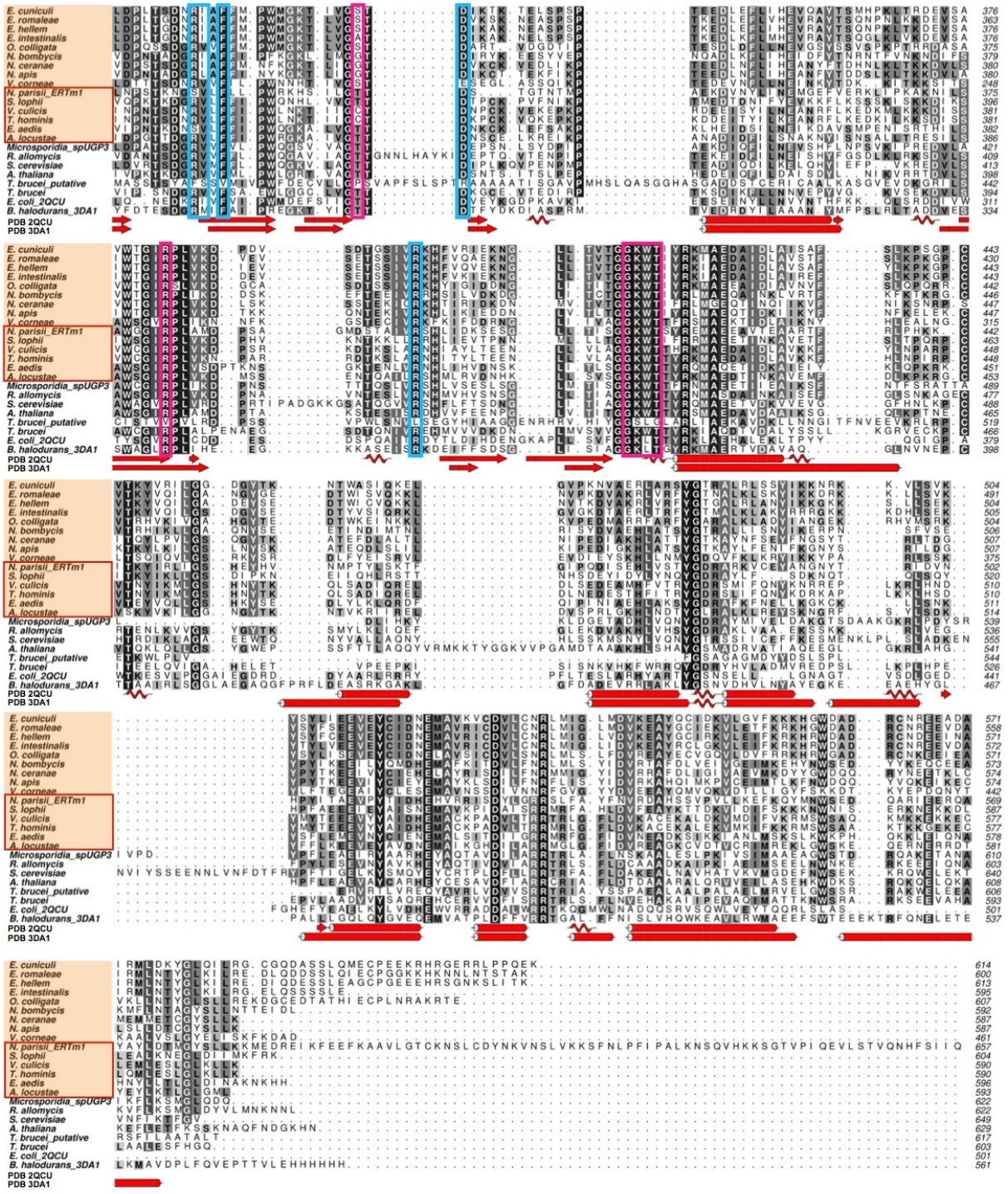

Figure 3.12 continued

Cleavable N-terminal presequence of *S. cerevisiae* Gut2P was indicated with the blue underline (K. Esser et al., 2004). α-helices are presented as cylinders and β-strands are presented as arrows. The sites involved in binding of the flavin adenine dinucleotide (FAD) cofactor (magenta) and 1,3-dihydroxyacetone phosphate (turquoise; PDB id: 2R4E) in *E. coli* GlpD were mapped on the alignment. Alignment was generated using MUSCLE and formatted in ALINE, conserved residues were coloured using 'colouring by similarity' function implemented in ALINE with 0.15 low similarity cut-off.

3.3.2 Cloning and expression of T. hominis AOX, mtG3PDH and mtHSP70 homologues for polyclonal antibodies production

T. hominis mtG3PDH (orf_1639) gene excluding first 393 nucleotides on the 5' terminus, and 21 nucleotides on the 3' terminus was amplified from *T. hominis* genomic DNA using primers with a 5' CACC overhang (forward primer) required in TOPO cloning protocol and TAA stop codon at the 3' terminus. The first 108 nucleotides of removed 5' sequence correspond to a potential N-terminal targeting signal that may be proteolytically cleaved and hence not present in mature *T. hominis* mtG3PDH. The remaining 285 nucleotides correspond to an amino acid sequence sharing a high level of identity with the mtG3PDH homologue from the rabbit host that could cause antibodies raised against this sequence to potentially cross-react with the host protein. 21 nucleotides on the 3' terminus were removed due to problems with gene amplification using primers complementary to this sequence.

Full-length nucleotide sequence of *T. hominis* mtHSP70 excluding the start codon (ATG) was amplified from *T. hominis* genomic DNA using primers with a 5' CACC overhang (forward primer) required in TOPO cloning protocol.

Amplified sequences of *T. hominis* mtHSP70 and mtG3PDH were cloned into pET100 plasmid (Directional TOPO® cloning Kit). Sequencing of three clones of each construct confirmed correct insertion of the sequence into the plasmid. The recombinant proteins of expected size (recombinant mtG3PDH, 56 kDa; recombinant mtHSP70, 64 kDa) were expressed using a standard IPTG induction protocol in *E. coli* BL21 (DE3) transformed with pET100-*th*mtg3pdh (Figure 3.13 C and F) or pET100-*th*mthsp70 plasmids' constructs (Figure 3.13 B and E). The expected size of the proteins was calculated using using ExPASy "Compute pI/Mw tool" (http://web.expasy.org/compute_pi/).

Due to the presence of potential membrane interaction domains that could be poorly accessible to the antibodies, a synthetic *Th*AOX gene, which does not contain these regions was designed. Two 90-nucleotide long fragments that encode the amino acid sequences predicted to be transmembrane helices in TMHMM analysis and that map onto to the potential membrane interaction domains in the solved structure of *T. brucei* AOX (Figure 3.7 and Figure 3.9), (Shiba et al., 2013) were removed from *T. hominis* AOX gene sequence. The ATG start codon was removed from the synthetic AOX gene sequence and 5' KpnI and 3' PstI restriction sites were added. The synthetic gene was synthesized and subsequently cloned into pQE40 vector in frame with a mouse DHFR fusion protein by GenScript

(http://www.genscript.com). DHFR (dihydrofolate reductase) itself displays little immunogenicity in mouse and rat, can enhance antigenicity and stability of the fusion protein and it is recommended for poorly expressed proteins (QIAGEN, 2003). The synthetic *Th*AOX was fused with the DHFR in order to increase chances of high levels of expression in *E. coli* and increase the antigenicity of the fusion protein. The recombinant protein of expected size (53 kDa) was expressed using a standard IPTG induction protocol in *E. coli* M15 transformed with the pQE40-*th*aox plasmid (Figure 3.13 A and D).

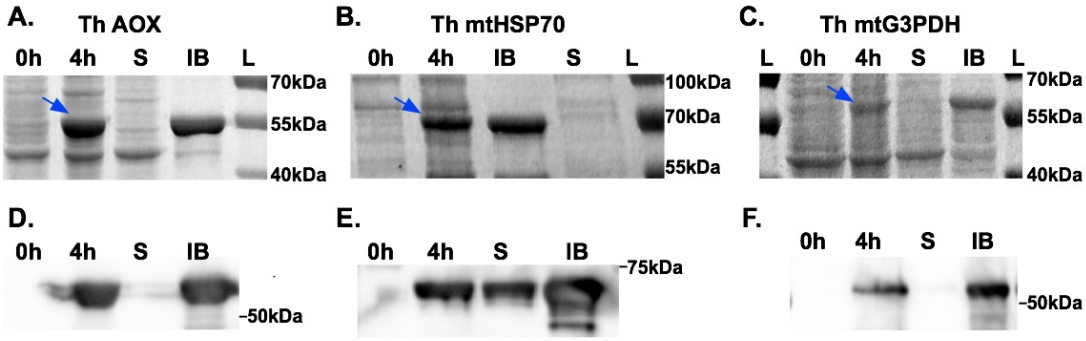

Figure 3.13 Expression and purification of *T. hominis* AOX, mtG3PDH and mtHSP70 from *E. coli*.

(A, B and C) Coomassie blue stained SDS polyacrylamide gels. Protein bands (blue arrows) corresponding to the expected molecular weights (A, 53 kDa; B, 64 kDA, C, 56 kDa). Samples loaded onto the gels: insoluble inclusion bodies (IB), soluble protein fraction (S). Molecular weight values correspond to the protein ladder bands (L).

(D, E and F) The same samples as in (A, B, C) were used in western blotting experiments with anti-His tag antibodies conjugated to HRP.

Recombinant *Th*AOX, *Th*mtG3PDH and *Th*mtHSP70 were extracted from bacteria and purified using BugBuster kit (Figure 3.13). All recombinant proteins were found mostly in the insoluble fraction. Recombinant *Th*mtHSP70 was also detected in soluble fraction using western blotting (Figure 3.13 E), however its concentration was below the detection limit of Coomassie blue (Figure 3.13 B). Around 1 mg of purified *Th*AOX, *Th*mtG3PDH and *Th*mtHSP70 inclusion bodies were run on SDS polyacrylamide gels and InstantBlue stained bands corresponding to the proteins were cut out of the gels and sent to Agrisera (http://www.agrisera.com/) for immunisation of rabbits (*Th*AOX, *Th*mtG3PDH) and rats (*Th*mtHSP70).

3.3.3 Testing of polyclonal antisera raised against recombinant T. hominis and AOX, mtG3PDH and mtHSP70 using western blotting

In western blotting experiments with rat polyclonal sera raised against recombinant *T. hominis* mtHSP70 a single band with an apparent relative molecular weight (rMW) of approximately 60 kDa was detected in extracts from *T. hominis* spores and *T. hominis* infected rabbit kidney cells (RK13) but not in extracts from the non-infected host (Figure 3.14 C). A band of the same size was detected using characterized rabbit anti-*Th*mtHSP70 antisera (Williams et al., 2002).

Weak parasite specific signals with a very high uniform background were detected in western blotting experiments with rabbit polyclonal sera raised against the recombinant *T. hominis* AOX and mtG3PDH (Figure 3.14 A and Figure 3.15 A**)**. In order to reduce the background (potentially caused by a presence of antibodies binding to milk used as the blocking agent) and to increase the concentration of specific antibodies the polyclonal sera were affinity purified against the recombinant *Th*AOX and *Th*mtG3PDH.

Affinity purified anti-*Th*AOX antibodies detected a single band in *T. hominis* spores with an apparent rMW of approximately 24 kDa (Figure 3.14 B**)**. A single band of the same rMW was also detected in *T. hominis spores* with monoclonal antibodies against plant AOX isolated from *Sauromatum guttatum* (Agrisera, AS10699). Monoclonal antibodies against plant AOX were already shown to detect microsporidian homologues on western blots (Williams et al., 2010). The observed MW is significantly lower than 36 kDa predicted (compute pI/Mw tool, ExPASy) for the full length *T. hominis* AOX. The difference between the predicted and the apparent molecular weight may reflect posttranslational modifications (e.g. removal of an N-terminal targeting signal during import of the protein to the mitosomes) and/or partial protein degradation during protein extraction process. All protein extracts were prepared with proteinase inhibitors and boiling of the protein extracts does not seem to affect the migration pattern as the 24 kDa band was detected in boiled (95°C) and non-boiled (30°C) protein extracts. The same band was also detected in protein extracts prepared in non-reducing conditions (Laemmli buffer without DTT, Figure 3.14 E).

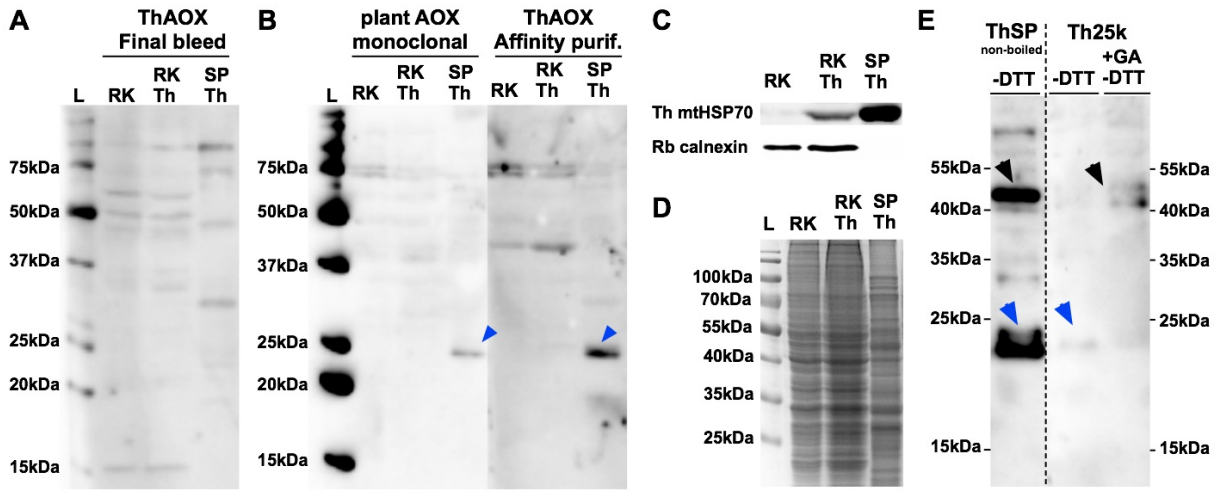

Figure 3.14 Testing the specificity of the anti-*Th*AOX and anti-*Th*mtHSP70 antibodies antibodies in total protein extracts from *T. hominis* spores, *T. hominis* infected and non-infected rabbit kidney (RK-13) cells

(A) Polyclonal antiserum from the final bleed of a rabbit immunised with the recombinant *T. hominis* AOX (1:200 dilution) was tested against total protein extracts from purified *T. hominis* spores (**SPTh**), *T. hominis* infected rabbit kidney cells (**RKTh**) and non-infected rabbit kidney cells control (**RK**). At least four parasite specific bands (not present in the RK control) had very week intensities and were detected only in the extracts from spores (SPTh).

(B) ThAOX antisera affinity purified against the immunogen (1:200 dilution of 0.2 mg/ml stock) and commercial monoclonal antibodies against plant AOX (Agrisera, 1:50 dilution) detect a single parasite specific band migrating with apparent molecular weights of ~24 kDa (**blue arrowhead**) in the parasite spores but not in the *T. hominis* infected RK cells and non-infected RK cells control.

(C) Rat anti-*Th*mtHSP70 antisera (1:1000 dilution) detect single band migrating with an apparent molecular weight of ~60 kDa in protein extracts from *T. hominis* infected RK cells and *T. hominis* spores but not in non-infected RK cells control. Commercial antibodies against **mammalian** calnexin detect single band (~80 kDa) in **RK** and **RKTh** but not in purified spores (**SPTh**).

(D) Coomassie blue stained polyacrylamide gel with total protein extracts from **RK**, **RKTh** and **SPTh**. Approximately 20 µg (based on BCA assay) of each extract was loaded onto the gel. The gel is an equivalent of the gels used in western blotting experiments (A), (B) and (**Figure 3.15).**

Blot probed with the affinity purified anti-ThAOX antibodies was exposed for 160 s in order to visualize all bands. Blot probed with final bleed was exposed for 10 s, as 160 s exposure time caused a uniform high background (completely black blot) possibly due to the cross-reaction of antibodies in the serum with the blocking reagent (milk).
Molecular weight of the bands was estimated using 'MW analysis tool' implemented in the Image Lab (Bio-Rad). Precision Plus Protein™ WesternC™ standard (Bio-Rad) was used in (A) and (B). PageRuler protein ladder (Thermo Scientific) was used in (D).

(E) Result of a preliminary experiment testing presence of the AOX dimer in *T. hominis* mitosomes based on (Umbach & Siedow, 2000). The resuspended 25.000 x g pellet from cell fractionation of RK13 cells infected with *T. hominis* (as in section 2.24 but all buffers were prepared without the addition of DTT) was split in half: the first aliquot was treated by the addition of Laemmli sample buffer without DTT **(-DTT)**; the second aliquot was incubated with 0.01 % glutaraldehyde for 30 minutes at room temperature followed by neutralization with 0.1 M Glycine, 0.1 M TRIS, pH 7.5 and addition of Laemmli - DTT **(+GA -DTT)**. Protein extract from purified *T. hominis* spores were prepared by suspending the spores in the Laemmli -DTT and heating the sample at 37°C for 10 min **(ThSP non-boiled)**. Bands corresponding to the observed size of the *Th*AOX monomers (24 kDa, **blue arrowheads**) and predicted size of the dimeric form (48 kDa, **black arrowheads**) were observed. As could be expected the band corresponding to the AOX dimer was more prominent in the protein extracts from mitosome enriched fraction (25.000 x g) treated with the cross-linking agent, glutaraldehyde.

Published (Williams et al., 2010) western blotting experiments with membrane preparations from *E. coli* expressing the full-length recombinant *T. hominis* AOX show that the recombinant protein migrates with a similar apparent rMW (not specified) to the AOX purified from plant (*Sauromatum guttatum*), (Williams et al., 2010). The plant AOX usually migrates with an apparent rMW (36 kDa) close to the predicted value (Elthon et al., 1989). In the western blots with recombinant *T. hominis* AOX, bands of lower rMW than the that of full-length protein were also detected indicating that the protein may be prone to proteolysis during the extraction process (Williams et al., 2010).

Polyclonal antisera from the final bleeds of rabbits immunised with the recombinant *T. hominis* mtG3PDH detected parasite specific bands (not present in the RK control) of very week intensities and were detected only in the extracts from spores (SPTh, Figure 3.15 A). Affinity-purified anti-*Th*mtG3PDH antibodies detected two major bands of apparent rMWs of approximately 61 kDa and 70 kDa in the protein extracts from purified *T. hominis* spores (Figure 3.15 B). This result seems to be consistent with published western blotting data with specific antibodies against *A. locustae* mtG3PDH where two bands corresponding to predicted size of unprocessed (66 kDa) and mature (61 kDa) mtG3PDH were detected in protein extracts from *A. locustae* spores (Burri et al., 2006). The 70 kDa band detected in purified *T. hominis* spores seems to correspond to the the full-length *T. hominis* mtG3PDH (67 kDa). Bands of apparent rMW of around 70 kDa were also detected in uninfected host indicating that the antibodies cross-react with a host protein of similar size to the possible full-length *T. hominis* mtG3PDH. The likely candidate could be a mature form of the rabbit homologue of mtG3PDH (gpd2), (Lu et al., 2008). Rabbit and *T. hominis* sequences share the highest identity at N-terminus that was removed from the recombinant *T. hominis* mtG3PDH in order to reduce the possibility of cross-reaction of the antibodies. However, the two sequences also share relatively high identity in other regions of the alignment that may be long enough to serve as epitopes responsible for potential cross-reactivity. Due to the cross-reactivity the presence of *T. hominis*-specific 70kDa band in the infected RK cells could not be verified. The major band migrating with the rMW of 61 kDa seems to correspond to the mature form of mtG3PDH detected in *A. locustae* spores and is only detected in spores and infected host and not in non-infected host control.

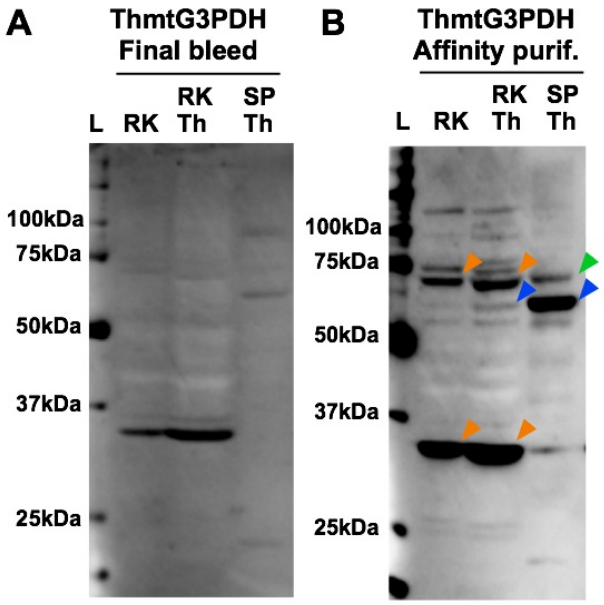

Figure 3.15 Testing the specificity of the anti-*Th*mtG3PDH in total protein extracts from *T. hominis* spores, *T. hominis* infected and non-infected rabbit kidney (RK-13) cells using western blotting

(A) Polyclonal antiserum from the final bleed of a rabbit immunised with the recombinant *T. hominis* mtG3PDH (1:200 dilution) was tested against total protein extracts from purified *T. hominis* spores (**SPTh**), *T. hominis* infected rabbit kidney cells (**RKTh**) and non-infected rabbit kidney cells control (**RK**).

(B) mtG3PDH antisera affinity-purified against the immunogen (1:100 dilution of 0.4 mg/ml stock) detected two major bands in purified *T. hominis* spores migrating with apparent molecular weights of ~70 kDa (**green arrowhead**) and ~61 kDa (**blue arrowhead**). Bands migrating with apparent molecular weights of ~70 kDa and ~33 kDa were detected in RKTh and RK (**orange arrowheads**).

Approximately 20 µg (based on BCA assay) of each extract was loaded onto the gel. Blot probed with the affinity-purified anti-*Th*mtG3PDH antibodies was exposed for 100 s (overexposure evident as an oversaturation of the major bands) in order to visualize all detected bands. Blot probed with final bleed was exposed for 10 s, as 100 s exposure caused a uniform high background (completely black blot) possibly due to the cross-reaction of antibodies in the serum with the blocking reagent (milk).

Controls and analysis of the blots were the same as described in (**Figure 3.14)**

3.3.4 Investigating intracellular localisation of the AOX and mtG3PDH in Trachipleistophora hominis cells using immunofluorescence microscopy and cell fractionation experiments

Cell fractionation

In western blotting analysis of fractions from differential centrifugation of *T. hominis* infected rabbit kidney cell lysates, affinity purified antisera against *T. hominis* AOX detected bands in 1,000 x g (1 k), 12,000 x g (12 k) and 25,000 x g (25 k) fractions but not in 100,000 x g (100 k) and the final supernatant, (S, Figure 3.16 A). Intesities of signals detected with anti-T. hominis AOX antibodies as well as antibodies raised against known mitosomal markers ThTom70 and ThmtHsp70 were higher in 1 k and 25 k fractions and weaker in 12 k fraction (Figure 3.16 A). Nuclear membrane marker ThMPS3 and cell membrane marker ThNTT3 were detected mainly in 1 k fraction and weaker signals in 12 k and 25 k fractions (Figure 3.16 A). No signals were detected in 100 k fraction and final supernatant (S, Figure 3.16 A) fractions suggesting that integrity of the membrane compartments has not been disrupted during homogenisation process. The 1 k fraction consists mostly of spores (not lysed with Dounce homogeniser), unbroken host cells and intracellular stages of *T. hominis*, large cell debris and compartments such as nuclei (demonstrated by the detection of parasite nuclear marker MPS3 mostly in this fraction as well as increase of viscosity due to DNA release after addition of SDS). Signals detected with specific antisera against two mitosomal marker proteins (*Th*TOM70 and *Th*mtHSP70) have the strongest intensities in 25 k pellet indicating that it is a fraction enriched in mitosomes from the intracellular stages of the parasite. The AOX signal seems to be more intense in 1 k fraction which is consistent with the enrichment of the AOX in microsporidian spores rather than the intracellular stages**.**

The apparent mitosome enriched fraction (25 k), was subjected to a proteinase K protection assay (Figure 3.16 A) in which all proteins that localize on the surface or outside of membrane vesicles can be degraded by the proteinase whereas the proteins localized inside the membrane compartments are protected from the proteinase activity. Signal detected with antisera against the *T. hominis* homologue of a mitochondrial outer surface protein TOM70, as expected, disappears in the proteinase treated samples (Figure 3.16 A). Bands detected with antibodies against AOX and mtHSP70 are present in the proteinase treated samples, but disappear after addition of the detergent (Triton X-100; Figure 3.16 A, +TX) -that disrupts

membranes of the vesicles causing an exposure of previously protected proteins to the proteinase activity- consistent with their localization inside a membrane compartment. The proteinase K protection assay was performed prior to affinity purification of anti-mtG3PDH of sufficient concentration for the western blotting experiments and needs to be repeated with these affinity-purified antibodies in the future.

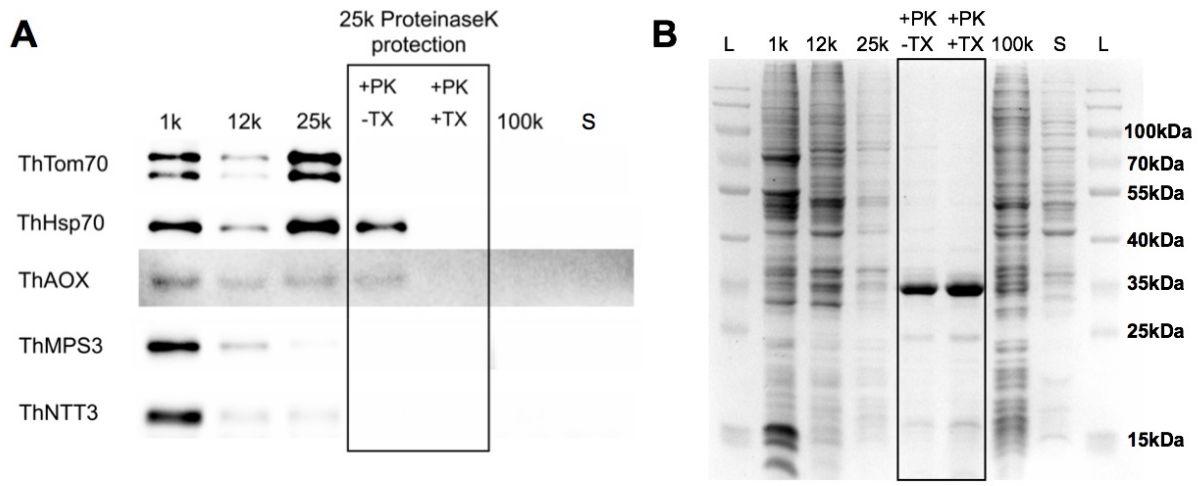

Figure 3.16 Western blotting analysis of fractions from differential centrifugation of *T. hominis* infected rabbit kidney cells lysates and proteinase K protection assay of mitosomal enriched fraction

(A) A sample of *T. hominis* infected rabbit kidney-13 cell line culture was lysed with a Dounce homogeniser and subjected to subcellular fractionation using differential centrifugation. Analysed fractions correspond to 1,000 x g (1 k), 12,000 x g (12 k), 25,000 x g (25 k) and 100,000 x g (100 k) pellets and the final supernatant (S). The 25 k pellet was split into three aliquots of equal volume. The black box indicates the two 25 k aliquots that were incubated with an addition of proteinase K and Triton x-100 (+TX) or with the proteinase K without the detergent (-TX). *Th*AOX band has the same MW as the 24 kDa band detected in protein extracts from *T. hominis* spores (Figure 3.14 B). Weak signal of the band detected with anti *Th*AOX antibody and a high background levels are due to long exposure time (100 s as opposed to 10 s in case of the remaining antibodies) and are consistent with enrichment of the AOX in the spore stages.

(B) Protein concentration in fractions was assessed with BCA assay and equal amounts (10 µg) of each fraction (1 k, 12 k, 100 k and supernatant) were loaded onto polyacrylamide gels. Due to a limited amount of material only 3 µg of 25 k fractions were loaded. Amount of proteinase K treated samples loaded onto the gels was the same as that of 25 k fraction. Blotting efficiency was assessed with Ponceau S (Sigma Aldrich), (not shown).

Immunofluorescence microscopy

In immunofluorescence microscopy experiments affinity purified polyclonal antisera against T. hominis AOX detect punctate fluorescent signals inside the parasite cells similar in number and distribution to the signals detected using characterized antibodies against known mitosomal marker mtHSP70 (Williams et al., 2002). Double labelling experiments with the purified anti-AOX antisera raised in rabbit and antisera against mtHSP70 raised in rat indicate colocalization of fluorescent signals detected with these two antibodies inside the parasite cells (Figure 3.17 A, B and C). Laser scanning confocal microscopy (LCSM) (Figure 3.17 A) and deconvolution of the acquired images (Figure 3.17 B) were used in order to reduce out of focus fluorescent signals, increase signal to noise ratio, and improve image contrast and resolution, relative to conventional widefield fluorescence microscopy (Figure 3.17 C). The colocalization pattern was observed in single confocal sections collected using LCSM (Figure 3.17 A) as well as in deconvolved LCSM images (Figure 3.17 B). Affinity purified antisera raised against mtG3PDH also detected fluorescent signals that colocalized with signals detected using rat polyclonal sera against *Th*mtHSP70 inside *T. hominis* cells (Figure 3.18). These results are consistent with the mitosomal localization of *T. hominis* AOX and mtG3PDH.

No primary antibody controls, single labelling experiments as well as experiments where primary antibodies raised in different animals (rats and rabbits) were used sequentially in a reverse order (i.e. first incubation with either antibody raised in rat or in rabbit) indicate that the detected signals are not due to cross-reactivity between the antibodies or unspecific binding of secondary antibodies.

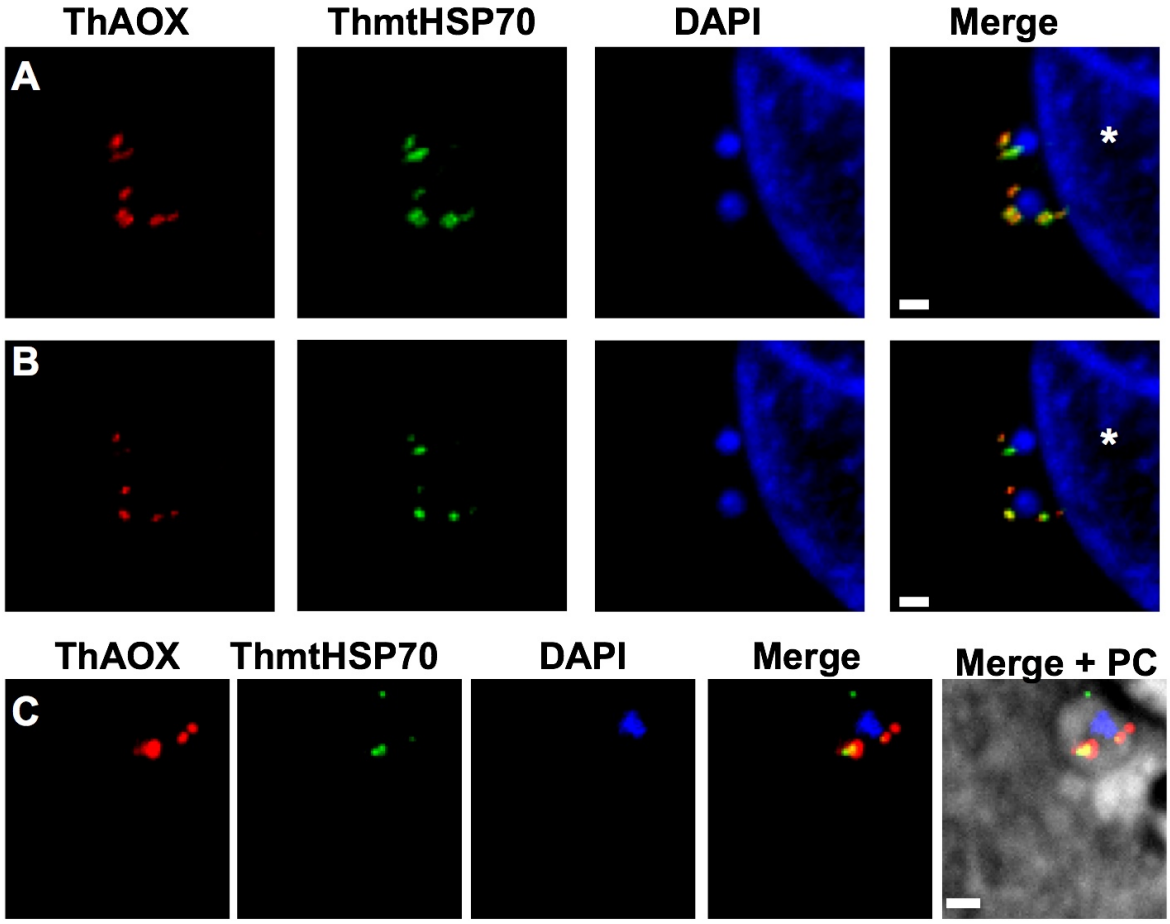

Figure 3.17 Fluorescence microscopy images of fixed samples of *T. hominis* infected rabbit kidney cells probed with anti-*Th*AOX and anti-*Th*mtHSP70 antibodies

(A, B and C) Affinity purified rabbit polyclonal sera raised against *T. hominis* AOX (red) label punctate structures that colocalize with signals detected using rat polyclonal sera against known mitosomal marker *Th*mtHSP70 (green) inside one (C) and two (A and B) uninucleate parasite cells. Some of the mitosomal signals appear to be closely associated with the DAPI-stained nuclei (blue) of the parasite. White asterisks indicate DAPI-stained nucleus of the host.

(A) A single optical section acquired using Nikon A1R confocal microscope (2 times linear averaging, 60x/1.4 lens).

(B) The same optical section as (A) after deconvolution. Red and green channels from Z-stack (20 sections) sampled according to Nyquist rate were deconvolved using experimentally verified (with images of 0.1 µm fluorescent microspheres, TetraSpeck™, Molecular Probes) point spread functions in Volocity (PerkinElmer).

(C) Maximum intensity Z-projections of Z-stack acquired using Zeiss Axioimager II fluorescence microscope (100x/1.46 Oil phase contras lens). Phase contrast image (PC) that was overlaid on the fluorescent image represents a single optical section.

Scale bars correspond to 1 µm.

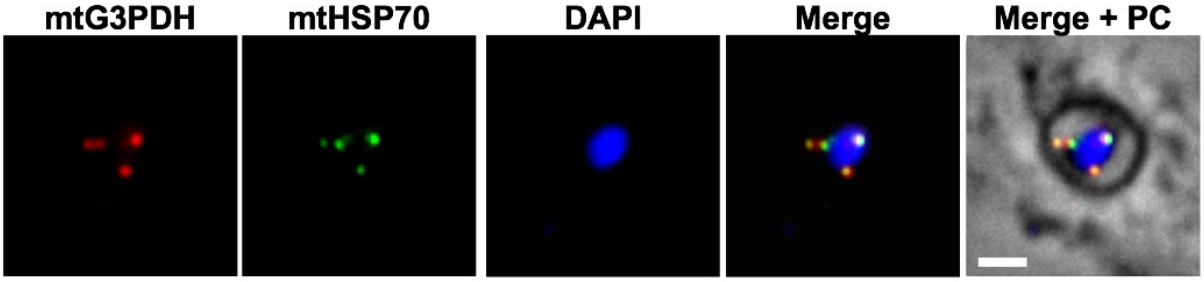

Figure 3.18 Fluorescence microscopy images of fixed samples of *T. hominis* infected rabbit kidney cells probed with anti-*Th*mtG3PDH and anti-ThmtHSP70 antibodies

Affinity purified rabbit polyclonal sera raised against *T. hominis* mtG3PDH (red) label punctate structures that colocalize with signals detected using rat polyclonal sera against known mitosomal marker *Th*mtHSP70 (green) inside a single uninucleate parasite cell. Nucleus of the parasite was stained with DAPI. The fluorescence images are maximum intensity Z-projections of Z-stack acquired and processed as described in (Figure 3.17). Phase contrast image (PC) represents a single optical section. Scale bars correspond to 1 µm.

3.3.5 Investigating mitosomal localisation of the AOX and mtG3PDH in different stages of the T. hominis life cycle

Detailed examination of the immunofluorescence images of the samples double labeled with antibodies against mtHSP70 and AOX or mtHSP70 and mtG3PDH (Figure 3.19) suggested that numbers of AOX and mtG3PDH signals that colocalize with mtHSP70 signals is different in various morphotypes of the parasite. The clearest difference was observed between small uninucleate parasite cells (diameter of around 2 µm) and large (diameter of around 6 µm - 8 µm) multinucleate cells (Figure 3.19). In the small cells only a small number of mtHSP70 fluorescent signals wese detected and usually all of them colocalized with similar number of AOX or mtG3PDH signals (Figure 3.19 A and 3.19 C). In the large cells the number of the mtHSP70 signals seemed to be much higher than in the small cells whereas the AOX and mtG3PDH signals were either not present or present in very small numbers (Figure 3.19 B and 3.19 D). These results seem to indicate that enzymes potentially involved in the microsporidian alternative respiratory pathway (AOX and mtG3PDH) are present in concentrations above the detection limit mostly in the mitosomes of the small cells and only in a small fraction of the mitosomes in the large parasite cells.

As images of the small and large cells were taken from the same samples, acquired and processed using the same settings (Figure 3.19) it is possible to

qualitatively compare the intensities of the fluorescent signals detected in this two morphotypes. In all acquired images fluorescent signals of the AOX and mtG3PDH seemed to be more intense in the small cells than in the large cells whereas the mtHSP70 signals seemed to be more intense in large cells than in the small cells. When the same exposure times were used to visualize fluorescent signals in both the small and the large cells many of the AOX and mtG3PDH signals detected in the small cells were over-saturated while signals detected using the same antibodies in the large cells were only slightly more intense than the background. These observations are consistent with the enrichment of AOX and mtG3PDH in the mitosomes of the small cells. Intensities of the detected fluorescent signals can potentially be analysed quantitatively as part of the future work. Quantitative analyses of fluoreccence intensities will require modification of existing protocols for sample preparation and image acquisition including imaging of multiple samples prepared by titering antibodies as well as avoiding acquisition of overexposed fluorescent signals (Kirkeby and Thomsen, 2005; Waters, 2009).

As opposed to AOX and mtG3PDH, all punctate fluorescence signals labeled with antisera against mtHSP70 in both the small and the large cells, colocalized with signals labeled using characterized antisera against mitosomal cysteine desulfurase (NFS1, Figure 3.19 E and F), (Goldberg et al., 2008) indicating that the proteins involved in biosynthesis of iron-sulfur clusters are present in concentrations above the detection limit in all mtHSP70-labeled mitosomes of the two observed parasite morphotypes.

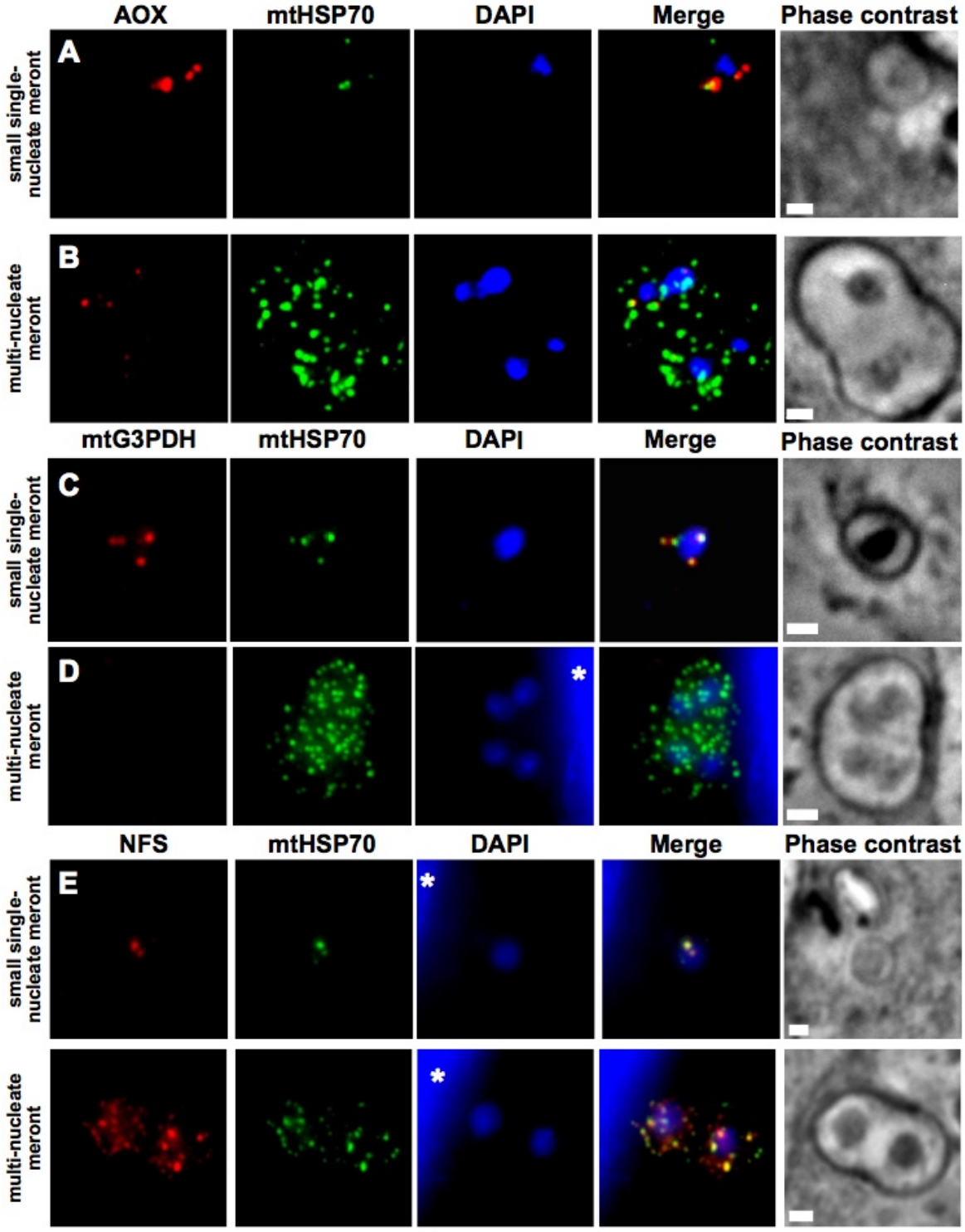

Figure 3.19 Fluorescence images of two distinct *T. hominis* morphotypes double-labelled with antibodies against different mitosomal proteins

Fluorescence images of the parasite cells double labelled with antibodies against *T. hominis* mtHSP70 and *T. hominis* AOX (A and B), mtHSP70 and *T. hominis* mtG3PDH (C and D) or mtHSP70 and *T. hominis* NFS (E and F). (A, C and E) are representative images of small single-nucleate meronts. (B, D and F) are representative images of proliferative multi-nucleate meronts. Image (A) is the same as (Figure 3.17 C) and image (C) is the same as (Figure 3.18). Images of the two morphotypes (A and B), (C and D) or (E and F) were acquired using the same setting and processed in the identical way. The fluorescence images are maximum intensity Z-projections of Z-stack acquired and processed as described in (Figure 3.17). White asterisks indicate DAPI-stained nucleus of the host cell. Phase contrast images (PC) represent single optical sections. Scale bars correspond to 1 µm.

Time course of infection

In order to correlate observed morphotypes with different stages of the *T. hominis* life cycle and to track the observed changes in numbers and intensities of the AOX signals during the life cycle, different time points from a time course of infection experiment were double labeled with anti-AOX and anti-mtHSP70 antibodies (Figure 3.20).

In phase contrast images the small cell morphotypes (single nucleate cells with an average diameter of around 2.2 µm) were observed just after the infection process (0.5 hour – 6 hours after addition of spores to non-infected host cells) and correspond to the first intracellular stage in the *T. hominis* life cycle, early meronts (Figure 3.20). Anti-AOX fluorescent signals always colocalized with anti-HSP70 in all of the observed early meronts.

An increased number of the anti-mtHSP70 fluorescent signals, and a decreased number of the anti-AOX signals were first observed 12 hours post infection (Figure 3.20, 12h) in single-nucleate parasite cells with an increased cell diameter (on average approximately 3.2 µm). As only a single nucleus per parasite cell was observed, this morphotype most likely corresponds to the life cycle stage where cells increase their biomass before entering the proliferative stage. Usually only a single cell of this intermediate morphotype (intermediate meront) was observed in a single host cell (Figure 3.20, 16h). The two parasite cells observed inside the single host cell in the image of the 12 h time point (Figure 3.20, 12h) are most likely due to infection of the same host cell by two different spores. In order to initiate the infection, spores were incubated with the non-infected RK13 monolayer for two hours. The presence of the two apparently different life cycle stages of *T. hominis* in the single host cell could correspond to the infection of the host cell by the first spore in the beginning of the incubation and by the second spore in the end of the incubation. The image of the two parasite cells in the single host cell allows for the direct comparison of numbers and observed intensities of the AOX and mtHSP70 fluorescent signals. A higher number of seemingly more intense anti-mtHSP70 signals was detected in the larger intermediate meront whereas number and intensity of the anti-AOX signals seemed to be higher in the smaller early meront. The observed higher number of the anti-mtHSP70 signals in the intermediate meronts could be explained by division of the mitosomes, by dispersion of the organelles in the cell volume from an initial point of origin (i.e. spindle pole body), or by both processes occurring at the same time. Mitosomes with the size of around 50 nm x

100 nm (Williams et al., 2002) are subresolution structures (resolution in the microscopy systems used in this study is around 250 nm), and can be often observed in clusters, meaning that single fluorescent signal can correspond to more than one mitosome. Thus, the observed higher intensity of mtHSP70 signals could be due to increase in concentration of the mtHSP70 in the mitosomes or increase in number of the mitosomes. The lower number and the lower intensity of the AOX signals in the intermediate meronts could be explained by a decrease in concentration of the mitosomal AOX either by a dilution of the protein during division of the mitosomes (assuming the reduction in expression levels of the AOX) or by a specific degradation of the protein inside the mitosomes. A reduced accessibility of the antibodies to the epitopes or a reduced affinity of the antibodies to the modified epitopes due to protein modification could be an alternative explanation. However, it seems less likely as similar labeling pattern was observed using antibodies against the second mitosomal component of the alternative respiratory pathway, mtG3PDH (Figure 3.19 C and 3.19 D).

First multinucleate cells indicating start of nuclear divisions and proliferative stage of the life cycle (late merogony) were observed 18 hours post infection. The observed late meronts had between 2 and 8 nuclei, high numbers of anti-mtHSP70 fluorescent signals and a very small number of faint anti-AOX signals. Around 40 hours post infection first spore forming stages (sporonts) were observed. Similar to published results (Williams et al., 2002; Heinz et al., 2014) no fluorescent signals were detected inside the spore forming stages and the spores probably due to the presence of the impermeable cell wall.

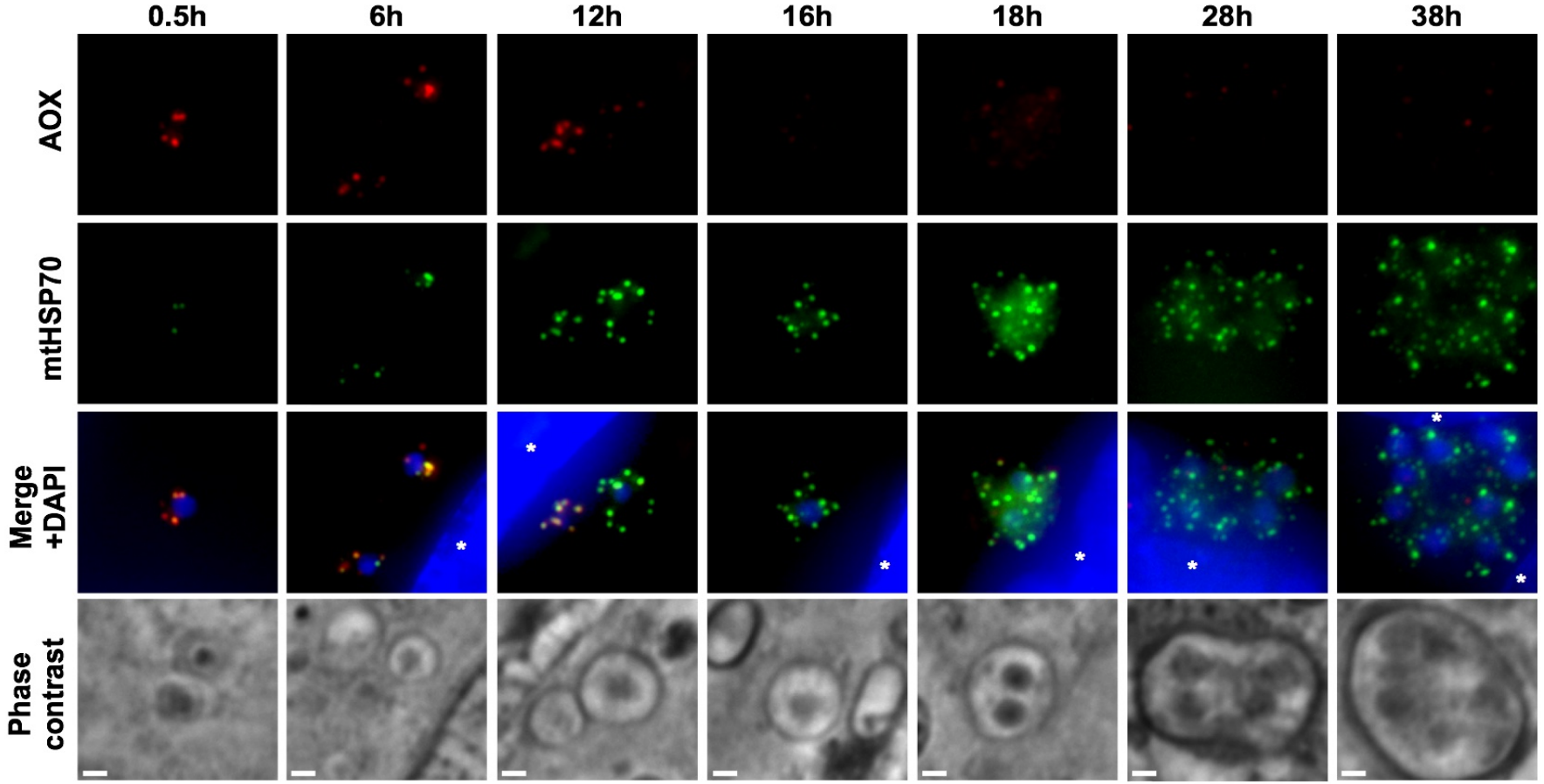

Figure 3.20 Investigating colocalization of mtHSP70 and AOX to the mitosomes in a time course of *T. hominis* infection of rabbit kidney cells monolayer

Fluorescent signals detected with the affinity purified anti-*T. hominis* AOX antibodies (red) colocalize with signals detected using anti-*T. hominis* mtHSP70 sera (green) to punctate structures in early meront stage of *T. hominis* life cycle visible in early time-points (0.5 h, 6 h and 12 h post infection) but not in intermediate and late meront stages of the life cycle detected in later time-points post infection (12 h - 38 h).

Presented images are representative examples of *T. hominis* cells from the time points where a significant change in the parasite cell size, number of fluorescent signals, number of the parasite nuclei or number of parasite cells per host cell were observed. All images were acquired using Zeiss AxioImager II with 100x (NA=1.46) Plan-Apochromat objective lens and processed using FiJI software package (Schindelin et al., 2012). Presented fluorescence images are maximum intensity z-projections of acquired z-stacks. Scale bars correspond to 1 μm.

Semi-quantitative analysis of the detected fluorescent signals

A semi-quantitative analysis of the fluorescent signals was performed in order to test the significance of observed difference in numbers of the anti-HSP70 and anti-AOX signals detected in various stages of the *T. hominis* life cycle. To compare different stages of the parasite life cycle, all images were from the same sample (single microscopy slide) of the mixed population of the parasite (all three stages were present); and were acquired, and analyzed using the same settings (the same microscope using the same lens, the same exposure time settings, ant the same detection thresholds in the analysis software). Fields of view were selected so that different parts of the glass slide were sampled and so that representatives of at least two life cycle stages were present within one field of view.

Three distinct morphotypes of the parasite cells labeled with the anti-AOX and anti-mtHSP70 antibodies were identified and classified based on a cell diameter and a number of nuclei (Figure 3.21 C). These morphotypes corresponded to early meront-, intermediate meront-, and late meront-life cycle stages established in the time course of infection experiment (Figure 3.20). Early meronts on average had significantly more AOX fluorescent signals (5.49 ± 2.97; mean ± SD depicted in Figure 3.21 A) than mtHSP70 signals (4.04 ± 2.11). Intermediate meronts had on average significantly more mtHSP70 (21.35 ± 15.78) signals and significantly less AOX signals (4.37 ± 4.81) than the early meronts. Late meronts had on average significantly more mtHSP70 (57.05 ± 26.84) signals and significantly less AOX signals 1.63 ± 2.25) than the intermediate meronts (Figure 3.21 A). Overall the number of anti-AOX signals was negatively correlated with the diameter of the cells (Figure 3.22). These results indicate that the observed differences in numbers of the fluorescent signals for anti-AOX and anti-mtHSP70 are significant and provide support for the hypothesis that the activity of the alternative respiratory pathway is involved in the survival of *T. hominis* spores and/or the infection process rather than in the later growth and proliferation stages of the parasite life cycle.

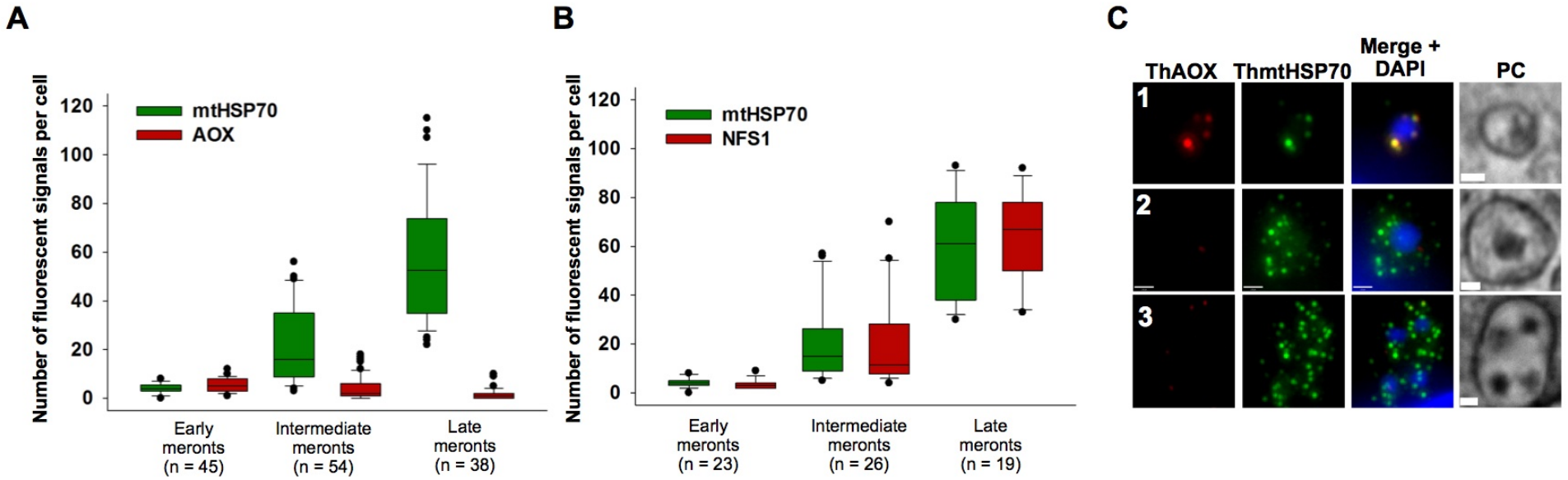

Figure 3.21 Semi-quantitative analysis of a number of fluorescent signals of mitosomal proteins: alternative oxidase (AOX), cysteine desulfurase (NFS) and mtHSP70 detected with specific antibodies in different stages of *T. hominis* life cycle

Number of fluorescent signals (detected using Find Spots function implemented in Volocity, PerkinElmer) detected within each parasite cell double labeled with anti-AOX and anti-mtHSP70 antibodies **(A)** or with anti-NFS and anti-mtHSP70 antibodies **(B)** were quantified. Mean values of quantified point fluorescent signals were plotted onto the graphs (**A** and **B**) with bars representing standard deviations. **(A)** Average number of green fluorescent signals (mtHSP70) is significantly different (Mann-Whitney Rank Sum Test, $P < 0.001$) between all three cell phenotypes. The number of red fluorescent signals (AOX) is significantly different between small and medium cells (Mann-Whitney Rank Sum Test, $P < 0.007$) as well as medium and large cell phenotypes (Mann-Whitney Rank Sum Test, $P < 0.003$). Difference between average numbers of green and red fluorescence signals is significant for early meronts (Mann-Whitney Rank Sum Test, $P = 0.02$**)** as well as for intermediate and late meronts (Mann-Whitney Rank Sum Test, $P < 0.001$**)**. **(B)** There are no significant (Mann-Whitney Rank Sum Test, $P > 0.2$) differences between average number of NFS (red) fluorescent signals and mtHSP70 (green) fluorescent signals in any of the *T. hominis* morphotypes.

Average number of red (AOX) and green (mtHSP70) signals was measured for a total of 137 cells observed in **20** z-stacks from two independent biological replicates corresponding to two independently infected and cultured populations of *T. hominis* infected RK13 cells (10 z-stack for each of the replicates). No statistically significant difference was found between the replicates for any of the measurements (Mann-Whitney Rank Sum Test).

(C) Three different morphotypes of *T. hominis* that are labeled with the specific antibodies were identified based on cell diameter and number of nuclei. Early meronts (C.1) have an avarage diameter of around 2.2 μm and a single nucleus. Single nucleate intermediate meronts (C.2) with the avarage diameter of around 3.2 μm are significantly larger (Student's t-test, $P < 0.001$) than the early meronts. Late meronts (C.3) have 2 to 4 nuclei and the average diameter of around 5.2 μm. Each of the morphotypes corresponds to a different stage of the *T. hominis* life cycle.

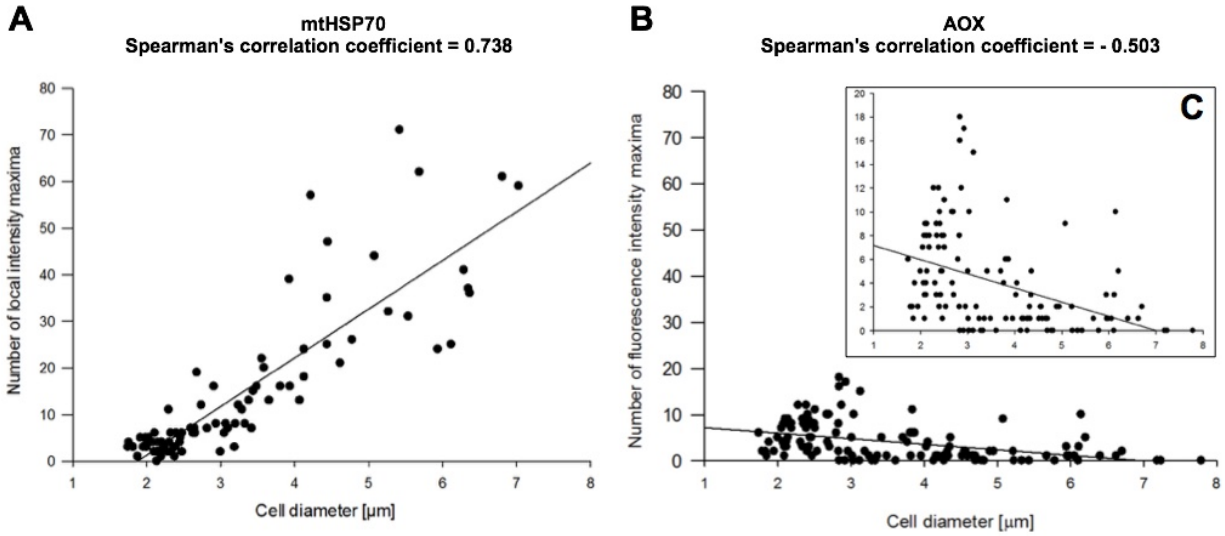

Figure 3.22 Correlation of the number of detected fluorescent mtHSP70 and AOX signals with the parasite cell diameter

(A) The number of mtHSP70 (green) fluorescent signals has a very strong positive correlation (Spearman's Correlation = 0.872, P = 2 x 10^{-7}) with the cell diameter. This indicates that the number of mitosomal mtHSP70 signals is increasing with the volume of the parasite's cells. **(B)** The number of the red signals has a moderate negative correlation with the cell diameter (Spearman's Correlation = -0.503, P = 2 x 10^{-9}) indicating that the number of AOX signals is decreasing with the volume of the *T. hominis* cells. **(C)** is the same as **(B)** with the Y axis scale displayed up to 20. Analyses was performed on the same dataset as in Figure 3.21.

As opposed to the anti-AOX fluorescent signals, there was no statistically significant difference between the number of anti-mtHSP70 and anti-NFS signals detected in the double labelling experiments (Figure 3.21 B). Numbers of the anti-mtHSP70 and anti-NFS fluorescent signals were positively correlated with the diameter of the cells (Figure 3.21 A), which seems to be consistent with the important function of the mitosomes in biosynthesis of the essential iron sulfur clusters during the cell growth and proliferation.

Analyses of relative intensities of the bands detected in western blots

As evident in the results of the time course experiment the early meronts can be observed in the host cells as soon as 30 minutes after initiation of the infection process (the addition of purified *T. hominis* spores). It is likely that proteins detected in the early meronts were already present in the spores. However, microsporidian spores are not labelled with anti-AOX or mtHSP70 antibodies regardless of the fixatives (1:1 methanol:acetone, methanol, acetone, ethanol, 4% paraformaldehyde) and permeabilization agents (0.2% TritonX-100, 0.5% saponin, 0.5% Tween-20) used, likely due to the presence of the complex spore wall that is impermeable to the

antibodies. In order to further investigate the presence of the mitosomal proteins in *T. hominis* spores, intensities of the bands detected using the specific antibodies on western blots with protein extracts from the purified spores and *T. hominis* infected rabbit kidney cells were analysed semiquantitatively (Figure 3.23). Intensities of signals detected with antibodies against proteins involved in nuclear division (MPS3), mitosomal biogenesis (mtHSP70, TOM70), and iron sulfur cluster biosynthesis (mtHSP70) are between five-fold and ten-fold lower in protein extracts from spores in comparison to the intensity of the signals detected in the protein extracts from *T. hominis* infected host. As opposed to these proliferative markers signals detected with antibodies against microsporidian alternative respiratory pathway components (AOX and mtG3PDH) have equal (AOX) or a four-fold higher (mtG3PDH) intensities in extracts from spores in comparison to the signals detected in the extracts from *T. hominis* infected host.

Protein extracts from *T. hominis* infected host were extracted from a mixed population containing different stages of the parasite's intracellular development (including spores and spore forming stages) and should be treated as a population enriched in the proliferative stages of the parasite as established by microscopy observations. Based on the observed presence of spores and spore forming stages and detection of fluorescent anti-AOX and anti-mtG3PDH signals mainly in the early meronts, AOX and G3PDH signals detected in the protein extracts from the infected host cells, most likely correspond to the proteins extracted from early meronts and also likely from a subpopulation of mature spores present inside the host cells.

Higher intensities of the bands of proliferative markers in the samples enriched in the proliferative stages of the parasite as well as higher intensities of the alternative respiratory pathway components in the protein extracts from purified environmental spores are consistent with the enrichment of the AOX and mtG3PDH in spores rather than the proliferative stages of the parasite.

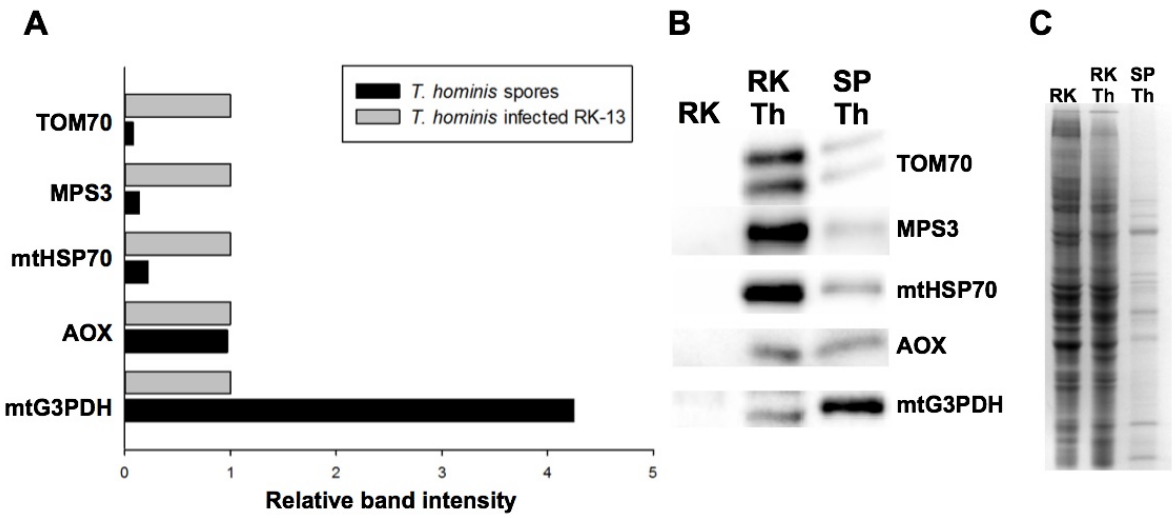

Figure 3.23 Measurements of relative intensities of the specific bands detected with antibodies against different microsporidian proteins in protein extracts from *T. hominis* infected rabbit kidney cells and purified *T. hominis* spores

(A) The relative intensities of signals detected with antibodies against *T. hominis* MPS3, mtHSP70, and TOM70 are between five-fold and ten-fold lower in protein extracts from spores in comparison to the intensity of the signals detected in the protein extracts from *T. hominis* infected host. The relative intensities of the signals detected with antibodies against *T. hominis* AOX and mtG3PDH have equal (AOX) or a four-fold higher (mtG3PDH) values in spores in comparison to the signals detected in the *T. hominis* infected host. Measured intensity values of the detected specific bands **(B)** in *T. hominis* infected rabbit kidney cells (RKTh) and spores (SPTh) were displayed **(A)** as values relative to the signal detected in the infected host (RKTh).

(B) Western blots used for the band intensity measurements. Antibodies used in the experiments: anti-mtG3PDH affinity purified antisera (1:100 dilution of 0.4 mg/ml stock), anti-AOX affinity purified antisera (1:50 dilution of 0.2 mg/ml stock), anti-MPS3 antisera (1:2000), anti-mtHSP70 antisera (1:2000), anti-TOM70 antisera (1:2000). Blots with anti-AOX antibodies were exposed for 40 seconds and the remaining blots were exposed for 1 second or 10 seconds.

(C) Polyacrylamide gel stained with Instant blue. Gels used in western blotting experiments were loaded with 10 µg (based on BCA assay) of total protein extracts from *T. hominis* infected RK-13 cell (RKTh) and non-infected RK-13 cells (RK), or 3 µg of total protein extracts from purified *T. hominis* spores (SPTh).

The same samples and conditions were used in two technical replicates of the experiment performed on two consecutive days. Intensity measurements of the two replicates were performed using FIJI (Schindelin et al., 2012) and Image Lab (Bio-Rad). Relative intensity values from the two replicates using both software packages were identical.

3.4 Discussion

The only currently known metabolic function of the mitosomes in all studied microsporidia is their involvement in biosynthesis of the essential iron-sulfur clusters (Goldberg et al., 2008). Genomes of some microsporidia, including that of *T. hominis,* encode homologues of AOX and mtG3PDH (Williams et al., 2010; Heinz et al., 2012) the two enzymes that constitute an alternative respiratory pathway (ARP) in mitochondria of bloodstream stage of *Trypanosoma brucei* (Chaudhuri et al., 2006). Presence of the ARP components encoded by the genome of *T. hominis* indicates that its mitosomes may have additional metabolic functions.

3.4.1 Mitosomal localization of the T. hominis AOX and mtG3PDH homologues

The results of the experiments with the affinity purified polyclonal antisera against *T. hominis* AOX and mtG3PDH raised in this study are consistent with the hypothesis that AOX and mtG3PDH localize to the mitosomes of *T. hominis.* In immunofluorescence microscopy experiments the anti-AOX and anti-mtG3PDH antibodies detect punctate fluorescent signals that colocalize with the signals detected using antisera against the mitosomal marker mtHSP70 (Figure 3.17 and 3.18). On western blots of protein extracts from the cell fractionation experiments the anti-AOX antibodies detect the specific bands in the same fractions as antibodies against other two mitosomal proteins (mtHSP70 and TOM70), (Figure 3.16). In the proteinase K protection assay using the mitosomal enriched fraction (25,000 x g) the AOX and mitosomal matrix protein mtHSP70 are protected against the proteinase activity as opposed to the mitosomal surface receptor, TOM70, which is degraded in samples treated with the proteinase (Figure 3.16). These results are consistent with the localization of the AOX inside the mitosome of *T. hominis* and are further supported by published immunoelectron microscopy results showing the detection of immunogold dots using the specific antibodies against the AOX and mtG3PDH inside the apparent double membrane bound organelles of the distant relative of *T. hominis,* microsporidian infecting insects *A. locustae* (Dolgikh et al., 2011). AOX in all studied organisms localizes on the inner surface of the inner mitochondrial membrane whereas the mtG3PDH localizes on the outer surface of the inner membrane. Further immunoelectron microscopy experiments using anti-AOX and anti-mtG3PDH antibodies characterized in this study could be used to test if the proteins localize to

the same two subcompartments inside the *T. hominis* mitosomes. Anti-mtG3PDH antibodies were not used in the cell fractionation and proteinase protection experiments as the purified antisera of a required concentration were only obtained in the final stage of this project. These experiments should be repeated with affinity purified anti-mtG3PDH as part of future work.

3.4.2 Potential presence of the N-terminal mitosomal targeting presequences in T. hominis AOX and mtG3PDH

The N-terminus of the AOX is the least conserved region of the protein in comparisons of the sequences from the broad range of eukaryotes: it has a variable length and is predicted to be highly disordered (Figure 3.8, 3.7, and 3.9). In microsporidia the weakly conserved N-terminal region ranges in length from 9 amino acids in *N. parisii* to 90 amino acids in *T. hominis* (Figure 3.7) whereas the corresponding regions in plants are from 70 to 100 amino acids long and in *T. brucei* around 50 amino acids long (Figure 3.9). Plant and *T. brucei* AOX homologues posses N-terminal and internal mitochondrial targeting signals (Tanudji, Sjöling, Glaser, & Whelan, 1999b; Hamilton et al., 2014). The presence of N-terminal mitochondrial targeting signal was predicted by at least one of three prediction programs (with score above 50 %) in AOX homologues from *T. hominis, V. culicis, S. lophii,* and *A. locustae* (Table 3.1). Mitochondrial targeting signals were not predicted in the two sequences with the shortest N-termini from *E. aedis* and *N. parisii.* The N-terminal presequence (41 amino acids long) is essential for import of the AOX into the purified plant mitochondria and transport mechanism seems to be dependent on the membrane potential (Tanudji, Sjöling, Glaser, & Whelan, 1999b). Import of AOX into the mitochondria isolated from the procyclic forms of trypanosome also seems to be dependent on the membrane potential as opposed to mitochondria from bloodstream stage of the parasite where addition of a mitochondrial membrane-dissipating agents (valinomycin and CCCP) did not inhibit the protein import (Williams et al., 2008). Membrane potential was not detected in mitosomes of *T. hominis* using Mitotracker Red (Williams et al., 2002) and the import mechanism of AOX into the organelle could resemble that of the bloodstream stage of *T. brucei. In vivo* localization of the HA-tagged AOX as well as *in vitro* import of the radiolabeled AOX to the purified trypanosome mitochondria was observed even after deletion of the first 40 amino acids indicating that the N-terminal targeting signals are not

essential for import of *T. brucei* AOX into the mitochondria (Hamilton et al., 2014). Variation in the size between N-termini of AOX from different microsporidia could potentially indicate that AOX homologues with shorter N-terminus such as *N. parisii* AOX rely more on the internal targeting signals than the N-terminal transit peptide (Figure 3.7).

In plants (Tanudji, Sjöling, Glaser, & Whelan, 1999a) and possibly in *T. brucei* (Hamilton et al., 2014) the N-terminal targeting signal of AOX is proteolytically removed by the activity of mitochondrial processing peptidase (MPP). Homologues of MPP were not identified in microsporidian genomes (Heinz & Lithgow, 2012) and other proteins with confirmed mitosomal localization do not have any detectable N-terminal transit peptides (Williams et al., 2002; Goldberg et al., 2008). Apparent rMW of the bands detected with affinity purified anti-*T. hominis* AOX antibodies as well as monoclonal antibodies raised against plant AOX is 12 kDa lower than that predicted for the full length *T. hominis* AOX (Figure 3.14). This difference could be due to an aberant migration pattern of *T. hominis* AOX in reducing SDS polyacrylamide gels and/or due to a proteolytic processing of the protein. The aberant migration is unlikely as highly similar AOX homologues from plants, fungi and *T. brucei* seem to migrate with molecular weights corresponding to their predicted size. In previous studies *T. hominis* and *A. locustae* homologues expressed in *E. coli* and detected using monoclonal antibodies against plant AOX were shown to migrate with the rMW (exact value was not indicated) similar to that of a plant AOX purified from *Sauromatum gutattum* (Williams et al., 2010). *A. locustae* AOX was also detected using specific antibodies in protein extracts from spores and had an apparent rMW of 30 kDa, 2 kDa less than predicted 32 kDa (Dolgikh et al., 2011). Hypothetically the AOX could migrate with lower apparent rMW than predicted due to the presence of highly hydrophobic regions that may bind an excess SDS and affect its migration pattern. Although it is unlikely that the full-length *T. hominis* AOX migrates with rMW 12 kDa lower than expected, the migration pattern of the non-tagged full length *T. hominis* AOX expressed in *E. coli* should be verified in the experimental system used in this study (the same SDS-PAGE and protein extraction protocols) as part of the future work.

The more likely explanation for the smaller than expected size of the *T. hominis* AOX is that it is a result of processing inside the mitosome or partial protein degradation during the protein extraction. Low temperature (extraction on ice and using ice cold reagents) as well as addition of proteinase inhibitors cocktail and

PMSF should inhibit the activity of endogenous proteinases during the extraction process however possible presence of the non-inhibited proteinase processing the AOX in the protein extracts cannot be excluded. Published western blots of the recombinant *T. hominis* AOX expressed in *E. coli* show additional bands migrating with the lower rMW than the monomer indicating the protein could be susceptible to degradation (Williams et al., 2010). The observed difference of 12 kDa could correspond to around 110 amino acids of highly disordered region predicted at the N-terminus of *T. hominis* AOX (Figure 3.7). In the structure of *T. brucei* the poorly conserved and disordered N-terminus forms an extension (N-terminal arm) to a compact cylinder consisting of six α-helices (Shiba et al., 2013). The model of *T. hominis* AOX (Figure 3.9) suggests similar organization of its N-terminus that could potentially be susceptibility to degradation during protein extraction. Possibility of the protein processing during import into the mitosome could not be excluded. Although microsporidian homologue of MPP was not identified, candidate members of M16 peptidase family are present in microsporidian genomes (data not shown) one of which could be a divergent homologue of MPP. Immunoprecipitation of the *T. hominis* AOX using antibodies characterized in this study together with mass spectroscopic analysis and N-terminal protein sequencing could be used in order to further investigate possible processing of the protein. The possible processing could also be investigated in western blotting experiments with proteins extracts from isolated mitochondria of *Saccharomyces cerevisiae* expressing *T. hominis* AOX (Williams et al., 2010) similar to the published experimental work with *A. locustae* mtG3PDH (Burri et al., 2006).

Mitochondrial N-terminal targeting presequences were predicted with very low probabilities in microsporidian mtG3PDH homologues (Table 3.2). In published studies bands that seem to be corresponding to the mature and processed mtG3PDH were detected using specific antibodies in protein extracts from *A. locustae* spores as well as in mitochondria isolated from yeast (*S. cerevisiae*) expressing full length *A. locustae* mtG3PDH (Burri et al., 2006). Out of the three prediction programs used here (Table 3.2), only one (MitoProt II (Claros & Vincens, 1996)) predicted the presence of a mitochondrial targeting presequence in mtG3PDH from *A. locustae* (with probability of 65.6 %) indicating that the models implemented in the available prediction software may not be suitable for detection of mitochondrial targeting presequences in microsporidian mtG3PDH homologues. Neither of the programs predicted the presence of an N-terminal presequence in *T. hominis*

mtG3PDH (Table 3.2). Specific antibodies against *T. hominis* mtG3PDH detected two bands in protein extracts from purified *T. hominis* spores that seem to correspond to the mature and full-length mtG3PDH (Figure 3.15 B).

Although N-terminal targeting signal (31 amino acids) of *A. locustae* mtG3PDH fused with GFP localized to mitochondria when heterogously expressed in *S. cerevisiae*, N-terminally truncated *A. locustae* mtG3PDH fused with GFP was also targeted into the yeast mitochondria indicating a presence of the internal targeting signals (Burri et al., 2006). In mitochondria of *S. cerevisiae* N-terminal presequence of mtG3PDH is processed by the activity of Mitochondrial inner membrane protease (IMP), (K. Esser et al., 2004). One of the possible import mechanisms of proteins processed by the IMP such as cytochromes C_1 and B_2 is so called 'stop-transfer' mechanism (Glick et al., 1992). In the stop-transfer mechanism translocation of the protein across the inner membrane is arrested after the N-terminal targeting signal enters the TIM23 channel and the protein is subsequently released into the intermembrane space by a proteolytic removal of the presequence (activity of the IMP). Detection of two bands that seem to correspond to the mature and full-length mtG3PDH in protein extracts from *T. hominis* (this study) and *A. locustae* (Burri et al., 2006) spores as well as possible presence of the N-terminal presequence (Figure 3.12 and Burri et al., 2006) indicate that the mtG3PDH may be imported into the mitosomes of these species by the stop transfer mechanism.

The IMP gene was detected in the EST library of *Antonospora locustae* however it is not present in the genome survey of *A. locustae* (Corradi et al., 2007) or in any other available microsporidian genome sequences including that of *T. hominis* (Heinz et al., 2012). It is possible that the *T. hominis* IMP homologue is highly divergent thus difficult to detect using currently available bioinformatic tools.

3.4.3 Enrichment of the AOX and mtG3PDH in T. hominis spores and early meronts rather than the proliferative late meronts

Analyses of the relative intensities of bands detected using specific antibodies in protein extracts from purified *T. hominis* spores and protein extracts from *T. hominis* infected host cells that contain mostly the intracellular stages of the parasite, mtG3PDH and AOX appear to be enriched in the spores rather than the intracellular stages as opposed to the proliferative markers (MPS3, mtHSP70 and TOM70) that seem to be enriched in the intracellular stages of the parasite (Figure 3.23). These

data together with published results of quantitative immunoelectron microscopy showing enrichment of glycolytic enzyme PGK-3 in spores rather than the intracellular stages of *T. hominis* (Heinz et al., 2012) are consistent with the role of glycolysis in ATP generation mainly in microsporidian spores. The intracellular stages of *T. hominis* can use the nucleotide transporter proteins (NTTs) to steal purine nucleotides, including ATP, from the host in order to fuel their energy requirenments (Heinz et al., 2014). However, the extracellular dispersive spore cannot rely on its host and may need to use glycolysis and alternative respiratory pathway for generation of energy that it may require for survival and/or germination process (Heinz et al., 2012; Williams et al., 2014).

In immunofluorescence microscopy experiments the AOX and mtG3PDH proteins were detected in the intracellular stages of the parasite (Figure 3.17 and 3.18). Careful examination of the images of the samples double labelled with the anti-mtHSP70 and anti-AOX or anti-mtHSP70 and anti-mtG3PDH antibodies reveal that although the mtHSP70 signals are detected in all intracellular stages of the parasite life cycle the colocalizing AOX and mtG3PDH signals are detected mostly in the early meront stage (Figure 3.19). Early meronts are small (diameter below 2 μm) round cells that are detected inside the RK13 host cells 30 minutes to 12 hours after addition of *T. hominis* spores to the monolayer of uninfected host cells (Figure 3.20). Detection of the early meronts 30 minutes after addition of the spores indicates that these cells correspond to the stage of microsporidian life cycle just after injection of the spore contents into the host RK13 cell and are likely to contain proteins that were already present in the spore.

Detection of AOX signals in early meronts for 12 hours after the infection process (Figure 3.20) adds an additional possible function of the ARP. It could be speculated that the parasite is not able fully utilize the host resources required for its own development in the first hours of infection and instead relies on the ARP and glycolysis before it is able to tap into the host metabolism and initiate the intermediate growth phase that precedes the proliferation (Figure 3.20). An alternative explanation for these observations could be that the AOX is not removed from the mitosomes but its activity is downregulated when the parasite starts stealing ATP from the host. These possible roles of the ARP in different stages of the parasite life cycle could be further investigated by studying the effects of the AOX inhibitors (salicylhydroxamic acid and ascofuranone) on the *T. hominis* spores and intracellular stages. In my preliminary experiments the culture of rabbit kidney cells (RK13) was

incubated in medium containing salicylhydroxamic acid (SHAM) in concentrations (0.01 mM, 0.1 mM, 1 mM and 10 mM) based on those that were required to inhibit germination of conidia of plant pathogenic fungus *Magnaporthe grisea* (Avila Adame & Köller, 2003), and cause a loss of motility and damage to the cells of *T. brucei* in *in vitro* conditions (Clarkson & Brohn, 1976). No negative effects on the progression of *T. hominis* infection in RK13 cells were observed as evident by formation of new spores that were capable of infecting non-infected host cells after 3 days of incubation (established based on the microscopy observations). The results of these preliminary experiments are difficult to interpret due to the localization of the parasite inside the host cell that could potentially reduce the final concentration of the inhibitor inside the parasite cells. Additional experiments with more specific and potent inhibitor of the AOX, ascofuranone, that was already shown to inhibit the *in vitro* activity of microsporidian AOX (Williams et al., 2010), could be performed to further investigate the effects of inhibition of AOX on the parasite cultured in the mammalian host cells. Furthermore the purified *T. hominis* spores could be also incubated with the AOX inhibitors and later used to infect healthy cells. Comparison of the infection levels (number of detected intracellular stages) after initiation of infection with spores that were incubated either with or without the inhibitor could be used to test its effects on the spore survival. In addition to the possible roles in spore survival and/or germination, and metabolism of the early meronts, the ARP and glycolysis could also function during the process of the spore formation. It is unknown if the spore forming stages can utilize host resources as efficiently as the proliferative stages because of the presence of the forming spore wall. During the spore formation the parasite might have to utilize its own metabolism to produce intermediates required for biosynthesis of major spore wall component chitin and reserve carbohydrate trehalose. The possible functions of the AOX during the spore formation could be investigated by testing if the addition of AOX inhibitors can interfere with formation of mature spores and/or infection of the new hosts.

AOX and mtG3PDH most likely are expressed and imported into the mitosomes during the spore formation. Localization to the spore-forming stages could not be tested using immunofluorescence microscopy because of the apparent impermeability of the spore wall to the antibodies. It future work it could be further investigated by immunofluorescence of ultrathin cryosection and/or immunoelectron microscopy using the specific antibodies generated in this study. My preliminary immunofluorescence experiments on the ultrathin cryosections were not successful

because of the problems with acquiring the sections of required thickness. Sections of around 5 μm were routinely acquired with optimal cutting temperature compound (OCT) embedded polyformaldehyde (PFA) fixed samples however they were too thick to section through spores and spore forming stages. Further optimization of the sectioning protocol will be required in order to obtain section that are less than 1 μm thick.

The fluorescent AOX signals were detected mostly in the intracellular *T. hominis* cells until 12 hours post-infection when the first intermediate meronts were observed (Figure 3.20). The cells of intermediate meronts have significantly larger diameters (on average around 3.2 μm) than the early meronts, and significantly more mtHSP70 signals but significantly less AOX signals (Figure 3.21). Qualitative comparison of the observed intensities of the fluorescent signals seems to indicate that the few AOX signals detected in the intermediate meronts also had lower intensities than the signals detected in the early meronts (Figure 3.20). This change in cell diameter, as well as the number and possibly intensities of the fluorescent anti-mtHSP70 signals indicate transition into a growth phase that precedes the proliferative stage of the *T. hominis* life cycle. First double nucleate cells - an indicative of the nuclear divisions - were observed 6 hours after the observation of the first intermediate meronts (18 hours post infection). Observation of the single nucleate meronts followed by the multinucleate 2-4 nuclei meronts and transition into the sporogony corresponds to the first description of the *T. hominis* life cycle in RK13 cell line using light and electron microsocopy (Hollister et al., 1996). The lower number (Figure 3.21) and the lower intensity (Figure 3.20) of the AOX signals in the intermediate meronts could be explained by a decrease in concentration of the mitosomal AOX either by a dilution of the protein during division of the mitosomes and/or by a specific degradation of the protein inside the mitosomes. Further work including a semi-quantitative analysis of the number of the AOX and mtHSP70 signals in the large samples of cells from time points where intermediate meronts are first observed (around 12 hours post-infection) could help in distinguishing between these two possibilities. Observation of a population in which an increasing number of mtHSP70 fluorescent signals is correlated with decreasing number of the AOX and mtG3PDH signals would be consistant with the dilution of the protein during the organelle division events. Observation of cells that have similar number of the mtHSP70 signals but decreasing number (or intensity) of AOX signals could be consistent with the degradation of the protein. These experiments could require

development of the super-resolution microscopy methods for *T. hominis* infected RK13 cell samples in order to overcome the major difficulty in resolving the sub-resolution organelles such us mitosomes that can be observed in close proximity of one another in electron micrographs. Application of quantitative immunoelectron microscopy in this case may not be feasible due to the difficulty with finding high number of the organelles reacquired for the quantification using this methodology.

The observed changes in numbers and intensity of the mitosomal proteins during the transition between early and intermediate meronts seems to indicate change in function of the organelle. AOX and mtG3PDH are detected mostly in spores and early meronts which is consistent with the hypothetical function of the mitosomes in reoxidation of NAD possibly required for ATP generation via glycolysis in this stages. The energy in the form of ATP could be used for housekeeping and survival of the spore, the infection process or establishment of the parasite inside the host cell in the first hours of the infection. However during the intermediate growth phase and proliferation the parasite seems dependent on the ATP stolen from the host using nucleotide membrane transporters (NTT), (Heinz et al., 2014). At the same time the number (Figure 3.21) and intensity (Figure 3.20) of the detected anti-mtHSP70 signals suggests the increase in number of the mitosomes and likely increase in concentration of the mtHSP70 inside the mitosomes. Fluorescent signals detected using specific antibodies against the component of mitosomal iron sulfur clusters biosynthesis (NFS1) colocalize with mtHSP70 in all observed stages of the parasite (Figure 3.19) and there are no siginificant differences in numbers of the signals detected using ant-NFS and anti-mtHsp70 antibodies (Figure 3.21). Furthermore the number of the mtHSP70 signals has a strong positive correlation with the parasite cell diameter (Figure 3.22 A) as opposed to the number of AOX signals, which is negatively correlated, with the cell diameter (Figure 3.22 B). Increase in number of the mitosomes containing the components of the iron-sulfur clusters biosynthesis machinery is consistent with the important function that this organelle plays in biosynthesis of these essential cofactors rather than energy metabolism during growth and proliferation of the parasite.

3.4.4 Presence of the conserved functional and regulatory features in the protein sequences of the T. hominis AOX and mtG3PDH homologues

Multiple sequence alignment of microsporidian AOXs with homologues from diverse eukaryotes (Figure 3.8) indicate that highly conserved residues involved in substrate and iron cofactor binding are present in microsporidian sequences. This is consistent with the previous experimental results showing that the recombinant AOX from *A. locustae* and *T. hominis* expressed in *Escherichia coli* can catalyze a cyanide- and antimycin-resistant reduction of an ubiquinol-1 (Williams et al., 2010). The most characteristic feature of microsporidian AOX sequences seems to be the lack of an otherwise highly conserved tryptophan residue (W151 in *T. brucei*). In the solved crystal structure of the *T. brucei* AOX, W151 is involved in the hydrophobic interaction between α-helix 3 and α-helix 6 through stacking with phenylalanine 276 (F276) and mutation of the W151 to alanine causes a 95% respiratory inhibition (Moore et al., 2013). The F276 is weekly conserved in AOX among aligned homologues from different eukaryotes (Figure 3.8) and other amino acids (usually alanine or leucine but also methionine, lysine or arginine) can be found in the position corresponding the *T. brucei* F276. In previous studies W151 was suggested to play a role as an electron donor in one of the possible mechanisms of electron transfer from ubiquinol to molecular oxygen (Moore & Albury, 2008; Affourtit et al., 2002) and lack of this residue in microsporidian AOX may indicate some differences in the mechanism of catalysis. In addition to W151 only 2 out of 35 universally conserved residues, according to (Moore et al., 2013), are not conserved in microsporidian homologues. These are methionine 164 (in microsporidia with an exception of *N. parisii* replaced by glutamine) that in *T. brucei* AOX structure is involved in interface between two subunits of a dimer via interaction with N-terminal arm, and alanine 243 in *T. brucei* (replaced by serine in *T. hominis, V. culicis* and *S. lophii)* involved in hydrophobic interactions between the short α-helix 3 and α-helix 3 (Moore et al., 2013). Comparison of the 3D model of the *T. hominis* AOX generated *in silico* (Figure 3.9) with solved structure of *T. brucei* AOX (Shiba et al., 2013) suggested that the secondary structure and tertiary structure of the protein are well conserved. Presence of proposed membrane interaction regions in microsporidian sequences indicates that microsporidian AOX is an integral membrane protein (Figure 3.8).

In plants activity of AOX can be regulated by at least two mechanisms: reduction of disulfide bridge between two well conserved cysteine residues and/or

addition of succinate or pyruvate (Moore et al., 2013). Neither of the two cysteine residues are present in microsporidian AOX homologues, however the region containing a glutamic acid, asparagine, and valine (ENV) motif that may be crucial for pyruvate activation in non-thermogenic plants is at least partially conserved in some microsporidia (Figure 3.8). Only the sequence of the *A. locustae* AOX has the complete ENV motif whereas most of the microsporidian AOX homologues including that of *T. hominis* have a positively charged lysine in place of negatively charged glutamic acid (KNV).

Based on the crystal structure of *T. brucei* AOX the N-terminus was also hypothesized to play a role in interaction between subunits of the AOX homodimer. AOX is known to form homodimers *in vivo* in plant mitochondria but not in Fungi such as *Neuropsora crassa* and *Pichia stipites* (Umbach & Siedow, 2000). In published western blots of protein extracts from membrane preparations of *E. coli* expressing *T. hominis* and *A. locustae* AOX specific antibodies detected bands corresponding to the size of a monomer and dimer (Williams et al., 2010). Results of my preliminary experiments with a protein linker, 1% glutaraldehyde (Figure 3.14 E), also suggested presence of the AOX dimers (48 kDa) in the mitosome-enriched fraction (25,000 x g) from *T. hominis* infected RK13 cells.

Both components of the glycerol-3-phosphate (G3P) shuttle: cytosolic (cytG3PDH) and mitochondrial (mtG3PDH) glycerol-3-phosphate dehydrogenases were identified in all but two available microsporidian genomes, the *Enterocytozoon bieneusi* and *Anncaliia algerae,* encoding only the homologue of cytG3PDH. *E. bieneusi* and *A. algerae* also do not have a homologue of AOX and it is possible that these species use cytG3PDH to generate G3P that could be used mainly for biosynthesis of triacylglycerol, a major component of membrane lipids (Nakjang et al., 2013).

All residues involved in the substrate (1,3-dihydroxyacetone phosphate) binding in crystal structure of *Homo sapiens* cytG3PDH are conserved in all microsporidian homologues with an exception of a *S. lophii* homologue (Figure 3.11). Residues involved in cofactor (NAD) binding that are well conserved in yeast (*S. cerevisiae*) and human homologues, are more variable in sequences from microsporidia and *T. brucei* (glycosomal G3PDH). Glycosomal and cytosolic G3PDH of *T. brucei* seem to follow the same catalytic mechanism although they differ in most of the tested parameters including pH profile, sensitivity to ionic strength of a buffer and affinity for the NAD (glycosomal homologue has 5-10 lower affinity than the

cytG3PDH), (Lambeir et al., 1991). It was hypothesized that the measured low affinity of the glycosomal G3PDH for NAD is due to a relatively high concentration of this cofactor inside the glycosome that may be required to sustain a high efficiency of glycolysis measured in *Trypanosoma* (Lambeir et al., 1991). Glycolytic enzymes were among the most abundant proteins detected in the proteomic analysis of *T. hominis* spores (Heinz et al., 2012) and the high abundance of these enzymes could result in a high rate of glycolysis, which could be required in order to fuel a rapid (lasting only few seconds) infection process (Troemel & Becnel, 2015).

FAD- and 1,3-dihydroxyacetone phosphate-binding sites identified in the crystal structure of bacterial homologue of mtG3PDH are well conserved in sequences from microsporidia and other eukaryotes (Figure 3.12). In future work modelling of microsporidian mtG3PDH could be used in order to investigate a possible presence of hydrophobic plateau that is likely the ubiquinone-binding site in bacterial homologue (Yeh et al., 2008).

3.4.5 Phylogenetic analyses of the AOX

In phylogenetic trees microsporidian AOX protein sequences group with the homologues from their closest relatives (*Rozella allomycis* and *Mitosporidium daphniae*) and basal fungi, which is consistent with a vertical inheritance of the AOX coding gene from the last common ancestor of these organisms (Figure 3.10). Overall topologies of the phylogenetic trees are similar to other published phylogenies of the AOX (Williams et al., 2010) but interpretation of higher level relationships is difficult due to the poor resolution and a likelihood of lateral gene transfer. The AOX is a ‘plug and play’ enzyme that can be heterogously expressed in distantly related organisms and confer a cyanide resistant respiration (even if the genome of a recipient organism initialy does not encode AOX orthologue) provided only with a reduced pool of ubiquinone in membrane and oxygen, as evident by the measured activity of AOX from *Arabidopsis thaliana* expressed in *Escherichia coli* (Kumar & Söll, 1992), AOX from *Ciona intestinalis* expressed in human cell lines (Hakkaart et al., 2006), or AOX from *Histoplasma capsulatum* expressed in *Saccharomyces cerevisiae* (Vemuri et al., 2007). Many of the relationships within the tree are not resolved (polytomies) or are weakly supported with a noteworthy exception of a long and highly supported branch separating most eukaryotic sequences from sequences from a group including sequences from plants, red algae,

microsporidia, *R. allomycis* and basal fungi. Grouping of the sequences from microsporidia, *R. allomycis* and basal Fungi with plants rather than with Basidiomycetes and Ascomycetes fungi indicate that microsporidian AOX sequences are more similar to the homologues from plants rather than the basidiomycetes and ascomycetes fungi. Analyses of multiple sequence alignment of AOX homologues from different eukaryotes indicated the presence of conserved sequence features in sequence from the group 1 (that includes plants and microsporidia) but not in sequences from the group 2 (including representative of Ascomycetes and Basidiomycetes) such as the sequence adjacent to first membrane-binding region and conserved region containing regulatory ENV motif (Figure 3.8). Characterized fungal AOX homologues are up regulated by GMP (e.g. *Neurospora crassa* (Umbach & Siedow, 2000)), or AMP and pyruvate (e.g. *Ustilago maydis* (Sierra-Campos et al., 2009)), whereas plant AOX homologues are up-regulated by addition of α-keto acids (such as pyruvate) and by reduction of two conserved cysteine residues (Moore et al., 2013). Further biochemical characterization of the microsporidian AOX will be required in order to test if its activity is upregulated by pyruvate and/or purine monophosphates. In experiments with protein linkers such as glutaraldehyde the protein dimers are detected in plants but not in Fungi (Umbach & Siedow, 2000). Potential dimers of the microsporidian homologue were detected in *E. coli* expressing *T. hominis* and *A. locustae* AOX (Williams et al., 2010) as well as in protein extracts from *T. hominis* in my preliminary experiments with the protein linker, glutaraldehyde (for more details see section 3.3.3).

3.4.6 Possible functions of the microsporidian alternative respiratory pathway

AOX gene is present in genomes of many distantly related microsporidians including nematode parasite *Nematocida parisii*, insect parasite *Antonospora locustae,* and fish parasite *Spraguea lophii* (Figure 3.25). AOX was hypothesized to function in microsporidia together with the glycerol-3-phosphate shuttle in reoxidation of NAD (Williams et al., 2010) a process required for production of ATP in glycolysis (Figure 3.24). As microsporidia are able to steal ATP from their hosts during proliferative intracellular stages of their life cycle it seems likely that they require their own energy metabolism to be active mostly while outside of the host in the dispersive spore stage. Production of ATP could be required for spore survival, rapid infection process and/or just after the infection process before the parasite is able to

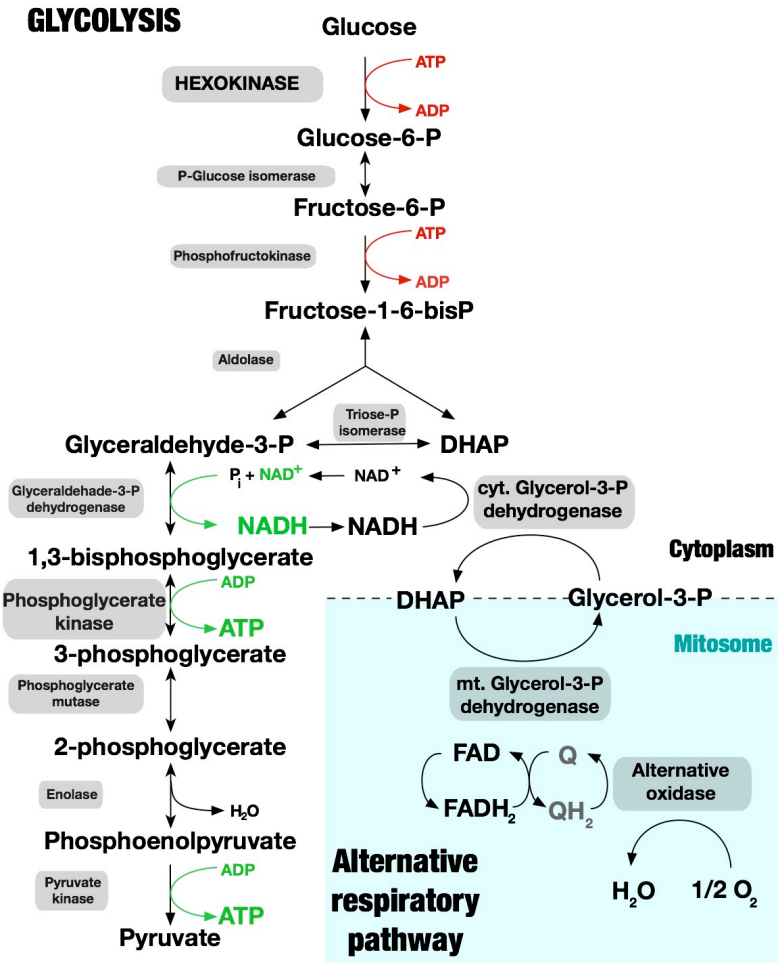

Figure 3.24 Hypothetical model of energy metabolism in *T. hominis*

Reoxidation of NAD is required for continuous generation of ATP in glycolysis and can be carried out by a homologue of cytosolic glycerol-3-P dehydrogenase. The product of the reaction, dihydroxyacetone phosphate (DHAP), can potentially cross the external mitosomal membrane in order to be reoxidised by a *T. hominis* homologue of mitochondrial FAD dependent glycerol-3-P dehydrogenase (mtG3PDH) that localizes to an outer surface of the inner mitochondrial membrane in *S. cerevisiae.* In *S. cerevisiae* mtG3PDH couples DHAP oxidation with reduction of ubiquinone (Q) from the inner mitochondrial membrane. Ubiquinone (Q) is in gray to indicate that the presence of a complete ubiquinone biosynthetic pathway in microsporidia is uncertain. Turquoise colour and dashed line indicate compartmentalisation of the alternative respiratory pathway within the mitosomes of T. hominis.

establish interactions with its host. The spore could utilize the trehalose reserve as a source of glucose for glycolysis although it is uncertain if it is able to metabolise pyruvate, the final product of the pathway. In analysed microsporidian genomes genes encoding only two subunits of the pyruvate dehydrogenase complex (PDH E1 alpha and beta) but not PDH E2 and E3 were identified (Heinz et al., 2012; Katinka et al., 2001; Keeling et al., 2010). It was hypothesized that microsporidia can metabolise pyruvate to acetate using a system based on PDH E1, ferredoxin and ferredoxin oxidoreductase similar to hydrogenosomal pyruvate:ferredoxin

oxidoreductase (Katinka et al., 2001). Alternatively pyruvate could be the final product of glycolysis as in the case of bloodstream stages of *T. brucei* in aerobic conditions (Opperdoes, 1987).

AOX can use ubiquinol (QH_2, Figure 3.24) as an electron donor and transfer electrons to the oxygen, forming the final product of the pathway a water molecule (H_2O, Figure 3.24). Although a complete pathway for biosynthesis of a polyprenyl side chain precursors (mevalonate pathway) seem to be conserved in microsporidia (KEGG pathways (Kanehisa et al., 2014) and BlastP searches), neither of the enzymes required for biosynthesis of the quinoid nucleus and the ubiquinone in yeast, bacteria or animals (Meganathan, 2001) were identified in microsporidian genomes. More detailed bioinformatics investigation will be required in order to test presence of any alternative pathways, possibility of acquiring ubiquinone from the host (Das et al., 2002) or presence of alternative electron carriers such as rhodoquinone proposed to be present in mitochondrial homologue of Pygsuia biforma (Stairs et al., 2014).

The AOX coding gene seems to have been lost independently at least twice in microsporidian evolution: in mosquito parasite capable of infecting humans *Anncaliia algerae* (Williams, et al., 2008) and in the last common ancestor of the lineage that includes microsporidia with smaller genomes (e.g. *Encephalitozoon cuniculi* (Katinka et al., 2001)), and the single microsporidian species that seems to have lost almost entire glycolytic pathway, *E. bieneusi* (Akiyoshi et al., 2009; Keeling et al., 2010), (Figure 3.25). Most of these species have retained a homologue of the mtG3PDH suggesting a possible presence of an 'alternative' terminal oxidase that could have replaced the activity of the AOX in the alternative respiratory pathway. Specific antibodies against *E. cuniculi* mtG3PDH in western blotting experiments detected only a single band corresponding the size of full-length protein (Burri et al., 2006) suggesting that it may not localize to the mitosomal intermembrane space by the specific stop-transfer mechanism. In immunofluorescence experiments the anti-*Ec*mtG3PDH antibodies detected parasite specific fluorescent signals that did not seem consistent with the mitosomal localization indicating possible relocalization of the protein to another cellular compartment (Williams, et al., 2008). This possible relocalization of the mtG3PDH could potentially suggest that the glycerol-3-phospahte shuttle of *E. cuniculi* functions with an uncharacterized 'alternative' terminal oxidase to reoxidize the NAD from the glycolysis in other cellular compartment than the mitosome. It was also hypothesized that *E. cuniculi* may no

longer use glycolysis to generate ATP as its main product (Keeling et al., 2010) but rather in order to provide substrates for biosynthetic reactions (e.g. 1,3-dihydroxyacetone phosphate for biosynthesis of triacylglycerol), (Nakjang et al., 2013).

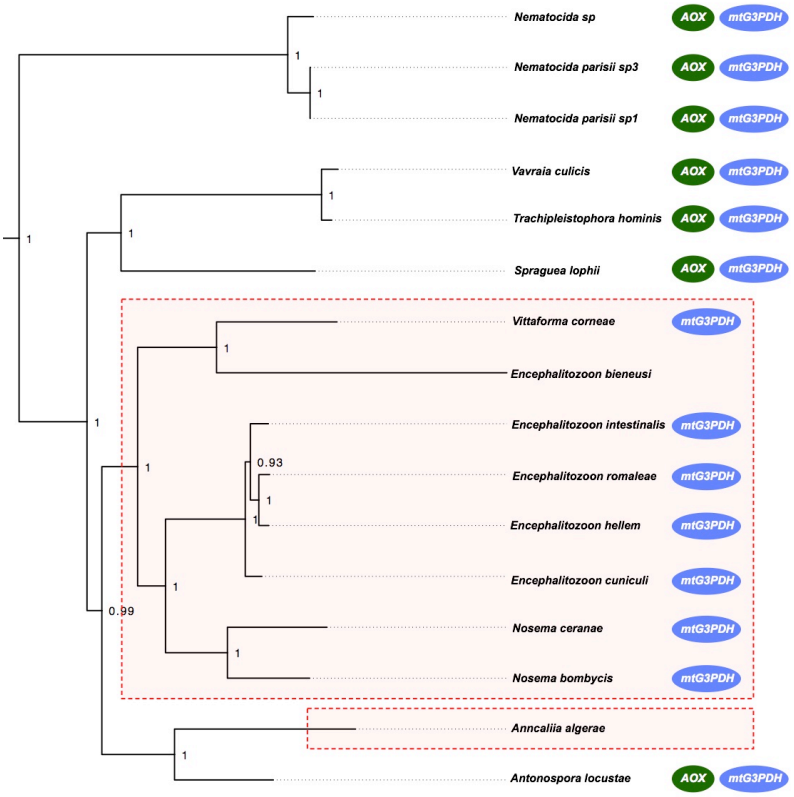

Figure 3.25 Distribution of an alternative oxidase across available microsporidian genome sequences

Distribution of genes encoding the AOX (green) and mtG3PDH (blue) was overlaid on a Bayesian phylogenetic tree of microsporidia inferred from a concatenated alignment of 20 proteins conserved across all of the analyzed microsporidian species (values of posterior probabilities are indicated on the tree). Red dashed line indicates lineages without the AOX gene.

The complete loss of ability to produce ATP in some microsporidia is not unlikely as currently available genomic data suggests that the single microsporidian species; *E. bieneusi,* has almost completely lost its glycolytic pathway together with mtG3PDH and AOX and may be fully dependent on its host for energy generation. *T. hominis* AOX, G3PDH (this study), and glycolytic enzyme PGK-3 (Heinz et al., 2012) are enriched in spores rather than the proliferative intracellular stages of the *T. hominis* life cycle and glycolytic enzymes are among the most abundant proteins in *T. hominis* spore proteomics (Heinz et al., 2012) suggesting that the energy metabolism may be required for infection process and/or survival of *T. hominis* spores. It was speculated that *E. bieneusi* spores might have lost some specific physiological function that could require energy in form of ATP such as an ability to infect the host cell using microsporidian specific infection apparatus (polar tube),

(Williams et al., 2014). This could potentially explain the difficulty in establishing a continuous *in vitro* culture of *E. bieneusi* in mammalian host cell lines as opposed to other human pathogenic microsporidia such as *E. cuniculi* or *T. hominis* (Keeling et al., 2010; Visvesvara, 2002). However it does not explain the loss of AOX in other microsporidian species (e.g. *E. cuniculi*), as they seem to use their polar tube during the infection process (Xu & Weiss, 2005). It was also hypothesized that different microsporidian species could use different mechanisms to induce changes in osmotic pressure that is believed to initiate germination of the spore, and some of these mechanisms could involve conversion of trehalose to glucose - the primary glycolytic substrate - whereas the others not (Undeen & Vander Meer, 1999), but the exact spore germination mechanism is unclear and requires further studies. Alternatively it could be speculated that the non-AOX encoding species do not require energy metabolism because their spores are not exposed to severe environmental conditions such as freezing and/or desiccation, however *E. cuniculi* spores are infective after drying, freezing and storage at -24°C for 24 hours, as well as incubation at room temperature for weeks (Didier et al., 2004).

T. hominis AOX and G3PDH were also detected in the mitosomes of early meronts (this study) that could suggest that *T. hominis* relies on its own energy metabolism just after entering the host cell and before the initiation of the intermediate growth phase that precedes proliferation. The species that do not have AOX might be able to acquire ATP from the host immediately after invading the host cell.

Chapter 4. Molecular detection and characterization of microsporidian spindle pole body

4.1 Introduction

4.1.1 Mechanisms of mitochondrial inheritance

During the cell division process, daughter cells inherit a set of organelles from the mother cell. Some of the organelles, including mitochondria, cannot be formed *de novo,* therefore their presence in the daughter cells depends strictly on the specific organelle partitioning mechanisms (Warren & Wickner, 1996). In model organisms, interactions of mitochondria with cytoskeletal components, including actin microfilaments and microtubules are involved in segregation of mitochondia during the cell division. (See section *1.2.2. Mechanisms of mitochondrial division and segregation*).

The interactions of mitochondria and mitochondrial homologues with other organelles have been also observed in a number of distantly related eukaryotic microorganisms. In apicomplexan parasites such as *Plasmodium falciparum* and *Toxoplasma gondii* physical tethering of multiple organelles to the centrosome - a microtubule organizing center (MTOC) of the mitotic spindle - was proposed to ensure fidelity of their segregation during the cell division (Francia & Striepen, 2014). Each cell of the human malaria parasite *P. falciparum* has a single elongated mitochondrion and a single apicoplast, a relict plastid acquired *via* secondary endosymbiosis. The apicoplasts are partitioned into the daughter cells by association with the centrosome and mitochondria seem to be associated with the apicoplasts (Okamoto et al., 2009).

In the causative agent of the African sleeping sickness, *Trypanosoma brucei,* the single mitochondrion and its genome (kinetoplast) are physically tethered to the flagellar basal body *via* filaments that span through the inner and outer mitochondrial membranes (Ogbadoyi et al., 2003). The basal body is the MTOC, responsible for nucleation of the microtubules of flagella and cilia (Lüders & Stearns, 2007). The association between the MTOC and mitochondrion ensures that each of the *T. brucei* daughter cells inherits a single mitochondrion with a single kinetoplast (Robinson & Gull, 1991). Association with the basal body is also thought to be involved in the inheritance of centrally located mitosomes of *Giardia intestinalis* while the rest of the mitosomes (peripheral mitosomes) seem to be segregated stochastically during the

cell division process (Regoes et al., 2005).

In electron micrographs microsporidian mitosomes are often observed close to the electron-dense plaques inside the nuclear envelope that resembles fungal-specific MTOC, called a spindle pole body (SPB) (Figure 4.1), (Vavra, 2005; Tsaousis et al., 2008; Bigliardi et al., 1998).

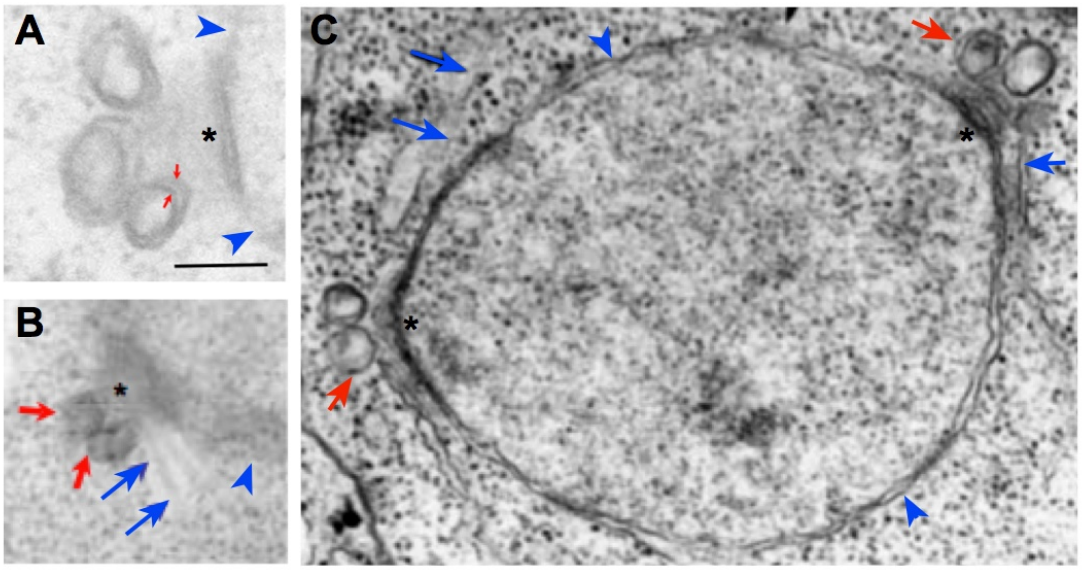

Figure 4.1 Electron micrographs of microsporidian mitosomes observed next to the electron-dense spindle plaques

Electron micrographs were reproduced from (A and B) (Tsaousis et al., 2008) and (C) (Bigliardi et al., 1998).

Double membrane bound vesicles **(red arrows)** reminiscent of the mitosomes characterized in other microsporidian species (Williams et al., 2002) were observed next to the nuclear electron-dense plaques **(black asterisk)** in ultrathin sections of fixed *E. cuniculi* **(A and B)** and *E. intestinalis* **(C)** cells. Nuclear membranes **(blue arrowheads)** and microtubules **(blue arrows)** were indicated.

4.1.2 Fungal spindle pole body

The fungal SPB is an organelle considered as analogous to the centrosome (Leidel & Gönczy, 2003) and serves as MTOC, a site of microtubule assembly (nucleation). In budding yeast, *Saccharomyces cerevisiae,* SPB is localized inside the pore in the nuclear envelope throughout the life cycle whereas in fission yeast, *Schizosaccharomyces pombe,* it is inserted into the nuclear envelope before initiation of mitosis. Owing to the fact that the nucleus of yeast is intact throughout their cell cycle (closed mitosis) the SPB is a site of microtubule assembly on both sides of the nuclear envelope (cytosolic and nucleoplasmic), (Winey & Bloom, 2012; Muller et al.,

2005; Jaspersen & Winey, 2004).

The SPB of *S. cerevisiae* is a large protein complex that consists of at least 18 core components assembled into three main layers (plaques), namely: central, inner and outer plaque (Figure 4.2 C), (Muller et al., 2005; Jaspersen & Winey, 2004). The central plaque is located inside a pore in the nuclear envelope, interconnects the outer and the inner plaques, and is involved in anchoring to the nuclear membrane. The inner plaque faces the nucleoplasm and is a site of nuclear microtubules nucleation whereas the outer plaque faces the cytosol and nucleates the cytoplasmic microtubules. In addition to the three plaques electron micrographs indicated the presence of a protrusion parallel to the nuclear membrane that extends from the central plaque on one side of the organelle. This protrusion is called a half-bridge and is involved in duplication of the SPB.

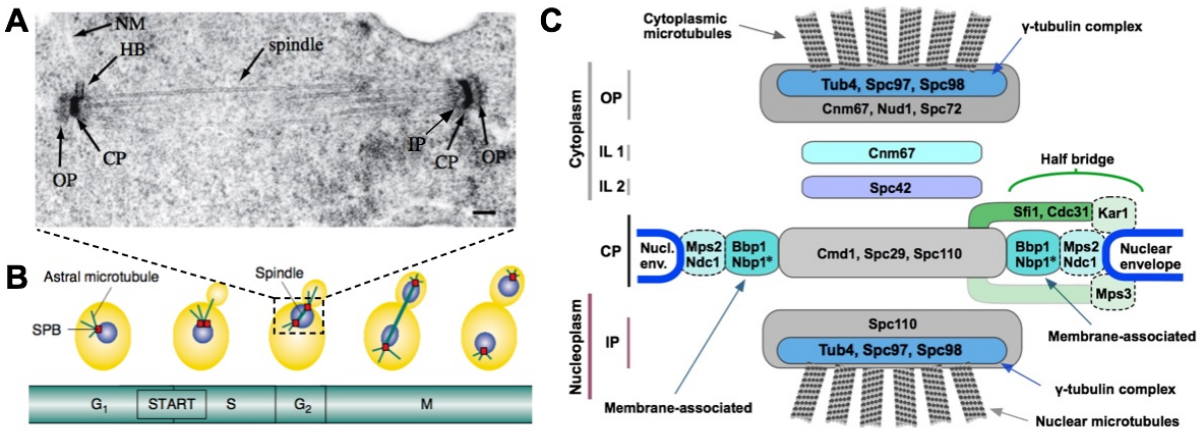

Figure 4.2 Structure and localization of *S. cerevisiae* spindle pole body
Images were adapted from (Kilmartin, 2014), (A) and (Segal & Bloom, 2001), (B).
(A) Thin section through a *S. cerevisiae* spindle apparatus showing two SPBs. Spindle microtubules **(spindle)**; nuclear membrane **(NM)**; as well as major elements of the SPB structure: central plaque **(CP)**, outer plaque **(OP)**, inner plaque **(IP)**, and half-bridge **(HB)** are visible. Scale bar indicates 100 nm.
(B) Duplication and segregation of the SPBs during *S. cerevisiae* cell cycle. The SPB nucleates both the astral and the spindle microtubules. In early G1 phase yeast cell contain only one SPB that starts duplicating in the late G1 phase. Duplication of the SPB ends in the early G1 phase and the two SPBs remain next to each other throughout DNA replication. During mitosis each of the daughter cells inherits single SPB.
(C) Model of the *S. cerevisiae* SPB showing the localization of its major components. Dashed boxes and asterisks indicate nuclear membrane proteins. Central plaque **(CP)**, outer plaque **(OP)**, inner plaque **(IP)**, and inner layer 1 **(IL 1)** and 2 **(IL 2)** were indicated.

The SPB is duplicated only once per cell cycle, and a single nucleus with a single SPB is transferred to each of the daughter cells during the cell division (Figure 4.2 B), (Seybold & Schiebel, 2013). In G2 phase of the *S. cerevisiae* cell cycle two SPBs migrate to the opposite sides of the nucleus to form two poles of the mitotic spindle (Muller et al., 2005; Jaspersen & Winey, 2004). A similar arrangement of two SPB-like plaques on two opposite sides of the nucleus has been observed in microsporidia (Figure 4.1 C), (Bigliardi et al., 1998).

4.2 Aims

Representatives of different eukaryotic lineages seem to rely on different mechanisms for segregation of mitochondrial during the cell division process. Parasitic protists such as *P. falciparum* (Okamoto et al., 2009) and *T. brucei* (Ogbadoyi et al., 2003) have only a single mitochondrion that seems to be associated with the microtubule organizing center (MTOC) of these organisms (in case of *P. falciparum* indirectly through the apicoplast). As each daughter cell inherits a single MTOC it also inherits the single mitochondrion. A similar mechanism has been proposed in *Giardia intestinalis* where a small subpopulation of the mitosomes seems to be associated with the MTOC through the cell cycle (Regoes et al., 2005).

Microsporidia such as *E. cuniculi* can have only a few mitosomes per cell (Tsaousis et al., 2008; Williams et al., 2002; Tachezy & Šmíd, 2008b) and it seems highly unlikely that they could rely on the stochastic mechanisms of inheritance to provide all daughter cells with the organelle. Electron micrographs indicate a possible presence of yeast-type MTOC, the SPB, in microsporidian nuclear envelope usually observed in close proximity of tiny double membrane bound organelles reminiscent of microsporidian mitosomes. Here I used bioinformatics tools and specific antibodies that I have generated against the microsporidian SPB protein candidates to test the hypothesis that microsporidian electron-dense spindle plaque is an organelle homologous to the fungal SPB in the two microsporidian species *T. hominis* and *E. cuniculi*. The specific antibodies were also used in double labeling experiments with antibodies against the known mitosomal marker (mtHSP70) in order to test the hypothesis that the mitosomes of *T. hominis* and *E. cuniculi* are associated with the SPB in all stages of their life cycle.

4.3 Results

4.3.1 Identification of fungal spindle pole body protein homologues in microsporidian genomes

BlastP (Altschul et al., 1990) and hidden Markov model (HMM) profile searches (Eddy, 2001) were performed in order to identify microsporidian homologues of characterized *Saccharomyces cerevisiae* and *Schizosaccahromyces pombe* spindle pole body proteins. Sequences of yeast homologues were downloaded from NCBI protein sequence database (http://www.ncbi.nlm.nih.gov/protein/) and used as queries in BlastP searches against a local database of microsporidian protein sequences from *T. hominis, E. cuniculi E. intestinalis, E. bieneusi, N. ceranae, A. locustae* and *N. parisii* ERTm1 (Table 4.1**)**. Microsporidian homologue candidates of yeast Tub4, Mps3 (Sad1) were found using BlastP searches. Multiple sequences containing common calcium binding motifs (EF hand) were identified in BlastP searches using Cmd1 (Cam1) and Cdc31 as queries however apart from the region containing EF hand neither of the microsporidian sequences aligned well with the yeast proteins. BlastP searches using Nud1 as query have identified multiple protein sequences containing leucine-rich repeat (LRR4) motif in *A. locustae* but not in other microsporidia.

Table 4.1 Identification of spindle pole body protein candidates in microsporidian genomes using BlastP and HMMER searches

SPB protein	Query gi number	BlastP result	HMMER result (PFAM)	Hit gi number (*T. hom / E. cun*)
Homologue candidates				
Tub4	6323241	+ (1 e^{-78})	+ (Tubulin/TubulinC)	440493798/19173393
Spc97/Spc98 (*Alp4/Alp6*)	6321966/6324203 (4757365/7649808)	-	+ (SPC97_SPC98)	440491835/19074786
Mps3 (*Sad1*)	398364651 (162312233)	+ (5 e^{-12})	+ (Sad1_UNC)	440491828/ 19074959
Weak homologue candidates (contain common protein motifs/domains)				
Cmd1 (*Cam1)*	536373	+ (5 e^{-15})	+ (EF_hand_5)	440492623/19173343
Cdc31	1420581	+ (2 e^{-9})	+ (EF_hand_5)	440492623/ 19173343
No microsporidian homologue candidates identified				
Nud1	4068	+ (1 e^{-19} only in *A. locustae*)	+ (LRR_4)	
Spc110 (*Nuf1)*	398366517	-		
Kar1	1302177	-		
Mps2	6321363	-		
Spc29	462707	-		
Cnm67	6324104	-	- (SID)	
Ndc1	575688	-	- (Ndc1-Nup)	
Sfi1	1235597	-	- (Sfi1/Sfi1C)	
Bbp1	1113129	-		
Spc72	330443372	-	- (Mto2_bdg)	
Spc42	398364591	-	- (Spc42p)	
Pcp1	2842697	-	- (Microtub_assoc/ PACT_coil_coil)	
Cut11	159883974	-	- (Ndc1-Nup)	
Ppc89	1184024	-	- (Cep57_CLD/ Cep57_MT)	
Ima1	3581922	-	- (DUF2349)	
Kms1	19115110	-	- (KASH)	
Kms2	2894299	-	- (KASH)	
Sid4	3184072	-	- (SID)	

Sequences **(Query gi number)** of characterized *S. cerevisiae* and *S. pombe* (***italicised***) SPB proteins were used as queries in BlastP searches against the local database of microsporidian protein sequences encoded in genomes of *T. hominis, E. cuniculi E. intestinalis, E. bieneusi, N. ceranae, A. locustae and N. parisii ERTm1*. In the **BlastP result** '+' indicates detection of microsporidian sequences with E-value lower than 0.01 (the lowest E-values were indicated) whereas '-' indicates that all detected sequences had E- values above 0.01.

The yeast sequences **(Query gi number)** were also used to identify hmm profiles (**PFAM)** in the PFAM database using PFAM search tool. The identified hmm profiles were used as queries in the hmmer profile searches against the microsporidian protein database (the same as in the BlastP searches). In **HMMER result** '+' indicates detection of the sequence above the default inclusion threshold (E-values below 0.01) whereas '-' indicates that all detected sequences were below the inclusion threshold.

The 'Hit gi numbers' are gi numbers of the highest scoring sequences from *T. hominis* and *E. cuniculi* from both BlastP and HMMER searches.

Many of the microsporidian protein sequences share low percentage of identity with their fungal homologues, thus Blast searches are often not sensitive enough to detect homologues of fungal proteins in microsporidia. More sensitive HMM profile searches use a probabilistic model of a consensus of a multiple sequence alignment (with a position-specific scoring system for substitutions, insertions, and deletions) rather than a single sequence as a query (as in BlastP) and use a probabilistic theory to set scoring parameters rather than using fixed parameters (as in PSI-Blast). Profiles of the protein families containing the yeast SPB proteins were identified using Pfam search tool (http://pfam.xfam.org/search) and downloaded from Pfam database (http://pfam.xfam.org). HMM profile searches identified two microsporidian proteins containing an SPC97/SPC98 specific domain (*T. hominis* gi: 440492072 and 440491835) in addition to the sequences that were initially found using BlastP searches. Analyses of the multiples sequence alignment of the microsporidian SPC97/98 homologue candidates indicated that one of the *T. hominis* sequences (gi 440492072) is missing the C-terminal region (300 amino acids) present in other microsporidian sequences. The tBlastN searches and manual analysis of the region of *T. hominis* genome encoding the gi 440492072 open reading frame (ORF) indicated that the sequence is truncated due to presence of a premature stop codon caused by an insertion of a singe nucleotide. Sequencing of a PCR amplified and cloned nucleotide sequence containing the ORF and 900 nucleotides downstream (ORF+900) from the premature stop codon has confirmed that the frame shift is an error in the genome sequence. The sequence of the ORF+900 can be found in Appendix A.

Maximum likelihood phylogeny of the eukaryotic gamma tubulin complex proteins (GCP) that contain the SPC97/SPC98 domain including sequences from *Homo sapiens* (GCP 2, 3, 4 and 5), *S. cerevisiae* (Spc97 and Spc98) and *S. pombe* (Alp4 and Alp6), as well as sequences identified in microsporidia was generated with RAxML under LG+I+G model with 100 rapid bootstrap replicates (Figure 4.3 B). The microsporidian homologues formed long branches at the base of the GCP3/SPC98/Alp6 clade and GCP2/SPC97/Alp4 clade, which is consistent with them being highly divergent SPC98/Alp6 (ORF+900) and SPC97/Alp4 (gi 440491835) orthologues.

BlastP and hmm profile searches using respectively yeast γ-tubulin (Tub4) sequence and Tubulin/TubulinC profiles have identified three sequences in each of the analyzed microsporidian genomes annotated as alpha - tubulin, beta - tubulin and

gamma - tubulin (Figure 4.3 A). Result of the phylogenetic analyses of the tubulin homologues from yeast, humans and microsporidia, was in agreement with the original annotation.

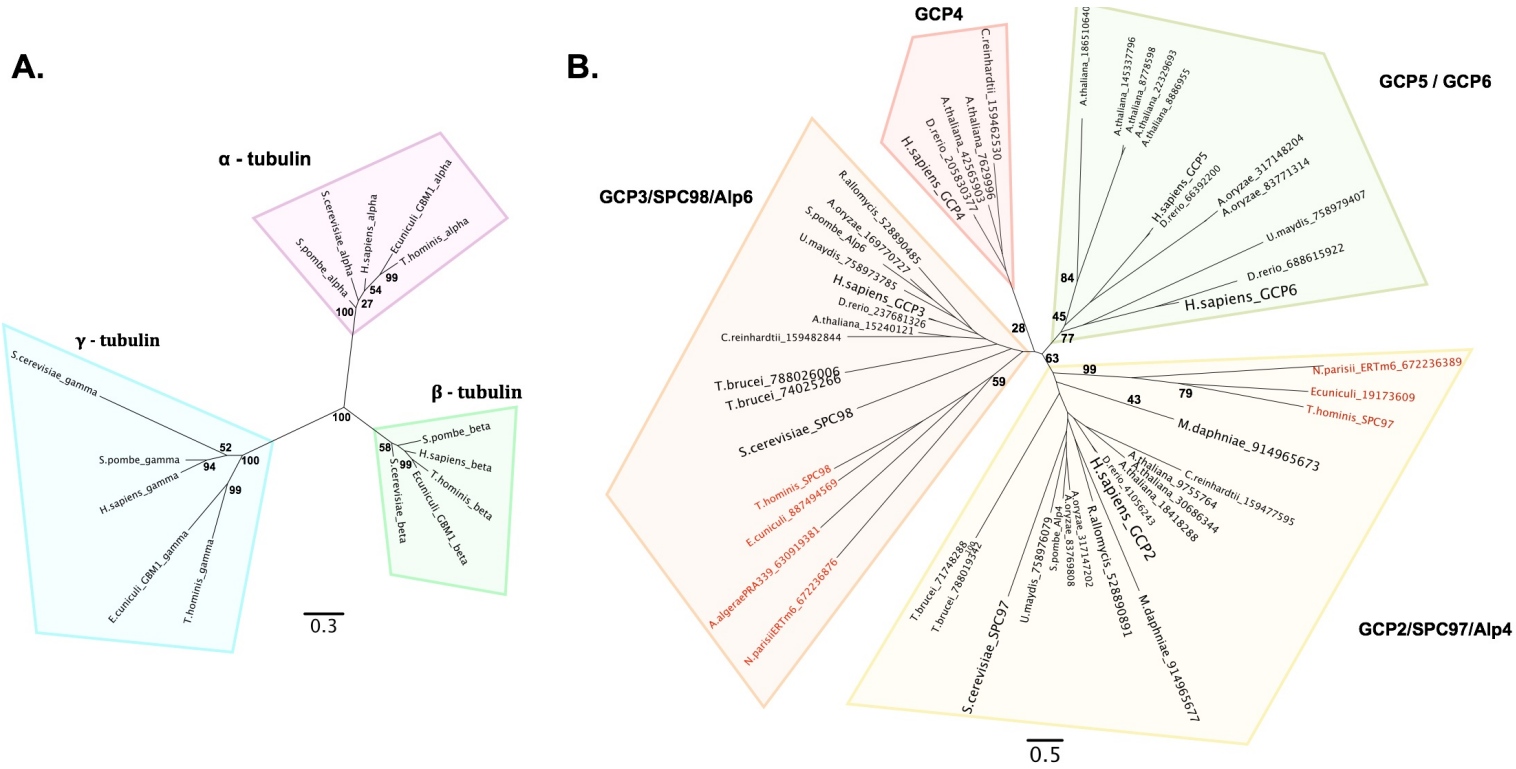

Figure 4.3 Phylogenetic trees of eukaryotic tubulins (α, β, γ) and γ-tubulin complex proteins (2, 3, 4, 5, and 6) including homologues from microsporidia

(A.) Three tubulin homologues annotated in *E. cuniculi* and *T. hominis* genome sequences as α -, β - and γ - tubulin in phylogenetic trees group together with the respective homologues from yeast and human with high bootstrap values (100). The tree was generated using RAxML under LG+I+G model with 100 rapid bootstrap replicates in RAxML based on trimmed (trimAL, gappyout method) alignment (MUSCLE) of 15 sequences of 433 amino acid positions.

(B.) Microsporidian sequences identified based on the HMMER profile search with SPC97_SPC98 PFAM profile form long branches at the base of the GCP3/SPC98/Alp6 group (low bootstrap value of 59) and GCP2/SPC97/Alp4 group (high bootstrap value of 99). Overall topology of the tree is consistent with previously published phylogenies of the eukaryotic GCP proteins (Murata et al., 2007). The tree was generated using RAxML under LG+I+G model with 100 rapid bootstrap replicates in RAxML based on trimmed (trimAL, gappyout method) alignment (MUSCLE) of 51 sequences of 440 amino acid positions.

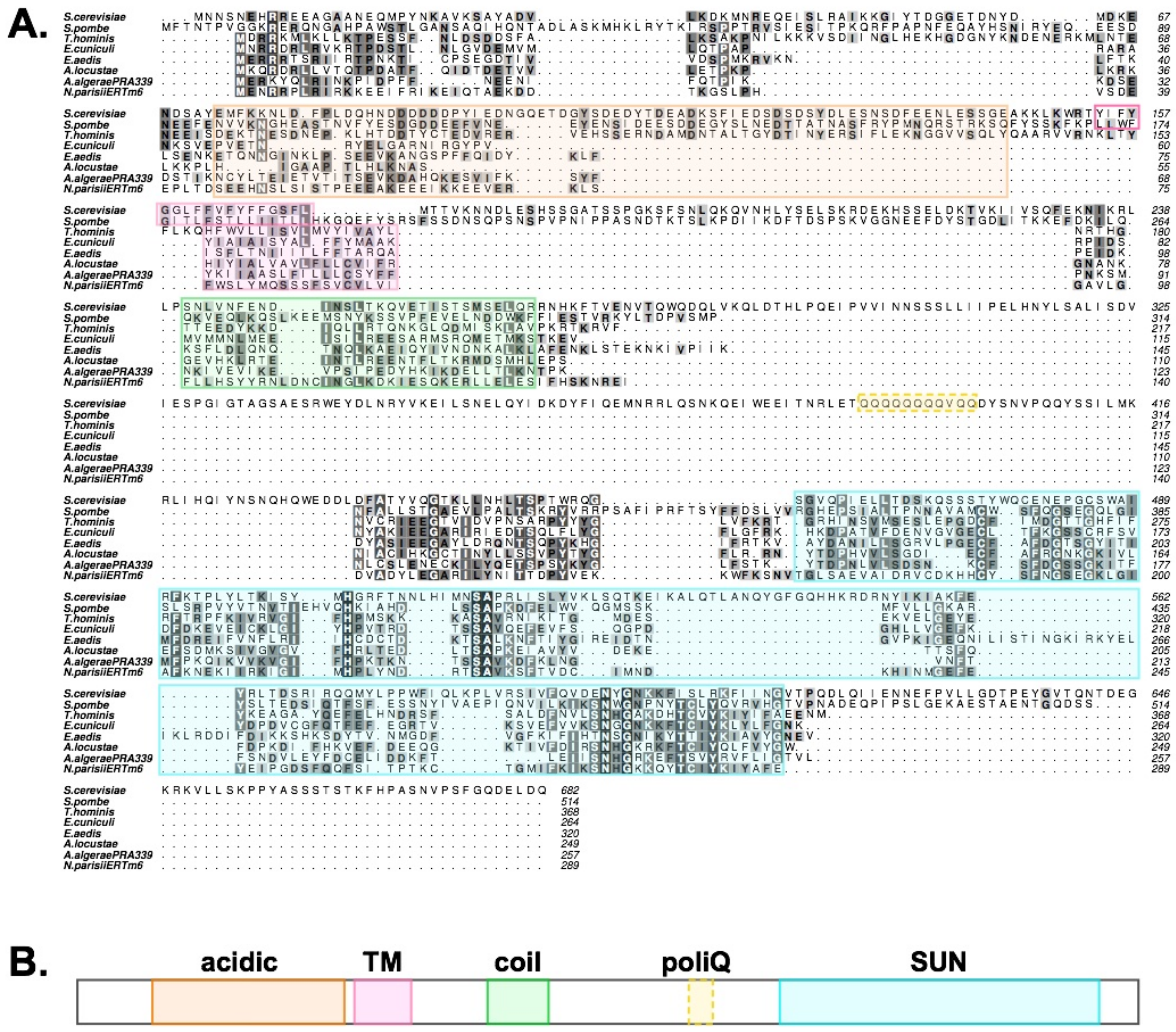

Figure 4.4 A multiple sequence alignment and protein domain architecture of *S. cerevisiae* MPS3, *S. pombe* Sad1 and microsporidian homologues

(A.) Transmembrane domains predicted using TMHMM (magenta), coil-coiled region predicted with COIL (green), and SUN domain predicted with InterProScan5 (blue) were indicated on the alignment. *S. cerevisiae* specific poliQ domain (yellow) and acidic domain (orange) were indicated based on the published sequence analyses of the MPS3 and Sad1 (Jaspersen, 2006).

(B.) Domain architecture conserved in analysed SUN-domain containing proteins from *S. cerevisiae*, *S. pombe* and *T. hominis*. The poliQ domain is present only in the *S. cerevisiae* homologue.

Bioinformatic analyses of microsporidian and yeast MPS3 homologues predicted the presence of transmembrane domain (TMHMM), coiled coil region (COIL), and SUN domain (InterProScan5) in the regions of the multiple sequence alignment corresponding to the MPS3/Sad1 domain architecture described in the literature (Jaspersen, 2006), (Figure 4.4). The *S. cerevisiae*-specific poliQ region was not detected in the microsporidian homologues or *S. pombe* Sad1. The region corresponding to the full-length yeast acidic N-terminal domain was identified only in MPS3 homologue from *T. hominis* as opposed to other microsporidian homologues

where the corresponding region seems to be truncated. In all microsporidian homologues the sequence between the predicted transmembrane domain and the predicted coiled coil region is significantly shorter (around 60 amino acids) than in yeast homologues.

4.3.2 Cloning and expression of E. cuniculi TUB4, and T. hominis SPC98, MPS3 and TUB4 homologues for polyclonal antibodies production

Full-length *T. hominis* TUB4 and *E. cuniculi* TUB4 coding genes were amplified from respectively *T. hominis* and *E. cuniculi* genomic DNA using primers with NdeI or BamHI restriction sites (*T. hominis*) and NdeI or XhoI restriction sites (*E. cuniculi*).

T. hominis SPC98 coding gene excluding first 66 nucleotides on the 5' end, and 84 nucleotides on the 3' terminus was amplified from *T. hominis* genomic DNA using primers with NdeI or BamHI restriction sites. The 5' and 3' termini sequences were removed due to problems with amplification of the gene using primers complementary to the sequence within these regions potentially caused by a high AT contents.

Two fragments of *T. hominis* MPS3 gene adjacent to the sequence encoding a predicted transmembrane domain (5' CACTTTTGGGTTCTTCTTATTTCAGTACTTATGGTCTACATCGTCGCGTAT 3'), were amplified using external primers with KpnI or PstI restriction sites and internal primers (in region adjacent to the transmembrane domain) with EcoRI restriction sites. The two fragments were ligated using the EcoRI restriction site in order to form a fusion polypeptide corresponding to the MPS3 without the transmembrane domain-coding region and without 45 nucleotides at the 3' terminus. The 45-nucleotide 3' terminus sequence was removed based on the high probability to form a hairpin structure within this region based on the analysis using Primer3 (http://primer3.ut.ee).

Amplified sequences of *T. hominis* tub4, spc98, and *E. cuniculi* tub4 coding genes were cloned into pET16b plasmid. Sequencing of three clones of each construct confirmed correct insertion of the sequence into the plasmid. The recombinant proteins of expected size (recombinant *T. hominis* SPC98, 66 kDa; recombinant *T. hominis* TUB4, 50 kDa; recombinant *E. cuniculi* TUB4, 50 kDa) were expressed using a standard IPTG induction protocol in *E. coli* BL21 (DE3), (Figure

4.5 A, B and C). The expected size of the proteins was calculated using ExPASy Compute pI/Mw tool (http://web.expasy.org/compute_pi/).

The amplified mps3 sequence, without the transmembrane domain-coding region and without 45 nucleotides at the 3' terminus, was cloned into pQE40 plasmid in frame with the DHFR in order to increase chances of high levels of expression in *E. coli* and increase the antigenicity of the fusion protein (DHFR fusion protein is discussed in more detail in section 3.2.2). Sequencing of three clones of the construct confirmed correct insertion of the sequence into the plasmid. The recombinant protein of expected size (62 kDa) was expressed using a standard IPTG induction protocol in *E. coli* M15 transformed with the pQE40-*th*mps3 plasmid construct (Figure 4.5 D).

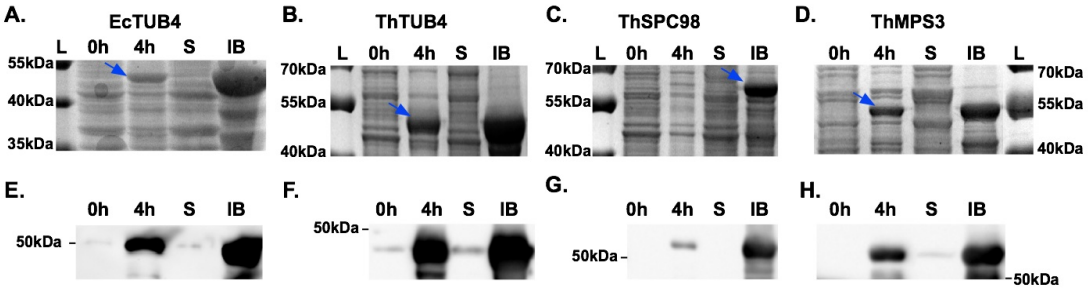

Figure 4.5 Expression and purification of *E. cuniculi* TUB4 and *T. hominis* TUB4, SPC98 and MPS3 from *E. coli.*

(A, B, C and D) Coomassie blue stained SDS polyacrylamide gels showing expression of recombinant EcTUB4 (A), ThTUB4 (B), ThSPC98 (C) and *T. hominis* MPS3 (D). Protein bands (blue arrows) corresponding to the expected molecular weights (A, 50 kDa; B, 50 kDa; C, 66 kDa; and D, 62 kDa). Molecular weight values correspond to the protein ladder bands (L).

(E, F, G and H) The same samples were used in western blotting experiments with anti-His tag antibodies conjugated to HRP. Protein bands corresponding to the expected molecular weights were detected in insoluble IB fractions as well as in protein extracts from bacteria expressing recombinant *Ec*TUB4 (E), *Th*TUB4 (F), *Th*SPC98 (G) and *Th*MPS3 (H).

Recombinant *Ec*TUB4, *Th*TUB4, *Th*SPC98 and *Th*MPS3 were extracted from bacteria and purified using BugBuster kit (Figure 4.5). All recombinant proteins were found mostly in the insoluble fraction. 1 mg of purified *Ec*TUB4, *Th*TUB4, *Th*SPC98 and *Th*MPS3 inclusion bodies were separated on SDS polyacrylamide gels and InstantBlue (Expedeon) stained bands corresponding to the proteins were cut out of the gels and sent to Agrisera (http://www.agrisera.com/) for immunisation of rats (*Th*MPS and *Th*SPC98) and to Eurogentec (http://www.eurogentec.com/) for

immunisation of rabbits (*Ec*TUB4, *Th*TUB4). *Th*SPC98 rather than *Th*SPC97 was used to generate antibodies due to the low expression levels of the *Th*SPC97 in *E. coli* (not shown).

4.3.3 Testing of polyclonal antisera raised against recombinant E. cuniculi TUB4, and T. hominis SPC98, MPS3 and TUB4 using western blotting

In western blotting experiments with rat polyclonal sera raised against recombinant *T. hominis* MPS3 a single band with an apparent relative molecular weight (rMW) of approximately 44 kDa (predicted size of the full length protein, 43 kDa) was detected in protein extracts from *T. hominis* spores and *T. hominis* infected rabbit kidney cells (RK13) but not in extracts from the non-infected host (Figure 4.6 B). Rat polyclonal sera against recombinant *T. hominis* SPC98 detected two parasite specific bands in protein extracts from *T. hominis* spores and *T. hominis* infected rabbit kidney cells (RK13) but not in extracts from the non-infected RK cells (Figure 4.6 A). The rMW of the more intense band corresponded to the predicted molecular weight of the full-length *T. hominis* SPC98 (76 kDa). Lower rMW of the less intense band (approximately 60 kDa) suggests that it may be a degradation product of the full-length protein.

Rabbit polyclonal sera against recombinant *E. cuniculi* TUB4 detected very strong signal in the *E. cuniculi* infected and non-infected RK cells indicating a cross-reactivity of the sera with a host protein that migrated with an apparent rMW matching the predicted size of the full-length *E. cuniculi* TUB4 (48 kDa), (Figure 4.7 A). Very faint -potentially parasite specific- signal of the same rMW was detected in protein extracts from purified *E. cuniculi* spores. In order to increase the concentration of specific antibodies and to reduce concentration of the unspecific antibodies (potentially responsible for the detection of the host specific signal) the polyclonal sera were affinity purified against the recombinant *E. cuniculi* TUB4. The affinity purified anti-*Ec*TUB4 antibodies detected a parasite specific signal of the expected size (48 kDa) in protein extracts from *E. cuniculi* spores and *E. cuniculi* infected rabbit kidney cells (RK13) but not in extracts from the non-infected host. Also, the contaminating host specific signal was no longer detected (Figure 4.7 B).

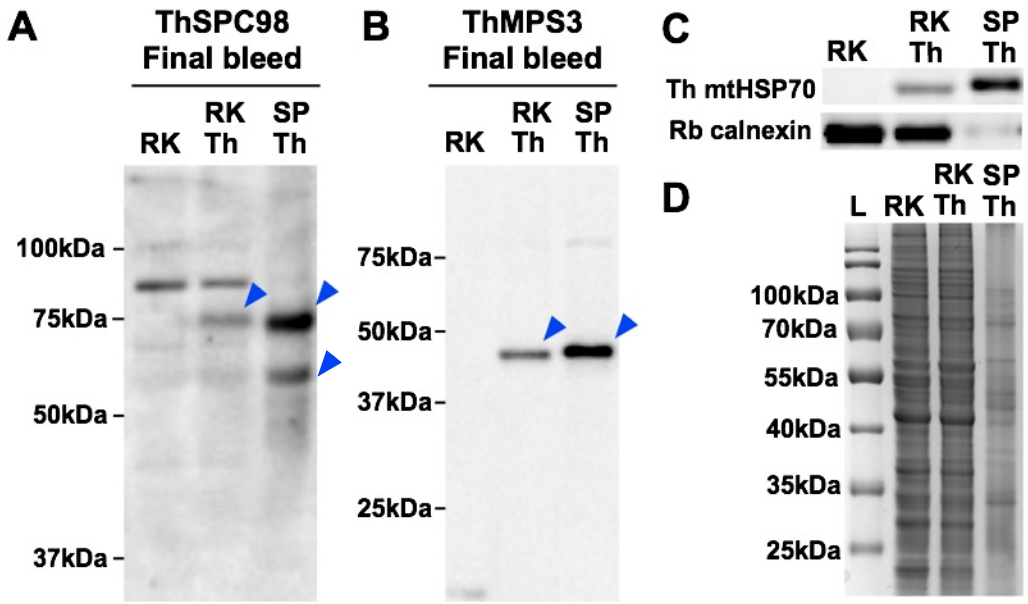

Figure 4.6 Testing the specificity of the anti-ThSPC98 and anti-*Th*MPS3 antibodies in total protein extracts from *T. hominis* spores, *T. hominis* infected and non-infected rabbit kidney (RK-13) cells

(A) Polyclonal antiserum from the final bleed of a rabbit immunised with the recombinant *T. hominis* SPC98 (1:500 dilution) was tested against total protein extracts from purified *T. hominis* spores (**SPTh**), *T. hominis* infected rabbit kidney cells (**RKTh**) and non-infected rabbit kidney cells control (**RK**). Two parasite specific bands migrating with relative apparent molecular weights of ~60kDa and ~70kDa were detected in RKTh and ThSP but not in the RK control (**blue arrowhead**).

(B) Polyclonal antiserum from the final bleed of a rabbit immunised with the recombinant *T. hominis* MPS3 (1:500 dilution) detected a single parasite specific band migrating with an apparent relative molecular weight of ~44 kDa (**blue arrowhead**) in the RKTh and the SPTh but not in the RK.

(C) Rat anti-*Th*mtHSP70 antisera (1:1000 dilution) detected single band migrating with an apparent molecular weight of ~60 kDa in the RKTh and the SPTh but not in the RK control. Commercial antibodies against mammalian calnexin detected single band (~80 kDa) in the RK and the RKTh but not in the SPTh.

(D) Coomassie blue stained polyacrylamide gel with total protein extracts from RK, RKTh and SPTh. Approximately 20 µg (based on BCA assay) of each extract was loaded onto the gel. The gel is an equivalent of the gels used in western blotting experiments (A), (B) and (C).

Blot probed with final bleeds were exposed for 10 - 20 s.

Molecular weights of the bands were estimated using 'MW analysis tool' implemented in the Image Lab (Bio-Rad). Precision Plus Protein™ WesternC™ standard (Bio-Rad) was used in (A) and (B). PageRuler protein ladder (Thermo Scientific) was used in (D).

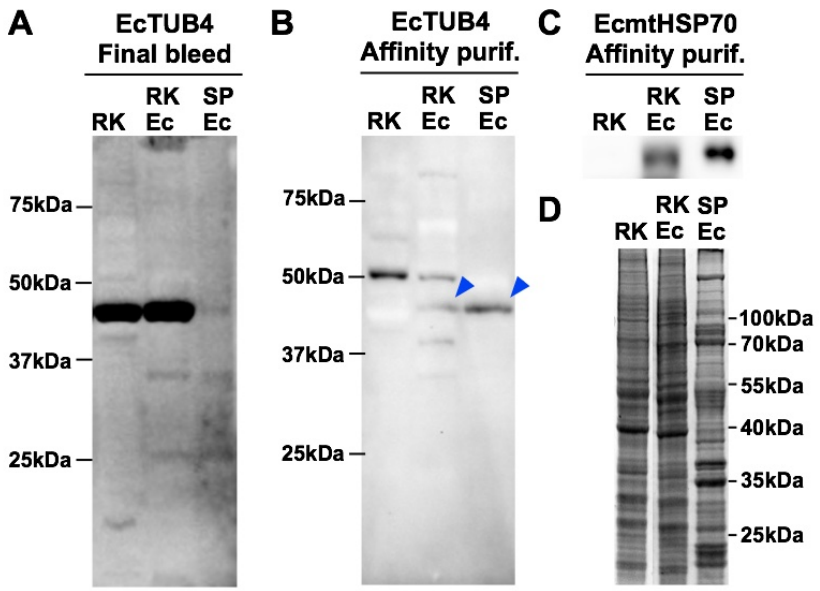

Figure 4.7 Testing the specificity of the anti-*Ec*TUB4 antibodies in total protein extracts from *E. cuniculi* spores, *E. cuniculi* infected and non-infected rabbit kidney (RK-13) cells

(A) Polyclonal antiserum from the final bleed of a rabbit immunised with the recombinant *E. cuniculi* TUB4 (1:1000 dilution) was tested against total protein extracts from purified *E. cuniculi* spores (**SPEc**), *E. cuniculi* infected rabbit kidney cells (**RKEc**) and non-infected rabbit kidney cells control (**RK**). A single intense band migrating with an apparent molecular weight of ~48 kDa was detected in RK and RKEc but only a very faint band of the same size was detected in SPEc.

(B) EcTUB4 antisera affinity purified against the immunogen (1:250 dilution of 0.22 mg/ml stock) detected a single parasite specific band migrating with apparent molecular weights of ~48 kDa (**blue arrowhead**) in the RKEc and the SPEc but not in the RK control.

(C) Affinity purified rabbit anti-*Ec*mtHSP70 antisera (1:500 dilution of 0.16 mg/ml stock) detected single band migrating with an apparent molecular weight of ~65 kDa in protein extracts from *E. cuniculi* infected RK cells and purified *E. cuniculi* spores but not in non-infected RK cells control.

(D) Coomassie blue stained polyacrylamide gel with total protein extracts from RK, RKEc and SPEc. Approximately 20 µg (based on BCA assay) of each extract was loaded onto the gel. The gel is an equivalent of the gels used in western blotting experiments (A), (B) and (C)**.**

Blot probed with the affinity purified anti-*Ec*TUB4 antibodies was exposed for 600 s in order to visualize all bands. Blot probed with final bleed was exposed for 60 s.

Molecular weights of the bands were estimated using 'MW analysis tool' implemented in the Image Lab (Bio-Rad). Precision Plus Protein™ WesternC™ standard (Bio-Rad) was used in (A) and (B). PageRuler protein ladder (Thermo Scientific) was used in (D).

Polyclonal sera raised against recombinant *T. hominis* TUB4 did not detect any signals on western blots with protein extracts from *T. hominis* spores or RK-13 cells. They also failed to detect any signals in western blots with the recombinant *Th*TUB4 used as an immunogen indicating that the immunogen has not sufficiently induced production of specific antibodies in the immunised rabbits. Sera were further

tested with other microsporidian recombinant proteins used in this study in order to rule out the possibility of mixing up the samples and also did not detect any signals. It is likely that microsporidian γ-tubulins display weak immunogenicity in rabbits as only one out of two sera from rabbits immunized with *E. cuniculi* TUB4 detected the immunogen (recombinant *Ec*TUB4) in western blotting experiments and affinity purification of 20 ml of this serum against the immunogen yielded only 100 µl of 1 mg/ml purified antibodies while affinity purification of sera against other proteins raised in this study routinely had ten times higher yield (100 µl of 1 mg/ml antibodies out of 2 ml of serum).

4.3.4 Investigating intracellular localisation of the SPC and MPS3 in Trachipleistophora hominis cells and TUB4 in Encephalitozoon cuniculi cells using immunofluorescence microscopy experiments

In immunofluorescence microscopy experiments rat polyclonal antisera against *T. hominis* SPC98 and MPS3 detected punctate fluorescent signals at the circumference of the DAPI stained round nuclei of the parasite (observed either in the XY or in the XZ plane of the Z-stack), which is consistent with the localization of the detected protein to the nuclear envelope of the parasite (Figure 4.8 A and 4.8 B). Signals detected in experiments with polyclonal antisera against ThSPC98 had very low signal to noise ratio and the punctate signals above the background level were observed only in a small fraction of the parasite nuclei. Affinity purification of the antibodies, titering the dilution (between 1:2 and 1:2000) of the antibodies, testing different incubation times (30 minutes to overnight) and conditions (room temperature or 4°C) of the incubation with the primary antibody as well as testing different cell fixation and permeabilization protocols did not improve the signal to noise ratio indicating that it may be due to the low affinity of the specific antibodies to the detected protein. In addition to the punctate signals the anti-*Th*SPC98 antibodies detected a very weak dispersed signal inside the DAPI stained nucleus that might be due to the presence of a non-SPB associated potentially soluble fraction of *T. hominis* SPC98 inside the parasite nucleus or due to the unspecific binding of the antibodies to another nuclear protein (Figure 4.8 A). The number of the punctate signals detected in experiments with rat polyclonal antisera against *Th*MPS3 was different in different stages of the parasite life cycle. In the early meronts (small round cells observed in the first hours of the infection), either a single MPS3 signal or two

MPS3 signals, at the opposite sides of the DAPI stained nucleus were observed (Figure 4.8 B).

Affinity purified rabbit polyclonal antisera against *E. cuniculi* TUB4 (*Ec*TUB4) detected punctate fluorescent signals that colocalized with DAPI stained nuclei (Figure 4.8 C). Similar to the *Th*SPC98 and *Th*MPS3 detected in *T. hominis* cell the *Ec*TUB4 signals were always observed at the circumference of the round DAPI stained nuclei of *E. cuniculi*. Similar to *Th*MPS3 most often two *Ec*TUB4 signals were observed at the opposite sides of the DAPI stained nucleus although nuclei with a single *Ec*TUB4 signal were also observed.

Antibodies raised against *T. hominis* proteins did not detect any fluorescence signals in *E. cuniculi* cells and antibodies raised against *E. cuniculi* TUB4 did not detect any fluorescence signals inside *T. hominis* cells.

As expected based on the results of western blotting experiments antibodies raised against *T. hominis* TUB4 did not detect any fluorescence signals in *T. hominis* or *E. cuniculi* cells.

In double labelling experiments with the anti-*T. hominis* MPS3 antisera raised in rat and the affinity-purified antisera against *T. hominis* mitosomal proteins: mtHSP70 (Figure 4.9 B) or AOX (Figure 4.9 A) raised in rabbit, the punctate fluorescent MPS3 signals were partially overlapping with the fluorescent signals corresponding to the mitosomal proteins but never fully colocalized. Similar localization pattern was observed in *E. cuniculi* cells using affinity purified anti-*E. cuniculi* mtHSP70 antisera raised in rabbit and affinity purified anti-*E. cuniculi* TUB4 antisera raised in rabbit and covalently linked to a fluorophore (using Alexa488 APEX™ Antibody Labeling Kit, Invitrogen). Directly labelled primary antibodies were always used in the second primary antibody incubation following thorough washes after the incubation with anti-rabbit fluorophore-linked secondary antibodies in order to avoid cross-reaction of the directly labelled primary antibodies with the labelled secondary antibodies.

In double labelling experiments the anti-*T. hominis* SPC98 sera failed to detect the punctate signals that were observed in the single labelling experiments regardless of whether the antibody was used in the first primary antibodies incubation, the second primary antibodies incubation, or when both primary antibodies were incubated at the same time.

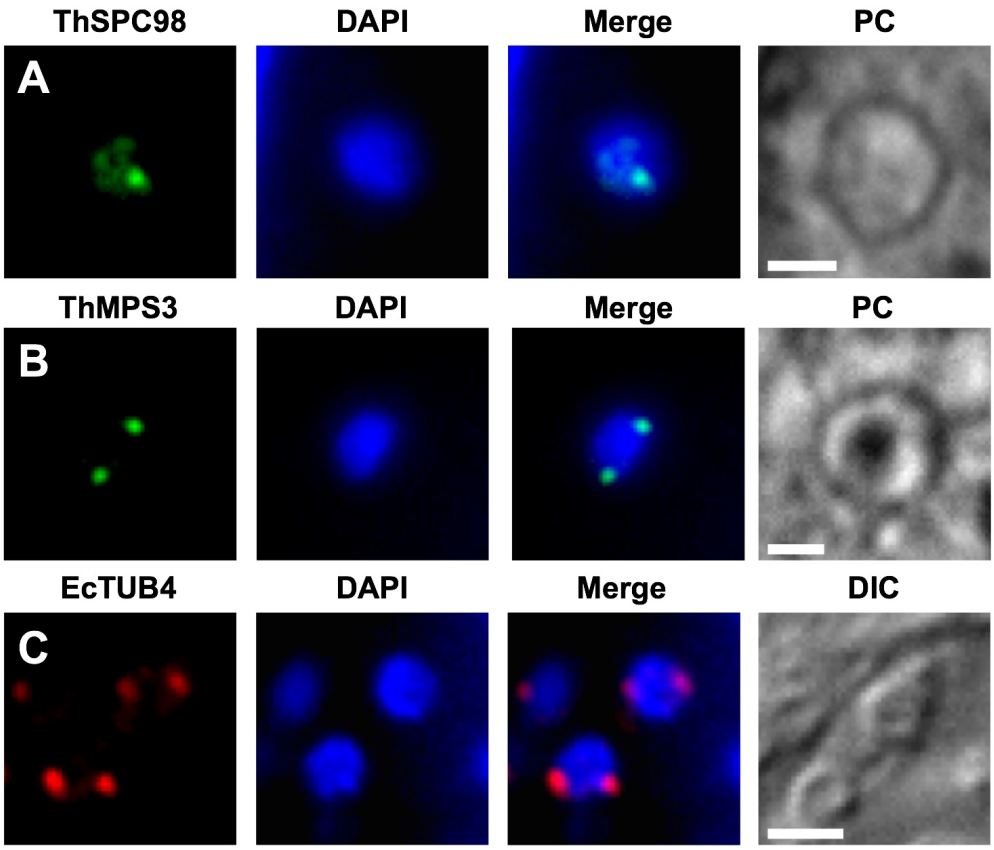

Figure 4.8 Fluorescence microscopy images of fixed samples of *T. hominis* or *E. cuniculi* infected rabbit kidney cells probed with anti-*Th*MPS3, anti-*Th*SPC98 or anti-*Ec*TUB4 antibodies

(A) Polyclonal sera raised in rat against *T. hominis* SPC98 (green) detect a single punctate signal at the circumference of the DAPI stained nucleus (blue) and weak dispersed signal inside the nucleus of a small single nucleate cell (early meront) of *T. hominis*.
(B) Polyclonal rat sera against *T. hominis* MPS3 (green) detect two punctate signals at the opposite sides of the DAPI stained nucleus (blue) of an early meront of *T. hominis*.
(C) Affinity purified polyclonal sera raised in rabbit against *E. cuniculi* TUB4 (red) detect two punctate signals at the opposite sides of the DAPI stained nucleus (blue) of an early meront of *E. cuniculi.*

Images (A, B and C) are maximum intensity Z-projections of Z-stack acquired using Zeiss Axioimager II fluorescence microscope with 100x/1.46 Oil phase contras lens (A and B) or 63x/1.4 Oil DIC lens (C). Differential interference contrast (DIC) and phase contras (PC) images represent single optical sections. Scale bars correspond to 1 μm.

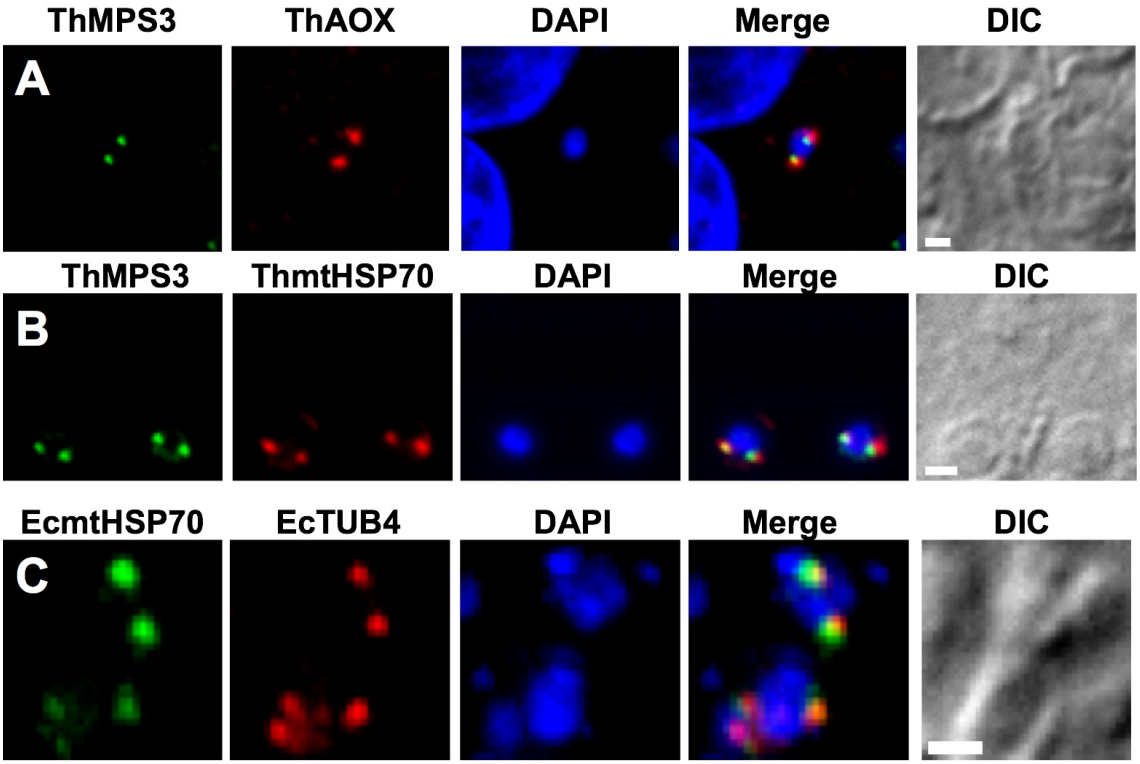

Figure 4.9 Fluorescence microscopy images of fixed samples of *T. hominis* or *E. cuniculi* infected rabbit kidney cells double labelled with mitosomal and SPB markers

Antibodies raised against SPB proteins: *Th*MPS3 **(A and B)** or *Ec*TUB4 **(C)** detected punctate fluorescent signals that partially overlapped with the signals detected using antibodies against the mitosomal markers: *Th*AOX **(A)**, *Th*mtHSP70 **(B)**, or *Ec*mtHSP70 **(C)** at the periphery of the DAPI stained nuclei of *T. hominis* **(A and B)** or *E. cuniculi* **(C)**.

Images (A, B and C) are single optical sections acquired using Zeiss Axioimager II fluorescence microscope (63x/1.4 Oil DIC lens). Scale bars correspond to 1 µm.

In order to further investigate the extent of the overlap between the mitosomal fluorescent signals (*Th*AOX, *Th*mtHSP70 or *Ec*mtHSP70) and the SPB fluorescent signal (*Th*MPS3 or *Ec*TUB4), the fluorescence intensity profiles were measured along the lines drawn across the *E. cuniculi* and *T. hominis* cells double labelled with the antibodies against the mitosomal and SPB proteins (Figure 4.10). In the analysed line profiles, the major peaks of fluorescence intensities of the mitosomal marker (mtHSP70) and spindle pole body markers (*Ec*Tub4 or *Th*MPS3) were separated by the distance corresponding to an estimated 50 nm - 100 nm, which seems to match the observed distances separating microsporidian mitosomes and spindle pole bodies in the available electron micrographs (Figure 4.10). However due to the resolution limit of the microscope used in the experiments (approximately 250 nm) this estimates are unreliable and further experimental work using superresolution microscopy would be required in order to investigate the distance separating the

detected fluorescence signals. To test the protein localization in the context of the ultrastructural detail of the studied organelles (different compartments of the mitosomes and different elements of the SPB structure) and to reliably assess the distances separating them the immunoelectron microscopy experiments using antibodies against the SPB and mitosomal markers will be required and are already planned as part of the future work.

In the analysed *E. cuniculi* and *T. hominis* cells the major fluorescence intensity peaks of the SPB markers were observed in between the major DAPI (nuclear) peaks and the major peaks of the mitosomal markers that is consistent with the localization of the mitosomes in the cytosol next to the microsporidian SPB localized inside a pore in the nuclear envelope or adjacent to the nuclear envelope. In order to ensure that images of the same field of view acquired with different fluorescent channels (green, red and blue) are correctly aligned (not affected by the distortion caused by chromatic aberration) image registration was verified using subresolution microspheres labelled with three fluorophores (green, red and blue; Molecular Probes, TetraSpeck™ Microspheres). Analyses of the line profiles in the image of samples double labelled with the antisera against the two mitosomal proteins (*Th*AOX in rabbit and *Th*mtHSP70 in rat) that were characterized in this study show perfect colocalization of the red and green fluorescence intensity peaks (Figure 4.10). This result is consistent with the localization of both proteins within a single organelle.

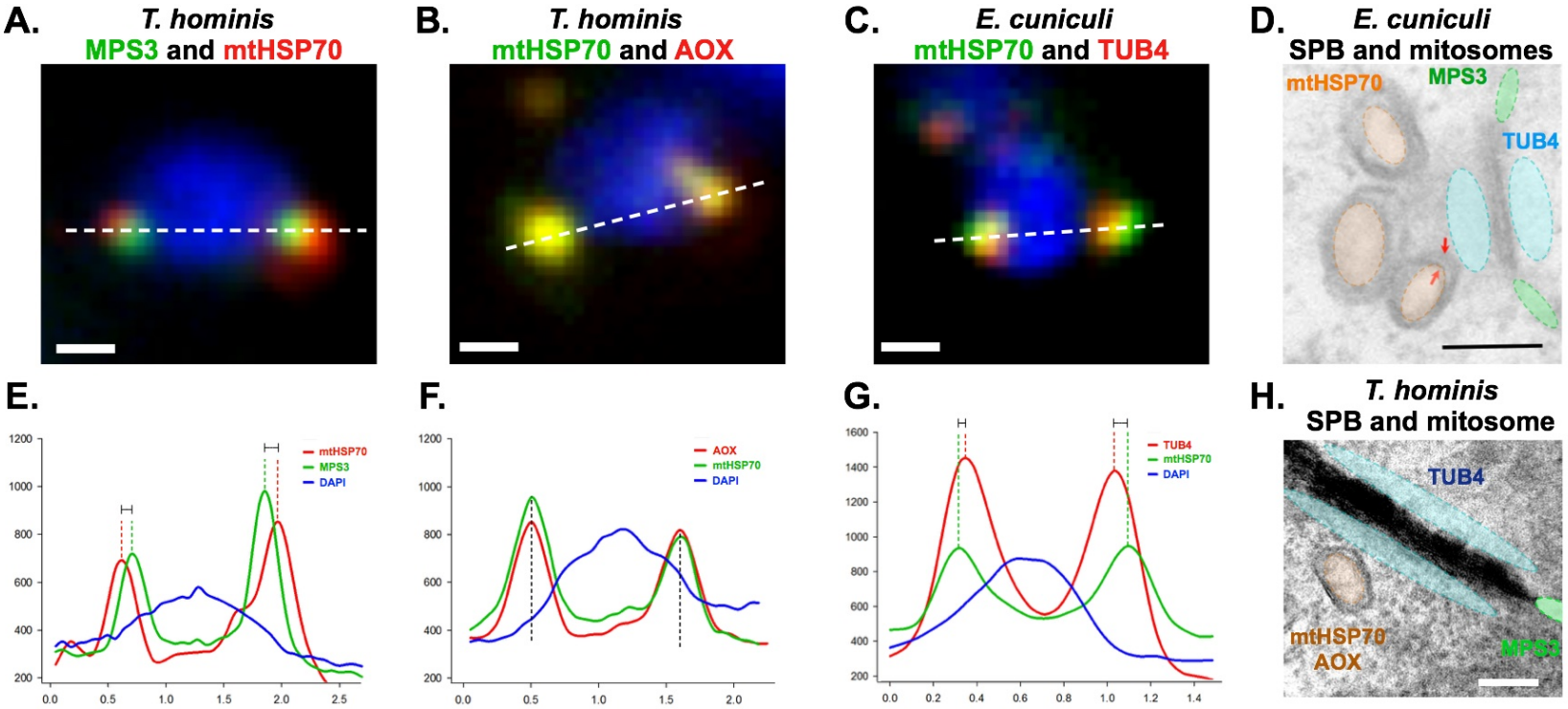

Figure 4.10 Line profiles of the fluorescence intensity across the *E. cuniculi* and *T. hominis* cells double labelled with the antibodies against the mitosomal and SPB proteins

(A and B) Representative images of the *T. hominis* cells double labelled with the antibodies against the SPB protein *Th*MPS3 and the mitosomal marker *Th*mtHSP70 (A) or double labelled with the antibodies against the two mitosomal proteins: *Th*AOX and *Th*mtHSP70 (B). **(C)** Representative image of the *E. cuniculi* cell double labelled with the antibodies against SPB protein *Ec*TUB4 and antibodies against the mitosomal marker *Ec*mtHSP70. Line profiles of the fluorescence intensity were measured along the **white dashed lines** drawn on the fluorescent images (A, B, and C). Scale bars correspond to 1 µm.

(E, F, G) Plots depict line profiles of the fluorescence intensity measured in all three channels (red, green and blue) along the line crossing centres of the green and red signals (A, B, C)**.** In all three plots the major peak of the red and green fluorescence intensity (indicated by vertical dashed lines above or below the peaks) flank the major peak of blue fluorescence intensity (DAPI) from both sides. Major peaks of the red and green fluorescence were aligned in the same position of the line profile of the *T. hominis* cell double labelled with two mitosomal markers (B and F) indicating colocalization to the same pixel of the image. In the line profile drawn across the *E. cuniculi* (C) and *T. hominis* (A) cells double labelled with the SBP and mitosomal markers, the major fluorescence intensity peaks detected with anti-mitosomal HSP70 antibodies did not align with the fluorescence intensity peaks of the SPB marker and were separated by an estimated distance of 50 nm - 100 nm. Based on the available electron micrographs (D and H) the microsporidian mitosomes and the microsporidian SPB can be separated by the distance of approximately 50 nm - 100 nm.

(D and H) Electron micrograph (D.) was adapted from (Tsaousis et al., 2008) and electron micrograph (H.) was acquired in this study. Colouring on the electron micrographs (D and H) indicates possible localization of the mitosomal proteins mtHSP70 and AOX (orange) as well as SPB components MPS3 (green) and TUB4 (blue). Scale bars on the electron micrographs correspond to 100 nm. Fluorescent images (A, B, and C) were acquired exactly the same way as the images in Figure 4.9.

4.3.5 Investigating localisation of the MPS3 in different stages of the T. hominis life cycle

In order to test if the partial overlap of the fluorescent signals detected using antibodies against the SPB marker MPS3 and antibodies against mitosomal marker mtHSP70 can be observed in all of the identified stages of the *T. hominis* life cycle double labelling with these antibodies was performed on the samples collected in different time points of the time course of infection experiment. Localization of at least one mtHSP70 signal partially overlapping with the anti-MPS3 signal was observed in all cells from all the time points collected in the experiment.

In the earliest stages after the initiation of the infection process (Figure 4.11 B, 0.5 h and 6 h) most of the *T. hominis* cells had two anti-MPS3 fluorescent signals at the opposite sides of the DAPI stained nucleus with a single anti-mtHSP70 signal partially overlapping with each of them. In the later time points (Figure 4.11 B, 12 h and 16 h) the parasite cell's diameter increased and significantly more mtHSP70 signals was detected but the subpopulation of the mtHSP70 fluorescent signals partially overlapping with the MPS3 signals was still observed. The partial overlap between the fluorescent signals was also observed in the multinucleate cells at 18 h and 28 h time points (Figure 4.11 B).

In addition to the one or -most often- two high intensity punctate fluorescent signals the anti-MPS3 antibodies also detected less intense signals at the circumference of the DAPI stained nuclei. These additional signals were first observed 12 h post infection and became more intense in later stages of the parasite life cycle. Frequently they seemed to spread out of the major punctate signal along the periphery (nuclear envelope) of the DAPI stained nuclei.

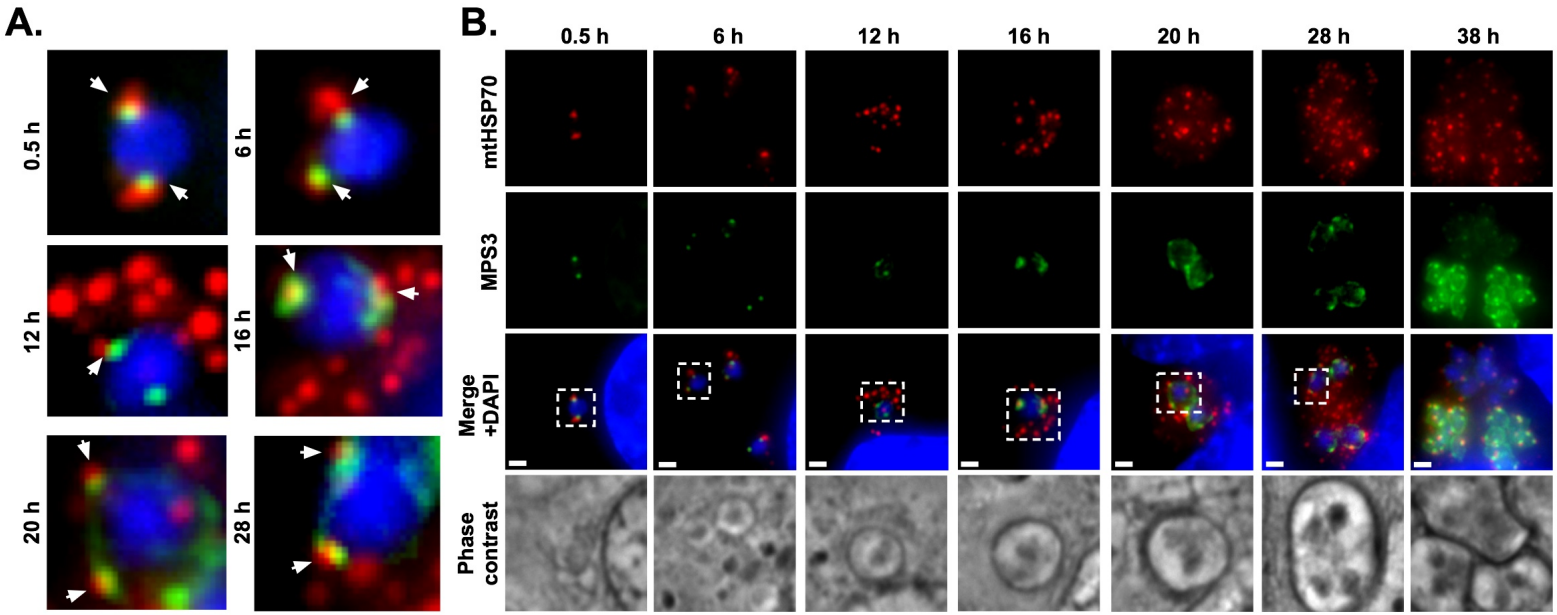

Figure 4.11 Investigating localization of mtHSP70 and MPS3 inside the parasite cells in a time course of *T. hominis* infection of rabbit kidney cells monolayer

Zoom in **(A)** at the nuclei of the cells from different time-points of the time-course of infection experiment **(B)** double labeled with the specific anti-*T. hominis* MPS3 sera (green) and affinity-purified anti-*T. hominis* mtHSP70 antibodies (red). At least one (usually two) green (anti-*Th*MPS3) signal observed at the circumference of all DAPI stained nuclei partially overlaped with a single red signal (anti-*Th*mtHSP70) in cells from all time points.

(B) One of the cells observed at the 38 h time point (top of the image) in comparison to other cells visible in the same field of view is weakly labeled with both MPS3 and mtHSP70 fluorescent signals. In addition, in a phase contrast image the weakly labeled cell appears to have more angular shape rather than round shape observed in earlier stages of the infection. Changes in shape of the cell and decreased permeability for the antibodies are most likely due to deposition of the spore coat material indicating early stage of the spore formation (sporogony). In later time point spore coat seems to be resistant to standard permeabilization agents (detergents and organic solvents) resulting in an observation of irregular shaped cells (sporonts) that are not labelled with antibodies.

For a more detailed discussion of different cell morphotypes and numbers of mitosomal fluorescent signals in a time course of *T. hominis* infection please see *section: 3.2 Investigating mitosomal localization of the AOX and mtG3PDH in different stages of the T. hominis life cycle.*

All images were acquired using Zeiss AxioImager II with 100x (NA=1.46) Plan-Apochromat objective lens and processed using FiJI software package (Schindelin et al., 2012). Presented fluorescence images are maximum intensity z-projections of acquired z-stacks. Intensity values in **(A)** were adjusted so that even the weakest red (anti-mtHSP70) fluorescent signals could be observed. Scale bars correspond to 1 μm.

In the last time point a phenotype of the parasite cell in which most of the *Th*mtHSP70 signals partially overlapped with the *Th*MPS3 signals was observed (Figure 4.11 and 4.12). In these cells the number and the apparent intensity of the peripheral mitosomes (not adjoining the DAPI or MPS3 signals) seemed to be reduced in comparison to the earlier stages (Figure 4.12). In addition, the volume of the cell that did not contain any of the mitosomal signals appeared to be larger than in the earlier stages. Semi-quantitative analysis of a number of the fluorescent *Th*MPS3 and *Th*mtHSP70 signals that partially overlap will be required in order to test the significance of these observations.

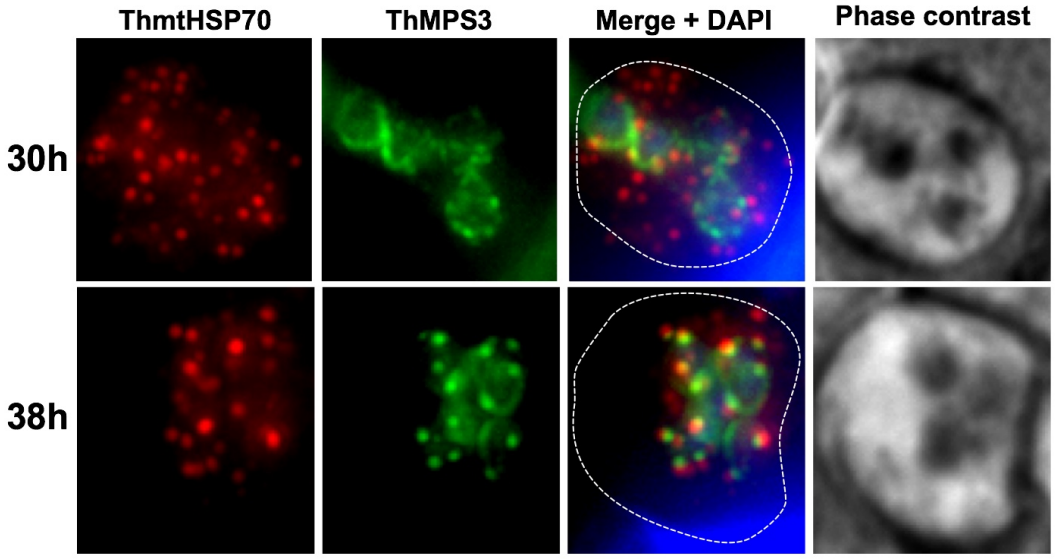

Figure 4.12 Comparison of two distinct labeling patterns observed in multinucleate *T. hominis* cells double labeled with mtHSP70 and MPS3 after 30 hours of infection

Mitosomal signals observed in multinucleate cells 30 hours post infection **(30h)** appeared to be evenly distributed in the volume of the cell. In the multinucleate cells first observed 38 hours post infection **(38h)** number of peripheral mitosomal signals (not overlapping with DAPI or MPS3 fluorescent signals) seemed to decrease in both number and intensity as opposed to the SPB associated signals that seemed to be more intense.

Images were acquired and processed as described in the Figure 4.11**.** White dashed line indicates the periphery of the cell based on the phase contrast image.

4.4 Discussion

Characterization of microsporidian spindle pole body

In electron micrographs microsporidian mitosomes are often observed close to the electron-dense spindle plaque that seems to be localized within a pore inside the nuclear envelope (Vavra, 2005; Tsaousis et al., 2008; Bigliardi et al., 1998). Its morphology and intracellular localization as well as observation of the microtubules originating at the plaque led to the hypothesis that it is a microtubule-organizing centre (MTOC) homologous to the yeast SPB (Vavra, 2005; Tsaousis et al., 2008).

In this study, candidates for homologues of the yeast SPB components were identified in microsporidian genomes using BlastP and HMMER profile searches (Figure 4.13 A). Out of the 17 characterized SPB components from *S. cerevisiae* and 13 characterized SPB components from *S. pombe* used in the analyses only 4 homologues namely, *S. cerevisiae* Mps3 (*S. pombe* Sad1), Tub4 (Tub4), Spc97 (Alp4), and Spc98 (Alp6) were detected in microsporidian genomes. Based on the phylogenetic analyses microsporidian TUB4, SPC97 and SPC98 (Figure 4.3) are orthologues of the yeast Tub4, Spc97 (Alp4), and Spc98 (Alp6). *T. hominis* MPS3 homologue has a conserved domain architecture with predicted transmembrane and SUN domains, predicted coiled coil region, and region corresponding to the yeast acidic domain (Figure 4.4). In addition, proteins containing common calcium binding EF-hand motif were identified in searches using the *S. cerevisiae* Cmd1 (*S. pombe* Cam1) and Cdc31 as queries however more detailed bioinformatics analysis including phylogenies of the identified microsporidian EF-hand containing proteins will be required in order to test if any of them are microsporidian Cmd1 and Cdc31 orthologues.

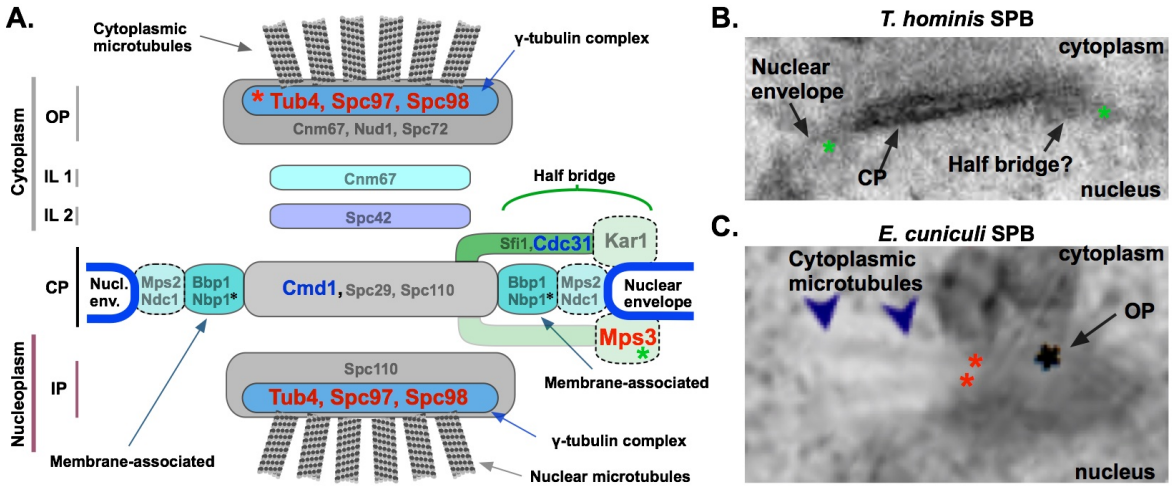

Figure 4.13 Microsporidian spindle pole body

(A) Homologues of the yeast spindle pole body proteins identified in microsporidian genomes based on BlastP and HMMER profile searches were indicated in **red** on a model of *S. cerevisiae* SPB (Figure 4.2 C). Among the conserved proteins are all of the key components of the γ-tubulin complex (TUB4, SPC97 and SPC98), the structures essential for a nucleation of microtubules; as well as homologue of Mps3, a nuclear membrane protein with an essential role in duplication of the SPB in yeast. Candidates for the microsporidian homologues of Cmd1 and Cdc31 -protein sequences containing common calcium binding motifs- were also detected in the microsporidian genomes (indicated in **blue**). Hypothetical localization of the MPS3 **(green asterisks)** and the γ-tubulin complex components **(red asterisks)** were indicated on the electron micrographs of the *T. hominis* **(B)** and *E. cuniculi* **(C)** electron-dense spindle plaques. Hypothetical location of the outer plaque **(OP)** and central plaque **(CP)** were indicated on the electron micrographs.

Electron micrograph **(C)** was reproduced from Tsaousis et al., 2008 and electron micrograph **(B)** is a courtesy of Mr. Andrew Watson (ICAMB, Newcastle University).

Identification of the microsporidian homologues of only 25 % of the yeast SPB proteins investigated in the bioinformatics analyses seems to be consistent with the observed trends of reduction in many of the studied microsporidian protein complexes (e.g. mitosomal import machinery components see *section 3.1.2 - The mitochondrial protein translocation machinery*). Alternatively, microsporidian homologues of the *S. cerevisiae* and/or *S. pombe* SPB components could be too divergent (share low sequence identity with yeast homologues) to be identified using the available bioinformatics tools. The protein composition of the SPB in fungi seems to be variable as evident in comparison between SPBs of *S. pombe* and *S. cerevisiae* (Rosenberg et al., 2006). Further homologue searches in the recently sequenced genomes of the representatives of basal fungal lineages (available from MycoCosm 1000 fungal genomes project, Grigoriev et al., 2014) as well as close relatives of microsporidia namely *Rozella allomycis* (James et al., 2013) and

Mitosporidium daphniae (Haag et al., 2014) could provide sequences of additional orthologues required for investigating possible presence of the more divergent SPB proteins in microsporidia.

Detection of the punctate signals at the circumference of the DAPI-stained nuclei using the specific antibodies against the microsporidian SPB proteins (*T. hominis* MPS3 and SPC98 as well as *E. cuniculi* TUB4) generated in this project is consistent with the localization of these proteins in or adjacent to the nuclear envelope and is reminiscent of the published fluorescent images from the localization studies of the yeast SPB proteins (Jaspersen et al., 2002; Li et al., 2015). In addition to usually one or two major punctate signals, the anti-MPS3 antibodies detect additional, often elongated signals along the circumference of the DAPI-stained nuclei of *T. hominis.* In published images of *S. cerevisiae* cells, fluorescent signal of Mps3 are enriched but not limited to the SPB (Nishikawa et al., 2003; Conrad et al., 2007). In *S. cerevisiae* Mps3 is involved in the formation of the biochemical link between the core SPB and the half-bridge (Jaspersen, 2006), and has an essential role in duplication of the SPB, but also functions in karyogamy, sister chromatid cohesion and anchoring telomeres to the nuclear envelope during S-phase and meiosis (Nishikawa et al., 2003, Antoniacci et al., 2004, Jaspersen, 2006; Conrad et al., 2007, Li et al., 2015). The region corresponding to the acidic domain that is necessary and sufficient for telomere tethering during S-phase in *S. cerevisiae* (Bupp et al., 2007) is present in *T. hominis* but seems to be truncated in other microsporidia including *E. cuniculi*. Presence of the additional MPS3 immunofluorescent signals coincides with increase of the microsporidian cell diameter and increase in the number of observed nuclei (associated with the cell growth and proliferation, see sections 3.3.5 and 3.4.3) in microsporidian cells, which seems to be consistent with the possible additional functions of the MPS3 during cell growth and proliferation.

Further immunoelectron microscopy experiments using the antibodies against SPB proteins generated and characterized in this study will be required to investigate the localization of the *Th*MPS3, *Th*SPC98 and *Ec*TUB4 to the electron-dense spindle plaques of *T. hominis* and *E. cuniculi*.

DAPI-stained nuclei were observed in all cells of all stages of the parasite life cycle and all detected MPS3 and TUB4 fluorescent signals were coincident with the DAPI signals suggesting that microsporidian nuclear envelope remains intact during the entire cell cycle of the parasite (‘closed’ mitosis or closed nuclear division). These results are in agreement with previous characterization of microsporidian cell cycle,

mainly based on the electron microscopy observations (Vavra & Larsson, 2014). Nuclei of model Ascomycete fungi *S. cerevisiae* and *S. pombe* undergo the 'closed' mitosis and the results of detailed studies of their cell cycle including measured changes of the surface and volume of the nuclei as well as the number of fluorescent signals of the SPB markers in correlation with the stage of the cell cyle are available (De Souza & Osmani, 2007; Zhang & Oliferenko, 2013; Segal & Bloom, 2001). Quantitative analyses of the fluorescent signals detected using antibodies against microsporidian SPB proteins generated in this study together with the volumetric and surface measurements of the DAPI stained microsporidian nuclei could be used in further studies of the microsporidian life cycle.

Investigating link between the microsporidian mitosomes and the SPB

In order to test the hypothesis that the mitosomes of *T. hominis* and *E. cuniculi* are connected to the SPB in all stages of their life cycle the anti-*T. hominis* MPS3 and anti-*E. cuniculi* TUB4 antibodies were used in double labelling experiments with the antibodies against known mitosomal markers mtHSP70 and AOX. Detection of the partially overlapping fluorescence signals in the double labelling experiments using the SPB and mitosomal markers is consistent with observation of a subpopulation of mitosomes (SPB mitosomes) in a close proximity of the electron-dense spindle plaque resembling the yeast SPB in the electron micrographs of microsporidian cells (Vavra, 2005; Tsaousis et al., 2008). The difficulty with resolving the fluorescence signals detected using the mitosomal and the SPB markers (the observed partial overlap of the signals) using a microscope with the resolution limit of approximately 250 nm is consistent with the observation of the mitosomes and the SPB at the distance of less than 100 nm from each other in the available electron micrographs (Figure 4.10).

In yeast, each of the daughter cells inherits a single SPB during the cell division process and electron micrographs (Bigliardi et al.,1998) suggests similar pattern of the organelle segregation in microsporidia. Small numbers of the mitosomes per microsporidian cell such as that of *E. cuniculi* (Tsaousis et al., 2008; Williams et al., 2002; Tachezy & Šmíd, 2008b) make stochastic inheritance of the organelle unreliable. Anchoring of the mitosomes to the microsporidian MTOC (SPB) could provide a reliable mechanism of the organelle segregation similar to that observed in other eukaryotic microorganisms such as *Trypanosoma brucei* (Ogbadoyi et al., 2003). Results of the double labeling experiments with the

antibodies raised against the SPB and mitosomal markers suggest that the connection between the subpopulation of mitosomes and the SPBs is maintained throughout the parasites life cycle (Figure 4.14). These observations are consistent with the hypothesis that attachment of the mitosomes to the SPB is a mechanism responsible for ensuring mitosome inheritance during cell division process. The exact mechanism responsible for attaching the mitosomes to the SPB is unknown and further immuno-EM experiments could be used to investigate if MPS3 or TUB4 are involved in mandating the interaction between the mitosome and the SPB.

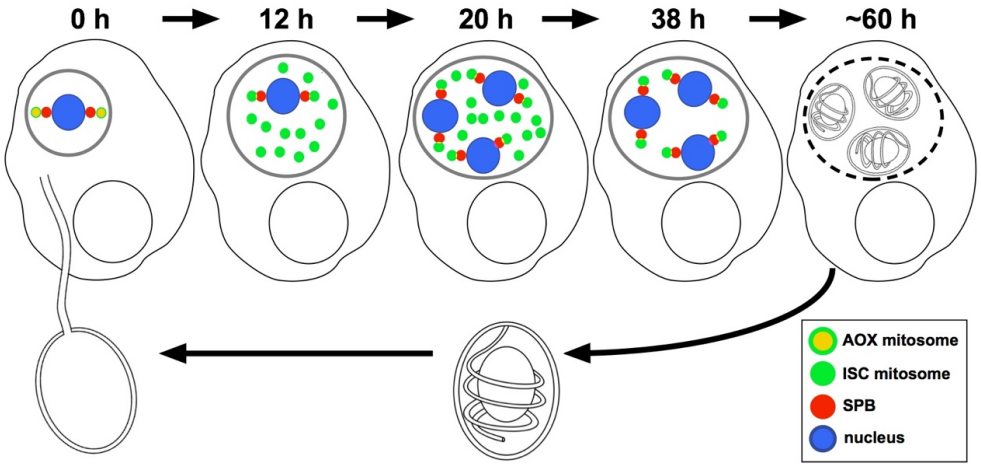

Figure 4.14 Model of changes in numbers, localization and function of the *T. hominis* mitosomes in different stages of the parasite life cycle, based on the results of immunofluorescence microscopy experiments using specific antibodies generated in this study

In the earliest time-points of *T. hominis* infection **(0 h),** just after addition of the spores to the uninfected host cells, the mitosomes are enriched in the AOX and mtG3PDH fluorescent signals **(AOX mitosomes)**, and these fluorescent signals are partially overlapping with the fluorescent signals detected using antibodies against the SPB marker **(SPB)**, MPS3. During the parasite cell growth **(12 h)** and proliferation (**20 h)** number of the fluorescent signals detected using antibodies against the mitosomal iron sulfur cluster biosynthesis markers mtHSP70 and NFS **(ISC mitosomes)** is significantly increased in comparison to the earlier stages, whereas the number of the AOX signals is significantly decreased. The partially overlapping SPB and mitosomal fluorescent signals are observed in all cells during cell growth (12 h) and proliferation (20 h). In the latest observed stages **(38 h)** of the parasite life cycle, that are labelled with the specific antibodies, fluorescent signals of the peripheral mitosomes seem to disappear, whereas the signals of the SPB-linked mitosomes are more prominent and appear to be more intense. In the time points later than the 38 h fluorescent signals are no longer detected, most likely due to deposition of the spore wall, indicating initiation of the spore formation stage of the life cycle (sporogony), followed by observation of the first mature spore, approximately 60 hours post infection.

In the multinucleate cell observed in the late time points of the time course of infection experiments majority of the mitosomal signals seemed to overlap with the SPB signals and the number of the peripheral mitosomes seemed to decrease (38 h

post infection Figure 4.14 and 4.12). This could indicate either a specific mechanism of transporting the mitosomes to the SPB at this stage of the life cycle or selective mitophagy (autophagy of the mitochondria) of the peripheral but not the SPB associated mitosomes. Degradation of the mitosomes by mitophagy is unlikely, as microsporidia seem to have lost components of the autophagic machinery (Duszenko et al., 2011). Transport of the mitosomes along the cytoskeleton seems to be more likely and could be mediated by the cytoplasmic microtubules that originate at the SPB. Antibodies against *T. hominis* alpha or beta tubulin could be generated as part of the future work in order to investigate the hypothetical attachment of the mitosomes to the microtubules. The observed changes in the distribution of the mitosomes in late time points of *T. hominis* life cycle seem to coincide with the transition between proliferative merogony and the spore formation stage (sporogony, see sections 3.3.5 and 3.4.3). During the spore formation process microsporidian cell undergoes complex morphological changes including deposition of double-layered spore wall and formation of a complex microsporidian-specific infection apparatus that consist of the polar tube and the posterior vacuole (Vavra & Larsson, 2014). Redistribution of the peripheral mitosomes to the SPBs may be a part of a mechanism responsible for segregating the mitosomes to the forming spores. Within each of the microsporidian spore-forming cells (sporonts) at least four single-nucleate (in *T. hominis*) spores are formed (Hollister et al., 1996) and the attachment of the mitosomes to the SPB could ensure that every spore inherits mitosomes.

The SPB-mitosomes observed in the latest stages of *T. hominis* life cycle that are labelled with antibodies, similar to those observed during the growth phase and proliferation, are labelled with intense fluorescent signals of the ISC markers but not with the AOX (Figure 3.20). AOX and mtG3PDH are enriched in the spore stages rather than the intracellular stages of *T. hominis* (section 3.4.3) suggesting that the expression and import of these proteins to the mitosomes occurs mainly during the spore formation stage. Based on that it could be hypothesized that the AOX and the mtG3PDH are enriched in the mitosomes of the spore forming stages of *T. hominis* shortly after redistribution of the peripheral mitosomes to the SPB and deposition of the spore wall that most likely is the cause of apparent impermeability of the sporonts to antibodies (section 3.4.3). This to events, namely redistribution of the peripheral mitosomes to SPBs and enrichment of the AOX and mtG3PDH inside the mitosomes could be the hallmarks of the change of the main mitosomal function from the ISC biosynthesis to the alternative respiration.

Chapter 5. Identification, *in silico* characterization and investigation of the intracellular localization of microsporidian dynamin related proteins

5.1 Introduction

Division of mitochondria is essential in order to provide all daughter cells with the organelles during proliferation. Nevertheless, so far there is no convincing published evidence for mitosomal division in microsporidia. In most eukaryotes the size, shape and number of mitochondria is dependent on a balance between division and fusion events (Yamano & Youle, 2011). Mitochondrial fusion is responsible for the formation of interconnected network of organelles (Bach et al., 2003). On the other hand mitochondrial fission produces many smaller mitochondria that may be easily transported along the cytoskeleton (Westermann, 2011).

A key component of all studied mitochondrial division machineries is the force generating 'constrictase' Dnm1 (Kageyama et al., 2011). Yeast Dnm1 and its mammalian homologue Drp1 are members of the dynamin-related protein family (Heymann & Hinshaw, 2009). Classical dynamin (the first described member of the dynamin superfamily) takes part in scission of clathrin coated vesicles during endocytosis and has five characteristic domains: a N-terminal GTPase domain, a middle domain (MD), a pleckstrin homology domain (PH), a GTPase effector domain (GED) and a proline rich domain (PRD), (Ferguson & De Camilli, 2012; Ford et al., 2011). The GTPase domain has a lower affinity for GTP and higher hydrolysis rate than small regulatory GTPases and does not require special nucleotide exchange factors or activating proteins (Ferguson & De Camilli, 2012).

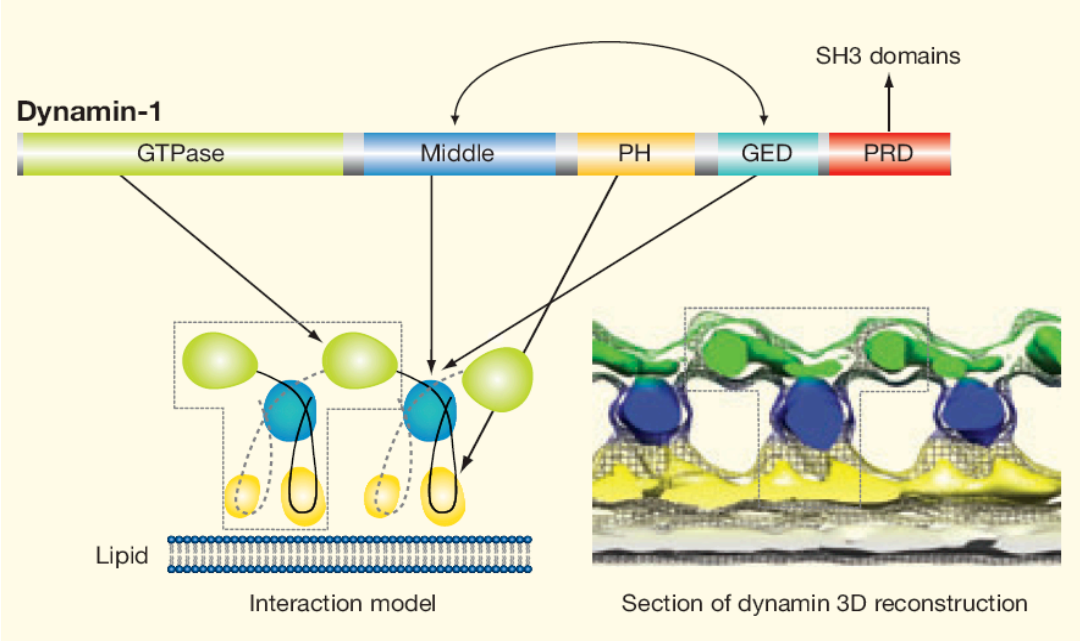

Figure 5.1 Domain architecture and mechanisms of self-assembly and oligomerization of Dynamin-1

GTPase domain interacts with the middle domain and the GTPase effector domain (GED) in self-assembly and oligomerization of Dynamin-1. A pleckstrin homology domain (PH) interacts with the lipid bilayer and a proline rich domain (PRD) is responsible for interaction with other proteins. Figure was taken from (Heymann & Hinshaw, 2009)

Interaction between the GTPase, GED and MD domains drives self-assembly, dimerization and further oligomerization into helical-ring structures around lipid vesicles (Mears et al., 2007), (Figure 5.1). Dynamin oligomerization is nucleotide-independent, however GTPase activity rises after self-assembly and oligomerization and drives the conformational changes responsible for constriction and depolymerization of the dynamin ring (Ferguson & De Camilli, 2012; Ford et al., 2011). The PH domain is responsible for interaction with lipids whereas PRD is a binding site for interaction partners and modifiers (Ferguson & De Camilli, 2012). Dynamin-related proteins (DRPs) have at least 3 of these domains (GTPase, GED and MD) and take part in division of mitochondria, chloroplasts, vacuoles and peroxisomes; cytokinesis; fusion of mitochondria; release of transport vesicles; and endocytosis (Ferguson & De Camilli, 2012).

Dynamin related proteins do not work alone in membrane remodeling. Besides the ability of DRPs to directly interact with lipids, the connection of DRPs with mitochondria at the constriction site is mediated by binding partners. In mammals, Mff1 is the only mitochondrial integral membrane protein known to interact directly with Drp1 (Griffin et al., 2005). In *S. cerevisiae* there are two known mechanisms

mediating interaction between the mitochondrial membrane and the Dnm1 ring. In the first mechanism, the integral mitochondrial membrane protein Fis1p anchors Dnm1 via one of the adaptor proteins Mdv1p or Caf4p (Griffin et al., 2005). Additionally Mdv1p was shown to be a nucleation factor promoting Dnm1 oligomerization on mitochondria (Koirala et al., 2010). In the second mechanism, a membrane associated protein Mdm36p links a cortical protein Num1p and Dnm1 to mitochondria (Hammermeister et al., 2010). Num1p is also involved in interaction of mitochondria with the actin cytoskeleton, tethering of mitochondria to the cell cortex and transport of mitochondria and retention of the organelles in the mother cell after cell division (Cerveny et al., 2007). In addition the activity of DRPs can be regulated by covalent post-translational modifications, including phosphorylation, sumoylation and ubiquitination (Cribbs & Strack, 2007).

Although in *in vitro* experiments Dnm1 was shown to constrict lipid vesicles independently, *in vivo* it oligomerizes at already constricted sites (Mears et al., 2010). The diameter of dynamin ring is only around 100nm and is much smaller than the diameter of mitochondria (Mears et al., 2010), (Ingerman et al., 2005). The size difference may explain the *in vivo* requirement for the primary dynamin-independent constriction of mitochondria. Recent discoveries suggest that endoplasmic reticulum (ER) may provide the primary constriction (Rambold & Lippincott-Schwartz, 2011). Interaction between ER and mitochondria mediates the exchange of lipids and calcium between the organelles (De Brito & Scorrano, 2010). Lately it has been shown that endoplasmic reticulum tubules form rings around constricted mitochondria and that in most of the cases the contact with ER marks sites of mitochondrial division (Friedman et al., 2011).

Dynamin related proteins are not the only contractile ring forming proteins involved in the division of mitochondria. Some eukaryotes have retained the FtsZ ring that was a core component of the cell division machinery of the bacterial ancestor of the mitochondria (Beech et al., 2000; Kuroiwa, 2010). Nevertheless FtsZ homologues involved in mitochondrial division have been lost in many eukaryotic lineages including all studied animals, higher plants and Fungi (Tachezy & Šmíd, 2008b; Arimura & Tsutsumi, 2002).

The mitosomal division machinery has not yet been investigated, however DRP-coding sequences have been found in distantly related pathogenic microbial eukaryotes containing the mitochondrial homologues. The single DRP of *Giardia intestinalis* is involved in secretion and endocytosis but does not seem to be involved

in the mitosomal division (Gaechter et al., 2008) and one of the two DRP homologues from *Entamoeba histolytica* was shown to localize around the nucleus and throughout the cytoplasm. The DRPs seem to be involved in the division of mitochondria in *Trypanosoma brucei* (Morgan et al., 2004) and hydrogenosomes in *Trichomonas vaginalis* (Wexler-Cohen et al., 2014). Two out of three DRPs from another parasitic protozoan *Toxoplasma gondii* were studied and one of them DrpA was shown to be involved in division of the plastid organelle (the apicoplast). However, the possibility that DrpA also participates in division of mitochondria could not be excluded (Breinich et al., 2009; van Dooren et al., 2009).

5.2 Aims

In order to maintain numbers of mitosomes in proliferating population of microsporidia, mitosomes have to divide. Dynamin related proteins (DRP) are responsible for formation of a contractile ring around mitochondrial division site that drives the division of mitochondrial membranes in representatives of many eukaryotic lineages including that of fungi and animals (Kageyama et al., 2011).

Here bioinformatics tools have been used to identify and characterize microsporidian homologues of DRPs and homologues of the DRP interaction partners. Specific antibodies against one of the homologues of DRPs identified in the genome of microsporidian capable of infecting humans *Trachipleistophora hominis* were generated and used to test the hypotheses that the *T. hominis* DRP homologue is involved in division of the mitosomes.

5.3 Results

5.3.1 Identification and bioinformatic analyses of microsporidian homologues of yeast and human Dnm1p/Drp1 interaction partners

BlastP (Altschul et al., 1990) and HMM (hidden Markov models) profile searches (Eddy, 2001) were used to identify potential microsporidian homologues of proteins involved in recruitment of Dnm1p or Drp1 to mitochondria of yeast or

mammals, respectively (Table 5.1). Both methods detected only microsporidian proteins containing common WD40 domain (Stirnimann et al., 2010) also found in two yeast homologues Mdv1p and Caf4p (Table 5.1).

Caf4p and Mdv1p were the only of the investigated proteins that clustered together with microsporidian sequences in a published analysis of clusters of homologues from 11 microsporidian, 7 fungal and 3 animal genomes (Nakjang et al., 2013). Examination of the cluster (c_1599) containing Caf4p and Mdv1 reveled that it consists of 1054 protein sequences containing WD40 repeats (InterProScan 5 (Jones et al., 2014)), including 229 microsporidian proteins.

Examination of the pairwise alignments generated by BlastP revealed that proteins align only in C-terminal region of Caf4p and Mdv1p containing the WD40 repeats. No reciprocal best BlastP hits were identified between microsporidia and *S. cerevisiae* when Mdv1p and Caf4p were used as initial queries.

In maximum likelihood and Bayesian phylogenetic trees Caf4p and Mdv1p grouped together with orthologous from other Fungi (Figure 5.2). None of the microsporidian proteins used in construction of the WD40 domain phylogenies grouped together with Mdv1p and Caf4p (Figure 5.2).

HMM profile searches have also detected microsporidian proteins containing tetratricopeptide repeat (TPR) motif (D'Andrea & Regan, 2003), however none of the tested hits (e-value < 0.001) contained a predicted C-terminal trans-membrane domain (TMHMM, (Sonnhammer et al., 1998; Krogh et al., 2001)) present in yeast Fis1p and human Fis1.

Table 5.1 Identification of microsporidian homologues of yeast Dnm1 and human Drp1 interaction partners involved in mitochondrial division in microsporidian genomes using BlastP and HMMER searches

BlastP searche queries	BlastP resut	PFAM	HMMER result
Caf4p (Griffin et al., 2005)	-	4x WD domain; DUF3249	+ (common motif); -
Fis1p (Mozdy et al., 2000)	-	(pfamB profile)	-
Fis1 (Palmer et al., 2013)	-	Tetratricopeptide repeat (TPR6)	+ (common motif)
Mdv1p (Tieu et al., 2002)	-	Mdv1; 4x WD40	-; +(common motif)
Num1p (Cerveny et al., 2007; Lackner et al., 2013)	-	(pfamB profile)	-
Mdm36p (Hammermeister et al., 2010; Lackner et al., 2013)	-	(pfamB profile)	-
Mid49 (Palmer et al., 2011)	-		-
Mid51(Palmer et al., 2011)	-		-
Mff (Otera et al., 2010)	-	Miff	-

Sequences of characterized *S. cerevisiae* Dnm1 and *H. sapiens* Drp1 **(in green)** interaction partners were used as queries in BlastP searches against the local database of microsporidian protein sequences encoded in genomes of *T. hominis, E. cuniculi E. intestinalis, E. bieneusi, N. ceranae, A. locustae and N. parisii ERTm1*. In the **BlastP result** '+' indicates detection of microsporidian sequences with E-value lower than 0.01 (the lowest E-values were indicated) whereas '-' indicates that all detected sequences had E-values above 0.01.

The yeast and human sequences were also used to identify hmm profiles (**PFAM)** in the PFAM database using PFAM search tool. The identified hmm profiles were used as queries in the hmm profile searches against the microsporidian protein database (the same as in the BlastP searches). In **HMMER result** '+' indicates detection of the sequence above the default inclusion threshold (E-values below 0.01) whereas '-' indicates that all detected sequences were below the inclusion threshold.

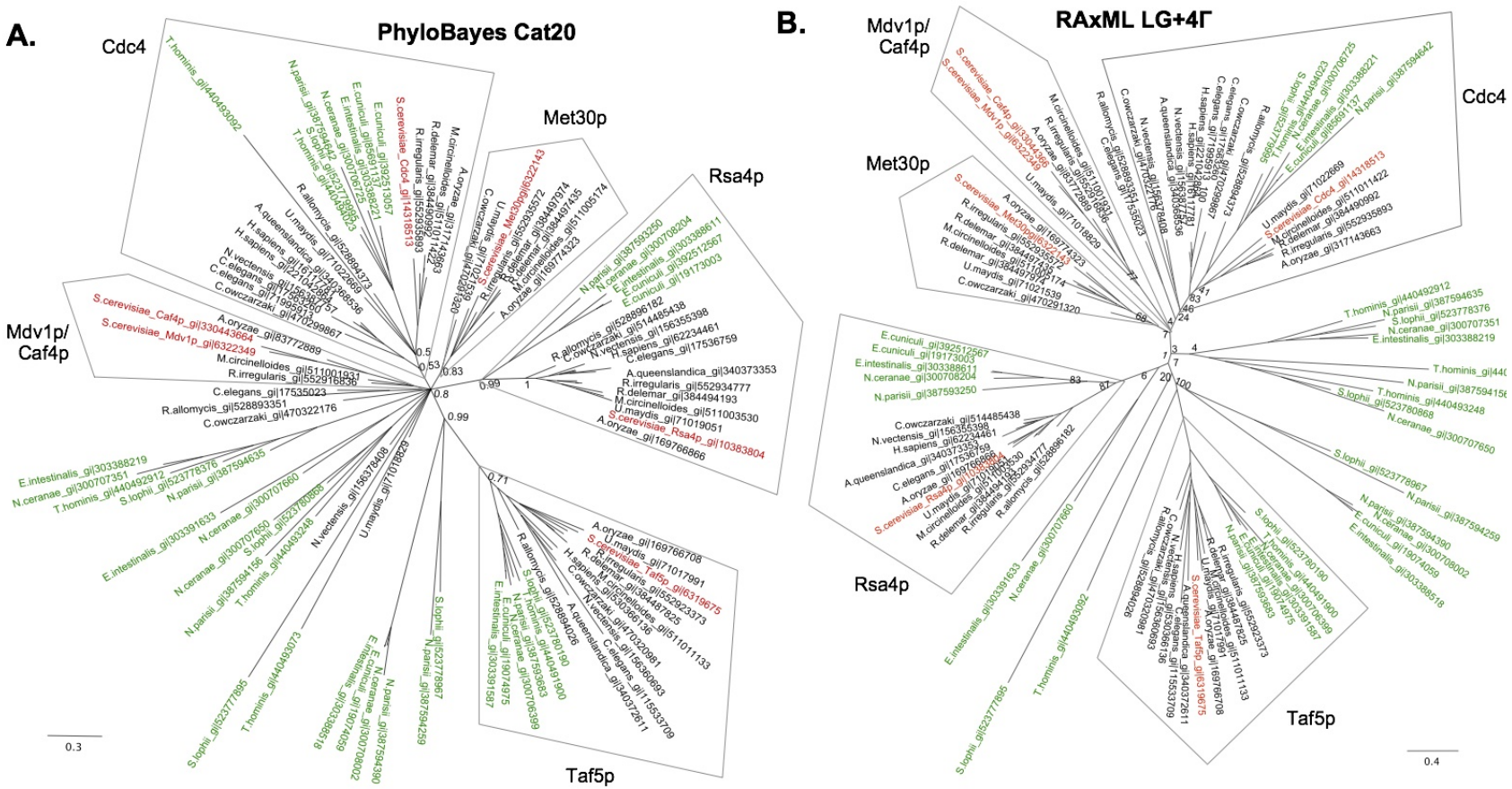

Figure 5.2 Phylogenetic trees of protein sequences containing WD40 domain from microsporidia, Fungi and Metazoa

Neither of the microsporidian WD40 protein sequences **(green)** grouped together with the fungal Mdv1/Caf4p homologues. WD40 protein sequences from *S. cerevisiae* were indicated in red. (A) Bayesian tree was generated with PhyloBayes (Lartillot et al., 2009) under C20 (Quang et al., 2008) model and (B) maximum likelihood tree was generated using RAxML (Stamatakis et al., 2005; Guindon & Gascuel, 2003) under LG+4Γ. Support values for key nodes of the trees correspond to (A) Bayesian posterior probabilities and (B) bootstrap values from 100 rapid boostrap replicates. Scale bar represents number of substitutions per site.

Sequences used in the analysis were selected as follows. Database of *S. cerevisiae* protein sequences (NCBI) was searched using BlastP (Altschul et al., 1990) with *S. cerevisiae* Mdv1p and Caf4p as queries and six best BlastP hits including queries were selected for the analysis. Subsequently BlastP searches with the six *S. cerevisiae* WD40 proteins as queries were performed against other fungi and Metazoa and the best hits were selected. The first six best BlastP hits were selected from Mdv1p and Caf4p searches against microsporidia. The selected sequences were aligned with MUSCLE (Edgar, 2004) and trimmed using trimAL (Capella-Gutiérrez et al., 2009) with gappyout method. Trimmed alignment had 230 positions and corresponded only to the WD40 region of the proteins.

5.3.2 Identification and sequence analysis of microsporidian Dynamin Related Proteins

BlastP searches were used to identify microsporidian homologues of Dynamin. With an exception of *Nematocida parisii* all analyzed microsporidian genomes contain two Dynamin Related Protein (DRP) homologues. Only one DRP homologue was identified in available genomic sequences fpr the three *N. parisii* isolates (Cuomo et al., 2012) using BlastP and tBlastN searches. Examination of a multiple sequence alignment of microsporidian DRPs with fungal (Dnm1p and Vps1p) and with metazoan (Drp1 and dynamin3) homologues generated with MUSCLE (Figure 5.4 *see Appendix B*) indicates that microsporidian homologues seem to have three conserved domains: the GTPase domain, the Middle domain (MD) and the GTPase effector domain (GED), (Figure 5.3). The sequence region corresponding to the Pleckstrin homology domain in classical dynamins or Insert B in mammalian Drp1 and yeast Dnm1p does not align well and appears to be either significantly reduced or lost in all of the microsporidian DRPs (Figure 5.4 *see Appendix B*). The microsporidian GTPase domain is the best conserved domain within the multiple sequence alignment of DRPs from four microsporidian species (*T. hominis, E. cuniculi*, *E. intestinalis* and *V. culicis*), *S. cerevisiae* and *R. allomycis* and shares considerably higher pairwise percentage of sequence identity with *S. cerevisiae* and *R. allomycis* than the MD and GED domains. Secondary structure prediction for both DRPs from *E. cuniculi, T. hominis* and *S. cerevisiae* (Figure 5.4 *see Appendix B*) suggests that despite low sequence identity alpha-helices and beta strands of GTPase, MD and GED are conserved between them and dynamins with solved crystal structures: human dynamin1 (Faelber et al., 2011), (pdb 3SHN), and human Drp1 (Fröhlich et al., 2013), (pdb 4BEJ).

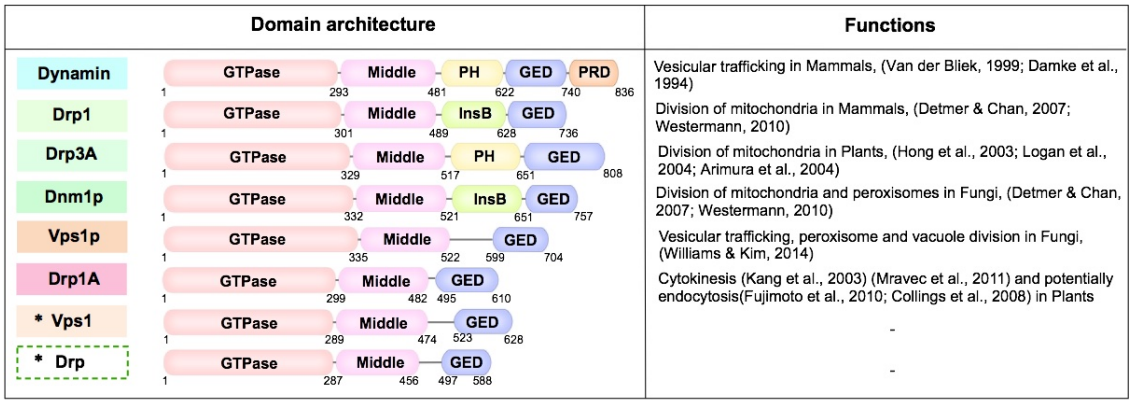

Figure 5.3 Domain architecture and functions of dynamins used in the phylogenetic analysis
Microsporidian DRPs have conserved domain architecture containing GTPase, middle and GTPase effector domains (GED). Region between middle and GED domains corresponding to pleckstrin homology domain (human dynamin1, plant Drp3A) and insert B (in human Drp1 and yeast Dnm1p) appears to be considerably reduced in microsporidia and is shorter then that in *S. cerevisiae* Vps1p.

Analysis of average pairwise percentage of sequence identities between full length proteins within the alignment revealed that one of the DRPs from each microsporidian species shared 24.7 % - 33.6 % identities with sequences from *S. cerevisiae* and *R. allomycis* whereas the second microsporidian homologue shared with them 36.3 % - 45.8 % identities.

Bayesian phylogenetic analysis of dynamin homologues was performed with Phylobayes under multiple models. The CAT model was selected as best fitting the data in biochemical specificity test statistics (Lartillot et al., 2007) based on posterior predictive simulations (Bollback, 2002), (Table 5.2). In the phylogenetic tree generated under the CAT model the microsporidian DRP homologues with higher pairwise percentage of sequence identities grouped together with fungal Vps1p with high posterior probability support values (Figure 5.5). The more divergent microsporidian DRP homologues grouped together with fungal Dnm1p sequences with low support values.

Table 5.2 Results of posterior predictive analysis

	WLSR5jtt	CAT60	CAT20	CAT
Number of cycles	42451	287708	360624	380487
Convergence test (bpcomp)				
	WLSR5jtt	**CAT60**	**CAT20**	**CAT**
maxdiff	0.0478661	0.0361473	0.0416964	0.0279542
meandiff	0.00334987	0.00349249	0.00294027	0.00255321
Biochemical specificity (ppred -div)				
	WLSR5jtt	**CAT60**	**CAT20**	**CAT**
observed diversity	7.20945	7.20945	7.20945	7.20945
posterior predictive	8.0758	7.38559	7.40373	7.33337
z-score	9.39425	2.16903	2.37128	1.44343
pp value	0 (0/2545)	0.0139539 (289/20711)	0.00837372 (235/28064)	0.0709783 (2038/28713)
Compositional homogeneity (ppred -comp) global test:				
	WLSR5jtt	**CAT60**	**CAT20**	**CAT**
max	**failed**	**failed**	**failed**	**failed**
observed	0.0151779	0.0151779	0.0151779	0.0151779
mean pred	0.00344779	0.00373492	0.00375565	0.00364374
p-value	0.0043222	0.0118982	0.0107338	0.000219106
z-score	7.31185	5.29397	5.3986	8.16652
mean	**failed**	**failed**	**failed**	**failed**
observed	0.00244215	0.00244215	0.00244215	0.00244215
mean pred	0.00123243	0.00127504	0.0012745	0.00127936
p-value	0	0	0	0
z-score	13.0007	11.6648	11.3163	11.7757
Saturation test (ppred -sat)				
	WLSR5jtt	**CAT60**	**CAT20**	**CAT**
observed subs number	28.6641 +/- 0.584616	32.2318 +/- 0.977331	30.3249 +/- 0.850851	33.3372 +/- 1.15292
posterior predictive	28.9361 +/- 0.741473	32.3368 +/- 1.05332	30.2768 +/- 0.913987	33.4473 +/- 1.20961
pvalue	0.715521	0.602103	0.43943	0.602542
observed homoplasy	19.9146 +/- 0.543871	23.2793 +/- 0.908263	21.4546 +/- 0.786745	24.4764 +/- 1.08807
posterior predictive	19.6085 +/- 0.690755	23.3326 +/- 0.976285	21.3488 +/- 0.842512	24.5239 +/- 1.14114
pvalue	0.230255	0.554234	0.363855	0.549956

Fit of models used to construct Bayesian phylogenies was evaluated with posterior predictive analysis (Bollback, 2002) implemented in ppred program of PhyloBayes package (Lartillot et al., 2009). P-values above 0.05 and Z-scores below 1.96 were indicated in green.

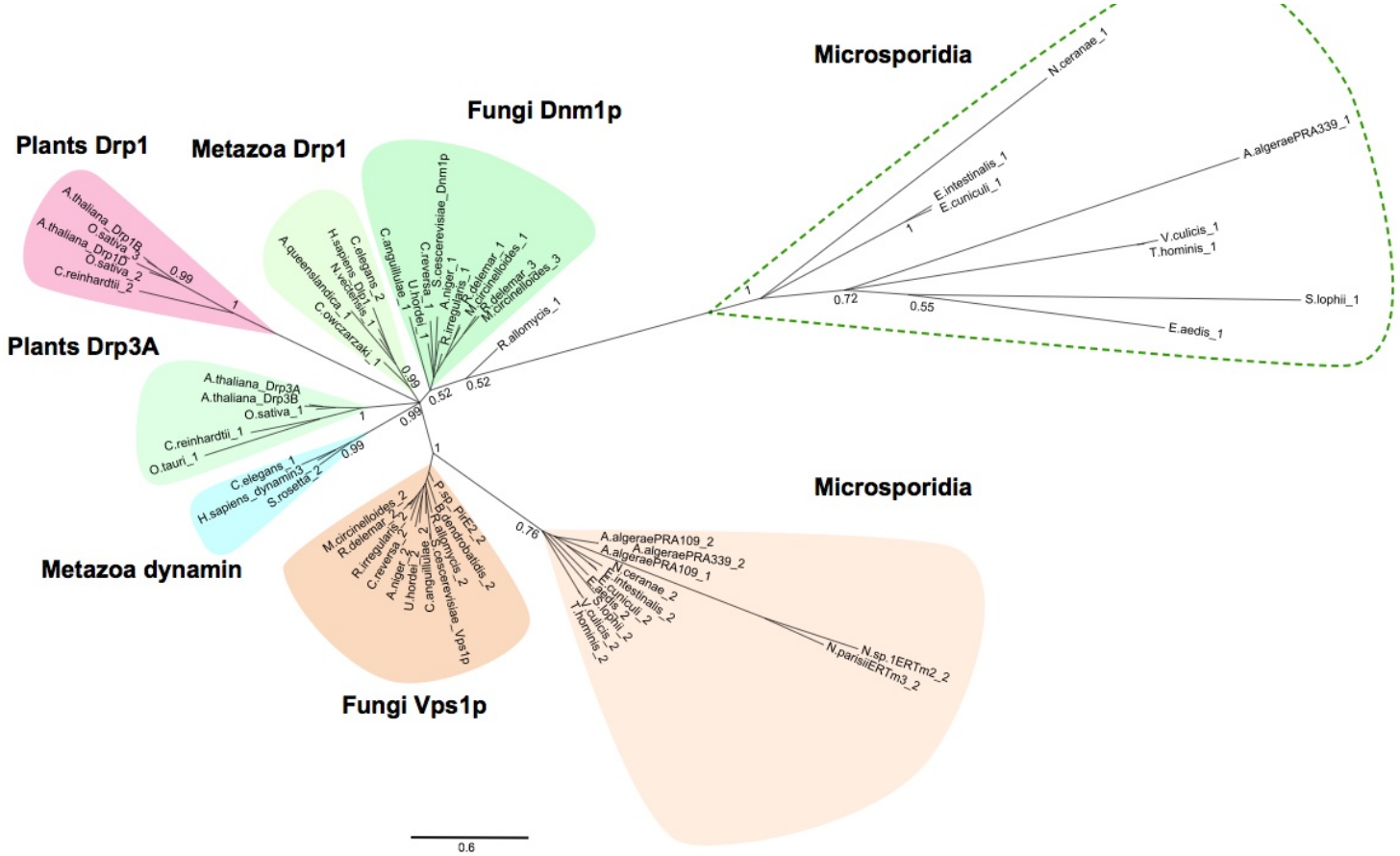

Figure 5.5 Bayesian phylogenetic tree of dynamin homologues

Microsporidian DRPs group together with their fungal homologues: Vps1p and Dnm1p. Dashed line around microsporidian Dnm1p orthologue candidate indicates low support value (0.52) for grouping with fungal Dnm1p.

The tree was generated using PhyloBayes (Lartillot et al., 2009) under the CAT model based on trimmed alignment of 62 sequences of 487 amino acid positions. Model was selected based on fit of model to data tested with posterior predictive analysis (Bollback, 2002) implemented in ppred program of PhyloBayes package (Lartillot et al., 2009) Posterior probability support values were displayed only for the key branches. Scale bar represents number of substitutions per site.

5.3.3 Cloning and expression of T. hominis DRP1 *for polyclonal antibodies production*

The full-length nucleotide sequence of *T. hominis* DRP1 excluding the start codon (ATG) was amplified from *T. hominis* genomic DNA using primers with a 5' CACC overhang (forward primer) required in TOPO cloning protocol.

The amplified sequence of *T. hominis* DRP1 was cloned into pET100 plasmid (Directional TOPO® cloning Kit). Sequencing of three clones of the construct confirmed correct insertion of the sequence into the plasmid. The recombinant proteins of expected size (78 kDa) were expressed using a standard IPTG induction protocol in *E. coli* BL21 (DE3) transformed with pET100-*th*drp1 (Figure 5.6). An additional band of approximately 75 kDa was detected in both coomassie blue-stained gels and western blots with anti-His-Tag antibodies indicating that it corresponds to a C-termianly truncated (His-Tag is located at the N-terminus of the recombinant protein) recombinant *Th*DRP1. Presence of the 75 kDa band could be explained by a premature termination of the protein translation or protein processing/degradation in bacterial cells. Only the band corresponding to the full-length recombinant *Th*DRP1 was used to generate the polyclonal antisera. The expected size of the protein was calculated using using ExPASy Compute pI/Mw tool (http://web.expasy.org/compute_pi/).

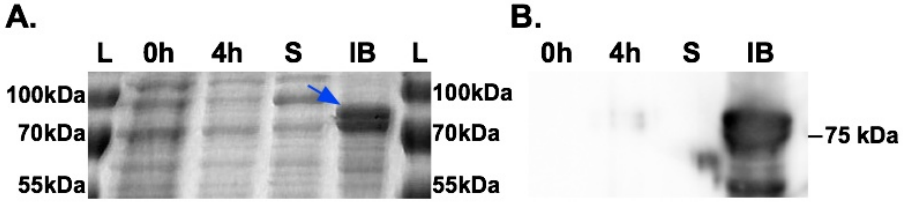

Figure 5.6 Expression and purification of *T. hominis* DRP1

(A.) Coomassie blue stained SDS polyacrylamide gel showing expression of recombinant *Th*DRP1. Protein band (blue arrow) corresponding to the expected molecular weight (78 kDa) was not detected in protein extracts from bacteria before (0h) or 4 hours after IPTG induction (4h). BugBuster reagent was used to lyse bacterial cell and purify insoluble protein fraction in form of inclusion bodies (IB). Band corresponding to the recombinant protein was detected in the insoluble IB fraction but not in a supernatant (S) corresponding to the soluble protein fraction. Molecular weight values correspond to the protein ladder bands (L).

(B.) The same samples were used in western blotting experiments with anti-His tag antibodies conjugated to HRP. Protein bands corresponding to the expected molecular weights were detected in insoluble IB fractions as well as in protein extracts from bacteria expressing recombinant *Th*DRP1 (weak signal)

Additional 75 kDa band potentially corresponding to C-terminally truncated recombinant *Th*DRP1 was detected in both (A) and (B).

5.3.4 Testing of polyclonal antisera raised against recombinant T. hominis and DRP1 using western blotting

In western blotting experiments with rabbit polyclonal sera raised against recombinant *T. hominis* DRP1, multiple bands were detected in protein extracts from purified *T. hominis* spores but neither of them migrated with a predicted molecular weight of 74 kDa (Figure 5.7 A). In order to increase the concentration of specific antibodies and to reduce concentration of the unspecific antibodies (potentially responsible for the detection of the additional bands detected in extracts from spores) the polyclonal sera were affinity purified against the recombinant C-terminus of *T. hominis* DRP1. Antibodies were purified against the C-terminal fragment of the protein (328 amino acids, cloned in frame with DHFR into pQE40 vector and expressed in *E. coli* M15 strain) instead the full-length sequence (645 amino acids) in order to avoid enriching in antibodies raised against common and well conserved (Figure 5.4 *see Appendix B*) N-terminal GTPase domain. The affinity purified antibodies detected a single parasite-specific band with an apparent relative molecular weight (rMW) of approximately 74 kDa in extracts from *T. hominis* spores and *T. hominis* infected rabbit kidney cells (RK13) but not in extracts from the non-infected host (Figure 5.7 B).

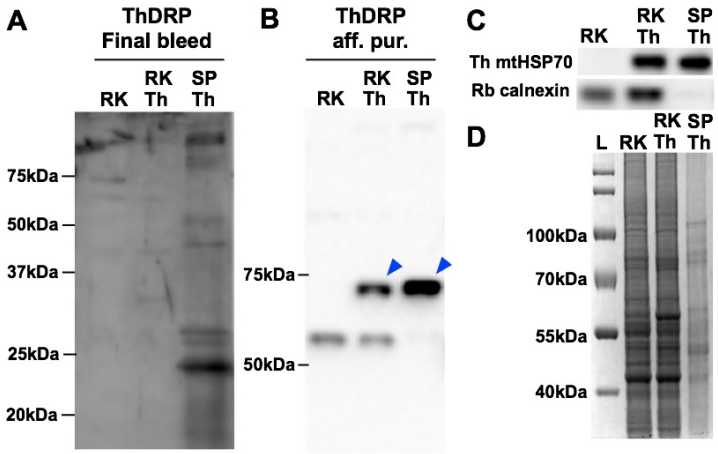

Figure 5.7 Testing the specificity of the anti-*Th*DRP1 antibodies in total protein extracts from *T. hominis* spores, *T. hominis* infected and non-infected rabbit kidney (RK-13) cells

(A) Polyclonal antiserum from the final bleed of a rabbit immunised with the recombinant *T. hominis* DRP1 (1:200 dilution) was tested against total protein extracts from purified *T. hominis* spores (**SPTh**), *T. hominis* infected rabbit kidney cells (**RKTh**) and non-infected rabbit kidney cells control (**RK**). Multiple parasite specific bands were detected in ThSP but not in the RK or RKTh and neither of them had predicted apparent relative molecular weight of 74 kDa.

(B) ThDRP1 antisera affinity-purified against the C-terminal region of the immunogen (1:100 dilution of 0.3 mg/ml stock) detected a single parasite specific band migrating with apparent molecular weights of ~74 kDa (**blue arrowhead**) in the RKTh and the SpTh but not in the RK control.

(C) Rat anti-*Th*mtHSP70 antisera (1:1000 dilution) detected single band migrating with an apparent molecular weight of ~60 kDa in the RKTh and the SPTh but not in the RK control. Commercial antibodies against mammalian calnexin detected single band (~80 kDa) in the RK and the RKTh but not in the SPTh.

(D) Coomassie blue stained polyacrylamide gel with total protein extracts from RK, RKTh and SPTh. Approximately 20 µg (based on BCA assay) of RK and RKTh extracts and 5 µg of SPTh was loaded onto the gel. The gel is an equivalent of the gels used in western blotting experiments (B) and (C). The gels used in western blotting experiment (B and C) as well as coomassie blue stained gel (D) were run longer in order to optimize resolution of the parasite specific and host specific bands detected with the affinity purified anti - ThDRP1 antisera (B).

Blot probed with final bleed (A) was exposed for 120 s whereas the rest of the blots (B and C) were exposed for 20 s.

Molecular weights of the bands were estimated using 'MW analysis tool' implemented in the Image Lab (Bio-Rad). Precision Plus Protein™ WesternC™ standard (Bio-Rad) was used in (A) and (B). PageRuler protein ladder (Thermo Scientific) was used in (D).

5.3.5 Investigating intracellular localisation of the DRP1 in Trachipleistophora hominis cells using immunofluorescence microscopy experiments

Fluorescent signals detected using anti-*Th*DRP1 rabbit polyclonal sera affinity purified against recombinant C-terminal *Th*DRP1 localized along the cell membrane of the intracellular stages of *T. hominis* observed in the DIC images (Figure 5.8). The fluorescent signals were detected in small single nucleate parasite cells (early meronts, Figure 5.8 A) as well as the large multinucleate cells (late meronts, Figure 5.8 B). In some cells the fluorescent signals that appeared to protrude from the surface of the cell were observed (Figure 5.8 B). No signals above the background levels were detected inside the parasite cytoplasm.

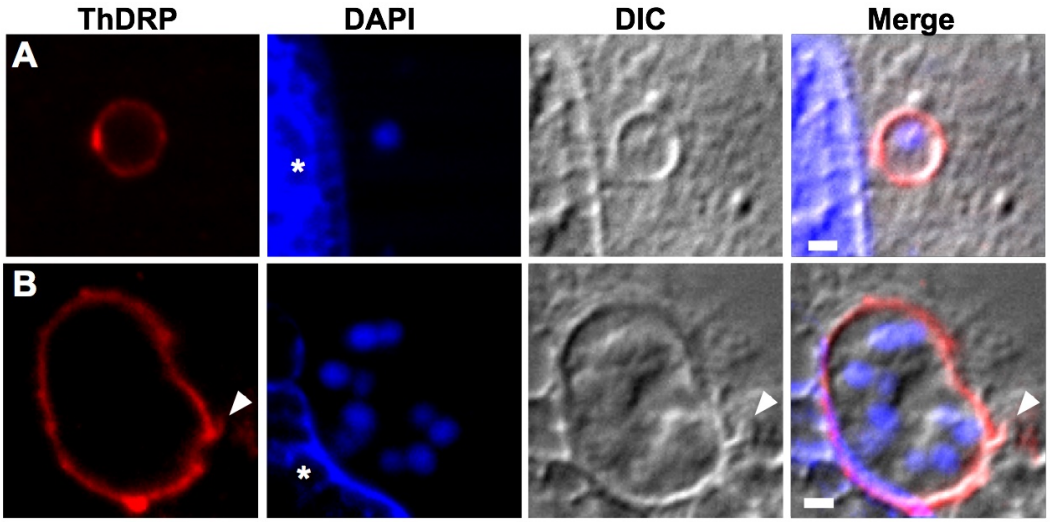

Figure 5.8 Fluorescence microscopy images of fixed samples of *T. hominis* infected rabbit kidney cells probed with the affinity purified anti-*Th*DRP1 polyclonal rabbit sera

Fluorescence signals detected using affinity-purified anti-ThDRP1 polyclonal rabbit sera (red) appeared to localize along the cell membrane of the small single-nucleate parasite **(A)** as well as the large multinucleate **(B)** *T. hominis* cells. In the image of the large cell, red anti-*Th*DRP1 signal (white arrowhead) was also detected along a small structure (visible in the DIC image) that appeared to protrude from the surface of the parasite cell. White asterisks indicate DAPI-stained nucleus of the host.

Images were acquired using Zeiss Axioimager II fluorescence microscope with 63x/1.4 Oil DIC lens. Scale bars correspond to 1 µm.

5.4 Discussion

In this study two dynamin related protein (DRP) homologues were identified in all analyzed microsporidian genomes apart from the three sequenced *Nematocida parisii* isolates that contain only one DRP homologue. Two DRPs were also found in representatives of two taxa most closely related to microsporidia, namely Fungi and Cryptomycota. In phylogenetic analyses (Figure 5.5) the DRP2 homologue was present in all microsporidia groups together with yeast Vps1p. This grouping seemed to be robust as it was retrieved with high support in all constructed phylogenies and suggested orthologous relationship between fungal Vps1p and the microsporidian homologue (DRP2 from now on is referred to as VPS1). The only DRP homologue present in available *N. parisii* genomes is the most divergent of microsporidian VPS1 orthologues, forming a long branch within microsporidian VPS1 clade. The second microsporidian homologue (DRP1) grouped together with Dnm1p homologues from Fungi and *R. allomycis* with low support. This result together with close phylogenetic relationship of microsporidia, Fungi and Cryptomycota suggests, that the second microsporidian DRP could be a highly divergent Dnm1p orthologue. Detection of the DRP1 coding gene in genomes of *R. allomyces* and all microsporidia, with the exception of *N. parisii,* indicates that the gene loss is specific to *N. parisii* lineage. It could be speculated that the *N. parisii* VPS1 can perform functions of both DRP1 and VPS1, which could potentially explain the long branch formed by the *N. parisii* VPS1 orthologues within the microsporidian VPS1 clade (Figure 5.5).

Protein sequence comparison revealed the presence of GTPase, MD and GED domains in microsporidian DRPs as well as the potential loss or at least high reduction of the region corresponding to the Insert B in mammalian Drp1 and yeast Dnm1p, from microsporidian sequences. In *S. cerevisiae* Dnm1p Insert B interacts with an N-terminal WD40 domain of one of the adaptor proteins Mdv1p or Caf4p (Bui & Shaw, 2013). The C-terminal region of either of the adaptors interacts with outer mitochondrial membrane anchor protein Fis1p (Bui & Shaw, 2013). The results of BlastP and HMMER searches, together with phylogenetic analysis suggest, that microsporidian homologues of proposed interaction partners involved in recruitment of Dnm1p/Drp1 to mitochondria in yeast or mammals might have been either lost in microsporidia or might be too divergent to be identified.

Recent studies indicate that the diverse lineages of microbial eukaryotes may still use the bacterial-derived FtsZ-based system to divide their mitochondria (Leger *et al.*, 2015). However the Opisthokonta (group of eukaryotes including animals, Fungi, and microsporidia) is one of the eukaryotic lineages that have lost the ancestral FtsZ-based system and instead rely on the dynamin related protein (Dnm1p in yeast, Drp1 in mammals) for division of their mitochondria (Leger *et al.*, 2015). A highly divergent orthologue of Dnm1p, microsporidian DRP1, is the only homologue of mitochondrial division machinery components identified in this study.

In order to test the hypothesis that the *T. hominis* DRP1 (*Th*DRP1) localizes to the constriction site of the dividing mitosomes, specific antibodies against the *Th*DRP1 generated in this study were tested in immunofluorescence microscopy experiments. In these experiments labelling inside the *T. hominis* cytoplasm was not detected but instead the labelling along the parasites cell membrane was observed. In published studies of *S. cerevisiae* DRPs, Dnm1p seems to localize mainly in the cytosol of *S. cerevisiae,* based on the western blotting experiments (Otsuga *et al.*, 1998), whereas in microscopy images of yeast cells fluorescence signals of GFP - tagged or immuno-labelled Dnm1p localized mainly to punctate structures colocalizing with the mitochondrial fluorescence signals (Bleazard *et al.*, 1999; Sesaki and Jensen, 1999; Kuravi *et al.*, 2006). YFP-tagged Vps1 showed moderate cytoplasmic localization, with an additional spotted accumulations, most likely in the Golgi apparatus and a minor fraction that seemed to colocalize with the peroxisomes (Hoepfner *et al.*, 2001). Additional experimental work is required in order to further investigate a possible presence of punctate DRP1 signals localizing at the mitosomal constriction sites in *T. hominis*. Due to a small number of mitosomes per cell, their tiny size and possibly a transient nature of the mitosomal division event, the mitosomal DRP1 signals may be difficult to observe in a population of the fixed *T. hominis* cells. The specific dynamin inhibitors that can stabilize dynamin rings around membrane constriction sites could be used to address this difficulty (Takei et al., 1995). The anti-*Th*DRP1 antibodies should also be tested in western blotting experiments with protein extracts from the cell fractionation experiments in order to test the possible presence of a cytosolic fraction that could not be detected in immunofluorescence experiments, as it was in case of *S. cerevisiae* Dnm1p (Bleazard *et al.*, 1999). In published immunoelectron microscopy (immuno-EM) experiments the immunogold signals corresponding to *S. cerevisiae* Dnm1p clustered at constricted sites on yeast mitochondria, that appeared to be dividing

(Bleazard *et al.*, 1999). The anti-*Th*DRP1 antibodies could also be tested in the immunoelectron microscopy experiment to investigate a possible presence of DRP1 division rings around the mitosomal fission sites.

A single DRP homologue can be involved in different cellular processes, for example *S. cerevisiae* Vps1p functions in vesicular trafficking as well as peroxisome and vacuole division in Fungi (Williams & Kim, 2014). *S. cerevisiae* Dnm1p in addition to its function in division of mitochondria seems to play a limited (Williams & Kim, 2014) role in division of the peroxisomes: *vps1* deletion strains contain two or more peroxisomes but *vps1 dnm1* double deletion strains contain only a single peroxisome (Kuravi *et al.*, 2006). The orthologue of Vps1p but not that of Dnm1p was identified in available genome assemblies of *N. parisii.* As it seems unlikely that *N. parisii* does not require specific machinery for mitosomal division the VPS1 seems to be the best candidate to perform this function in this microsporidian. The possibility that the VPS1 is involved in mitosomal division in all microsporidia cannot be excluded and, in order to investigate this hypothesis the specific antibodies against the *T. hominis* VPS1 should be generated as part of future work.

Observed localization of the fluorescence signals detected with anti-*T. hominis* DRP1 antibodies indicates that in addition to its hypothetical role in the division of the mitosome it may also be involved in membrane remodelling processes along the parasite's cell membrane. In published electron micrographs of fixed host cells infected with *T. hominis* the parasite's meronts are surrounded by an electron-dense surface coat, which forms protrusions (also described as 'processes extending from the surface coat', 'reticular extensions', or 'branched surface ribbon-like extensions') extending from the parasite's surface into an electron-lucent zone of modified host cytoplasm (clear zone) adjacent to the surface of *T. hominis* cells (Hollister *et al.*, 1996; Lafranchi-Tristem *et al.*, 2001; Curry *et al.*, 2005), (Figure 5.9). These protrusions are often observed next to -possibly host derived- vesicles observed in the host cytosol (Hollister *et al.*, 1996). The exact nature or function of these protrusions is unknown but it could be speculated that they play a role in interaction with the host, other cells of the parasite, and/or are responsible for increasing the surface area of the interface between the host and the pathogen. *T. hominis* DRP1 could potentially be involved in membrane remodelling processes that may be required for the formation and maintenance of this potentially complex interface between the host and the parasite. Observation of the fluorescence signals extending out of the parasite's surface seems to be consistent with localization to the

protrusions of the parasite surface coat (Figure 5.9). Further immuno-electron microscopy experiments will be required in order to investigate if the DRP1 localizes to the constriction sites of the parasite cell membrane or an outer thin membrane-like layer separating the parasite surface coat from the host cytosol (Vavra *et al.*, 2006).

Dynamins are involved in different types of endocytic membrane trafficking pathways in mammalian cells (Harper et al., 2013; Mayor & Pagano, 2007). The microsporidian DRP1 could also be involved in endocytosis, although convincing experimental evidence of endocytosis in microsporidia is missing. The anti-*Th*DPR1 antibodies could be used together with the commercially available dynamin inhibitors to further study these processes in microsporidia (Harper et al., 2013).

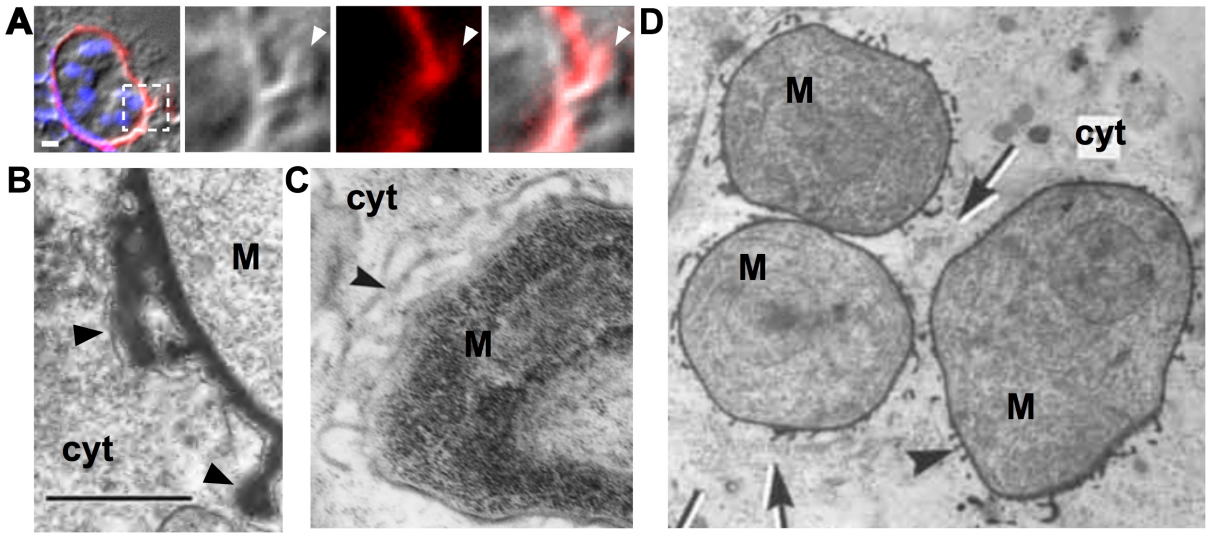

Figure 5.9 Projections of the *T. hominis* surface coat at the interface between the host and the parasite

(A) Zoom in at the small structure (white arrow) that appeared to protrude from the surface of the *T. hominis* cell (Figure 5.7 B) labelled with affinity purified anti-*Th*DRP1 sera (red).

(B, C and D) The short projections of the parasite surface coat (black arrowheads) were previously observed in electron micrographs of thin sections of fixed host cells infected with *T. hominis.* Images B and D were adapted from (Hollister et al., 1996); and image C was adapted from (Lafranchi-Tristem et al., 2001).

Annotation of images: M, *T. hominis* meronts; cyt, host cytoplasm; arrowheads, extensions of the parasite surface coat. Scale bar corresponds to 500 nm.

Chapter 6. General discussion

Microsporidia are a group of highly successful eukaryotic obligate intracellular parasites infecting broad range of eukaryotic hosts including immunocompromised patients. Microsporidia grow and proliferate exclusively inside their host cells and the only stage of their life cycle that can survive outside the host cell is a dispersive environmental spore. Analyses of microsporidian genomes revelled extreme reduction of their metabolic capabilities including a lack of complete metabolic pathways for *de novo* biosynthesis of nucleotides, and amino acids; as well as pathways involved in energy metabolism including the tricarboxylic acid cycle, beta-oxidation of fatty acids, and the electron transport chain (Nakjang et al., 2013). Microsporidia have to steal metabolites that they cannot synthesise on their own using a range of membrane transporter proteins encoded in their genomes including members of the NTT-transport protein family (Heinz et al., 2012; Nakjang et al., 2013). Microsporidian NTTs were localized to the cell membrane of the intracellular stages of *Trachipleistophora hominis* and *Encephalitozoon cuniculi* and can transport nucleotides in heterologous expression experiments (Tsaousis et al., 2008; Heinz et al., 2014). Many of the metabolic pathways that were lost from microsporidian genomes such as the tricarboxylic acid cycle and the electron transport chain usually are localized in mitochondria. Microsporidian mitochondrial homologues called mitosomes are tiny organelles (50 nm x 100 nm) with a single known conserved metabolic function in biosynthesis of the essential iron-sulfur clusters (Williams et al., 2002; Goldberg et al., 2008; Tsaousis et al., 2008).

The general aims of this study were to further investigate the functions of the microsporidian mitosomes and to characterize molecular mechanisms involved in inheritance of this organelle in two microsporidians capable of infecting humans *Trachipleistophora hominis* and *Encephalitozoon cuniculi.*

6.1 AOX and mtG3PDH localize to the mitosomes of *T. hominis*

Genomes of some microsporidia including that of *T. hominis* encode homologues of two mitochondrial metabolic enzymes namely the alternative oxidase (AOX) and the mitochondrial glycerol-3-phosphate dehydrogenase (mtG3PDH), (Williams et al., 2010; Heinz et al., 2012) the two enzymes that constitute an

alternative respiratory pathway (ARP) in mitochondria of the bloodstream stage of another eukaryotic microbial parasite *Trypanosoma brucei* (Chaudhuri et al., 2006).

In order to investigate the hypothetical localization of the AOX and mtG3PDH to the mitosomes of *T. hominis* I have expressed recombinant *Th*AOX and *Th*mtG3PDH in *E. coli* and generated rabbit polyclonal sera against these two proteins. I have also generated rat polyclonal sera against the known mitosomal marker *Th*mtHSP70 for use in double labelling experiments with sera raised in the two different animal species (i.e. rabbits and rats). The results of my immunofluorescence and western blotting experiments with the affinity purified polyclonal antisera against the *T. hominis* AOX and mtG3PDH were consistent with the initial hypothesis that AOX and mtG3PDH localize to the mitosomes of *T. hominis.* The mitosomal localization of the AOX and mtG3PDH indicates that the mitosomes of *T. hominis* can function in the ARP in addition to their role in biosynthesis of the essential iron-sulfur clusters (ISC).

The mitosomal ARP is the only known metabolic pathway encoded in microsporidian genomes capable of reoxidizing NADH, the process required for continuous generation of ATP in glycolysis. Published experimental data suggested enrichment of the glycolytic enzymes in spores rather than the intracellular stages of *T. hominis* (Heinz et al., 2012) and the results of my analyses of the relative intensities of bands detected in western blotting experiments indicated that the AOX and the mtG3PDH are also enriched in *T. hominis* spores rather than in the intracellular stages of the parasite. Apart from glycolysis together with the ARP microsporidia do not have any other metabolic pathways for energy generation. The intracellular stages of *T. hominis* can use the nucleotide transporter proteins (NTTs) to steal purine nucleotides, including ATP, from the host (Tsaousis et al., 2008; Heinz et al., 2014). However, the extracellular dispersive spore cannot rely on its host and can utilize glycolysis together with the ARP for generation of energy that it may require for survival and/or for the germination process (Heinz et al., 2012; Williams et al., 2014).

In my immunofluorescence microscopy experiments *T. hominis* AOX and G3PDH were detected in the mitosomes of early meronts (stage of the parasite life cycle observed just after the infection process) suggesting that *T. hominis* may also rely on its own energy metabolism just after entering the host cell and before the initiation of the growth and proliferation phases of its life cycle. Based on my semi-quantitative analyses of the fluorescence signals detected with the anti-*Th*mtHSP70,

anti-*Th*NFS, and anti-*Th*AOX the mitosomes seem to shift their function from the ARP to the ISC during the transition between early meront phase and cell-growth (intermediate meront) phase of the *T. hominis* life cycle. The ISC-containing proteins are involved in central metabolic processes including protein translation, as well as the synthesis and maintenance of DNA (Lill & Mühlenhoff, 2005; Netz et al., 2012). These processes are essential for cell growth and proliferation and observed increase in number of the mitosomes involved in biosynthesis of the ISCs but not in the ARP is consistent with an important role that mitosomes play in the proliferative stages of the *T. hominis* life cycle.

Future experimental work should focus on investigating the exact function of the ARP during the parasite life cycle using the specific inhibitors of the AOX as well as testing the effectiveness of this inhibitors as anti-microsporidian drugs.

6.2 Characterization of the microsporidian spindle pole body and investigating its role in inheritance of the mitosomes in *T. hominis* and *E. cuniculi*

In electron micrographs microsporidian mitosomes are often observed close to the electron-dense spindle plaque that seems to be localized within a pore inside the nuclear envelope and resembles fungal microtubule organizing center (MTOC), called a spindle pole body (SPB), (Bigliardi et al., 1998; Vavra, 2005; Tsaousis et al., 2008).

My bioinformatics analyses identified 4 microsporidian homologues of the 17 characterized SPB components from *Saccharomyces cerevisiae* and 13 characterized SPB components from *Schizosaccharomyces pombe* investigated in this study. I have expressed and generated polyclonal antibodies against three of the microsporidian SPB protein candidates, namely *T. hominis* SPC98, TUB4 and MPS3; and *E. cuniculi* TUB4. The specific antibodies against the *T. hominis* MPS3 and SPC98 as well as *E. cuniculi* TUB4 detected punctate fluorescence signals at the circumference of the DAPI stained nuclei of the parasites, which is consistent with the localization of these proteins in or adjacent to the nuclear envelope and is reminiscent of the published fluorescent images from the localization studies of the yeast SPB proteins (Jaspersen et al., 2002; Li et al., 2015). Further immunoelectron microscopy experiments will be required in order to investigate localization of the proteins to the electron-dense spindle plaques.

Anchoring to MTOC seems to be a mechanism responsible for the segregation of mitochondria or mitochondrial homologues during the cell division process in different eukaryotic microorganisms including *Giardia intestinalis* (Regoes et al., 2005) *Plasmodium falciparum* (Okamoto et al., 2009) or *Trypanosoma brucei* (Ogbadoyi et al., 2003). In my double labelling experiments using antibodies against the microsporidian SPB proteins and mitosomal markers the fluorescent signals detected with the two antibodies have partially, but not completely, overlapped. The observed labelling pattern was consistent with the observation of a subpopulation of mitosomes in a close proximity of the electron-dense spindle plaque in the electron micrographs of *E. cuniculi* (Tsaousis et al., 2008) and *T. hominis* (this study) cells. At least one mitosomal (mtHSP70) fluorescent signal partially overlapping with the SPB protein (MPS3) fluorescent signal was observed in all intracellular stages of the *T. hominis* life cycle. These observations suggest that the steady link between the SBP and mitosomes is maintained through the *T. hominis* life cycle and are consistent with the hypothesis that attachment of the mitosomes to the SPB is a mechanism responsible for ensuring mitosome inheritance during cell proliferation.

The exact nature of the link between the mitosomes and the SPB is unknown and further immunoelectron microscopy experiments could be used to investigate if MPS3 or TUB4 are involved in mediating the interaction between the SPB and the mitosome. Identification of the proteins involved in interaction between the SPB and the mitosomes could help in identifying drugs that could be used to disturb this interaction and test its effect on the segregation of the mitosomes.

Identification of the microsporidian homologues of the mitochondrial division machinery components

In addition to a reliable segregation mechanism, mitosomal division is essential in order to maintain the numbers of mitosomes in the population of proliferating microsporidian cells. The force generating 'constrictases' belonging to the family of dynamin related proteins (DRP) play important roles in division of mitochondria in fungi and mammals (Ferguson & De Camilli, 2012; Friedman & Nunnari, 2014).

My bioinformatics analyses have identified two homologues of the dynamin related proteins in available microsporidian genomes: VPS1 an orthologue of a yeast Vps1 involved in multiple membrane remodelling processes including peroxisome

division, vacuole division, and vesicular trafficking in *S. cerevisiae* (Williams & Kim, 2014); and DRP1 a highly divergent orthologue of fungal Dnm1 involved in division of mitochondria in *S. cerevisiae* (Detmer & Chan, 2007; Westermann, 2010). In order to test the hypotheses that the microsporidian DRP1 is involved in mitosomal division I have expressed recombinant *T. hominis* DRP1 in *E. coli* and used it to generate specific polyclonal antisera. Antibodies affinity purified from the sera detected bands corresponding to expected size of *T. hominis* DRP1 in western blotting experiments using protein extracts from purified *T. hominis* spores and host cells infected with *T. hominis.* Fluorescent signals detected using the affinity purified antibodies localized along the cell membrane of the intracellular stages of *T. hominis* indicating that *T. hominis* DRP1 may be involved in endocytosis and/or in remodelling of a potentially complex membrane system at the interface between the pathogen and its host. The antibodies did not detect any punctate signals inside the parasite cytoplasm, which would be expected for a protein involved in the mitosomal division. However, division of the mitosomes could be a transient event and additional experimental work using dynamin inhibitors that can stabilize dynamin rings around membrane constriction sites (Takei et al., 1995) may be needed in order to further test the hypothetical involvement of the DRP1 in the mitosomal division.

References

Abrahamsen, M.S., Templeton, T.J., Enomoto, S., Abrahante, J.E., Zhu, G., Lancto, C.A., Deng, M., Liu, C., Widmer, G., Tzipori, S., Buck, G.A., Xu, P., Bankier, A.T., Dear, P.H., Konfortov, B.A., Spriggs, H.F., Iyer, L., Anantharaman, V., Aravind, L., et al. (2004) Complete Genome Sequence of the Apicomplexan, *Cryptosporidium parvum*. *Science*. 304 (5669), 441–445.

Adl, S.M., Simpson, A.G.B., Lane, C.E., Lukeš, J., Bass, D., Bowser, S.S., Brown, M.W., Burki, F., Dunthorn, M., Hampl, V., Heiss, A., Hoppenrath, M., Lara, E., le Gall, L., Lynn, D.H., McManus, H., Mitchell, E.A.D., Mozley-Stanridge, S.E., Parfrey, L.W., et al. (2012) The Revised Classification of Eukaryotes. *Journal of Eukaryotic Microbiology*. 59 (5), 429–514.

Affourtit, C., Albury, M.S., Crichton, P.G. & Moore, A.L. (2002) Exploring the molecular nature of alternative oxidase regulation and catalysis. *FEBS Letters*. *510* (3), 121-126.

Akhter, S., McDade, H.C., Gorlach, J.M., Heinrich, G., Cox, G.M. & Perfect, J.R. (2003) Role of alternative oxidase gene in pathogenesis of *Cryptococcus neoformans*. *Infection and Immunity.* 71(10), 5794-5802.

Akiyoshi, D.E., Morrison, H.G., Lei, S., Feng, X., Zhang, Q., Corradi, N., Mayanja, H., Tumwine, J.K., Keeling, P.J. & Weiss, L.M. (2009) Genomic survey of the non-cultivatable opportunistic human pathogen, *Enterocytozoon bieneusi*. *PLoS Pathogens*, *5* (1), e1000261.

Ali, V., Shigeta, Y., Tokumoto, U., Takahashi, Y. & Nozaki, T. (2004) An intestinal parasitic protist, *Entamoeba histolytica*, possesses a non-redundant nitrogen fixation-like system for iron-sulfur cluster assembly under anaerobic conditions. *The Journal of Biological Chemistry*. 279 (16), 16863–16874.

Allen, J.F. (2015) Why chloroplasts and mitochondria retain their own genomes and genetic systems: Colocation for redox regulation of gene expression. *Proceedings of the National Academy of Sciences of the United States of America*. 112 (33), 10231–10238.

Altmann, K., Frank, M., Neumann, D., Jakobs, S. & Westermann, B. (2008) The class V myosin motor protein, Myo2, plays a major role in mitochondrial motility in *Saccharomyces cerevisiae*. *The Journal of Cell Biology*. 181 (1), 119–130.

Altschul, S.F., Gish, W., Miller, W., Myers, E.W. & Lipman, D.J. (1990) Basic local alignment search tool. *Journal of Molecular Biology*. 215 (3), 403–410.

Andreadis, T.G. (1985) Experimental transmission of a microsporidian pathogen from mosquitoes to an alternate copepod host. *Proceedings of the National Academy of Sciences of the United States of America*. 82 (16), 5574–5577.

Antoniacci, L.M., Kenna, M.A., Uetz, P., Fields, S., and Skibbens, R.V. (2004) The spindle pole body assembly component mps3p/nep98p functions in sister chromatid cohesion. *Journal of Biological Chemistry.* 279(47), 49542-49550.

Arimura, S.-I. & Tsutsumi, N. (2002) A dynamin-like protein (ADL2b), rather than FtsZ, is involved in *Arabidopsis* mitochondrial division. *Proceedings of the*

National Academy of Sciences of the United States of America. 99 (8), 5727–5731.

Arimura, S.-I., Aida, G.P., Fujimoto, M., Nakazono, M. & Tsutsumi, N. (2004) Arabidopsis dynamin-like protein 2a (ADL2a), like ADL2b, is involved in plant mitochondrial division. *Plant and Cell Physiology*. 45 (2), 236–242.

Audia, J.P. & Winkler, H.H. (2006) Study of the five *Rickettsia prowazekii* proteins annotated as ATP/ADP translocases (Tlc): Only Tlc1 transports ATP/ADP, while Tlc4 and Tlc5 transport other ribonucleotides. *Journal of Bacteriology*. 188 (17), 6261–6268.

Avila Adame, C. & Köller, W. (2003) Impact of alternative respiration and target-site mutations on responses of germinating conidia of *Magnaporthe grisea* to Qo-inhibiting fungicides. *Pest Management Science*. 59 (3), 303–309.

Bach, D., Pich, S., Soriano, F.X., Vega, N., Baumgartner, B., Oriola, J., Daugaard, J.R., Lloberas, J., Camps, M., Zierath, J.R., Rabasa-Lhoret, R., Wallberg-Henriksson, H., Laville, M., Palacín, M., Vidal, H., Rivera, F., Brand, M. & Zorzano, A. (2003) Mitofusin-2 determines mitochondrial network architecture and mitochondrial metabolism. A novel regulatory mechanism altered in obesity. *The Journal of Biological Chemistry*. 278 (19), 17190–17197.

Bakker, B.M., Overkamp, K.M., van Maris AJ, Kötter, P., Luttik, M.A., van Dijken JP & Pronk, J.T. (2001) Stoichiometry and compartmentation of NADH metabolism in *Saccharomyces cerevisiae*. *FEMS Microbiology Reviews*. 25 (1), 15–37.

Bakowski, M.A., Luallen, R.J. & Troemel, E.R. (2014) 'Microsporidia Infections in Caenorhabditis Elegans and Other Nematodes', in *Microsporidia*. Pathogens of Opportunity. [Online]. Chichester, UK: John Wiley & Sons, Inc. pp. 341–356.

Bakowski, M.A., Priest, M., Young, S., Cuomo, C.A. & Troemel, E.R. (2014) Genome Sequence of the Microsporidian Species *Nematocida* sp1 Strain ERTm6 (ATCC PRA-372). *Genome Announcements*. 2 (5), e00905–14.

Becnel, J.J. & Andreadis, T.G. (2014) 'Microsporidia in Insects', in *Microsporidia*. Pathogens of Opportunity. [Online]. Chichester, UK: John Wiley & Sons, Inc. pp. 521–570.

Beech, P.L., Nheu, T., Schultz, T., Herbert, S., Lithgow, T., Gilson, P.R. & McFadden, G.I. (2000) Mitochondrial FtsZ in a chromophyte alga. *Science*. 287 (5456), 1276–1279.

Bigliardi, E., Riparbelli, M.G., Selmi, M.G., Lanzarini, P., Corona, S., Gatti, S., Scaglia, M. & Sacchi, L. (1998) Mechanisms of microsporidial cell division: ultrastructural study on *Encephalitozoon hellem. Journal of Eukaryotic Microbiology.* 45 (3), 347–351.

Bjørnson, S. & Oi, D. (2014) 'Microsporidia Biological Control Agents and Pathogens of Beneficial Insects', in *Microsporidia*. Pathogens of Opportunity. [Online]. Chichester, UK: John Wiley & Sons, Inc. pp. 635–670.

Bleazard, W., McCaffery, J.M., Shaw, J.M., 8 (1999) The dynamin-related GTPase Dnm1 regulates mitochondrial fission in yeast. *Nature Cell Biology.* 1, 298–304.

Boldogh, I.R. & Pon, L.A. (2007) Mitochondria on the move. *Trends in Cell Biology*. 17 (10), 502–510.

Boldogh, I.R., Yang, H.C., Nowakowski, W.D., Karmon, S.L., Hays, L.G., Yates, J.R. & Pon, L.A. (2001) Arp2/3 complex and actin dynamics are required for actin-based mitochondrial motility in yeast. *Proceedings of the National Academy of Sciences of the United States of America*. 98 (6), 3162–3167.

Bollback, J.P. (2002) Bayesian model adequacy and choice in phylogenetics. *Molecular Biology and Evolution*. 19 (7), 1171–1180.

Bond, C.S. & Schüttelkopf, A.W. (2009) ALINE: a WYSIWYG protein-sequence alignment editor for publication-quality alignments. *Acta Crystallographica. Section D, Biological crystallography*. 65 (5), 510–512.

Branda, S.S., Cavadini, P., Adamec, J. & Kalousek, F. (1999) Yeast and human frataxin are processed to mature form in two sequential steps by the mitochondrial processing peptidase. *Journal of Biological Chemistry. 274(32), 22763-22769.*

Breinich, M.S., Ferguson, D.J.P., Foth, B.J., van Dooren, G.G., Lebrun, M., Quon, D.V., Striepen, B., Bradley, P.J., Frischknecht, F., Carruthers, V.B. & Meissner, M. (2009) A Dynamin Is Required for the Biogenesis of Secretory Organelles in *Toxoplasma gondii*. *Current Biology*. 19 (4), 277–286.

Brown, M.W., Sharpe, S.C., Silberman, J.D., Heiss, A.A., Lang, B.F., Simpson, A.G.B. & Roger, A.J. (2013) Phylogenomics demonstrates that breviate flagellates are related to opisthokonts and apusomonads. *Proceedings. Biological Sciences / The Royal Society*. 280 (1769), 20131755.

Bui, H.T., Karren, M.A., Bhar, D. & Shaw, J.M. (2012) A novel motif in the yeast mitochondrial dynamin Dnm1 is essential for adaptor binding and membrane recruitment. *The Journal of Cell Biology*. 199 (4), 613–622.

Bui, H.T., and Shaw, J.M. (2013) Dynamin Assembly Strategies and Adaptor Proteins in Mitochondrial Fission. *Current Biology.* 23, R891–R899.

Bupp, J.M., Martin, A.E., Stensrud, E.S., and Jaspersen, S.L. (2007) Telomere anchoring at the nuclear periphery requires the budding yeast Sad1-UNC-84 domain protein Mps3. *The Journal of Cell Biology.* 179, 845–854.

Burri, L. & Keeling, P.J. (2007) Protein targeting in parasites with cryptic mitochondria. *International Journal for Parasitology*. 37 (3-4), 265–272.

Burri, L., Williams, B.A.P., Bursac, D., Lithgow, T. & Keeling, P.J. (2006) Microsporidian mitosomes retain elements of the general mitochondrial targeting system. *Proceedings of the National Academy of Sciences of the United States of America*. 103 (43), 15916–15920.

Cali, A. & Takvorian, P.M. (1999) 'Developmental morphology and life cycles of the microsporidia', in Murray Wittner & M Louis Weiss (eds.) *The Microsporidia and Microsporidiosis*. [Online]. Washington D.C.: ASM Press. pp. 85–128.

Campbell, S.E., Williams, T.A., Yousuf, A., Soanes, D.M., Paszkiewicz, K.H. &

Williams, B.A.P. (2013) The Genome of *Spraguea lophii* and the Basis of Host-Microsporidian Interactions. *PLoS Genetics*. 9 (8), e1003676.

Capella-Gutiérrez, S., Marcet-Houben, M. & Gabaldón, T. (2012) Phylogenomics supports microsporidia as the earliest diverging clade of sequenced fungi. *BMC Biology*. 10 (1), 47.

Capella-Gutiérrez, S., Silla-Martínez, J.M. & Gabaldón, T. (2009) trimAl: a tool for automated alignment trimming in large-scale phylogenetic analyses. *Bioinformatics (Oxford, England)*. 25 (15), 1972–1973.

Cerveny, K.L., Studer, S.L., Jensen, R.E. & Sesaki, H. (2007) Yeast mitochondrial division and distribution require the cortical num1 protein. *Developmental Cell*. 12 (3), 363–375.

Cavalier-Smith, T. (1989) Archaebacteria and Archezoa. Nature 339: 100–101.

Chacinska, A., Koehler, C.M., Milenkovic, D., Lithgow, T. & Pfanner, N. (2009) Importing mitochondrial proteins: machineries and mechanisms. *Cell*. 138 (4), 628–644.

Chapman, H.C. (1974) Biological control of mosquito larvae. *Annual Review of Entomology*. 19 (1), 33–59.

Chaudhuri, M., Ott, R.D. & Hill, G.C. (2006) Trypanosome alternative oxidase: from molecule to function. *Trends in Parasitology*. 22 (10), 484–491.

Chen, X.J. & Butow, R.A. (2005) The organization and inheritance of the mitochondrial genome. *Nature Reviews Genetics*. 6 (11), 815–825.

Chen, Y.P., Pettis, J.S., Zhao, Y., Liu, X., Tallon, L.J., Sadzewicz, L.D., Li, R., Zheng, H., Huang, S., Zhang, X., Hamilton, M.C., Pernal, S.F., Melathopoulos, A.P., Yan, X. & Evans, J.D. (2013) Genome sequencing and comparative genomics of honey bee microsporidia, *Nosema apis* reveal novel insights into host-parasite interactions. *BMC Genomics*. 14 (1), 451.

Chiron, S., Bobkova, A., Zhou, H. & Yaffe, M.P. (2008) CLASP regulates mitochondrial distribution in *Schizosaccharomyces pombe*. *The Journal of Cell Biology*. 182 (1), 41–49.

Clarkson, A.B. & Brohn, F.H. (1976) Trypanosomiasis: an approach to chemotherapy by the inhibition of carbohydrate catabolism. *Science*. 194 (4261), 204–206.

Claros, M.G. & Vincens, P. (1996) Computational Method to Predict Mitochondrially Imported Proteins and their Targeting Sequences. *European Journal of Biochemistry.* 241 (3), 779–786.

Codes, G. (2000). Sequencher: Version 4.2. 2. Gene Codes Corporation. *Ann Arbor*.

Cole, C., Barber, J.D. & Barton, G.J. (2008) The Jpred 3 secondary structure prediction server. *Nucleic Acids Research*. 36 (Web Server issue), W197–201.

Collings, D.A., Gebbie, L.K., Howles, P.A., Hurley, U.A., Birch, R.J., Cork, A.H., Hocart, C.H., Arioli, T. & Williamson, R.E. (2008) *Arabidopsis* dynamin-like

protein DRP1A: a null mutant with widespread defects in endocytosis, cellulose synthesis, cytokinesis, and cell expansion. *Journal of Experimental Botany*. 59 (2), 361–376.

Conrad, M.N., Lee, C.-Y., Wilkerson, J.L., and Dresser, M.E. (2007) MPS3 mediates meiotic bouquet formation in *Saccharomyces cerevisiae*. *Proceedings of the National Academy of Sciences.* 104(21), 8863-8868.

Corradi, N. & Keeling, P.J. (2009) Microsporidia: a journey through radical taxonomical revisions. *Fungal Biology Reviews*. 23 (1), 1–8.

Corradi, N., Akiyoshi, D.E., Morrison, H.G., Feng, X., Weiss, L.M., Tzipori, S. & Keeling, P.J. (2007) Patterns of genome evolution among the microsporidian parasites *Encephalitozoon cuniculi, Antonospora locustae* and *Enterocytozoon bieneusi*. *PLoS ONE*. 2 (12), e1277.

Corradi, N., Haag, K.L., Pombert, J.-F., Ebert, D. & Keeling, P.J. (2009) Draft genome sequence of the *Daphnia* pathogen *Octosporea bayeri*: insights into the gene content of a large microsporidian genome and a model for host-parasite interactions. *Genome Biology*. 10 (10), R106.

Corradi, N., Pombert, J.-F., Farinelli, L., Didier, E.S. & Keeling, P.J. (2010) The complete sequence of the smallest known nuclear genome from the microsporidian *Encephalitozoon intestinalis*. *Nature Communications*. 1,77.

Cotte, L., Rabodonirina, M., Chapuis, F., Bailly, F., Bissuel, F., Raynal, C., Gelas, P., Persat, F., Piens, M.A. & Trepo, C. (1999) Waterborne outbreak of intestinal microsporidiosis in persons with and without human immunodeficiency virus infection. *The Journal of Infectious Diseases*. 180 (6), 2003–2008.

Cribbs, J.T. & Strack, S. (2007) Reversible phosphorylation of Drp1 by cyclic AMP-dependent protein kinase and calcineurin regulates mitochondrial fission and cell death. *EMBO Reports*. 8 (10), 939–944.

Cuomo, C.A., Desjardins, C.A., Bakowski, M.A., Goldberg, J., Ma, A.T., Becnel, J.J., Didier, E.S., Fan, L., Heiman, D.I., Levin, J.Z., Young, S., Zeng, Q. & Troemel, E.R. (2012) Microsporidian genome analysis reveals evolutionary strategies for obligate intracellular growth. *Genome Research*. 22 (12), 2478–2488.

Curry, A., Beeching, N.J., Gilbert, J.D., Scott, G., Rowland, P.L. & Currie, B.J. (2005) *Trachipleistophora hominis* infection in the myocardium and skeletal muscle of a patient with AIDS. *The Journal of Infection*. 51 (3), e139–144.

D'Andrea, L.D. & Regan, L. (2003) TPR proteins: the versatile helix. *Trends in Biochemical Sciences*. 28 (12), 655–662.

Damke, H., Baba, T., Warnock, D.E. & Schmid, S.L. (1994) Induction of mutant dynamin specifically blocks endocytic coated vesicle formation. *The Journal of Cell Biology*. 127 (4), 915–934.

Darriba, D., Taboada, G.L., Doallo, R. & Posada, D. (2011) ProtTest 3: fast selection of best-fit models of protein evolution. *Bioinformatics (Oxford, England)*. 27 (8), 1164–1165.

Das, S., Stevens, T., Castillo, C., Villasenõr, A., Arredondo, H. & Reddy, K. (2002) Lipid metabolism in mucous-dwelling amitochondriate protozoa. *International Journal for Parasitology*. 32 (6), 655–675.

De Brito, O.M. & Scorrano, L. (2010) An intimate liaison: spatial organization of the endoplasmic reticulum-mitochondria relationship. *The EMBO Journal*. 29 (16), 2715–2723.

De Souza, C.P.C. & Osmani, S.A. (2007) Mitosis, not just open or closed. *Eukaryotic Cell*. 6 (9), 1521–1527.

Dean, P., Major, P., Nakjang, S., Hirt, R.P. & Embley, T.M. (2014) Transport proteins of parasitic protists and their role in nutrient salvage. *Frontiers in Plant Science*. 5, 153.

Decraene, V., Lebbad, M., Botero-Kleiven, S., Gustavsson, A.-M. & Löfdahl, M. (2012) First reported foodborne outbreak associated with microsporidia, Sweden, October 2009. *Epidemiology and Infection*. 140, 519–527.

DeLano, W. L. (2002). The PyMOL molecular graphics system. [online]. Available from:https://www.pymol.org (Accessed 20 June 2015)

Deplazes, P., Mathis, A., Baumgartner, R., Tanner, I. & Weber, R. (1996) Immunologic and Molecular Characteristics of Encephalitozoon-Like Microsporidia Isolated from Humans and Rabbits Indicate That *Encephalitozoon cuniculi* Is a Zoonotic Parasite. *Clinical Infectious Diseases*. 22 (3), 557–559.

Desjardins, C.A., Sanscrainte, N.D., Goldberg, J.M., Heiman, D., Young, S., Zeng, Q., Madhani, H.D., Becnel, J.J. & Cuomo, C.A. (2015) Contrasting host-pathogen interactions and genome evolution in two generalist and specialist microsporidian pathogens of mosquitoes. *Nature Communications*. 6, 7121.

Detmer, S.A. & Chan, D.C. (2007) Functions and dysfunctions of mitochondrial dynamics. *Nature Reviews Molecular Cell Biology*. 8 (11), 870–879.

Didier, E.S. & Weiss, L.M. (2011) Microsporidiosis: not just in AIDS patients. *Current Opinion in Infectious Diseases*. 24, 490–495.

Didier, E.S., Didier, P.J., Snowden, K.F. & Shadduck, J.A. (2000) Microsporidiosis in mammals. *Microbes and Infection*. 2 (6), 709–720.

Didier, E.S., Stovall, M.E., Green, L.C., Brindley, P.J., Sestak, K. & Didier, P.J. (2004) Epidemiology of microsporidiosis: sources and modes of transmission. *Veterinary Parasitology*. 126 (1-2), 145–166.

Dolezal, P., Dagley, M.J., Kono, M., Wolynec, P., Likić, V.A., Foo, J.H., Sedinová, M., Tachezy, J., Bachmann, A., Bruchhaus, I. & Lithgow, T. (2010) The Essentials of Protein Import in the Degenerate Mitochondrion of *Entamoeba histolytica*. *PLoS Pathogens*. *6*(3), e1000812.

Dolezal, P., Likic, V., Tachezy, J. & Lithgow, T. (2006) Evolution of the molecular machines for protein import into mitochondria. *Science*. 313 (5785), 314–318.

Dolgikh, V.V., Seliverstova, E.V., Naumov, A.M., Senderskiy, I.V., Pavlova, O.A. &

Beznoussenko, G.V. (2009) Heterologous expression of pyruvate dehydrogenase E1 subunits of the microsporidium *Paranosema(Antonospora) locustae* and immunolocalization of the mitochondrial protein in amitochondrial cells. *FEMS Microbiology Letters*. 293 (2), 285–291.

Dolgikh, V.V., Senderskiy, I.V., Pavlova, O.A., Naumov, A.M. & Beznoussenko, G.V. (2011) Immunolocalization of an Alternative Respiratory Chain in *Antonospora (Paranosema) locustae* Spores: Mitosomes Retain Their Role in Microsporidial Energy Metabolism. *Eukaryotic Cell*. 10 (4), 588–593.

Dudek, J., Rehling, P. & van der Laan, M. (2013) Mitochondrial protein import: common principles and physiological networks. *Biochimica et Biophysica Acta*. 1833 (2), 274–285.

Dunn, A.M. & Smith, J.E. (2001) Microsporidian life cycles and diversity: the relationship between virulence and transmission. *Microbes and Infection.* 3 (5), 381–388.

Duszenko, M., Ginger, M.L., Brennand, A., Gualdrón-López, M., Colombo, M.-I., Coombs, G.H., *et al.* (2011) Autophagy in protists. *Autophagy.* 7, 127–158.

Eddy, R.S. (2001) *HMMER: Profile hidden Markov models for biological sequence analysis.* [online]. Available from: http://hmmer.wustl.edu/. (Accessed 16 July 2014).

Edgar, R.C. (2004) MUSCLE: multiple sequence alignment with high accuracy and high throughput. *Nucleic Acids Research*. 32 (5), 1792–1797.

El-Khoury, R., Dufour, E., Rak, M., Ramanantsoa, N., Grandchamp, N., Csaba, Z., Duvillié, B., Bénit, P., Gallego, J., Gressens, P., Sarkis, C., Jacobs, H.T. & Rustin, P. (2013) Alternative oxidase expression in the mouse enables bypassing cytochrome c oxidase blockade and limits mitochondrial ROS overproduction. *PLoS Genetics*. 9 (1), e1003182.

Elthon, T. E., Nickels, R. L., & McIntosh, L. (1989). Monoclonal Antibodies to the Alternative Oxidase of Higher Plant Mitochondria. *Plant Physiology.* 89 (4), 1311–1317.

Emanuelsson, O., Nielsen, H., Brunak, S. & Heijne, von, G. (2000) Predicting subcellular localization of proteins based on their N-terminal amino acid sequence. *Journal of Molecular Biology*. 300 (4), 1005–1016.

Embley, T.M. (2006) Multiple secondary origins of the anaerobic lifestyle in eukaryotes. *Philosophical Transactions of the Royal Society of London B: Biological Sciences*. 361 (1470), 1055–1067.

Embley, T.M. & Martin, W. (2006) Eukaryotic evolution, changes and challenges. *Nature*. 440 (7084), 623–630.

Embley, T.M., van der Giezen, M., Horner, D., Dyal, P., Bell, S. & Foster, P. (2003) Hydrogenosomes, Mitochondria and Early Eukaryotic Evolution. *IUBMB Life*. 55 (7), 387–395.

Emelyanov, V.V. (2003) Phylogenetic affinity of a *Giardia lamblia* cysteine

desulfurase conforms to canonical pattern of mitochondrial ancestry. *FEMS Microbiology Letters*. *226*(2), 257-266.

Esser, C., Ahmadinejad, N., Wiegand, C., Rotte, C., Sebastiani, F., Gelius-Dietrich, G., Henze, K., Kretschmann, E., Richly, E., Leister, D., Bryant, D., Steel, M.A., Lockhart, P.J., Penny, D. & Martin, W. (2004) A genome phylogeny for mitochondria among alpha-proteobacteria and a predominantly eubacterial ancestry of yeast nuclear genes. *Molecular Biology and Evolution*. 21 (9), 1643–1660.

Esser, K., Jan, P.S., Pratje, E. & Michaelis, G. (2004) The mitochondrial IMP peptidase of yeast: functional analysis of domains and identification of Gut2 as a new natural substrate. *Molecular Genetics and Genomics*. 271 (5), 616–626.

Estaquier, J., Vallette, F., Vayssiere, J.-L. & Mignotte, B. (2012) 'The Mitochondrial Pathways of Apoptosis', in *Advances in Mitochondrial Medicine*. Advances in Experimental Medicine and Biology. [Online]. Dordrecht: Springer Netherlands. pp. 157–183.

Estes, K.A., Szumowski, S.C. & Troemel, E.R. (2011) Non-Lytic, Actin-Based Exit of Intracellular Parasites from *C. elegans* Intestinal Cells *PLoS Pathogens*. 7, e1002227.

Faelber, K., Posor, Y., Gao, S., Held, M., Roske, Y., Schulze, D., Haucke, V., Noé, F. & Daumke, O. (2011) Crystal structure of nucleotide-free dynamin. *Nature*. 477 (7366), 556–560.

Favet, J., Lapanje, A., Giongo, A., Kennedy, S., Aung, Y.-Y., Cattaneo, A., Davis-Richardson, A.G., Brown, C.T., Kort, R., Brumsack, H.-J., Schnetger, B., Chappell, A., Kroijenga, J., Beck, A., Schwibbert, K., Mohamed, A.H., Kirchner, T., de Quadros, P.D., Triplett, E.W., et al. (2013) Microbial hitchhikers on intercontinental dust: catching a lift in Chad. *The ISME Journal*. 7 (4), 850–867.

Fayer, R. & Santin Duran, M. (2014) 'Epidemiology of Microsporidia in Human Infections', in *Microsporidia*. Pathogens of Opportunity. [Online]. Chichester, UK: John Wiley & Sons, Inc. pp. 135–164.

Ferguson, S.M. & De Camilli, P. (2012) Dynamin, a membrane-remodelling GTPase. *Nature Reviews Molecular Cell Biology*. 13 (2), 75–88.

Ford, M.G.J., Jenni, S. & Nunnari, J. (2011) The crystal structure of dynamin. *Nature*. 477 (7366), 561–566.

Francia, M.E. & Striepen, B. (2014) Cell division in apicomplexan parasites. *Nature Reviews Microbiology*. 12 (2), 125–136.

Franzen, C. (2008) Microsporidia: a review of 150 years of research. *The Open Parasitology Journal*. 21–34.

Franzen, C. (2004) Microsporidia: how can they invade other cells? *Trends in Parasitology*. 20, 275–279.

Franzen, C. & Müller, A. (2001) Microsporidiosis: human diseases and diagnosis. *Microbes and Infection.* 3, 389–400.

Friederichs, J.M., Ghosh, S., Smoyer, C.J., McCroskey, S., Miller, B.D., Weaver, K.J., *et al.* (2011) The SUN Protein Mps3 Is Required for Spindle Pole Body Insertion into the Nuclear Membrane and Nuclear Envelope Homeostasis. *PLoS Genetics.* 7, e1002365.

Friedman, J.R., Lackner, L.L., West, M., DiBenedetto, J.R., Nunnari, J. & Voeltz, G.K. (2011) ER Tubules Mark Sites of Mitochondrial Division. *Science*. 334 (6054), 358–362.

Friedman, J.R. & Nunnari, J. (2014) Mitochondrial form and function. *Nature.* 505, 335–343.

Fries, I. (2014) 'Microsporidia, Honeybees, and Colony Collapse Disorder', in *Microsporidia*. Pathogens of Opportunity. [Online]. Chichester, UK: John Wiley & Sons, Inc. pp. 571–577.

Fröhlich, C., Grabiger, S., Schwefel, D., Faelber, K., Rosenbaum, E., Mears, J., Rocks, O. & Daumke, O. (2013) Structural insights into oligomerization and mitochondrial remodelling of dynamin 1-like protein. *The EMBO Journal*. 32 (9), 1280–1292.

Fu, C., Jain, D., Costa, J., Velve-Casquillas, G. & Tran, P.T. (2011) mmb1p Binds Mitochondria to Dynamic Microtubules. *Current Biology*. 21 (17), 1431–1439.

Fujimoto, M., Arimura, S.-I., Ueda, T., Takanashi, H., Hayashi, Y., Nakano, A. & Tsutsumi, N. (2010) *Arabidopsis* dynamin-related proteins DRP2B and DRP1A participate together in clathrin-coated vesicle formation during endocytosis. *Proceedings of the National Academy of Sciences*. 107 (13), 6094–6099.

Gaechter, V., Schraner, E., Wild, P. & Hehl, A.B. (2008) The Single Dynamin Family Protein in the Primitive Protozoan *Giardia lamblia* Is Essential for Stage Conversion and Endocytic Transport. *Traffic*. 9 (1), 57–71.

Galván, A.L., Magnet, A., Izquierdo, F., Fenoy, S., Rueda, C., Fernández Vadillo, C., Henriques-Gil, N. & del Aguila, C. (2013) Molecular characterization of human-pathogenic microsporidia and *Cyclospora cayetanensis* isolated from various water sources in Spain: a year-long longitudinal study. *Applied and Environmental Microbiology*. 79 (2), 449–459.

Gannon, J. (1980) A survey of *Encephalitozoon cuniculi* in laboratory animal colonies in the United Kingdom. *Laboratory Animals*. 14 (2), 91–94.

Gasteiger, E., Gattiker, A., Hoogland, C., Ivanyi, I., Appel, R. D., & Bairoch, A. (2003). ExPASy: the proteomics server for in-depth protein knowledge and analysis. *Nucleic Acids Research*. *31*(13), 3784-3788.

Gill, E.E., Diaz-Triviño, S., Barbera, M.J., Silberman, J.D., Stechmann, A., Gaston, D., Tamas, I. & Roger, A.J. (2007) Novel mitochondrion-related organelles in the anaerobic amoeba *Mastigamoeba balamuthi. Molecular Microbiology*. 66 (6), 1306–1320.

Glick, B.S., Brandt, A., Cunningham, K., Müller, S., Hallberg, R.L. & Schatz, G. (1992) Cytochromes c1 and b2 are sorted to the intermembrane space of yeast mitochondria by a stop-transfer mechanism. *Cell*. 69 (5), 809–822.

Goldberg, A.V., Molik, S., Tsaousis, A.D., Neumann, K., Kuhnke, G., Delbac, F., Vivares, C.P., Hirt, R.P., Lill, R. & Embley, T.M. (2008) Localization and functionality of microsporidian iron–sulphur cluster assembly proteins. *Nature.* 452, 624–628.

Gouy, M., Guindon, S. & Gascuel, O. (2010) SeaView version 4: A multiplatform graphical user interface for sequence alignment and phylogenetic tree building. *Molecular Biology and Evolution*. 27 (2), 221–224.

Gray, M.W., Lang, B.F. & Burger, G. (2004) Mitochondria of protists. *Annual Review of Genetics*. 38, 477–524.

Griffin, E.E., Graumann, J. & Chan, D.C. (2005) The WD40 protein Caf4p is a component of the mitochondrial fission machinery and recruits Dnm1p to mitochondria. *The Journal of Cell Biology*. 170 (2), 237–248.

Grigoriev, I.V., Nikitin, R., Haridas, S., Kuo, A., Ohm, R., Otillar, R., *et al.* (2014) MycoCosm portal: gearing up for 1000 fungal genomes. *Nucleic Acids Research.* 42, D699–704.

Guindon, S. & Gascuel, O. (2003) A simple, fast, and accurate algorithm to estimate large phylogenies by maximum likelihood. *Systematic Biology*. 52 (5), 696–704.

Haag, K.L., James, T.Y., Pombert, J.-F., Larsson, R., Schaer, T.M.M., Refardt, D. & Ebert, D. (2014) Evolution of a morphological novelty occurred before genome compaction in a lineage of extreme parasites. *Proceedings of the National Academy of Sciences*. 111(43), 15480-15485.

Hacker, C., Howell, M., Bhella, D. & Lucocq, J. (2013) Strategies for Maximizing ATP Supply in the Microsporidian *E. cuniculi:* Direct Binding of Mitochondria to the Parasitophorous Vacuole and Clustering of the Mitochondrial Porin VDAC. *Cellular Microbiology*. 16(4), 565-579.

Hackstein, J., Baker, S., van Hellemond, J. & Tielens, A. (2008) 'Hydrogenosomes and Mitosomes: Mitochondria of Anaerobic Eukaryotes', in Jan Tachezy (ed.) *Microbiology Monographs*. [Online]. Springer Berlin / Heidelberg. pp. 147–162.

Haferkamp, I., Schmitz-Esser, S., Wagner, M., Neigel, N., Horn, M. & Neuhaus, H.E. (2006) Tapping the nucleotide pool of the host: novel nucleotide carrier proteins of *Protochlamydia amoebophila*. *Molecular Microbiology*. 60 (6), 1534–1545.

Hakkaart, G.A.J., Dassa, E.P., Jacobs, H.T. & Rustin, P. (2006) Allotopic expression of a mitochondrial alternative oxidase confers cyanide resistance to human cell respiration. *EMBO Reports*. 7 (3), 341–345.

Hamilton, V., Singha, U.K., Smith, J.T., Weems, E. & Chaudhuri, M. (2014) Trypanosome alternative oxidase possesses both an N-terminal and internal mitochondrial targeting signal. *Eukaryotic Cell*. 13 (4), 539–547.

Hammermeister, M., Schödel, K. & Westermann, B. (2010) Mdm36 is a mitochondrial fission-promoting protein in *Saccharomyces cerevisiae. Molecular Biology of the Cell*. 21 (14), 2443–2452.

Harper, C.B., Popoff, M.R., McCluskey, A., Robinson, P.J. & Meunier, F.A. (2013)

Targeting membrane trafficking in infection prophylaxis: dynamin inhibitors. *Trends in Cell Biology*. 23 (2), 90–101.

Hatefi, Y. (1985) The mitochondrial electron transport and oxidative phosphorylation system. *Annual Review of Biochemistry*. 54 (1), 1015–1069.

Heinz, E. & Lithgow, T. (2012) Back to basics: A revealing secondary reduction of the mitochondrial protein import pathway in diverse intracellular parasites. *Biochimica et Biophysica Acta (BBA)-Molecular Cell Research, 1833(2), 295-303.*

Heinz, E., Hacker, C., Dean, P., Mifsud, J., Goldberg, A.V., Williams, T.A., Nakjang, S., Gregory, A., Hirt, R.P., Lucocq, J.M., Kunji, E.R.S. & Embley, T.M. (2014) Plasma membrane-located purine nucleotide transport proteins are key components for host exploitation by microsporidian intracellular parasites*. PLoS Pathogens*, *10* (12), e1004547.

Heinz, E., Williams, T.A., Nakjang, S., Noël, C.J., Swan, D.C., Goldberg, A.V., Harris, S.R., Weinmaier, T., Markert, S., Becher, D., Bernhardt, J., Dagan, T., Hacker, C., Lucocq, J.M., Schweder, T., Rattei, T., Hall, N., Hirt, R.P. & Embley, T.M. (2012) The Genome of the Obligate Intracellular Parasite *Trachipleistophora hominis*: New Insights into Microsporidian Genome Dynamics and Reductive Evolution. *PloS Pathogens.* 8 (10), e1002979.

Henriquez, F.L., Richards, T.A., Roberts, F., McLeod, R. & Roberts, C.W. (2005) The unusual mitochondrial compartment of *Cryptosporidium parvum*. *Trends in Parasitology*. 21 (2), 68–74.

Hewitt, V., Lithgow, T. & Waller, R.F. (2014) 'Modifications and Innovations in the Evolution of Mitochondrial Protein Import Pathways', in *Endosymbiosis*. [Online]. Vienna: Springer Vienna. pp. 19–35.

Heymann, J.A.W. & Hinshaw, J.E. (2009) Dynamins at a glance. *Journal of Cell Science*. 122 (19), 3427–3431.

Hjort, K., Goldberg, A.V., Tsaousis, A.D., Hirt, R.P. & Embley, T.M. (2010) Diversity and reductive evolution of mitochondria among microbial eukaryotes. *Philosophical Transactions of the Royal Society B: Biological Sciences*. 365 (1541), 713–727.

Hoepfner, D., van den Berg, M., Philippsen, P., Tabak, H.F., and Hettema, E.H. (2001) A role for Vps1p, actin, and the Myo2p motor in peroxisome abundance and inheritance in *Saccharomyces cerevisiae*. *The Journal of Cell Biology* 155: 979–990.

Hollister, W.S., Canning, E.U., Weidner, E., Field, A.S., Kench, J. & Marriott, D.J. (1996) Development and ultrastructure of *Trachipleistophora hominis* n.g., n.sp. after in vitro isolation from an AIDS patient and inoculation into athymic mice. *Parasitology*. 112 (1), 143–154.

Hong, Z., Bednarek, S.Y., Blumwald, E., Hwang, I., Jurgens, G., Menzel, D., Osteryoung, K.W., Raikhel, N.V., Shinozaki, K., Tsutsumi, N. & Verma, D.P.S. (2003) A unified nomenclature for Arabidopsis dynamin-related large GTPases based on homology and possible functions. *Plant Molecular Biology*. 53 (3), 261–265.

Hrdý, I., Tachezy, J. & Müller, M. (2008) 'Hydrogenosomes and Mitosomes: Mitochondria of Anaerobic Eukaryotes', in Jan Tachezy (ed.) *Microbiology Monographs*. [Online]. Springer Berlin / Heidelberg. pp. 113–145.

Hunter, P.R. (2000) Waterborne outbreak of microsporidiosis. *The Journal of Infectious Diseases*. 182 (1), 380–381.

Huson, D. H., & Scornavacca, C. (2012). Dendroscope 3: an interactive tool for rooted phylogenetic trees and networks. *Systematic Biology*. sys062.

Ingerman, E., Perkins, E.M., Marino, M., Mears, J.A., McCaffery, J.M., Hinshaw, J.E. & Nunnari, J. (2005) Dnm1 forms spirals that are structurally tailored to fit mitochondria. *The Journal of Cell Biology*. 170 (7), 1021–1027.

Izquierdo, F., Castro Hermida, J.A., Fenoy, S., Mezo, M., González-Warleta, M. & Aguila, C.D. (2011) Detection of microsporidia in drinking water, wastewater and recreational rivers. *Water Research*. 45 (16), 4837–4843.

Jagow, G. & Klingenberg, M. (1970) Pathways of hydrogen in mitochondria of *Saccharomyces carlsbergensis*. *European Journal of Biochemistry*. 12(3), 583-592.

James, T.Y., Pelin, A., Bonen, L., Ahrendt, S., Sain, D., Corradi, N. & Stajich, J.E. (2013) Shared Signatures of Parasitism and Phylogenomics Unite *Cryptomycota* and Microsporidia. *Current Biology*. 23 (16), 1548–1553.

Janssen, M.J.F.W., van Voorst, F., Ploeger, G.E.J., Larsen, P.M., Larsen, M.R., de Kroon, A.I.P.M. & de Kruijff, B. (2002) Photolabeling Identifies an Interaction between Phosphatidylcholine and Glycerol-3-phosphate Dehydrogenase (Gut2p) in Yeast Mitochondria †. *Biochemistry*. 41 (18), 5702–5711.

Jaspersen, S.L. (2006) The Sad1-UNC-84 homology domain in Mps3 interacts with Mps2 to connect the spindle pole body with the nuclear envelope. *The Journal of Cell Biology*. 174 (5), 665–675.

Jaspersen, S.L. & Winey, M. (2004) The budding yeast spindle pole body: structure, duplication, and function. *Annual Review of Cell and Developmental Biology*. 20, 1–28.

Jaspersen, S.L., Giddings, T.H. & Winey, M. (2002) Mps3p is a novel component of the yeast spindle pole body that interacts with the yeast centrin homologue Cdc31p. *The Journal of Cell Biology*. 159 (6), 945–956.

Jedrzejewski, S., Graczyk, T.K., Slodkowicz-Kowalska, A., Tamang, L. & Majewska, A.C. (2007) Quantitative assessment of contamination of fresh food produce of various retail types by human-virulent microsporidian spores. *Applied and Environmental Microbiology*. 73 (12), 4071–4073.

John, P. & Whatley, F.R. (1975) *Paracoccus denitrificans* and the evolutionary origin of the mitochondrion. *Nature*. 254, 495–498.

Jones, P., Binns, D., Chang, H.-Y., Fraser, M., Li, W., McAnulla, C., McWilliam, H., Maslen, J., Mitchell, A., Nuka, G., Pesseat, S., Quinn, A.F., Sangrador-Vegas, A., Scheremetjew, M., Yong, S.-Y., Lopez, R. & Hunter, S. (2014) InterProScan 5:

genome-scale protein function classification. *Bioinformatics (Oxford, England)*. 30 (9), 1236–1240.

Joseph-Horne, T., Hollomon, D.W. & Wood, P.M. (2001) Fungal respiration: a fusion of standard and alternative components. *Biochimica et Biophysica Acta*. 1504 (2), 179-195.

Juárez, O., Guerra, G., Martínez, F. & Pardo, J.P. (2004) The mitochondrial respiratory chain of *Ustilago maydis*. *Biochimica et Biophysica Acta*. 1658 (3), 244–251.

Kageyama, Y., Zhang, Z. & Sesaki, H. (2011) Mitochondrial division: molecular machinery and physiological functions. *Current Opinion in Cell Biology*. 23 (4), 427–434.

Kampinga, H.H. & Craig, E.A. (2010) The HSP70 chaperone machinery: J proteins as drivers of functional specificity. *Nature Reviews Molecular Cell Biology*. 11 (8), 579–592.

Kanehisa, M., Goto, S., Sato, Y., Kawashima, M., Furumichi, M. & Tanabe, M. (2014) Data, information, knowledge and principle: back to metabolism in KEGG. *Nucleic Acids Research*. 42 (Database issue), D199–205.

Kang, B.-H., Busse, J.S. & Bednarek, S.Y. (2003) Members of the *Arabidopsis* dynamin-like gene family, ADL1, are essential for plant cytokinesis and polarized cell growth. *The Plant Cell*. 15 (4), 899–913.

Katinka, M.D., Duprat, S., Cornillot, E., Méténier, G., Thomarat, F., Prensier, G., Barbe, V., Peyretaillade, E., Brottier, P., Wincker, P., Delbac, F., El Alaoui, H., Peyret, P., Saurin, W., Gouy, M., Weissenbach, J., Vivarès, C.P. (2001) Genome sequence and gene compaction of the eukaryote parasite *Encephalitozoon cuniculi. Nature.* 414 (6862), 450–453.

Keeling, P.J. & Corradi, N. (2011) Shrink it or lose it: balancing loss of function with shrinking genomes in the microsporidia. *Virulence*. 2 (1), 67–70.

Keeling, P.J. & Fast, N.M. (2002) Microsporidia: Biology and Evolution of Highly Reduced Intracellular Parasites. *Annual Review of Microbiology*. 56, 93–116.

Keeling, P.J., Corradi, N., Morrison, H.G., Haag, K.L., Ebert, D., Weiss, L.M., Akiyoshi, D.E. & Tzipori, S. (2010) The Reduced Genome of the Parasitic Microsporidian *Enterocytozoon bieneusi* Lacks Genes for Core Carbon Metabolism. *Genome Biology and Evolution*. 2 (0), 304–309.

Keithly, J.S., Langreth, S.G., Buttle, K.F. & Mannella, C.A. (2005) Electron tomographic and ultrastructural analysis of the *Cryptosporidium parvum* relict mitochondrion, its associated membranes, and organelles*. Journal of Eukaryotic Microbiology.* 52(2), 132-140.

Kelley, L.A., Mezulis, S., Yates, C.M., Wass, M.N. & Sternberg, M.J.E. (2015) The Phyre2 web portal for protein modeling, prediction and analysis. *Nature Protocols*. 10 (6), 845–858.

Kent, M.L., Harper, C. & Wolf, J.C. (2012) Documented and Potential Research

Impacts of Subclinical Diseases in Zebrafish. *ILAR Journal*. 53 (2), 126–134.

Kent, M.L., Shaw, R.W. & Sanders, J.L. (2014) 'Microsporidia in Fish', in *Microsporidia*. Pathogens of Opportunity. [Online]. Chichester, UK: John Wiley & Sons, Inc. pp. 493–520.

Kirkeby, S., and Thomsen, C.E. (2005) Quantitative immunohistochemistry of fluorescence labelled probes using low-cost software. Journal of Immunological Methods 301: 102–113.

Kilmartin, J.V. (2014) Lessons from yeast: the spindle pole body and the centrosome. *Philosophical Transactions of the Royal Society of London B: Biological Sciences*. 369 (1650), 20130456.

Klingenberg, M. (2008) The ADP and ATP transport in mitochondria and its carrier. *Biochimica et Biophysica Acta - Biomembranes*. 1778 (10), 1978–2021.

Koirala, S., Bui, H.T., Shaw, J.M. (2010) Molecular architecture of a dynamin adaptor: implications for assembly of mitochondrial fission complexes. *The Journal of Cell Biology*. 191 (6), 1127–1139.

Krogh, A., Larsson, B., Heijne, von, G. & Sonnhammer, E.L. (2001) Predicting transmembrane protein topology with a hidden Markov model: application to complete genomes. *Journal of Molecular Biology*. 305 (3), 567–580.

Kumar, A.M. & Söll, D. (1992) *Arabidopsis* alternative oxidase sustains *Escherichia coli* respiration. *Proceedings of the National Academy of Sciences of the United States of America*. 89 (22), 10842–10846.

Kuravi, K., Nagotu, S., Krikken, A.M., Sjollema, K., Deckers, M., Erdmann, R., *et al.* (2006) Dynamin-related proteins Vps1p and Dnm1p control peroxisome abundance in *Saccharomyces cerevisiae*. *Journal of Cell Science.* 119, 3994–4001.

Kuroiwa, T. (2010) Mechanisms of organelle division and inheritance and their implications regarding the origin of eukaryotic cells. *Proceedings of the Japan Academy, Series B*. 86 (5), 455–471.

Künzel, F. & Joachim, A. (2009) Encephalitozoonosis in rabbits. *Parasitology research*. 106 (2), 299–309.

Lackner, L.L., Ping, H., Graef, M., Murley, A. & Nunnari, J. (2013) Endoplasmic reticulum-associated mitochondria-cortex tether functions in the distribution and inheritance of mitochondria. *Proceedings of the National Academy of Sciences*. 110 (6), E458–E467.

Lafranchi-Tristem, N.J., Curry, A., Cheney, S.A. & Canning, E.U. (2001) Growth of *Trachipleistophora hominis* (Microsporidia: Pleistophoridae) in C2,C12 mouse myoblast cells and response to treatment with albendazole. *Folia Parasitologica*. 48 (3), 192–200.

Lambeir, A.M., Loiseau, A.M., Kuntz, D.A., Vellieux, F.M., Michels, P.A. & Opperdoes, F.R. (1991) The cytosolic and glycosomal glyceraldehyde-3-phosphate dehydrogenase from *Trypanosoma brucei*. Kinetic properties and

comparison with homologous enzymes. *European Journal of Biochemistry*. 198 (2), 429–435.

Lane, N. & Martin, W. (2010) The energetics of genome complexity. *Nature*. 467 (7318), 929–934.

Larsson, C., Påhlman, I.-L., Ansell, R., Rigoulet, M., Adler, L. & Gustafsson, L. (1998) The importance of the glycerol 3-phosphate shuttle during aerobic growth of *Saccharomyces cerevisiae*. *Yeast*. 14 (4), 347–357.

Lartillot, N., Brinkmann, H. & Philippe, H. (2007) Suppression of long-branch attraction artefacts in the animal phylogeny using a site-heterogeneous model. *BMC Evolutionary Biology*. 7, (Suppl 1), S4.

Lartillot, N., Lepage, T. & Blanquart, S. (2009) PhyloBayes 3: a Bayesian software package for phylogenetic reconstruction and molecular dating. *Bioinformatics (Oxford, England)*. 25 (17), 2286–2288.

Leger, M.M., Petrů, M., Zarsky, V., Eme, L., Vlček, Č., Harding, T., Lang, F.B., Elias, M., Dolezal, P., Roger, A.J. (2015) An ancestral bacterial division system is widespread in eukaryotic mitochondria. *Proceedings of the National Academy of Sciences.* 112 (33), 10239–10246.

Leidel, S. & Gönczy, P. (2003) SAS-4 Is Essential for Centrosome Duplication in *C. elegans* and Is Recruited to Daughter Centrioles Once per Cell Cycle. *Developmental Cell*. 4 (3), 431–439.

Leon-Avila, G. (2004) Mitosomes of *Entamoeba histolytica* are abundant mitochondrion-related remnant organelles that lack a detectable organellar genome. *Microbiology*. 150 (5), 1245–1250.

Li, P., Shao, Y., Jin, H. & Yu, H.-G. (2015) Ndj1, a telomere-associated protein, regulates centrosome separation in budding yeast meiosis. *The Journal of Cell Biology*. 209 (2), 247–259.

Li, T., Zheng, F., Cheung, M., Wang, F. & Fu, C. (2015) Fission yeast mitochondria are distributed by dynamic microtubules in a motor-independent manner. *Scientific Reports*. 5.

Lill, R. (2009) Function and biogenesis of iron–sulphur proteins. *Nature.* 460 (7257), 831–838.

Lill, R. & Mühlenhoff, U. (2006) Iron-sulfur protein biogenesis in eukaryotes: components and mechanisms. *Annual Review of Cell and Developmental Biology*. *22*, 457-486.

Lill, R. & Mühlenhoff, U. (2005) Iron–sulfur-protein biogenesis in eukaryotes. *Trends in biochemical sciences*. 30 (3), 133–141.

Lill, R., Hoffmann, B., Molik, S., Pierik, A.J., Rietzschel, N., Stehling, O., Uzarska, M.A., Webert, H., Wilbrecht, C. & Mühlenhoff, U. (2012) The role of mitochondria in cellular iron–sulfur protein biogenesis and iron metabolism. *Biochimica et Biophysica Acta (BBA) - Molecular Cell Research*. 1823 (9), 1491–1508.

Logan, D.C., Scott, I. & Tobin, A.K. (2004) ADL2a, like ADL2b, is involved in the control of higher plant mitochondrial morphology. *Journal of Experimental Botany*. 55 (397), 783–785.

Lom, Jirí & Dyková, I. (2005) Microsporidian xenomas in fish seen in wider perspective. *Folia Parasitologica*. 52, 69–81.

Lom, Jiří & Nilsen, F. (2003) Fish microsporidia: fine structural diversity and phylogeny. *International Journal for Parasitology*. 33 (2), 107–127.

Lu, B., Poirier, C., Gaspar, T., Gratzke, C., Harrison, W., Busija, D., Matzuk, M.M., Andersson, K.-E., Overbeek, P.A. & Bishop, C.E. (2008) A mutation in the inner mitochondrial membrane peptidase 2-like gene (Immp2l) affects mitochondrial function and impairs fertility in mice. *Biology of Reproduction*. 78 (4), 601–610.

Lucarotti, C.J. & Andreadis, T.G. (1995) Reproductive strategies and adaptations for survival among obligatory microsporidian and fungal parasites of mosquitoes: a comparative analysis of *Amblyospora* and *Coelomomyces*. *Journal of the American Mosquito Control Association*. 11 (1), 111–121.

Lüders, J. & Stearns, T. (2007) Microtubule-organizing centres: a re-evaluation. *Nature Reviews Molecular Cell Biology*. 8 (2), 161–167.

Magnani, T., Soriani, F.M., Martins, V. de P., Policarpo, A.C. de F., Sorgi, C.A., Faccioli, L.H., Curti, C. & Uyemura, S.A. (2009) Silencing of mitochondrial alternative oxidase gene of *Aspergillus fumigatus* enhances reactive oxygen species production and killing of the fungus by macrophages. *Journal of Bioenergetics and Biomembranes*. *40*(6), 631-636.

Mai, Z., Ghosh, S., Frisardi, M., Rosenthal, B., Rogers, R. & Samuelson, J. (1999) Hsp60 is targeted to a cryptic mitochondrion-derived organelle (‘crypton’) in the microaerophilic protozoan parasite *Entamoeba histolytica*. *Molecular and Cellular Biology*. 19 (3), 2198–2205.

Maralikova, B., Ali, V., Nakada-Tsukui, K., Nozaki, T., van der Giezen, M., Henze, K. & Tovar, J. (2010) Bacterial-type oxygen detoxification and iron-sulfur cluster assembly in amoebal relict mitochondria. *Cellular Microbiology*. 12 (3), 331–342.

Martins, V.P., Dinamarco, T.M., Soriani, F.M., Tudella, V.G., Oliveira, S.C., Goldman, G.H., Curti, C. & Uyemura, S.A. (2011) Involvement of an alternative oxidase in oxidative stress and mycelium-to-yeast differentiation in *Paracoccidioides brasiliensis*. *Eukaryotic Cell*. 10 (2), 237–248.

Mayor, S. & Pagano, R.E. (2007) Pathways of clathrin-independent endocytosis. *Nature Reviews Molecular cell biology*. 8 (8), 603–612.

McDonald, A.E. (2008) Alternative oxidase: an inter-kingdom perspective on the function and regulation of this broadly distributed‘cyanide-resistant’terminal oxidase. *Functional Plant Biology*. 35 (7), 535–552.

McDonald, A.E. & Vanlerberghe, G.C. (2006) Origins, evolutionary history, and taxonomic distribution of alternative oxidase and plastoquinol terminal oxidase. *Comparative Biochemistry and Physiology. Part D, Genomics & Proteomics*. 1 (3), 357–364.

McDonald, A.E., Amirsadeghi, S. & Vanlerberghe, G.C. (2003) Prokaryotic orthologues of mitochondrial alternative oxidase and plastid terminal oxidase. *Plant Molecular Biology*. 53 (6), 865–876.

McDonald, A.E., Vanlerberghe, G.C. & Staples, J.F. (2009) Alternative oxidase in animals: unique characteristics and taxonomic distribution. *The Journal of Experimental Biology*. 212 (16), 2627–2634.

Mears, J.A., Lackner, L.L., Fang, S., Ingerman, E., Nunnari, J. & Hinshaw, J.E. (2010) Conformational changes in Dnm1 support a contractile mechanism for mitochondrial fission. *Nature Publishing Group*. 18 (1), 20–26.

Mears, J.A., Ray, P. & Hinshaw, J.E. (2007) A Corkscrew Model for Dynamin Constriction. *Structure*. 15 (10), 1190–1202.

Meganathan, R. (2001) Ubiquinone biosynthesis in microorganisms. *FEMS Microbiology Letters*. 203 (2), 131–139.

Mi-ichi, F., Miyamoto, T., Takao, S., Jeelani, G., Hashimoto, T., Hara, H., Nozaki, T. & Yoshida, H. (2015) *Entamoeba* mitosomes play an important role in encystation by association with cholesteryl sulfate synthesis. *Proceedings of the National Academy of Sciences*. 112 (22), E2884–90.

Mi-ichi, F., Yousuf, M.A., Nakada-Tsukui, K. & Nozaki, T. (2009) Mitosomes in *Entamoeba histolytica* contain a sulfate activation pathway. *Proceedings of the National Academy of Sciences of the United States of America*. 106 (51), 21731-21736.

Millenaar, F.F. & Lambers, H. (2003) The alternative oxidase: in vivo regulation and function. *Plant Biology*. *5* (1), 2-15.

Mishra, P. & Chan, D.C. (2014) Mitochondrial dynamics and inheritance during cell division, development and disease. *Nature Reviews Molecular Cell Biology*. 15 (10), 634–646.

Mogi, T. & Kita, K. (2010) Diversity in mitochondrial metabolic pathways in parasitic protists *Plasmodium* and *Cryptosporidium*. *Parasitology International*. 59 (3), 305–312.

Moore, A.L. & Albury, M.S. (2008) Further insights into the structure of the alternative oxidase: from plants to parasites. *Biochemical Society Transactions*. 36 (5), 1022-1026.

Moore, A.L., Shiba, T., Young, L., Harada, S., Kita, K. & Ito, K. (2013) Unraveling the heater: new insights into the structure of the alternative oxidase. *Annual Review of Plant Biology*. 64, 637–663.

Morgan, G.W., Goulding, D. & Field, M.C. (2004) The single dynamin-like protein of Trypanosoma brucei regulates mitochondrial division and is not required for endocytosis. *The Journal of Biological Chemistry*. 279 (11), 10692–10701.

Mossmann, D., Meisinger, C. & Vögtle, F.N. (2012) Processing of mitochondrial presequences. *Biochimica et Biophysica Acta (BBA) - Gene Regulatory Mechanisms*. 1819 (9-10), 1098–1106.

Mozdy, A.D., McCaffery, J.M. & Shaw, J.M. (2000) Dnm1p GTPase-mediated mitochondrial fission is a multi-step process requiring the novel integral membrane component Fis1p. *The Journal of Cell Biology*. 151 (2), 367–380.

Mravec, J., Petrášek, J., Li, N., Boeren, S., Karlova, R., Kitakura, S., Pařezová, M., Naramoto, S., Nodzyński, T., Dhonukshe, P., Bednarek, S.Y., Zažímalová, E., de Vries, S. & Friml, J. (2011) Cell Plate Restricted Association of DRP1A and PIN Proteins Is Required for Cell Polarity Establishment in Arabidopsis. *Current Biology*. 21 (12), 1055–1060.

Muller, E.G.D., Snydsman, B.E., Novik, I., Hailey, D.W., Gestaut, D.R., Niemann, C.A., O'Toole, E.T., Giddings, T.H., Sundin, B.A. & Davis, T.N. (2005) The organization of the core proteins of the yeast spindle pole body. *Molecular Biology of the Cell*. 16 (7), 3341–3352.

Murata, T., Tanahashi, T., Nishiyama, T., Yamaguchi, K. & Hasebe, M. (2007) How do Plants Organize Microtubules Without a Centrosome? *Journal of Integrative Plant Biology*. 49 (8), 1154–1163.

Müller, M., Mentel, M., van Hellemond, J.J., Henze, K., Woehle, C., Gould, S.B., Yu, R.-Y., van der Giezen, M., Tielens, A.G.M. & Martin, W.F. (2012) Biochemistry and evolution of anaerobic energy metabolism in eukaryotes. *Microbiology and Molecular Biology Reviews*. 76 (2), 444–495.

Nakjang, S., Williams, T.A., Heinz, E., Watson, A.K., Foster, P.G., Sendra, K.M., Heaps, S.E., Hirt, R.P. & Embley, T.M. (2013) Reduction and expansion in microsporidian genome evolution: new insights from comparative genomics. *Genome Biology and Evolution*. *5* (12), 2285-2303.

Nargang, F.E., Adames, K., Rüb, C., Cheung, S., Easton, N., Nargang, C.E. & Chae, M.S. (2012) Identification of genes required for alternative oxidase production in the *Neurospora crassa* gene knockout library. *G3: Genes*| *Genomes*| *Genetics.* 2 (11), 1345–1356.

Netz, D.J.A., Stith, C.M., Stümpfig, M., Köpf, G., Vogel, D., Genau, H.M., Stodola, J.L., Lill, R., Burgers, P.M.J. & Pierik, A.J. (2012) Eukaryotic DNA polymerases require an iron-sulfur cluster for the formation of active complexes. *Nature Chemical Biology*. 8 (1), 125–132.

Neupert, W. & Herrmann, J.M. (2007) Translocation of proteins into mitochondria. *Annual Review of Biochemistry*. 76, 723–749.

Nishikawa, S.-I., Terazawa, Y., Nakayama, T., Hirata, A., Makio, T., and Endo, T. (2003) Nep98p is a component of the yeast spindle pole body and essential for nuclear division and fusion. *Journal of Biological Chemistry*. 278, 9938–9943.

Notredame, C., Higgins, D.G. & Heringa, J. (2000) T-Coffee: A novel method for fast and accurate multiple sequence alignment. *Journal of Molecular Biology*. 302 (1), 205–217.

Nývltová, E., Sutak, R., Harant, K., Sedinová, M., Hrdý, I., Pačes, J., Vlček, Č. & Tachezy, J. (2013) NIF-type iron-sulfur cluster assembly system is duplicated and distributed in the mitochondria and cytosol of *Mastigamoeba balamuthi*. *Proceedings of the National Academy of Sciences*. 110 (18), 7371–7376.

Ogbadoyi, E.O., Robinson, D.R. & Gull, K. (2003) A High-Order Trans-Membrane Structural Linkage Is Responsible for Mitochondrial Genome Positioning and Segregation by Flagellar Basal Bodies in Trypanosomes. *Molecular Biology of the Cell*. 14, 1769–1779.

Okamoto, N., Spurck, T.P., Goodman, C.D. & McFadden, G.I. (2009) Apicoplast and mitochondrion in gametocytogenesis of *Plasmodium falciparum*. *Eukaryotic Cell*. 8 (1), 128–132.

Opalińska, M. & Meisinger, C. (2015) Metabolic control via the mitochondrial protein import machinery. *Current Opinion in Cell Biology*. 33, 42–48.

Opperdoes, F.R. (1987) Compartmentation of carbohydrate metabolism in trypanosomes. *Annual Reviews in Microbiology*. *41*(1). 127-151.

Otsuga, D., Keegan, B.R., Brisch, E., Thatcher, J.W., Hermann, G.J., Bleazard, W., and Shaw, J.M. (1998) The dynamin-related GTPase, Dnm1p, controls mitochondrial morphology in yeast. *The Journal of Cell Biology.* 143, 333–349.

Otera, H., Wang, C., Cleland, M.M., Setoguchi, K., Yokota, S., Youle, R.J. & Mihara, K. (2010) Mff is an essential factor for mitochondrial recruitment of Drp1 during mitochondrial fission in mammalian cells. *The Journal of Cell Biology*. 191 (6), 1141–1158.

Palmer, C.S., Elgass, K.D., Parton, R.G., Osellame, L.D., Stojanovski, D. & Ryan, M.T. (2013) Adaptor Proteins MiD49 and MiD51 Can Act Independently of Mff and Fis1 in Drp1 Recruitment and Are Specific for Mitochondrial Fission. *Journal of Biological Chemistry*. 288 (38), 27584–27593.

Palmer, C.S., Osellame, L.D., Laine, D., Koutsopoulos, O.S., Frazier, A.E. & Ryan, M.T. (2011) MiD49 and MiD51, new components of the mitochondrial fission machinery. *EMBO reports*. 12 (6), 565–573.

Pan, G., Xu, J., Li, T., Xia, Q., Liu, S.-L., Zhang, G., Li, S., Li, C., Liu, H., Yang, L., Liu, T., Zhang, X., Wu, Z., Fan, W., Dang, X., Xiang, H., Tao, M., Li, Y., Hu, J., et al. (2013) Comparative genomics of parasitic silkworm microsporidia reveal an association between genome expansion and host adaptation. *BMC Genomics*. 14 (1), 186.

Parisot, N., Pelin, A., Gasc, C., Polonais, V., Belkorchia, A., Panek, J., Alaoui, El, H., Biron, D.G., Brasset, É., Vaury, C., Peyret, P., Corradi, N., Peyretaillade, E. & Lerat, E. (2014) Microsporidian genomes harbor a diverse array of transposable elements that demonstrate an ancestry of horizontal exchange with metazoans. *Genome Biology and Evolution*. 6 (9), 2289–2300.

Peraza Reyes, L., Crider, D.G. & Pon, L.A. (2010) Mitochondrial manoeuvres: Latest insights and hypotheses on mitochondrial partitioning during mitosis in *Saccharomyces cerevisiae*. *BioEssays*. 32 (12), 1040–1049.

Peyretaillade, E., Parisot, N., Polonais, V., Terrat, S., Denonfoux, J., Dugat-Bony, E., Wawrzyniak, I., Biderre-Petit, C., Mahul, A., Rimour, S., Gonçalves, O., Bornes, S., Delbac, F., Chebance, B., Duprat, S., Samson, G., Katinka, M., Weissenbach, J., Wincker, P., et al. (2012) Annotation of microsporidian genomes using transcriptional signals. *Nature Communications*. 3, 1137.

Pombert, J.-F., Haag, K.L., Beidas, S., Ebert, D. & Keeling, P.J. (2015) The Ordospora colligata Genome: Evolution of Extreme Reduction in Microsporidia and Host-To-Parasite Horizontal Gene Transfer. *mBio*. 6 (1), e02400–14.

Pombert, J.-F., Selman, M., Burki, F., Bardell, F.T., Farinelli, L., Solter, L.F., Whitman, D.W., Weiss, L.M., Corradi, N. & Keeling, P.J. (2012) Gain and loss of multiple functionally related, horizontally transferred genes in the reduced genomes of two microsporidian parasites. *Proceedings of the National Academy of Sciences of the United States of America*. 109 (31), 12638–12643.

QIAGEN (2003) The QIAexpressionist™. *A handbook for high-level expression and purification of 6xHis-tagged proteins*. [online]. Available from: https://www.qiagen.com/gb/resources/resourcedetail?id=79ca2f7d-42fe-4d62-8676-4cfa948c9435&lang=en . (Accessed 10 January 2012).

Quang, L.S., Gascuel, O. & Lartillot, N. (2008) Empirical profile mixture models for phylogenetic reconstruction. *Bioinformatics (Oxford, England)*. 24 (20), 2317–2323.

Rambaut, A. (2007). FigTree, a graphical viewer of phylogenetic trees. *See http://tree. bio. ed. ac. uk/software/figtree*.

Rambold, A.S. & Lippincott-Schwartz, J. (2011) SevERing Mitochondria. *Science*. 334 (6053), 186–187.

Ramsay, J.M., Watral, V., Schreck, C.B. & Kent, M.L. (2009) *Pseudoloma neurophilia* infections in zebrafish *Danio rerio*: effects of stress on survival, growth, and reproduction. *Diseases of Aquatic Organisms*. 88 (1), 69–84.

Regoes, A., Zourmpanou, D., León-Avila, G., van der Giezen, M., Tovar, J. & Hehl, A.B. (2005) Protein import, replication, and inheritance of a vestigial mitochondrion. *The Journal of biological Chemistry*. 280 (34), 30557–30563.

Roberts, C.W., Roberts, F., Henriquez, F.L., Akiyoshi, D., Samuel, B.U., Richards, T.A., Milhous, W., Kyle, D., McIntosh, L., Hill, G.C., Chaudhuri, M., Tzipori, S. & McLeod, R. (2004) Evidence for mitochondrial-derived alternative oxidase in the apicomplexan parasite *Cryptosporidium parvum*: a potential anti-microbial agent target. *International Journal for Parasitology*. 34 (3), 297–308.

Robinson, D.R. & Gull, K. (1991) Basal body movements as a mechanism for mitochondrial genome segregation in the trypanosome cell cycle. *Nature*. 352 (6337), 731–733.

Rodríguez-Ezpeleta, N. & Embley, T.M. (2012) The SAR11 Group of Alpha-Proteobacteria Is Not Related to the Origin of Mitochondria. *PLoS ONE*. 7 (1), e30520.

Rosenberg, J.A., Tomlin, G.C., McDonald, W.H., Snydsman, B.E., Muller, E.G., Yates, J.R., and Gould, K.L. (2006) Ppc89 links multiple proteins, including the septation initiation network, to the core of the fission yeast spindle-pole body. *Molecular Biology of the Cell.* 17 (9), 3793–3805.

Ruiz, O.H., Gonzalez, A., Almeida, A.J., Tamayo, D., Garcia, A.M., Restrepo, A. & McEwen, J.G. (2011) Alternative Oxidase Mediates Pathogen Resistance in

Paracoccidioides brasiliensis Infection. *PLOS Neglected Tropical Diseases*. 5 (10), e1353.

Sapir, A., Dillman, A.R., Connon, S.A., Grupe, B.M., Ingels, J., Mundo-Ocampo, M., Levin, L.A., Baldwin, J.G., Orphan, V.J. & Sternberg, P.W. (2014) Microsporidia-nematode associations in methane seeps reveal basal fungal parasitism in the deep sea. *Frontiers in Microbiology*. 5.

Saxton, W.M. & Hollenbeck, P.J. (2012) The axonal transport of mitochondria. *Journal of Cell Science*. 125 (9), 2095–2104.

Scanlon, M., Leitch, G.J., Visvesvara, G.S. & Shaw, A.P. (2004) Relationship between the host cell mitochondria and the parasitophorous vacuole in cells infected with *Encephalitozoon* microsporidia. *Journal of Eukaryotic Microbiology*. 51, 81–87.

Scheffler, I.E. (2002a) 'Metabolic Pathways Inside Mitochondria', in *Mitochondria*. [Online]. New York, USA: John Wiley & Sons, Inc. pp. 246–272.

Scheffler, I.E. (2002b) 'Mitochondrial Electron Transport and Oxidative Phosphorylation', in *Metabolic Pathways Inside Mitochondria*. [Online]. New York, USA: John Wiley & Sons, Inc. pp. 141–245.

Schilke, B., Williams, B., Knieszner, H., Pukszta, S., D'Silva, P., Craig, E.A. & Marszalek, J. (2006) Evolution of mitochondrial chaperones utilized in Fe-S cluster biogenesis. *Current Biology*. 16 (16), 1660–1665.

Schindelin, J., Arganda-Carreras, I., Frise, E., Kaynig, V., Longair, M., Pietzsch, T., Preibisch, S., Rueden, C., Saalfeld, S., Schmid, B., Tinevez, J.-Y., White, D.J., Hartenstein, V., Eliceiri, K., Tomancak, P. & Cardona, A. (2012) Fiji: an open-source platform for biological-image analysis. *Nature Methods*. 9 (7), 676–682.

Schrödinger, LLC (2010) *The PyMOL molecular graphics system, Version 1.7.4*. [online]. Available from:https://www.pymol.org (Accessed 20 June 2015)

Segal, M. & Bloom, K. (2001) Control of spindle polarity and orientation in *Saccharomyces cerevisiae*. *Trends in Cell Biology*. 11 (4), 160–166.

Sesaki, H., and Jensen, R.E. (1999) Division versus fusion: Dnm1p and Fzo1p antagonistically regulate mitochondrial shape. *The Journal of Cell Biology.* 147: 699–706.

Seybold, C. & Schiebel, E. (2013) Spindle pole bodies. *Current Biology*. 23 (19), R858–R860.

Sharma, S., Das, S., Joseph, J., Vemuganti, G.K. & Murthy, S. (2011) Microsporidial keratitis: need for increased awareness. *Survey of Ophthalmology*. 56 (1), 1–22.

Shen, W., Wei, Y., Dauk, M., Tan, Y., Taylor, D.C., Selvaraj, G. & Zou, J. (2006) Involvement of a glycerol-3-phosphate dehydrogenase in modulating the NADH/NAD+ ratio provides evidence of a mitochondrial glycerol-3-phosphate shuttle in *Arabidopsis*. *The Plant Cell*. 18 (2), 422–441.

Shiba, T., Kido, Y., Sakamoto, K., Inaoka, D.K., Tsuge, C., Tatsumi, R., Takahashi,

G., Balogun, E.O., Nara, T., Aoki, T., Honma, T., Tanaka, A., Inoue, M., Matsuoka, S., Saimoto, H., Moore, A.L., Harada, S. & Kita, K. (2013) Structure of the trypanosome cyanide-insensitive alternative oxidase. *Proceedings of the National Academy of Sciences*. 110 (12), 4580-4585.

Siedow, J.N. & Umbach, A.L. (2000) The mitochondrial cyanide-resistant oxidase: structural conservation amid regulatory diversity. *Biochimica et biophysica Acta*. 1459 (2), 432–439.

Sierra-Campos, E., Velázquez, I., Matuz-Mares, D., Villavicencio-Queijeiro, A. & Pardo, J.P. (2009) Functional properties of the *Ustilago maydis* alternative oxidase under oxidative stress conditions. *Mitochondrion*. 9 (2), 96–102.

Small, I., Peeters, N., Legeai, F. & Lurin, C. (2004) Predotar: A tool for rapidly screening proteomes for N-terminal targeting sequences. *Proteomics*. 4 (6), 1581–1590.

Sokolova, Y.Y., Paskerova, G.G., Rotari, Y.M., Nassonova, E.S. & Smirnov, A.V. (2014) Description of *Metchnikovella spiralis* sp. n. (Microsporidia: Metchnikovellidae), with notes on the ultrastructure of metchnikovellids. *Parasitology*. 1–15.

Sokolova, Y.Y., Paskerova, G.G., Rotari, Y.M., Nassonova, E.S. & Smirnov, A.V. (2013) Fine structure of *Metchnikovella incurvata* Caullery and Mesnil 1914 (microsporidia), a hyperparasite of gregarines *Polyrhabdina* sp. from the polychaete *Pygospio elegans*. *Parasitology*. 140, 855–867.

Sonnhammer, E.L., Heijne, von, G. & Krogh, A. (1998) A hidden Markov model for predicting transmembrane helices in protein sequences. *International Conference on Intelligent Systems for Molecular Biology*. 6, 175–182.

Stairs, C.W., Eme, L., Brown, M.W., Mutsaers, C., Susko, E., Dellaire, G., Soanes, D.M., van der Giezen, M. & Roger, A.J. (2014) A SUF Fe-S cluster biogenesis system in the mitochondrion-related organelles of the anaerobic protist *Pygsuia*. *Current Biology.* 24 (11), 1176–1186.

Stamatakis, A. (2014) RAxML Version 8: A tool for Phylogenetic Analysis and Post-Analysis of Large Phylogenies. *Bioinformatics (Oxford, England)*. 30 (9), 1312–1313.

Stamatakis, A., Ludwig, T. & Meier, H. (2005) RAxML-III: a fast program for maximum likelihood-based inference of large phylogenetic trees. *Bioinformatics (Oxford, England)*. 21 (4), 456–463.

Stechmann, A., Hamblin, K., Pérez-Brocal, V. & Gaston, D. (2008) Organelles in *Blastocystis* that blur the distinction between mitochondria and hydrogenosomes. *Current Biology*. 18 (8), 580–585.

Stentiford, G.D. & Dunn, A.M. (2014) 'Microsporidia in Aquatic Invertebrates', in *Microsporidia*. Pathogens of Opportunity. [Online]. Chichester, UK: John Wiley & Sons, Inc. pp. 579–604.

Stirnimann, C.U., Petsalaki, E., Russell, R.B. & Müller, C.W. (2010) WD40 proteins propel cellular networks. *Trends in Biochemical Sciences*. 35 (10), 565–574.

Szigyarto, C., Dessi, P., Smith, M.K., Knorpp, C., Harmey, M.A., Day, D.A., Glaser, E. & Whelan, J. (1998) A matrix-located processing peptidase of plant mitochondria. *Plant molecular Biology*. 36 (1), 171–181.

Szumowski, S.C. & Troemel, E.R. (2015) Microsporidia–host interactions. *Current Opinion in Microbiology*. 26, 10–16.

Škodová, I., Verner, Z., Bringaud, F., Fabian, P., Lukeš, J. & Horváth, A. (2013) Characterization of Two Mitochondrial Flavin Adenine Dinucleotide-Dependent Glycerol-3-Phosphate Dehydrogenases in *Trypanosoma brucei*. *Eukaryotic Cell*. 12 (12), 1664–1673.

Šmíd, O., Matusková, A., Harris, S.R., Kucera, T., Novotný, M., Horváthová, L., Hrdý, I., Kutejová, E., Hirt, R.P., Embley, T.M., Janata, J. & Tachezy, J. (2008) Reductive evolution of the mitochondrial processing peptidases of the unicellular parasites *Trichomonas vaginalis* and *Giardia intestinalis. PLoS Pathogens.* 4 (12), e1000243.

Tachezy, J. & Dolezal, P. (2011) The *Giardia* Mitosomes. *Giardia*. Springer Vienna. pp. 185–200.

Tachezy, J. & Šmíd, O. (2008a) 'Hydrogenosomes and Mitosomes: Mitochondria of Anaerobic Eukaryotes', in Jan Tachezy (ed.) *Microbiology Monographs*. [Online]. Springer Berlin / Heidelberg. pp. 201–230.

Tachezy, J. & Šmíd, O. (2008b) Mitosomes in parasitic protists. In *Hydrogenosomes and Mitosomes: Mitochondria of Anaerobic Eukaryotes*. Springer Berlin Heidelberg. pp. 201–230.

Takei, K., McPherson, P.S., Schmid, S.L. & Camilli, P.D. (1995) Tubular membrane invaginations coated by dynamin rings are induced by GTP-γS in nerve terminals. *Nature*. 374 (6518), 186–190.

Tanudji, M., Sjöling, S., Glaser, E. & Whelan, J. (1999a) Signals required for the import and processing of the alternative oxidase into mitochondria. *The Journal of biological Chemistry*. 274 (3), 1286–1293.

Tanudji, M., Sjöling, S., Glaser, E. & Whelan, J. (1999b) Signals required for the import and processing of the alternative oxidase into mitochondria. *The Journal of Biological Chemistry*. 274 (3), 1286–1293.

Teixeira, P.F. & Glaser, E. (2013) Processing peptidases in mitochondria and chloroplasts. *Biochimica et Biophysica Acta - Molecular Cell Research*. 1833 (2), 360–370.

Thomazella, D.P.T., Teixeira, P.J.P.L., Oliveira, H.C., Saviani, E.E., Rincones, J., Toni, I.M., Reis, O., Garcia, O., Meinhardt, L.W., Salgado, I. & Pereira, G.A.G. (2012) The hemibiotrophic cacao pathogen Moniliophthora perniciosa depends on a mitochondrial alternative oxidase for biotrophic development. *New Phytologist*. 194 (4), 1025–1034.

Tielens, A.G.M., Rotte, C., van Hellemond, J.J. & Martin, W. (2002) Mitochondria as we don't know them. *Trends in Biochemical Sciences*. 27 (11), 564–572.

Tieu, Q., Okreglak, V., Naylor, K. & Nunnari, J. (2002) The WD repeat protein, Mdv1p, functions as a molecular adaptor by interacting with Dnm1p and Fis1p during mitochondrial fission. *The Journal of Cell Biology*. 158 (3), 445–452.

Timmis, J.N., Ayliffe, M.A., Huang, C.Y. & Martin, W. (2004) Endosymbiotic gene transfer: organelle genomes forge eukaryotic chromosomes. *Nature Reviews Genetics*. 5 (2), 123–135.

Tjaden, J., Winkler, H.H., Schwöppe, C., Van Der Laan, M., Möhlmann, T. & Neuhaus, H.E. (1999) Two Nucleotide Transport Proteins in *Chlamydia trachomatis,* One for Net Nucleoside Triphosphate Uptake and the Other for Transport of Energy. *Journal of Bacteriology*. 181 (4), 1196–1202.

Touw, W. G., Baakman, C., Black, J., te Beek, T. A., Krieger, E., Joosten, R. P., & Vriend, G. (2015). A series of PDB-related databanks for everyday needs. *Nucleic Acids Research*. *43* (D1), D364-D368.

Tovar, J., Fischer, A. & Clark, C.G. (1999) The mitosome, a novel organelle related to mitochondria in the amitochondrial parasite *Entamoeba histolytica*. *Molecular Microbiology*. 32 (5), 1013–1021.

Tovar, J., León-Avila, G., Sánchez, L.B., Sutak, R., Tachezy, J., van der Giezen, M., Hernández, M., Müller, M. & Lucocq, J.M. (2003) Mitochondrial remnant organelles of *Giardia* function in iron-sulphur protein maturation*. Nature.* 426 (6963), 172–176.

Trentmann, O., Horn, M., van Scheltinga, A.C.T., Neuhaus, H.E. & Haferkamp, I. (2007) Enlightening energy parasitism by analysis of an ATP/ADP transporter from chlamydiae. *PLoS Biology*. 5 (9), e231.

Troemel, E.R. & Becnel, J.J. (2015) Genome analysis and polar tube firing dynamics of mosquito-infecting microsporidia. *Fungal Genetics and Biology*. 83, 41–44.

Tsaousis, A. D., Kunji, E. R., Goldberg, A. V., Lucocq, J. M., Hirt, R. P., & Embley, T. M. (2008). A novel route for ATP acquisition by the remnant mitochondria of *Encephalitozoon cuniculi*. *Nature*. *453* (7194), 553-556.

Umbach, A.L. & Siedow, J.N. (2000) The cyanide-resistant alternative oxidases from the fungi *Pichia stipitis* and *Neurospora crassa* are monomeric and lack regulatory features of the plant enzyme. *Archives of Biochemistry and Biophysics*. 378 (2), 234–245.

Undeen, A.H. & Vander Meer, R.K. (1999) Microsporidian intrasporal sugars and their role in germination. *Journal of Invertebrate Pathology*. 73 (3), 294–302.

US Department of Health and Human Services. National Institute of Allergy and Infectious Disease (2015) Biodefense and Emerging Infectious Diseases [online, accessed July 2015]. niaid.nih.gov/topics/biodefenserelated/biodefense/pages/cata.aspx

Van der Bliek, A.M. (1999) Functional diversity in the dynamin family. *Trends in Cell Biology*. 9 (3), 96–102.

Van Dooren, G.G., Reiff, S.B., Tomova, C., Meissner, M., Humbel, B.M. & Striepen,

B. (2009) A Novel Dynamin-Related Protein Has Been Recruited for Apicoplast Fission in *Toxoplasma gondii*. *Current Biology*. 19 (4), 267–276.

Vavra, J. (2005) "Polar vesicles" of microsporidia are mitochondrial remnants (‘mitosomes’)? *Folia Parasitologica*. 52 (1-2), 193–195.

Vavra, J., Horák, A., Modrý, D., Lukeš, J., and Koudela, B. (2006) *Trachipleistophora extenrec* n. sp. a new microsporidian (fungi: microsporidia) infecting mammals. *J Eukaryotic Microbiology.* 53: 464–476.

Vavra, J. & Lukeš, J. (2013) Microsporidia and 'the art of living together'. *Advances in Parasitology*. 82, 253–319.

Vavra, J. & Ronny Larsson, J.I. (2014) *Structure of Microsporidia*. in *Microsporidia*. Pathogens of Opportunity. [Online]. Chichester, UK: John Wiley & Sons, Inc. pp 1-70.

Vemuri, G.N., Eiteman, M.A., McEwen, J.E., Olsson, L. & Nielsen, J. (2007) Increasing NADH oxidation reduces overflow metabolism in Saccharomyces cerevisiae. *Proceedings of the National Academy of Sciences of the United States of America*. 104 (7), 2402–2407.

Visvesvara, G.S. (2002) In vitro cultivation of microsporidia of clinical importance. *Clinical Microbiology Reviews*. 15 (3), 401–413.

Vossbrinck, C.R. & Debrunner-Vossbrinck, B.A. (2005) Molecular phylogeny of the Microsporidia: ecological, ultrastructural and taxonomic considerations. *Folia Parasitologica*. 52, 131–42– discussion 130.

Vossbrinck, C.R., Maddox, J.V., Friedman, S., Debrunner-Vossbrinck, B.A. & Woese, C.R. (1987) Ribosomal RNA sequence suggests microsporidia are extremely ancient eukaryotes*. Nature.* 326 (6111), 411–414.

Waller, R.F., Jabbour, C., Chan, N.C., Celik, N., Likic, V.A., Mulhern, T.D. & Lithgow, T. (2009) Evidence of a Reduced and Modified Mitochondrial Protein Import Apparatus in Microsporidian Mitosomes. *Eukaryotic Cell*. 8 (1), 19–26.

Warren, G. & Wickner, W. (1996) Organelle Inheritance. *Cell*. 84 (3), 395–400.

Wasson, K. & Peper, R.L. (2000) Mammalian microsporidiosis. *Veterinary Pathology Online*. 37 (2), 113–128.

Waterhouse, A.M., Procter, J.B., Martin, D.M.A., Clamp, M. & Barton, G.J. (2009) Jalview Version 2-a multiple sequence alignment editor and analysis workbench. *Bioinformatics (Oxford, England)*. 25 (9), 1189–1191.

Waters, J.C. (2009) Accuracy and precision in quantitative fluorescence microscopy. The Journal of Cell Biology 185: 1135–1148.

Weidner, E., Canning, E.U., Rutledge, C.R. & Meek, C.L. (1999) Mosquito (Diptera: Culicidae) Host Compatibility and Vector Competency for the Human Myositic Parasite *Trachipleistophora hominis* (Phylum Microspora). *Journal of Medical Entomology*. 36 (4), 522–525.

Weiss, L.M. (2014) 'Clinical Syndromes Associated with Microsporidiosis', in *Microsporidia*. Pathogens of Opportunity. [Online]. Chichester, UK: John Wiley & Sons, Inc. pp. 371–401.

Weiss, L.M., Delbac, F., Russell Hayman, J., Pan, G., Dang, X. & Zhou, Z. (2014) 'The Microsporidian Polar Tube and Spore Wall', in *Microsporidia*. Pathogens of Opportunity. [Online]. Chichester, UK: John Wiley & Sons, Inc. pp. 261–306.

Westermann, B. (2010) Mitochondrial fusion and fission in cell life and death. *Nature Reviews Molecular Cell Biology*. 11 (12), 872–884.

Westermann, B. (2011) Organelle Dynamics: ER Embraces Mitochondria for Fission. *Current Biology*. 21 (22), R922–R924.

Wexler-Cohen, Y., Stevens, G.C., Barnoy, E., van der Bliek, A.M. & Johnson, P.J. (2014) A dynamin-related protein contributes to *Trichomonas vaginalis* hydrogenosomal fission. *The FASEB Journal*. 28 (3), 1113–1121.

Williams, B.A.P. & Keeling, P.J. (2005) Microsporidian Mitochondrial Proteins: Expression in *Antonospora locustae* Spores and Identification of Genes Coding for Two Further Proteins. *Journal of Eukaryotic Microbiology*. 52 (3), 271–276.

Williams, B.A.P., Cali, A., Takvorian, P.M. & Keeling, P.J. (2008) Distinct Localization Patterns of Two Putative Mitochondrial Proteins in the Microsporidian Encephalitozoon cuniculi. *Journal of Eukaryotic Microbiology*. 55 (2), 131–133.

Williams, B.A.P., Dolgikh, V.V. & Sokolova, Y.Y. (2014) 'Microsporidian Biochemistry and Physiology', in *Microsporidia*. Pathogens of Opportunity. [Online]. Chichester, UK: John Wiley & Sons, Inc. pp. 245–260.

Williams, B. A., Elliot, C., Burri, L., Kido, Y., Kita, K., Moore, A. L., & Keeling, P. J. (2010). A broad distribution of the alternative oxidase in microsporidian parasites. *PLoS Pathogens. 6* (2), e1000761.

Williams, B.A.P., Haferkamp, I. & Keeling, P.J. (2008) An ADP/ATP-Specific Mitochondrial Carrier Protein in the Microsporidian *Antonospora locustae*. *Journal of Molecular Biology*. 375 (5), 1249–1257.

Williams, B.A.P., Hirt, R.P., Lucocq, J.M. & Embley, T.M. (2002) A mitochondrial remnant in the microsporidian *Trachipleistophora hominis. Nature*. 418 (6900), 865–869.

Williams, B.A.P., Lee, R.C.H., Becnel, J.J., Weiss, L.M., Fast, N.M. & Keeling, P.J. (2008) Genome sequence surveys of *Brachiola algerae* and *Edhazardia aedis* reveal microsporidia with low gene densities. *BMC Genomics*. 9 (1), 200.

Williams, B.P. & Keeling, P. (2011) '2 Microsporidia – Highly Reduced and Derived Relatives of Fungi', in Stefanie Pöggeler & Johannes Wöstemeyer (eds.) *Evolution of Fungi and Fungal-Like Organisms*. [Online]. Springer Berlin Heidelberg. pp. 25–36.

Williams, M. & Kim, K. (2014) From membranes to organelles: Emerging roles for dynamin-like proteins in diverse cellular processes. *European Journal of Cell Biology*. 93 (7), 267–277.

Williams, S., Saha, L., Singha, U.K. & Chaudhuri, M. (2008) *Trypanosoma brucei*: Differential requirement of membrane potential for import of proteins into mitochondria in two developmental stages. *Experimental Parasitology*. 118 (3), 420–433.

Winey, M. & Bloom, K. (2012) Mitotic spindle form and function. *Genetics*. 190 (4), 1197–1224.

Xu, P., Widmer, G., Wang, Y., Ozaki, L.S., Alves, J.M., Serrano, M.G., Puiu, D., Manque, P., Akiyoshi, D., Mackey, A.J., Pearson, W.R., Dear, P.H., Bankier, A.T., Peterson, D.L., Abrahamsen, M.S., Kapur, V., Tzipori, S. & Buck, G.A. (2004) The genome of *Cryptosporidium hominis*. *Nature.* 431 (7012), 1107–1112.

Xu, Y. & Weiss, L.M. (2005) The microsporidian polar tube: A highly specialised invasion organelle. *International Journal for Parasitology*. 35, 941–953.

Xue, B., Dunbrack, R. L., Williams, R. W., Dunker, A. K., & Uversky, V. N. (2010). PONDR-FIT: a meta-predictor of intrinsically disordered amino acids. *Biochimica et Biophysica Acta (BBA)-Proteins and Proteomics*. 1804 (4), 996-1010.

Yabu, Y., Yoshida, A., Suzuki, T., Nihei, C.-I., Kawai, K., Minagawa, N., Hosokawa, T., Nagai, K., Kita, K. & Ohta, N. (2003) The efficacy of ascofuranone in a consecutive treatment on Trypanosoma brucei brucei in mice. *Parasitology International*. 52 (2), 155–164.

Yaffe, M.P. (1999) The Machinery of Mitochondrial Inheritance and Behavior. *Science*. 283 (5407), 1493–1497.

Yaffe, M.P., Stuurman, N. & Vale, R.D. (2003) Mitochondrial positioning in fission yeast is driven by association with dynamic microtubules and mitotic spindle poles. *Proceedings of The National Academy of Sciences of The United States of America*. 100 (20), 11424–11428.

Yamano, K. & Youle, R.J. (2011) Coupling mitochondrial and cell division. *Nature Publishing Group*. 13 (9), 1026–1027.

Yeh, J.I., Chinte, U. & Du, S. (2008) Structure of glycerol-3-phosphate dehydrogenase, an essential monotopic membrane enzyme involved in respiration and metabolism. *Proceedings of The National Academy of Sciences*. 105 (9), 3280–3285.

Zhang, D. & Oliferenko, S. (2013) Remodeling the nuclear membrane during closed mitosis. *Current Opinion in Cell Biology*. 25 (1), 142–148.

Zimorski, V., Ku, C., Martin, W.F. & Gould, S.B. (2014) Endosymbiotic theory for organelle origins. *Current Opinion in Microbiology*. 22, 38–48.

Appendices

Appendix A

Nucleotide sequence of T. hominis SPC97 orthologue (gi 440492072 + 900 nucleotides):

ATGCTCGAGGAGGTTCATTTTCAGAAAAGTTTCAATTTGGGCTATAATTTAACAAAAAATGAGGACCCTATGG
AAGAAAAATTGAATTTGCTTGTGGAAGAATTTTTTAAAATACATAACACAAAAGCCGAGGAATCATTCCTTAAA
TATCTTCGTCTATACCTTGAACCTAGTCAAGACATTACGTTGTCAACTAACGATGTGTTAAGCATCACAAAGAA
ATACAACTTAGATGTCAATTTGAGTATTTTTTCACCAATGGAAGTTAAATTAATTTATATATTTTGCAAATTGGC
TAGTATTCGGAGGAAAAGACCAAAAATAGTTCAGAAAAGCAAAATTAACCTTAAGAGAATTGCACTCGGTCTT
GAAACCGTAGAGAACTACAAGTTAAACATGGAACAGGATGAAATACTAGGAATTTTGCAGAACAACGCATTCA
TTTATACCAAATTCAAGAATGTAACAGACGGCCAGACCATGTCACAGTTACATTTTTACAAAATAGCGAAGGA
CAAAGTGAAAGAGTTTGAAATGCAGGTGCTTATTCTTGATGAGGAAGACATTTTGTTGTTTTACGTCCAGTTAA
AACCATATATAAAGACGTTCATTCTCCTAGATCAGATAAACAGCCACTTCCAAGACACGAAAAATCCCTACAAT
TTTCTAAAATTCTACAGCCGTGATTTTTTTACAAAGGAGGACACGCTGATATATAACATAGTTAGTAGCTGCAC
GAAGCAGCTCAACATCAATTTAAATGAGTGGTTGGTCAAGGGACAGTTTACTGATTACGCTAGAGAATTTTTT
ATTACGAAAAATACTAATGATTTCTGGTTATCGTACAATGTTGACACGGGAATGCTGCCTTTCTTCATTTCGGC
TGAAATTGCTCAAAAAATTCTATACATCGGCAAGGTTAGCAATCTCTTGGTGCGTATATCAAGCGTTTATGAG
GCTGACTATTCTAAACAAGCCACGAATAATTTGGAGATTGTCAACGATGGTCGTAACATACTAGAAACCCGGC
CACATTGCACTAAAGGTGGAAATGTTCCGTATGATTGCACGATAGGAAACGAAGCACAGCTCGTCGAAGTTC
TTGATAGAAATTTTGAAAATATAATTAATGAAAGGCTTTTAGCTGCAGACAGACAGGTTAAGGCCATTTTTCTT
GTACGATGCCAAATCATTGAATATCTAAATTTCTGTAAAGACACGTTTTTCTTCGCCCGTAACGATTTCATCGA
ACATCTTCTGCTCCACATGAAAGACATTAATACAAGCAGCTTGTGTAAAAGGAGCTATTCGTTCGTCTTGGAC
AGTGCAATCATGTCATCCTTCAAACAAATGAATAAGATCACATCCACGCTGGATATGTGCGTACTTAAAGATG
ATGATTTTTCGTTATTCTGCCATTTAGATTTTCCCATGAATGTAATTATTGAGAAGGACGTGGTTATGATTTTTC
TTAGCGTTTTTAAGTATTTGTGGAAGATAAAACGAATTGAGCACTTTTTGAGGAAAATGAAGAATGCGGCGAG
TAATGATCTAAGTAATGCCATTACGCTCAACAAATGGTATTTTTTGATCCAAAAAATATTTTTCTATTTTTTCTAC
GAGGTTATTGAGAAAGACTATGTAGAATTGATAAGTATTGTAGACAATAAAGTATTTGTGATTGATGAGCTACG
CAAGGGGGTAAAAAGGTTCCTGAGGAATGTTATAAAAGGCATTTTTCAGGAAAATGGGAACGGTAAGGAACA
GATGGATACATTTCTCAATGTTCTGGAACAGGAGTGTCTCAATTATAAGAAATACAGACGAGTTTTTGATGACT
GCCATATTAAGAAAAATTTAGAAAATCTTATTGTTGTGATAAATGATAAAGTTGAGAACACCACGCTGTTCAAC
ATAACAGCATACGTGTAA

Appendix B

Figure 5.4 Multiple sequence alignment of representative dynamin and DRP homologues sequences from Fungi, microsporidia and Metazoa

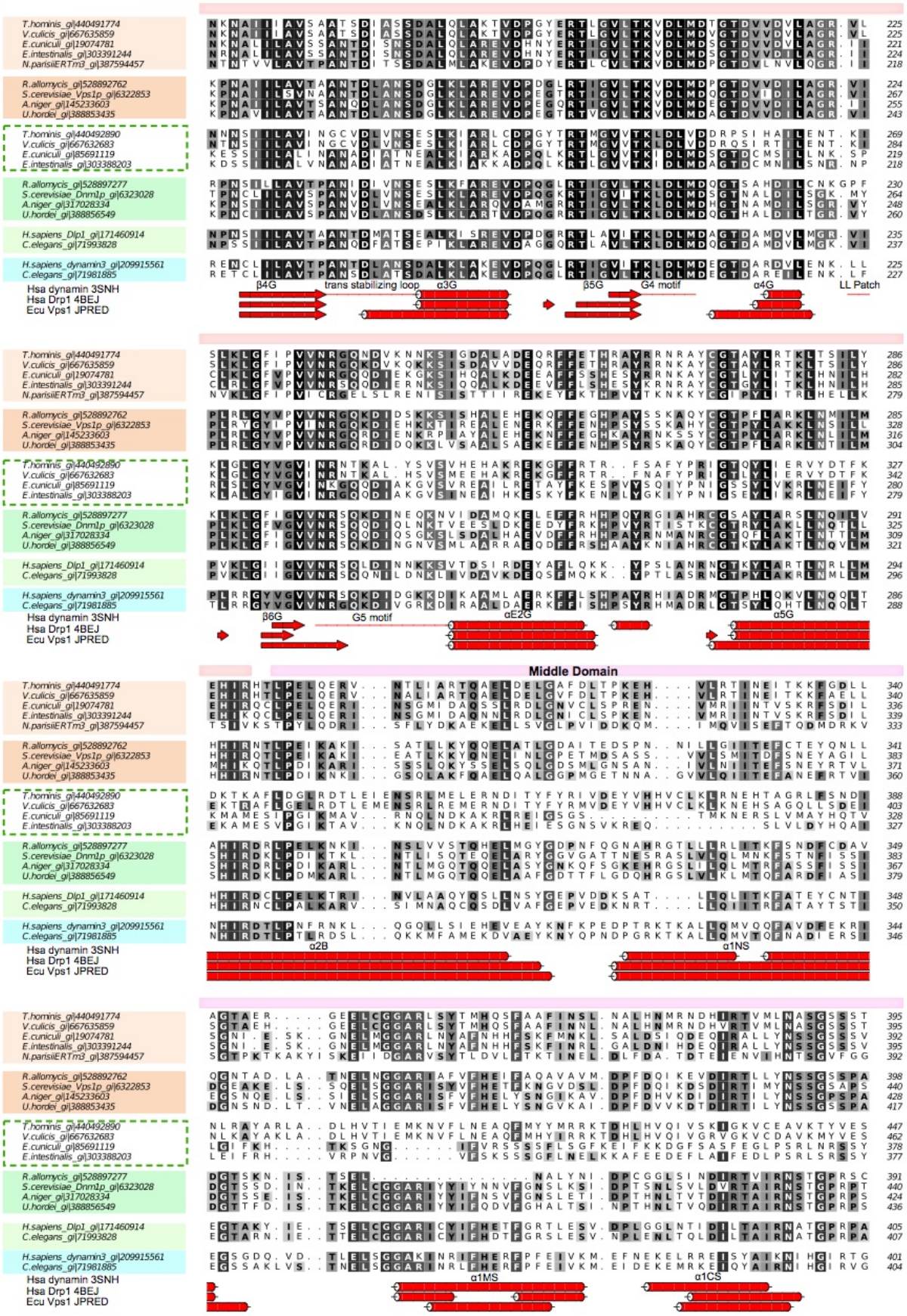

Figure 5.4 Multiple sequence alignment of representative dynamin and DRP homologues sequences from Fungi, microsporidia and Metazoa

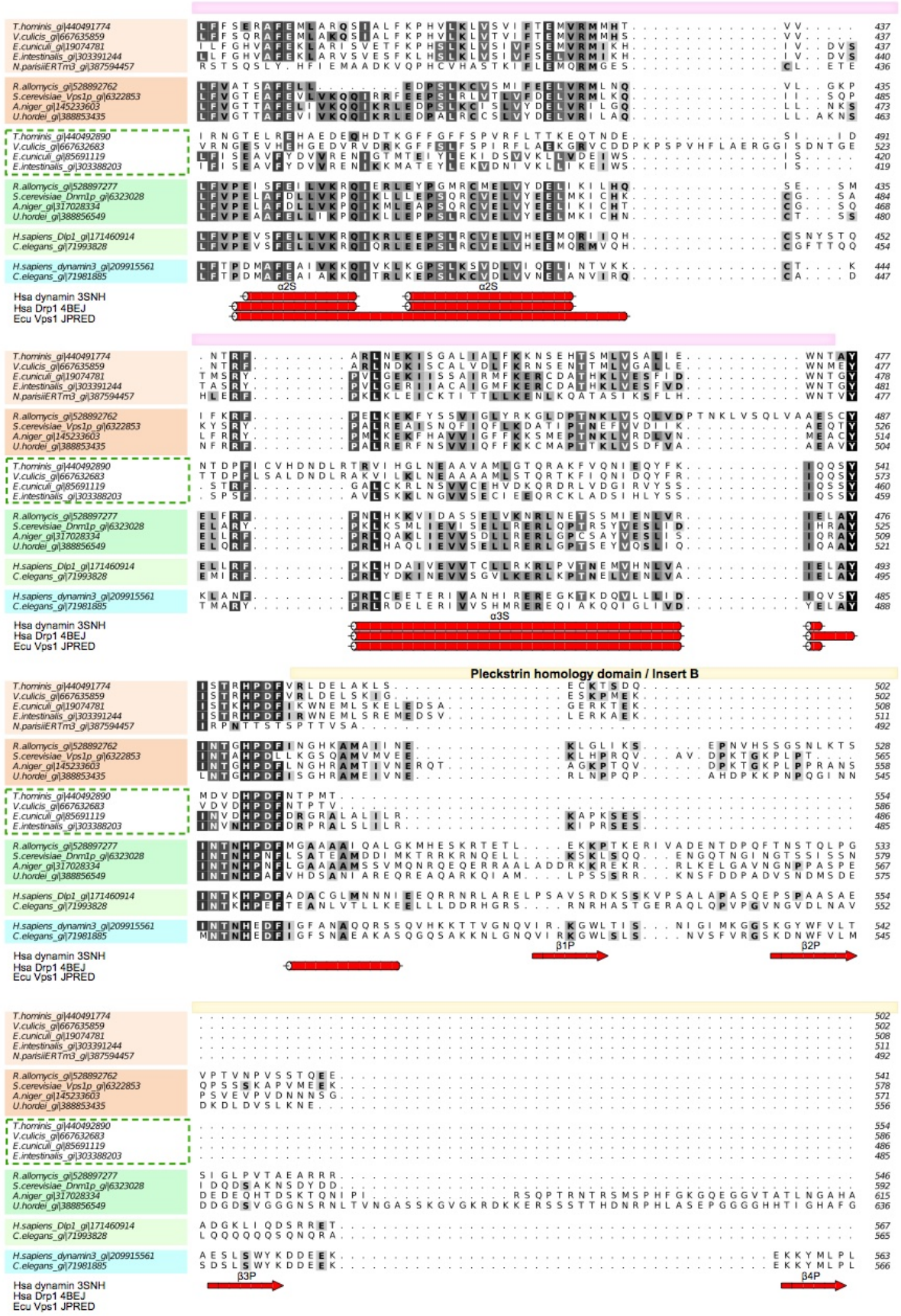

Figure 5.4 Multiple sequence alignment of representative dynamin and DRP homologues sequences from Fungi, microsporidia and Metazoa

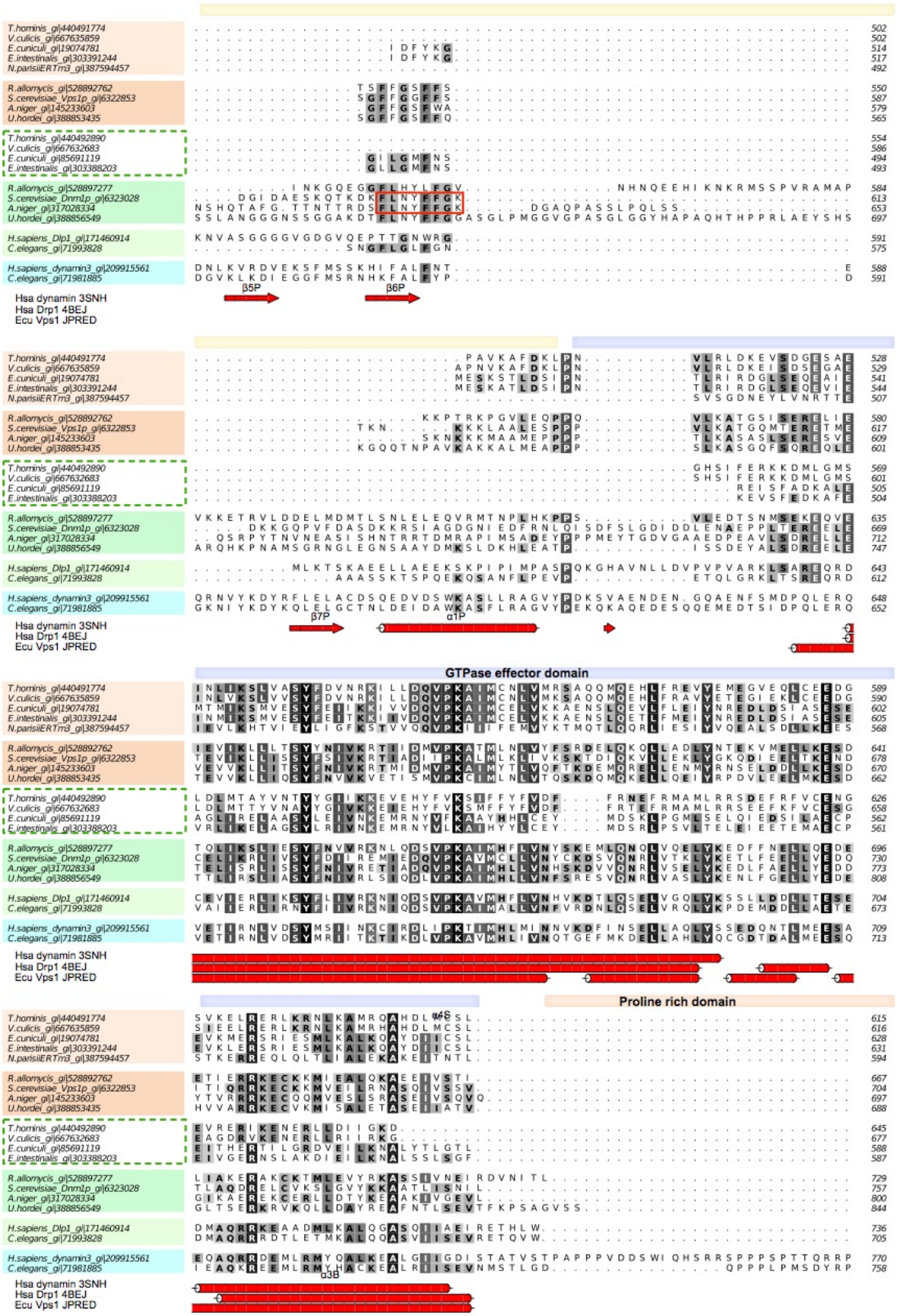

Figure 5.4 Multiple sequence alignment of representative dynamin and DRP homologues sequences from Fungi, microsporidia and Metazoa

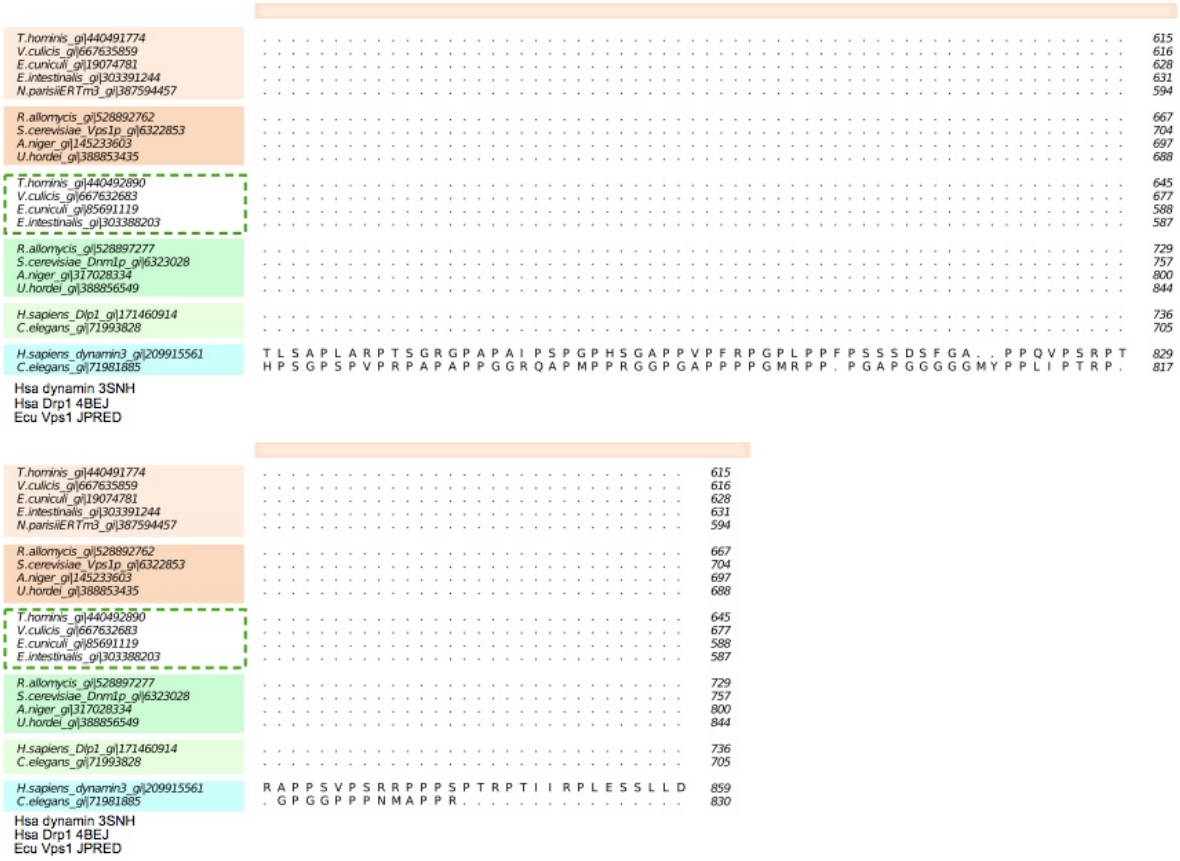

Figure 5.4 Multiple sequence alignment of representative dynamin and DRP homologues sequences from Fungi, microsporidia and Metazoa

Coloured boxes above alignment annotate domain architecture according to published data (Fröhlich et al., 2013; Faelber et al., 2011). Secondary structures below the alignment correspond to human dynamin1 (Faelber et al., 2011), (pdb 3SHN), human DNM1L (Fröhlich et al., 2013), (pdb 4BEJ) and secondary structure predictions for *E. cuniculi* Vps1p orthologue generated using Jpred 3 server (Cole et al., 2008) (www.compbio.dundee.ac.uk/jpred/). Secondary structure was annotated following Fröhlich et al., 2013. Alpha-helices are presented as cylinders and beta strands are presented as arrows. Red box indicates sequence motif responsible for interaction of Dnm1p with Mdv1p adaptor protein in *S. cerevisiae* (Bui et al., 2012). Groups of sequences were annotated with colours corresponding to those used in the trees. Alignment was formatted in ALINE (Bond & Schüttelkopf, 2009), conserved residues were coloured using 'colouring by similarity' function implemented in ALINE with 0.1 low similarity cut-off.

Sequences used in the alignment: *Trachipleistophora hominis* Drp1 (GI 440492890), *T. hominis* Vps1p (GI 440491774), *Vavraia culicis* Drp1 (GI 667632683), *V. culicis* Vps1p (GI 667635859), *Encephalitozoon cuniculi* Drp1 (GI 85691119), *E. cuniculi* Vps1p (GI 19074781), *Encephalitozoon intestinalis* Drp1 (GI 303388203), *E. intestinalis* Vps1p (GI 303391244), N. parisii ERTm3 Vps1p (GI 387594457), *Saccharomyces cerevisiae* Vps1p (GI 6322853), *S. cerevisiae* Dnm1p (GI 6323028), *Rozella allomycis* Vps1p (GI 528892762), *R. allomycis* Dnm1p (GI 528897277), *Aspergillus niger* Vps1p (GI 145233603), *A. niger* Dnm1p (GI 317028334), *Ustilago hordei* Dnm1p (GI 388856549), *U. hordei* Vps1p (GI 388853435), *Homo sapiens* Dlp1 (GI 171460914), *H. sapiens* dynamin 3 (GI 209915561), *Caenorhabditis elegans* dynamin (GI 71981885), *C. elegans* Dlp1 (GI 71993828).